From N to P: Examining Structure-Property Relationships of Ammonium- and Phosphonium-Containing Macromolecules

Sean T. Hemp

Dissertation submitted to the faculty of the Virginia Polytechnic Institute and State University in partial fulfillment of the requirements for the degree of

Doctor of Philosophy
In
Chemistry

Timothy E. Long, Chair
Robert B. Moore
Kevin J. Edgar
Tijana Z. Grove
Richey M. Davis

August 22nd, 2013
Blacksburg, VA

Keywords: phosphonium, ammonium, polyelectrolyte, RAFT polymerization

From N to P: Examining Structure-Property Relationships of Ammonium- and Phosphonium-Containing Macromolecules

Sean T. Hemp

ABSTRACT

An unprecedented comprehensive study of ammonium and phosphonium polyelectrolytes probed and examined structure-property relationships with a focus on different macromolecular properties. Conventional free radical polymerization readily generated a large library of ammonium- and phosphonium-containing polyelectrolytes. Along with the two different cationic atoms, the alkyl substituent lengths and counterions were varied to generate a thorough structure-property relationship analysis. Phosphonium macromolecules displayed improved thermal stabilities and improved ionic conductivities compared to ammonium analogs. Longer alkyl substituent lengths systematically decreased the glass transition temperatures of all polyelectrolytes; the larger, bulkier counterions also resulted in lower glass transition temperatures. Counterion also impacted the thermal stability of the polymerized ionic liquids with less basic counterions leading to improved thermal stability. For the first time, the efficacy of phosphonium macromolecules for nonviral nucleic acid delivery was examined. Phosphonium macromolecules more efficiently complexed nucleic acids than ammonium analogs and butyl-containing phosphonium macromolecules delivered nucleic acids more effectively than the ammonium analog. Controlled radical polymerization generated unprecedented phosphonium-containing diblock copolymers and these diblock copolymers displayed enhanced colloidal stability and lower cytotoxicity compared to the phosphonium homopolymer for nucleic acid delivery.

Step-growth polymerization techniques enabled the synthesis of well-defined, high molecular weight phosphonium ionenes for the first time. Phosphonium ionenes exhibited higher thermal stability and alkaline stability compared to ammonium ionenes. Due to their high thermal stability and relatively low glass transition temperatures, unprecedented melt rheology studies on polyelectrolytes probed the melt flow characteristics of phosphonium ionenes. Novel phosphonium gemini surfactants displayed interesting solution properties in aqueous and chloroform solutions. Electrospinning of the phosphonium gemini surfactants created uniform fibers. The synthesis and characterization of sulfonium polyelectrolytes enabled the first examination of sulfonium macromolecules for nonviral nucleic acid delivery. Sulfonium polyelectrolytes successfully bound nucleic acids and delivered them *in vitro*. Controlled radical polymerization generated innovative AB diblock and ABA triblock copolymers that displayed salt- and temperature-responsive properties suitable for biological applications such as drug delivery vehicles and hydrogels. Finally, adenine-containing polyelectrolytes were synthesized and they were successfully electrospun to generate adenine-decorated nanofibers appropriate for filtration and nonwoven applications.

Acknowledgements

Firstly, I would like to thank and acknowledge my Ph.D. advisor, Dr. Tim Long, who provided support and guidance throughout my graduate career at Virginia Tech. He is an excellent scientist and advisor who provided significant contributions to not only my research endeavors, but also to other skills required as a scientist. His consistent strive for excellence in oral presentations and writing helped strengthen my skills in both areas. I also thank Dr. Long for all of his personal support during my graduate career. I firmly believe no other advisor would have provided as much support and understanding as he did with my wife's illness. I also thank my committee members for their constant input and guidance: Dr. Kevin Edgar, Dr. Bob Moore, Dr. Tijana Grove, and Dr. Richey Davis. They always challenged me to be the best that I could possibly be.

I acknowledge funding from a broad range of federal and industrial partners whose support enabled me to serve as a research assistant instead of a teaching assistant. I received significant support from the Army Research Labs and a Materials Center of Excellence grant. I appreciate my industrial collaborations, which included Techulon, Inc., and Kimberly-Clark Corporation.

The Long research group is a fantastic group of scientists and I appreciate all of their support during graduate school. I would like to thank Dr. Shijing Cheng and Dr. Matthew Hunley first and foremost since they served as graduate student mentors to me when I first joined the group. Shijing always challenged me to think beyond the novelty of an idea and focus on the significance of the research. Matt Hunley taught me all I know about solution rheology and electrospinning; he also initiated me in the writing style of Dr. Long. I owe much of my success and research to two individuals who collaborated significantly on many projects: Dr. Adam

Smith and Dr. Mike Allen. Adam catalyzed much of the research reported and he taught me everything about RAFT polymerization. Mike is an invaluable friend and researcher who trained me on all cell bio experiments. Dr. Nancy Zhang, my fellow Tar Heel, always made lab enjoyable and was always willing to lend a hand with any experiment. I thank Dr. Asem Abdulahad for his friendship and support during my last year at Virginia Tech. His willingness to listen and his constant laughter helped brighten my time during the most difficult time of my graduate career. Finally, I would like to thank the rest of the Long group members who I interacted with who were pivotal during my graduate career: Joe Dennis, John Herlihy, Ashley Nelson, Evan Margaretta, Keren Zhang, Dan Buckwalter, Alie Schultz, David Inglefield, Renlong Gao, Matt Green, Steve June, Mana Tamami, and all of my undergraduates (Kerry DeMella, Sandeep Pole, and Zach Weinrich).

Finally and most importantly, I profusely thank my wife and family for their love and support during graduate school. My wife, Merileigh, provided constant love and grace to me during graduate school and I love her with all of my heart and soul. She truly is my better half and I look forward to starting "real life" together out of school. I appreciate all of the support from my parents, whose love and support strengthened me. I have the best in-laws possible in John and Beth with their constant strength and support and I am truly blessed to have them in my life. My siblings, Chris and Katie, and my siblings-in-law, Greg, Daniel, and Grant, also provided much needed support and friendship. I am thankful for the 5 nieces and nephews that I have been blessed to be a part of their lives while in graduate school.

All of this would not be possible without God's love and grace given freely to me every day. I am truly thankful for His love and support during graduate school and I would not have

had any success without His help. I hope to use my education to further His kingdom and I wish to bring Him glory for the rest of my life.

Attributions

Prof. Timothy E. Long
Professor of Chemistry at Virginia Tech and Research Advisor

Dr. Shijing Cheng
Past graduate student in Dr. Long's research group who mentored me during my first year. Contributed to Chapter 5.

Dr. Matthew Hunley
Past graduate student in Dr. Long's research group who mentored me during my first year. Contributed to Chapter 3.

Dr. Michael H. Allen, Jr.
Past graduate student in Dr. Long's research group who contributed significantly to Chapters 4, 5, 6, 7, 9, and 10.

Dr. Adam E. Smith
Post-doctoral researcher in Dr. Long's research group who contributed significantly to Chapters 6, 7, 10, and 11.

Dr. Matthew D. Green
Past graduate student in Dr. Long's research group who contributed to Chapter 6.

Dr. Musan "Nancy" Zhang
Past graduate student in Dr. Long's research group who contributed to Chapter 8.

Prof. Robert B. Moore
Professor of Chemistry at Virginia Tech and collaborator on Chapters 5 and 9.

Mingqiang Zhang
Graduate student in Dr. Moore's research group who contributed to Chapter 5.

Amanda G. Hudson
Graduate student in Dr. Moore's research group who contributed to Chapter 9.

Kerry DeMella
Past undergraduate student in Dr. Long's research group who contributed to Chapter 3.

Sandeep S. Pole
Past undergraduate student in Dr. Long's research group who contributed to Chapter 9.

Dr. Mana Tamami
Past graduate student in Dr. Long's research group who contributed to Chapter 8.

Dr. Clay Bunyard

Industrial collaborator at Kimberly-Clark Corporation who contributed to Chapter 11.

Prof. Michael Rubinstein
Professor of Chemistry at University of North Carolina at Chapel Hill who contributed to Chapter 11.

Dr. Joshua M. Bryson
Principal scientist at Techulon, Inc., who contributed to Chapter 7.

Table of Contents

List of Figures

List of Tables

List of Schemes

Chapter 1: Introduction

1.1 *Dissertation Overview*

The overall focus of this dissertation revolves around ammonium- and phosphonium-containing macromolecules with an emphasis on polyelectrolytes. Chapter 2 reviews the current literature focused on nucleobase-containing macromolecules with a perspective on the incorporation of electrostatic and complementary hydrogen bonding interactions in the same macromolecular system. Chapter 3 details the synthesis and characterization of adenine-containing polyelectrolytes with a focus on their solution and electrospinning behavior. Ammonium- and adenine-containing macromolecules displayed polyelectrolyte behavior and electrospinning generated adenine-decorated nanofibers.

Chapter 4 reviews literature focused on the comparison of ammonium- and phosphonium-containing macromolecules for biological applications including nonviral gene delivery and antimicrobials. Chapter 5 examines structure-property relationships of ammonium and phosphonium polyelectrolytes with a focus on thermal properties, ionic conductivities, and morphologies. Differences in the cationic atom, alkyl substituent lengths, and counterions impacted all macromolecular properties examined. Phosphonium polymerized ionic liquids exhibited improved thermal stabilities and ionic conductivities compared to ammonium analogs. Chapters 6 and 7 report on the novel utilization of phosphonium macromolecules for nonviral nucleic acid delivery. Specifically, Chapter 6 covers the direct comparison of ammonium and phosphonium polyelectrolytes as nucleic acid delivery vehicles. Phosphonium macromolecules bound nucleic acids more efficiently and they also displayed enhanced nucleic acid delivery compared to ammonium analogs. Chapter 7 examines the synthesis and characterization of phosphonium-containing diblock copolymers for nonviral nucleic acid delivery. These AB

diblock copolymers displayed enhanced colloidal stability and reduced cytotoxicity compared to the phosphonium homopolymer.

Chapter 8 focuses on the well-defined step-growth polymerization of ditertiary phosphines and alkyl dibromides to generate high molecular weight phosphonium ionenes. Phosphonium ionenes exhibited enhanced thermal stability and alkaline stability compared to ammonium ionenes. Melt rheology studies probed the melt flow dynamics of phosphonium ionenes, enabling a thorough understanding of charge density on the melt behavior of polyelectrolytes. Chapter 9 reports novel phosphonium gemini surfactants with controlled spacer lengths in between the head groups. The solution behavior of the phosphonium gemini surfactants were examined in aqueous and organic solutions. Electrospinning of phosphonium gemini surfactants from chloroform solution created uniform fibers.

Chapter 10 details the examination of sulfonium polyelectrolytes for nucleic acid complexation and delivery. Post-polymerization alkylation of a thioether-containing homopolymer and diblock copolymer generated sulfonium polyelectrolytes. These sulfonium macromolecules complexed nucleic acids effectively and they delivered nucleic acids *in vitro*. Chapter 11 examines salt- and temperature-responsive AB diblock and ABA triblock copolymers suitable for drug delivery and hydrogel applications. Precise structure control enabled tuning of the salt- and temperature-response to generate materials suitable for biological applications under physiological conditions. Finally, Chapters 12 and 13 provide overall conclusions of the dissertation and suggested future work to continue the enclosed research efforts, respectively.

Chapter 2: DNA Inspired Hierarchical Polymer Design: Electrostatics and Hydrogen Bonding in Concert

(Published in *Macromolecular Bioscience* **2012,** *12* (1), 29-39.)

Sean T. Hemp and Timothy E. Long*

Department of Chemistry and Macromolecules and Interfaces Institute, Virginia Tech,

Blacksburg, VA 24061

*To whom correspondence should be addressed. E-mail: telong@vt.edu. TEL: (540)231-2480

FAX: (540)231-8517

Keywords: hydrogen bonding, nucleobases, molecular recognition, supramolecular structures, templates

2.1 *Abstract*

Nucleic acids and proteins, two of nature's biopolymers, assemble into complex structures to achieve desired biological functions and inspire the design of synthetic macromolecules containing a wide variety of non-covalent interactions including electrostatics and hydrogen bonding. Researchers have incorporated DNA nucleobases into a wide variety of synthetic monomers/polymers achieving stimuli-responsive materials, supramolecular assemblies, and well-controlled macromolecules. Recently, scientists utilized both electrostatics and complementary hydrogen bonding to orthogonally functionalize a polymer backbone through supramolecular assembly. Diverse macromolecules with non-covalent interactions will create materials with properties necessary for biomedical applications.

2.2 *DNA Structure and Experimental Techniques*

Deoxyribose nucleic acids (DNA) contain all the required genetic information for reproduction and protein synthesis; their complex quaternary structure enables the storage of genetic information and the combination of many non-covalent interactions stabilize the quaternary structure.[1] For many years, researchers pursued the structure of DNA and James Watson and Francis Crick's seminal paper titled "Molecular structure of nucleic acids. A structure for deoxyribose nucleic acid" solved the mystery of the DNA structure and the inherent genetic information.[2,3] Since Watson and Crick's publication, scientists have discovered and characterized many different polymorphs of DNA including A-DNA, B-DNA, and Z-DNA shown in **Figure 2.1**.[4,5] While these polymorphs are geometrically different in structure (morphology), their basic chemical structure remains the same: a deoxyribose sugar and phosphate backbone with a nucleobase attached to each sugar.[6]

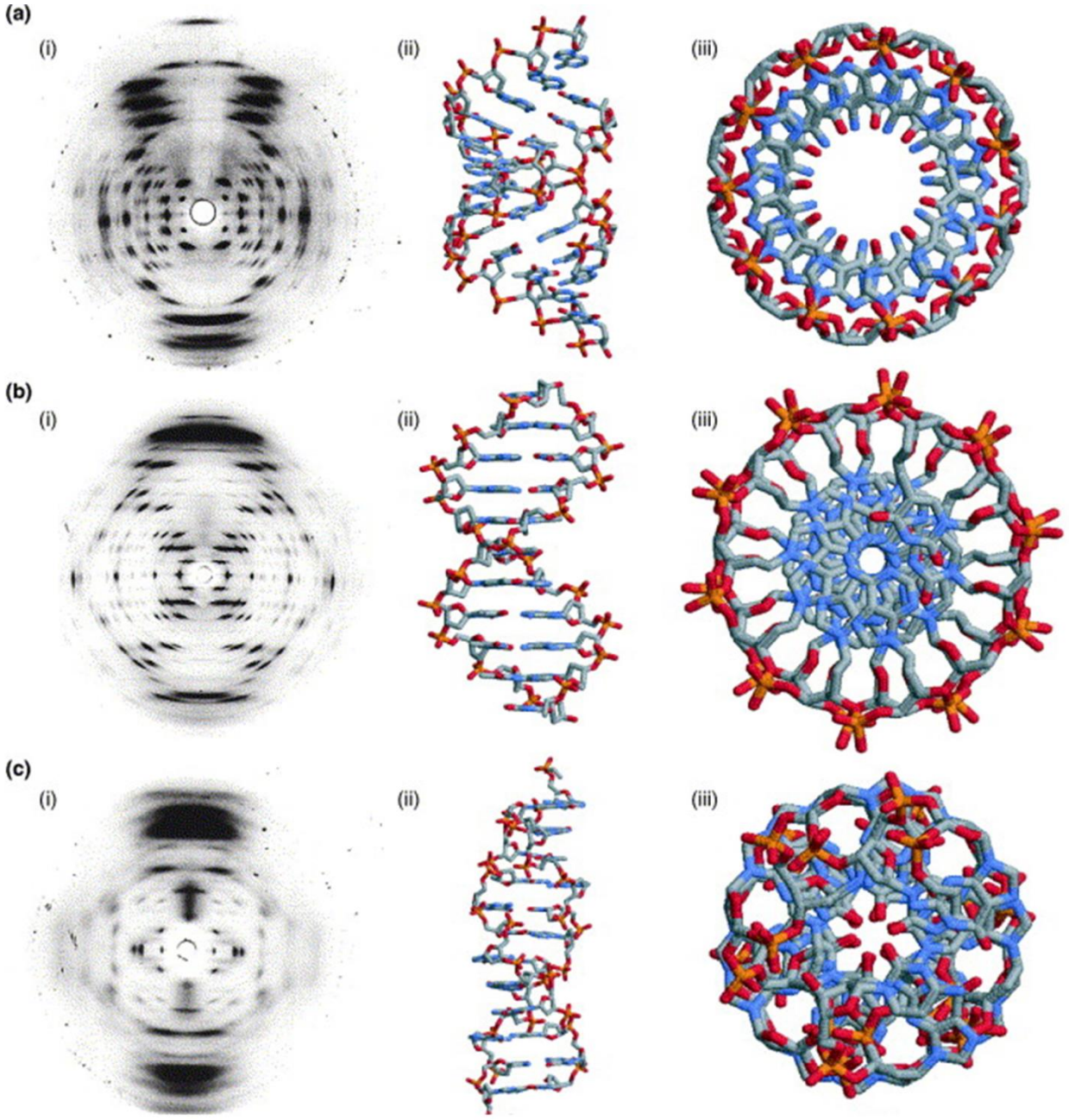

Figure 2.1. X-ray diffraction patterns of a) A-DNA, b) B-DNA, and c) Z-DNA along with structural depictions of each helix. Reprinted with permission from Ref. 7. ©2006 Elsevier.

The four nucleobases utilized in DNA are the pyrimidines (thymine and cytosine) and the purines (adenine and guanine).[8] Another common nucleobase is uracil, a pyrimidine, which replaces thymine in RNA. Attachment of the nucleobases to the deoxyribose sugar occurs at the

C1 position of the sugar and either the N1 position for pyrimidines or the N9 position for purines through a glycosidic bond that has two different conformations: syn and anti (the preferred conformation).[9] The ribose sugar itself has two different common sugar pucker conformations found within the different DNA polymorphs: C2'-*endo* and C3'-*endo.*[10] Phosphodiester bonds link together the nucleosides (ribose + nucleobase) at the 5'-OH and 3'-OH to generate one DNA strand[11] and they are also hydrolytically stable (rate constants estimated around 10^{-13} to 10^{-16} s^{-1})[12] except in the presence of DNA nucleases (catalyzed rate constants 10^{16} times larger than uncatalyzed rate constants).[13] Two complementary DNA strands dimerize in an anti-parallel fashion to generate a double stranded helical structure.[14] The supramolecular assembly of the DNA structure results from many different non-covalent interactions: hydrogen bonding,[15,16] electrostatics,[17-19] and π- π stacking.[20-22]

Figure 2.2 shows the chemical structure for DNA and three common hydrogen bonding configurations: Watson-Crick base pairing between adenine/thymine and guanine/cytosine and also a Hoogsteen base pair between uracil and adenine.[23] While the hydrogen bonding creates specificity and a method to copy the genetic code in DNA, hydrogen bonding itself does not greatly add to the stabilization of the DNA double helix.[1,24,25] Predominately, π-π stacking interactions between the nucleobases drive the self-assembly into double helices.[26,27] The double helix structures place the nucleobases in the proper orientation to base stack on top of each other allowing for favorable π- π interactions between their aromatic rings and also shields the hydrophobic bases from the hydrophilic aqueous solution.[22,28] Electrostatics also play a role in the double helix because the negatively charged phosphate groups electrostatically repel each other, similar to synthetic polyelectrolytes,[29] elongating the DNA strands.[19] Cations, specifically

monovalent and especially divalent, are vital to screen the negatively charged phosphates and aid in stabilizing the double helix.[30]

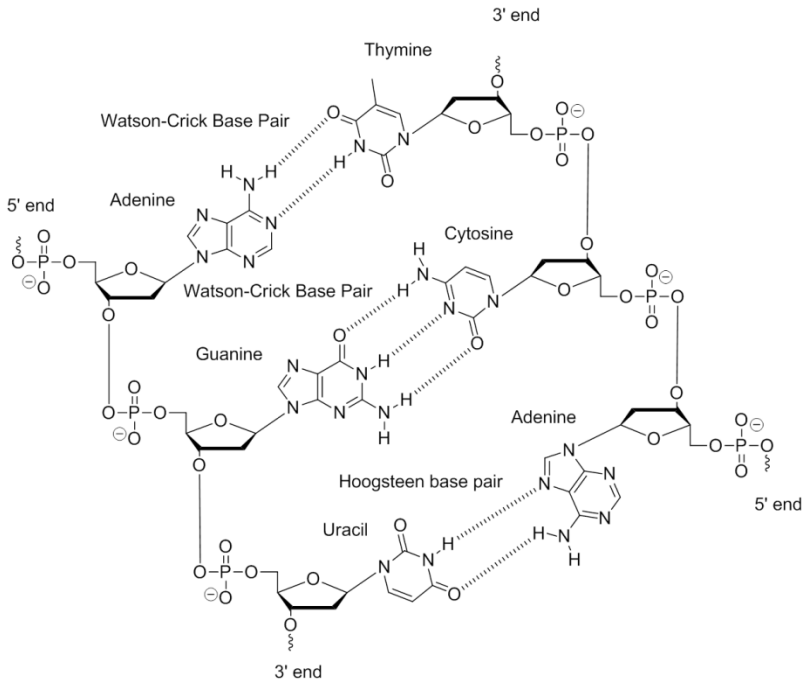

Figure 2.2. DNA chemical structure depicting the sugar and phosphate backbone and the five different nucleobases with Watson-Crick base pairing and Hoogsteen base pairing.

The DNA structure and the non-covalent forces used to generate the double helix have inspired researchers to utilize these same non-covalent interactions to generate unique macromolecules and structures. Supramolecular chemistry describes the formation and synthesis of macromolecules through specific, directional non-covalent interactions between small molecule monomers.[31-34] Typical non-covalent interactions employed in supramolecular chemistry are hydrogen bonding,[35] π-π interactions,[36] or metal coordination.[37] Supramolecular chemistry also focuses on the non-covalent interaction of small molecules with complementary functionality on covalently formed macromolecules.[38] Recently, researchers have focused on the incorporation of nucleobases into synthetic polymers to allow the supramolecular assembly of

nucleobase functionalized small molecules to these nucleobase-functionalized polymers and/or the supramolecular assembly of two nucleobase-functionalized polymers.

2.3 *Nucleobase-Containing Styrene Monomers*

Sedlák *et al.*[39] first synthesized all five nucleobase styrenic monomers shown in **Figure 2.3**; adenine required no protection chemistry before substitution, thymine/uracil and cytosine required trimethylsilyl protection prior to substitution and then hydrolysis/deprotection, and guanine required the utilization of the precursor 2-amino-6-chloropurine with hydroxyl substitution. One major concern in nucleobase chemistry results from the multiple nucleophilic positions in the heterocycles where substitution can occur. For example, adenine and guanine substitution can occur at both the N7 and N9 positions. Sedlák *et al.* modified their reaction conditions to synthesize and obtain only the N9 substitution product; ^{15}N NMR confirmed isolation of only the N9 substitution product.

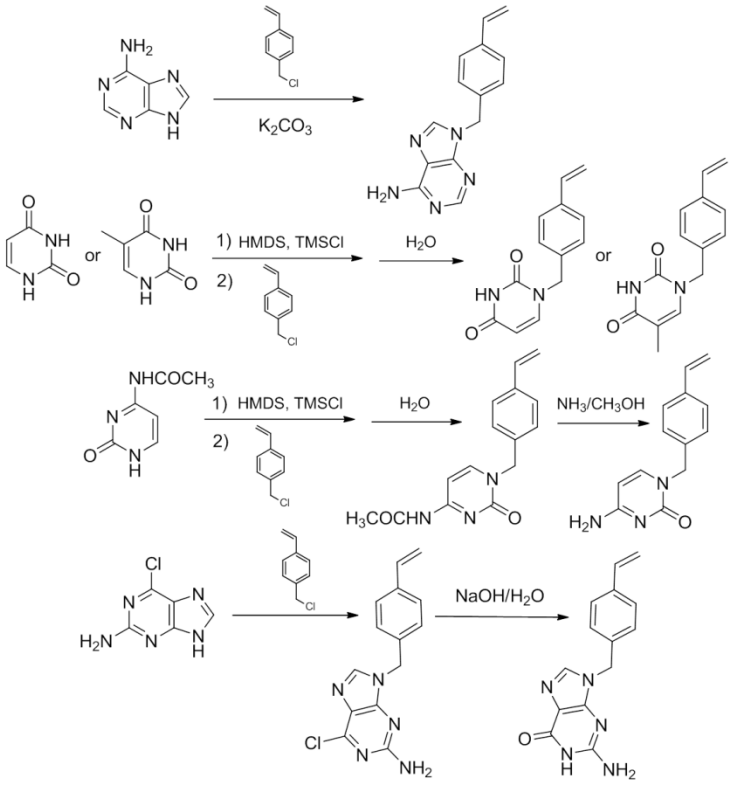

Figure 2.3. Synthesis of adenine, thymine, uracil, cytosine, and guanine containing styrene monomers.[39]

While a few researchers polymerized 1-vinylbenzylthymine prior to Lutz *et al.*'s work, Lutz *et al.*[40-42] first demonstrated the conventional free radical polymerization of 1-vinylbenzylthymine, 1-vinylbenzyluracil, and 9-vinylbenzyladenine. Since the homopolymers were insoluble in a majority of organic solvents except for highly polar, aprotic organic solvents such as dimethylsulfoxide (DMSO), *N*-methyl-2-pyrrolidone (NMP), and dimethylformamide (DMF), the authors copolymerized dodecyl methacrylate with either 1-vinylbenzylthymine or 9-vinylbenzyladenine utilizing atom transfer radical polymerization (ATRP). These copolymers were readily soluble in a greater variety of organic solvents with molecular weights between 7,000-17,000 g/mol and M_w/M_n's around 1.3. Ultraviolet (UV) spectroscopy, ^{1}H-NMR, and infrared spectroscopy confirmed association of the two copolymers via complementary hydrogen

bonding and at very high concentrations, the copolymers aggregated into micron-scale spheres shown using confocal fluorescence microscopy, optical microscopy, and dynamic light scattering (DLS).

Cheng *et al.*[43,44] were the first to control the radical homopolymerization of 1-vinylbenzylthymine, 1-vinylbenzyluracil, and 9-vinylbenzyladenine utilizing ATRP. Since the nucleobases coordinate to metals like copper, Cheng *et al.* utilized tris(2-dimethylaminoethyl)amine (Me_6TREN) as the copper ligand to minimize nucleobase coordination to the copper catalyst. They also needed very high temperatures (180 °C) to achieve the homopolymerization of the three monomers in *N*-methyl-2-pyrrolidone and were able to obtain high conversions with molecular weights ranging from 3,500-7,500 g/mol and M_w/M_n's from 1.2-1.4.

Nitroxide-mediated polymerization or stable-free radical polymerization (SFRP) eliminates the need for a metal catalyst avoiding nucleobase coordination issues. Long *et al.* [45] first published the synthesis of ABA triblocks utilizing a difunctional initiator $DEPN_2$ shown in **Figure 2.4** to synthesize a poly(n-butyl acrylate) precursor block and then subsequently polymerizing either 1-vinylbenzylthymine or 9-vinylbenzyladenine to generate an ABA triblock. They demonstrated that microphase separation occurred even with low molecular weight outer nucleobase blocks (1,500 g/mol) and they also showed a significant increase in solution viscosity and solution viscosity scaling factors upon the blending of adenine-containing triblocks and thymine-containing triblocks together in solution. A blend of the adenine and thymine ABA triblock copolymers also had the widest rubbery plateau as shown in the dynamic mechanical analysis (DMA) curves in **Figure 2.4** and annealing conditions greatly influenced the onset of flow.

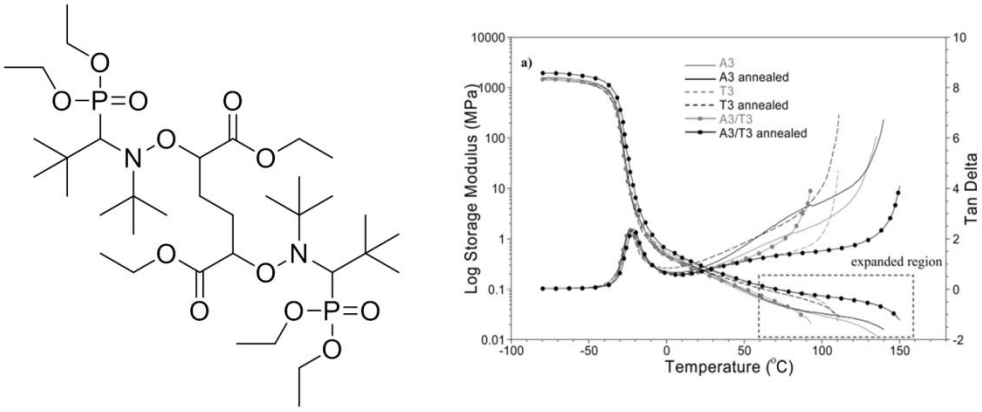

Figure 2.4. Structure of $DEPN_2$, a difunctional nitroxide initiator, and the resulting mechanical properties of the nucleobase-containing triblock copolymers and their blends. Annealing and also blending the thymine- and adenine-containing triblocks together increased the flow temperature. Reprinted with permission from Ref. 45. ©2007 American Chemical Society.

2.4 *Nucleobase-Containing Methacrylate Monomers*

Marsh *et al.*[46] synthesized uridine- and adenosine-functionalized methacrylate monomers utilizing *Candida Antarctic lipase* 435, an enzyme catalyzing the esterification regioselectively at the 5'-hydroxyl group of the nucleobase-functionalized ribose, shown in **Figure 2.5**. They silyl protected the uridine and adenosine monomers which improved their solubility allowing the authors to polymerize the monomers using ATRP in less polar solvents. Utilizing ethyl bromoisobutyrate as an initiator and *N*-(*n*-pentyl)-2-pyridiylmethanimine (NPMI) or Me_6TREN as the copper ligands, the authors controlled the polymerization of the trimethylsilyl (TMS)-protected 5'-methacryloyluridine to achieve molecular weights between 6,500-8,500 g/mol with M_w/M_n's between 1.12-1.17. *tert*-butyldimethylsilyl (TBDMS)-protected 5'-methacryloyladenosine polymerized utilizing the same conditions achieved molecular weights around 4,000 g/mol with a higher M_w/M_n around 1.4; the authors attributed the higher molecular

weight distribution to polymer-column interactions during size-exclusion chromatography (SEC) analysis. Marsh *et al.*[47] have also polymerized uridine and adenosine methacrylate polymers from silica gel functionalized with ATRP initiators and are currently investigating their use for nucleic acid chemistry in separations and syntheses.

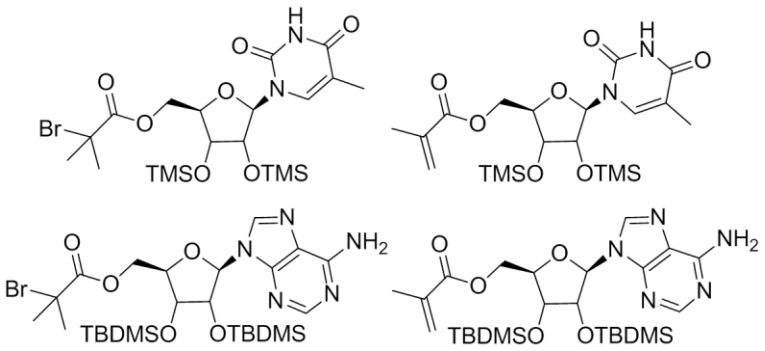

Figure 2.5. Nucleoside-containing ATRP initiators and methacrylate monomers protected with TMS and TBDMS groups to improve organic solubility. Reprinted with permission from Ref. 46. ©1999 American Chemical Society.

van Hest *et al.*[48] synthesized the four nucleobase monomers shown in **Figure 2.6**; they synthesized the adenine, thymine, and cytosine monomers without any protection chemistry via the S_N2 substitution of 3-bromopropyl methacrylate. The guanine methacrylate monomer required multiple protection and deprotection steps to afford the final guanine methacrylate in 24% overall yield. As shown in Table 1, the authors successfully controlled the polymerization of the adenine, thymine, and guanine monomers using ATRP achieving narrow M_w/M_n's and molecular weights around 7,000 g/mol using bipyridine (bpy) as the ligand. All three monomers exhibited pseudo-first order kinetics confirming their controlled character. Surprisingly, ^{1}H-NMR confirmed coordination of the guanine monomer to the Cu catalyst with no detriment to the control of the polymerization. On the other hand, the cytosine monomer required additional $CuCl_2$ and N,N,N′,N″,N″-Pentamethyldiethylenetriamine (PMDETA) as the Cu ligand to

minimize cytosine coordination to control the polymerization and achieve a M_n and M_w/M_n of 4,500 g/mol and 1.15, respectively.

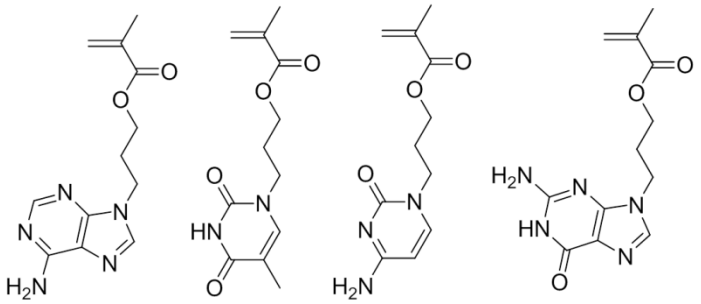

Figure 2.6. Adenine, thymine, cytosine, and guanine based methacrylate monomers for ATRP processes to generate well-controlled nucleobase-containing poly(alkyl methacrylates).[48]

van Hest *et al.*[49] also synthesized block copolymers containing a PEG block and either an adenine or thymine methacrylate block employing a bromine functionalized PEG macroinitiator and ATRP. They achieved pseudo-first order kinetics for the growth of the nucleobase block and quenched the polymerization using 1-phenyl-1-(trimethylsiloxy)-ethylene to obtain an M_w/M_n around 1.2. The diblock copolymers dissolved in water and DLS revealed the formation of micelles (20 nm in size) and large compound micelles (150-200 nm). DLS of the diblock copolymer blends in solution indicated a particle size increase from 20 nm to 73 nm with no larger aggregates showing complete mixing and complementary association of the two diblock copolymers. UV-vis spectroscopy confirmed the association of the adenine and thymine moieties in solution but the association may result from either complementary hydrogen bonding or π-π stacking.

2.5 *Nucleobase-Containing Polyesters*

In 2010, Li *et al.*[50] were the first to successfully synthesize a thymine-functionalized monomer suitable for step-growth polycondensation to generate a nucleobase-functionalized

polyester where the nucleobase occurs in every repeat unit. They polymerized the thymine-functionalized dimethyl isophthalate with a 600 g/mol poly(ethylene glycol) (PEG) diol and investigated the polyesters' self-assembly characteristics. The authors dissolved the polyester in chloroform and then evaporated the chloroform to synthesize nanospheres. Scanning electron microscopy (SEM) confirmed the formation of spherical aggregates with diameters ranging from 150-300 nm. Upon dissolution in water, the nanospheres remained and DLS confirmed similar sizes to the SEM data ranging from 190-255 nm. The authors theorized that the nanospheres contained an inner hydrophobic core containing the isophthalate and thymine nucleobase with an outer hydrophilic PEG shell.

To study the complementary hydrogen bonding of the thymine-functionalized polyester and adenine, Fourier transform infrared (FTIR) spectroscopy monitored various peaks corresponding to the nucleobases in the solid state as shown in **Figure 2.7**.[50] The free N-H peak at 3352 cm^{-1} of adenine disappeared when mixed with the nanospheres and a new peak at 3373 cm^{-1} appeared corresponding to the adenine N-H and the thymine carbonyl hydrogen bonding; these two peaks confirmed the complementary hydrogen bonding of the adenine and thymine inside the nanospheres. The carbonyl stretch of the thymine also shifted from 1685 cm^{-1} to 1680 cm^{-1} upon hydrogen bonding with the adenine. Upon heating the nanospheres, the carbonyl stretch of the thymine gradually returned to 1685 cm^{-1} and the 3375 cm^{-1} peak slowly decreased in intensity and then subsequently disappeared at 115 °C. The peak shift and peak loss confirmed the disruption of the hydrogen bonding between the adenine and thymine at elevated temperatures, as expected.

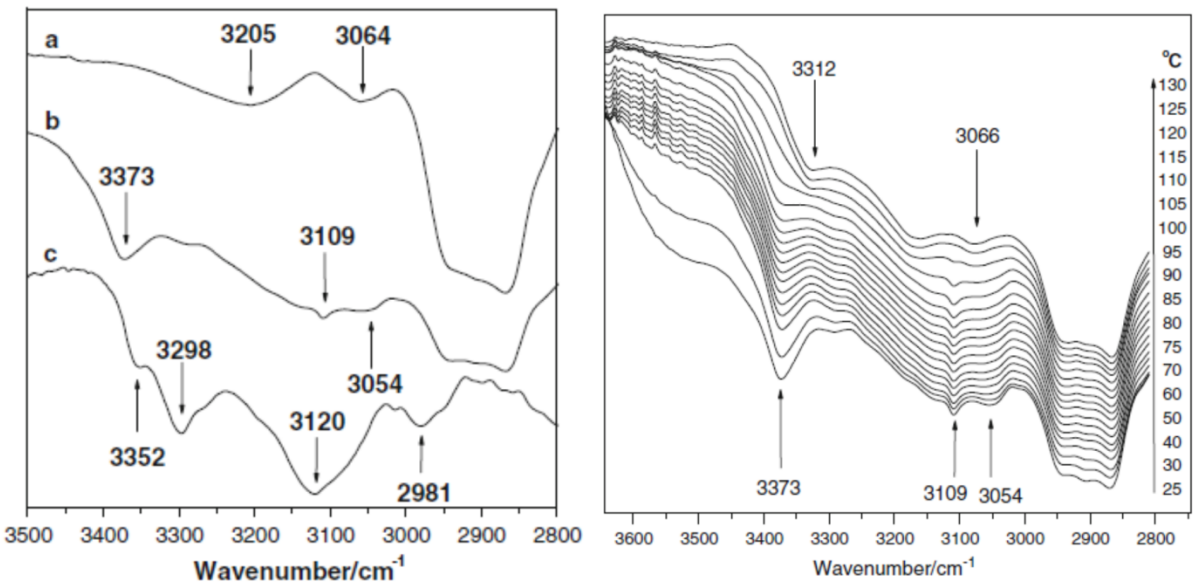

Figure 2.7. FTIR spectroscopic analysis of a) thymine-containing nanospheres, b) thymine-containing nanospheres with adenine, and c) adenine elucidating the supramolecular assembly between adenine and the thymine-containing polyesters. Variable temperature FTIR also demonstrated the disruption of the complementary hydrogen bonding at high temperatures. Reprinted with permission from Ref. 50. ©2009 Springer.

2.6 *Nucleobase-Functionalized Polysiloxanes*

Unlike the nucleobase-functionalized polymers discussed previously, researchers typically functionalize polysiloxanes post-polymerization to generate nucleobase-functionalized polysiloxanes. Hurduc *et al.*[51,52] utilized the same reaction conditions Sédlak *et al.* used to functionalize an azopolysiloxane with either adenine, thymine, uracil, or cytosine as shown in **Figure 2.8**. The resulting nucleobase-functionalized azopolysiloxanes were thermally more stable than the precursor[53] and the authors investigated the photoisomerizations of the azobenzene in the resulting polysiloxanes.[51,54] Hurduc *et al.*[54] demonstrated that the nucleobase-functionalized polysiloxanes exhibited slower cis-trans relaxation kinetics after UV trans-cis

isomerization which they attributed to the decreased mobility of the polymer chains resulting from the self-complementary hydrogen bonding between the nucleobases.

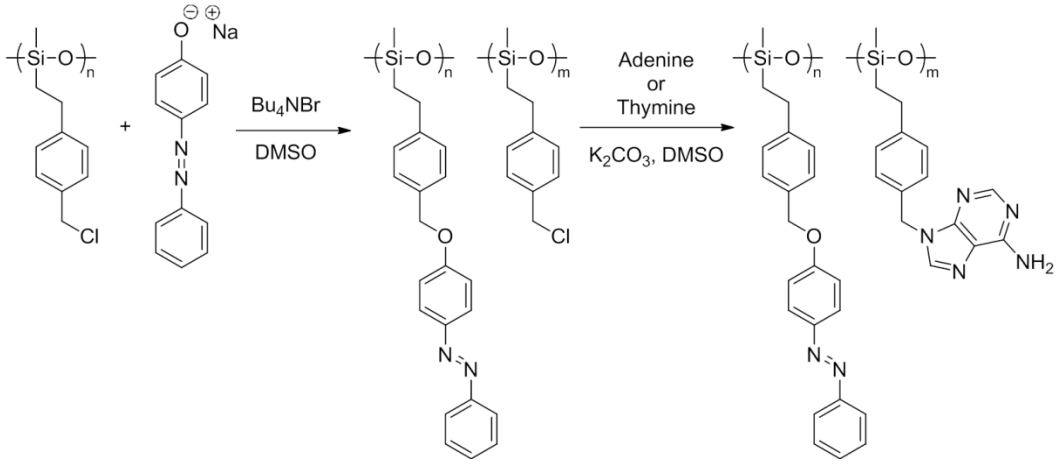

Figure 2.8. Post-polymerization functionalization of polysiloxanes with azobenzene and either adenine or thymine resulted in UV responsive nucleobase-containing polysiloxanes. Reprinted with permission from Ref. 51. ©2007 John Wiley and Sons.

2.7 *Nucleobase-Functionalized Oligothiophenes and Polythiophenes*

Polythiophenes are an important class of conjugated polymers with both conductive and fluorescent properties in polymers.[55-57] Typically, the morphology of the resulting polythiophene films drastically influences the resulting conductive and fluorescent properties. Dinucleotide-functionalized quaterthiophenes and quinquethiophenes synthesized generated unique self-assemblies due to the complementary hydrogen bonding, electrostatics, and π-π stacking between the thiophenes and nucleobases.[55,58] The chirality of the dinucleotides even influenced the morphology of the overall self-assemblies generating chiral self-assemblies.

Only a few in the literature have synthesized nucleobase-functionalized polythiophenes.[56,59,60] Bäuerle and Emge[59] were the first to synthesize *N*6-acetyladenine- and uracil-functionalized polythiophenes utilizing electropolymerization of nucleobase-

functionalized bithiophenes. Cyclic voltammetry and UV/vis spectroscopy confirmed that the addition of a complementary nucleobase modified the electrochemistry of the polythiophenes: the oxidation potential increased and the electroactivity decreased. Barbella *et al.*[56] oxidatively polymerized thymidine- and adenosine-functionalized bithiophenes using $FeCl_3$, shown in **Figure 2.9**, and examined their resulting crystalline film morphologies using optical microscopy and atomic force microscopy (AFM). Optical microscopy showed dendritic growth of crystallites for the thymine-functionalized polythiophene and long wire growth of crystallites for the adenine-functionalized polythiophene. AFM confirmed a helical crystalline morphology for the adenine-functionalized polythiophene, contrary to the typical lamellar crystalline structure of alkylated polythiophenes.

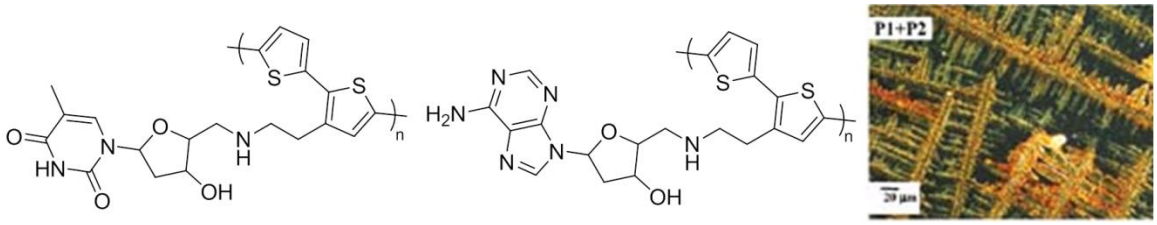

Figure 2.9. Adenosine- and thymidine-functionalized polythiophenes polymerized from nucleobase-functionalized bithiophenes. Polymer blends generated crystalline wires shown here using optical microscopy. Reprinted with permission from Ref. 56. ©2010 John Wiley and Sons.

While thymine complexes with Hg^{2+} generating very sensitive probes for Hg^{2+}, Hg^{2+} irreversibly binds to these sensors limiting the sensors to a single use.[61-63] Zhu *et al.*[60] recently published a thymine-functionalized polythiophene which strongly fluoresced before Hg^{2+} complexation and weakly fluoresced after Hg^{2+} complexation due to polymer aggregation as shown in **Figure 2.10**. Upon the addition of NaCl, the $HgCl_2$ precipitated from solution regenerating the uncoordinated thymine-functionalized polythiophene and resulting in 80% of

the previous fluorescence. The resulting Hg^{2+} sensor was also sensitive to Hg^{2+} and did not bind to other common cations nor lose fluorescence in the presence of other cations.

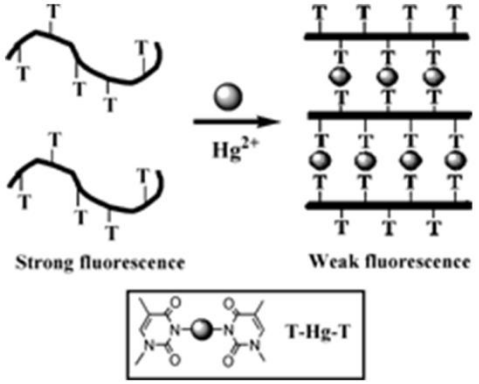

Figure 2.10. Thymine-functionalized polythiophene utilized as a Hg^{2+} sensor; fluorescence was quenched upon complexation of Hg^{2+} with two thymines and the addition of NaCl restored the fluorescence properties of the thymine-functionalized polythiophenes enabling them to function as reversible Hg^{2+} sensors. Reprinted with permission from Ref. 60. ©2006 John Wiley and Sons.

2.8 *Nucleobase-Functionalized Telechelic Polymers*

Nucleobase-functionalized telechelic polymers are widespread throughout the literature. For example, poly(tetramethylene oxide) and polycaprolactone terminally functionalized with nucleobases exhibited higher solution viscosities, nucleobase hard segment microphase separation, film formation, and thermally reversible hydrogen bonding.[64-66] Long *et al.*[67] investigated the self-complementary hydrogen bonding group 2-ureido-4[1*H*]-pyrimidone (UPy) telechelic functionalized poly(butylene terephthalate) (PBT) and poly(butylene isophthalate) (PBI). These telechelic UPy thermoplastic polyesters exhibited similar melt viscosities at 235 °C (a typical processing temperature) as unfunctionalized PBT and PBI but their impact strength and strain at break were superior. Long *et al.*[68] also synthesized adenine and thymine terminated

four armed stars of poly(D,L-lactide) (PDLLA) as shown in **Figure 2.11**. These nucleobase functionalized star polymers exhibited higher solution and melt viscosities; Long *et al.*[69] also successfully melt electrospun the star polymer blends generating fibers double the diameter size of the non-blended PDLLA-adenine or PDLLA-thymine.

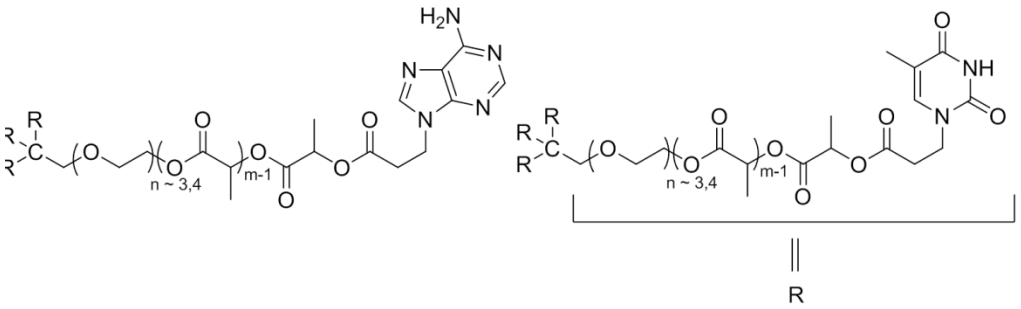

Figure 2.11. Four-armed PDLLA stars functionalized with adenine or thymine at each chain end using Michael addition. Reprinted with permission from Ref. 68. ©2007 American Chemical Society.

2.9 *Template Polymerization*

With the advent of the polymerization of many nucleobase-containing monomers and the synthesis of various nucleobase-containing polymers, researchers have focused on template polymerizations where a nucleobase template polymer dictates and drives the polymerization of the complementary nucleobase monomer. Inaki *et al.*[70-72] pioneered the investigation of template polymerization through the polymerization of nucleobase-functionalized methacrylates and methacrylamides in the presence of the complementary nucleobase-functionalized polymer. The rate of polymerization increased for the alkyl methacrylate monomers when in the presence of the complementary nucleobase template and decreased when both the monomer and polymer contained the same nucleobase. When Inaki *et al.*[71,73] polymerized the methacrylamide monomers in the presence of a template, a polymer precipitate formed during the polymerization

with no increase in the rate of polymerization. The polymerization of both the uracil and adenine methacrylamides together in the presence of poly(adenine methacrylamide) resulted in a polymer precipitate composed of a 1:1 mixture of poly(uracil methacrylamide) and poly(adenine methacrylamide) while the polymer remaining in solution was principally poly(adenine methacrylamide).

Marsh *et al.*[46] also utilized their nucleoside acrylate monomers shown in **Figure 2.5** in the template polymerization of the adenine acrylate in the presence of the uracil acrylate and poly(uracil acrylate). The resulting polymer precipitate resulted in a roughly 1:1 composition of uracil and adenine acrylate polymers while predominately poly(uracil acrylate) remained in solution. van Hest *et al.*[74] examined the ATRP polymerization of their adenine methacrylate shown in **Figure 2.6** with either their thymine methacrylate monomer or their poly(thymine methacrylate). The presence of either thymine monomer or thymine polymer increased significantly the rate of polymerization of the adenine methacrylate while the thymine methacrylate in the presence of the poly(thymine methacrylate) exhibited no rate enhancement; the authors theorized that the template effect helped screen and prevent adenine coordination to the Cu catalyst which typically deactivated and slowed down the catalyst activity in the ATRP polymerizations without the thymine template.

Ring-opening metathesis polymerization (ROMP) is another popular polymerization technique utilized to generate nucleobase- and diaminopyridine (DAP)-functionalized polymers. DAP self-associates via hydrogen bonding poorly but associates tightly through three hydrogen bonds with thymine.[75] Weck *et al.*[75] utilized DAP-functionalized polynorbornenes to template the ROMP of thymine-functionalized norbornenes. They demonstrated that the template polymer successfully enhanced the rate of polymerization due to an increase in the relative

monomer concentration near the template. Weck *et al.* also polymerized the thymine norbornene in the presence of a DAP template attached to a solid support. After polymerization, they removed the solid supported polymer and the isolated daughter thymine polymers exhibited a better controlled polymerization than the untemplated thymine polymers.

Sleiman *et al.*[76] synthesized a thymine template shown in **Figure 2.12** utilizing ROMP to achieve a template with a M_w/M_n of 1.04. They performed a Sonagashira coupling polymerization of an adenine-functionalized monomer in the presence of the thymine template, in the absence of the thymine template, and in the presence of the wrong DAP template. The correctly templated polymerization synthesized an adenine-functionalized polymer with a high degree of polymerization (25) and a low M_w/M_n (1.2) similar to the template polymer while both the incorrectly templated and untemplated polymerizations resulted in low molecular weight (DP<10) and high M_w/M_n (>2.2) polymers. Using a template polymerization, they controlled a step growth polymerization to have a similar DP as the template and also a M_w/M_n significantly lower than the expected M_w/M_n of 2.0 for a step-growth polymerization.

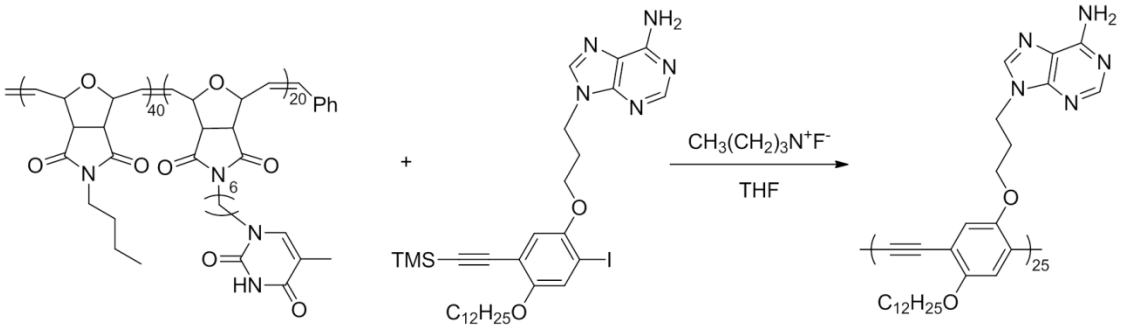

Figure 2.12. Step-growth Sonagashira polymerization of an adenine monomer in the presence of a ROMP synthesized thymine polymer to synthesize a well-controlled step-growth polymer. Reprinted with permission from Ref. 76. ©2009 American Chemical Society.

Tao *et al.*[77] recently examined the homopolymerization of a DAP-containing vinyl monomer utilizing conventional free radical polymerization and reversible addition-

fragmentation chain transfer (RAFT) polymerization. They demonstrated stereocontrol of the conventional free-radical polymerization utilizing 1-octylthymine as the mediator. Strong complementary hydrogen bonding between the DAP-containing vinyl monomer and 1-octylthymine generated predominantly syndiotactic polymer from 46% syndiotacticity without 1-octylthymine to 84% syndiotacticity with 1-octylthymine as the mediator. Utilizing RAFT, Tao *et al.* successfully synthesized an atactic-syndiotactic stereoblock copolymer through polymerization of the DAP-containing vinyl monomer without 1-octylthymine to generate the atactic stereoblock and then the subsequent addition of 1-octylthymine to generate the syndiotactic stereoblock.

2.10 *Electrostatics and Hydrogen Bonding in Concert*

Like DNA and RNA, proteins utilize a wide variety of non-covalent interactions including hydrogen bonding and electrostatics to generate complex secondary, tertiary, and quaternary structures which dictate their ultimate properties and function in biological systems.[1] Magainins, a class of antimicrobial polypeptides, assemble into α-helical structures shown in **Figure 2.13** through the interplay of 6 charged amino acids and 10 hydrogen bonding amino acids when in the presence of lipid bilayers.[78-81] When dissolved in pure water, the magainins denature into random coils. The amphiphilic nature of the α-helical magainins allows them to disrupt cell membranes causing enhanced permeability resulting in cell death.

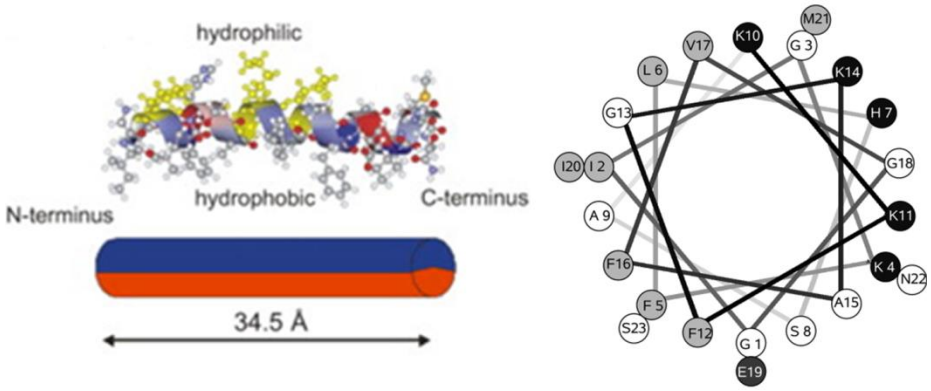

Figure 2.13. Alpha-helical structure of magainin, a 23 amino acid polypeptide, where 6 amino acids are charged and 10 amino acids participate in hydrogen bonding to create the alpha-helical structure. Reprinted with permission from Ref. 78, 80. ©2009 Elsevier.

Weck *et al.*[82] pioneered the combination of electrostatics and hydrogen bonding together in the same polymer backbone through the ROMP polymerization of ammonium and DAP-functionalized norbornenes to generate a random copolymer shown in **Figure 2.14**Error! No bookmark name given.. They investigated the influence of electrostatics and hydrogen bonding together with respect to supramolecular assembly through anion exchange and the addition of *N*-butylthymine. Weck *et al.* examined the influence of the order of functionalization on the efficiency of the supramolecular assembly and whether the hydrogen bonding or electrostatics would disrupt or prevent the other non-covalent interaction. They determined that the order of supramolecular assembly did not matter and that neither non-covalent interaction disrupted the other non-covalent interaction. ^{1}H NMR titration studies determined association constants (K_a) of around 500 M^{-1} for the *N*-butylthymine and DAP portion of the random copolymer and the association constants remained around 500 M^{-1} independent of the order of functionalization. Ultimately, Weck *et al.* found that both functionalizations could occur at the same time

demonstrating the utility of these orthogonal functionalization to modify a "universal polymer backbone" to generate new polymer structures.

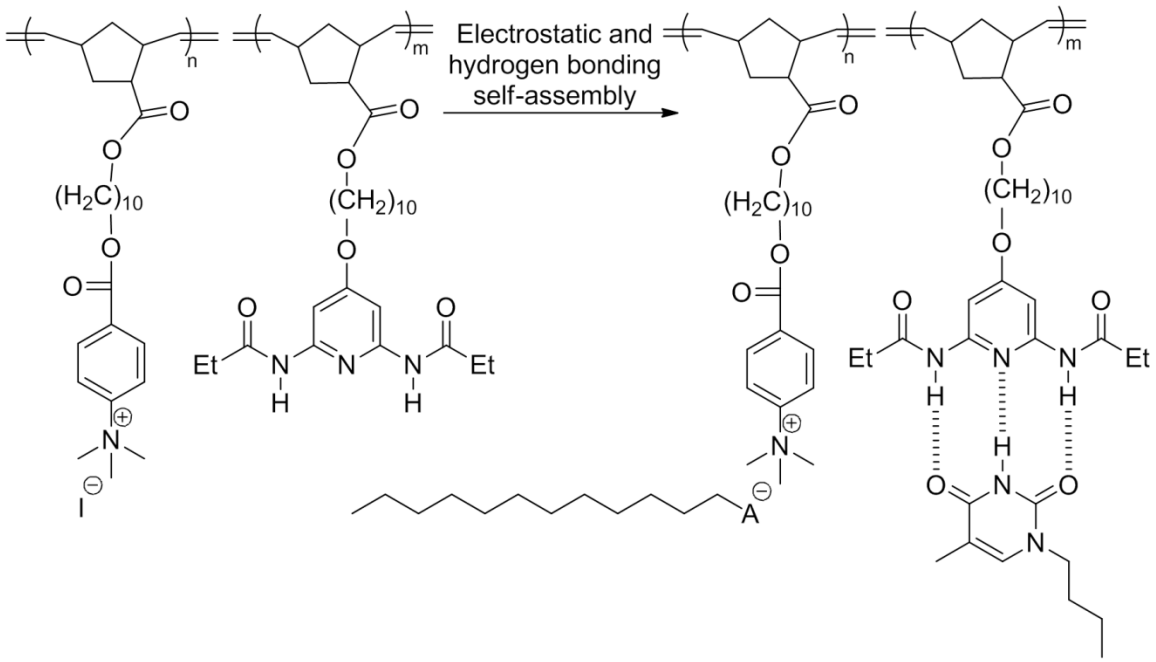

Figure 2.14. "Universal Polymer Backbone" functionalized utilizing hydrogen bonding interactions and/or electrostatic interactions to synthesize new, novel polymers. Reprinted with permission from Ref. 82. ©2006 American Chemical Society.

Another example of the interplay between hydrogen bonding and electrostatic interactions involved the addition of a tricotylphosphonium containing uracil salt (UP+) with the triblock copolymer poly(9-vinylbenzyladenine-*b*-*n*-butyl acrylate-*b*-9-vinylbenzyladenine) to selectively add the UP+ to the hard phase of the triblock copolymer.[83] Dynamic mechanical analysis (DMA) confirmed the selective incorporation of the UP+ into the hard phase since the soft phase T_g remained relatively the same after functionalization as shown in **Figure 2.15**. Also, the rubbery plateau storage modulus increased significantly upon supramolecular assembly due to an increase in the hard phase weight %. Rheological measurements in solution also demonstrated a significant decrease in viscosity upon the addition of the UP+ most likely due to

the prevention of the self-association of adenine. SAXS analysis of the unfunctionalized and UP+ functionalized triblock copolymers confirmed the bulk morphology transition from cylindrical to lamellar morphology upon the addition of the UP+.

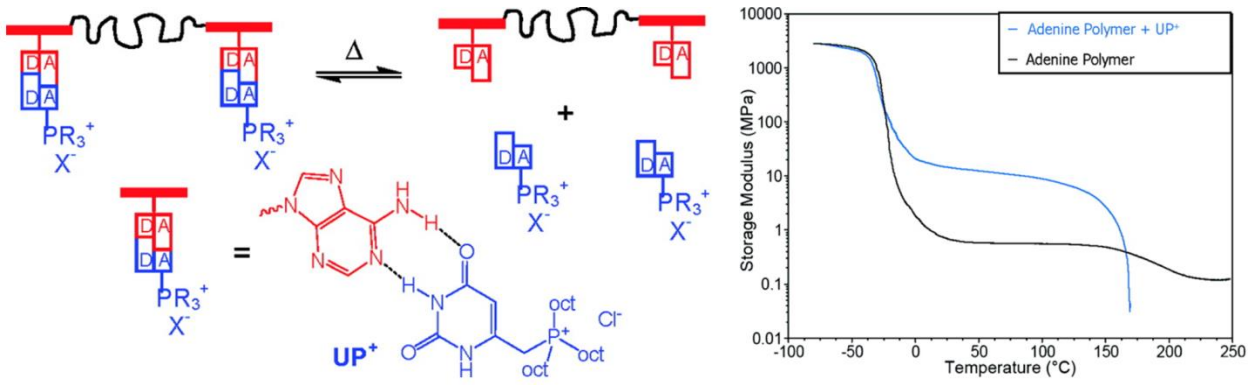

Figure 2.15. Complementary hydrogen bonding between an adenine-containing triblock copolymer and a trioctylphosphonium containing uracil salt increased the rubbery plateau modulus without plasticizing the poly(*n*-butyl acrylate) center block. Reprinted with permission from Ref. 83. ©2007 American Chemical Society.

2.11 *Conclusion*

Advances in controlled radical polymerization techniques continue to enable the synthesis of well-controlled block copolymers with a diverse range of functionality. Recently, researchers successfully incorporated nucleobases and other complementary hydrogen bonding functionality into well-defined block copolymers. For the first time, template polymerizations successful controlled a step-growth polymerization to achieve a targeted DP and narrow PDI similar to the template. Further research into template polymerizations will expand the range of narrow, monodisperse macromolecules through controlling polydispersities of both step-growth polymerizations and uncontrolled chain growth polymerizations through the use of a complementary, well-controlled block copolymer with narrow PDI. Non-covalent interactions

incorporated into a diverse macromolecular structure generate complex tertiary and quaternary structures; these interactions also enable the supramolecular assembly and modification of a parent macromolecule to achieve new, desired properties. Few examples in the literature incorporate both electrostatics and complementary hydrogen bonding together in one macromolecule. Orthogonal functionalization through ion exchange and complementary hydrogen bonding modify the polymer properties significantly allowing rapid modifications to achieve desired properties for specific biomedical applications.

2.12 *Acknowledgements*

This material is based upon work supported by the U.S. Army Research Laboratory and the U.S. Army Research Office under the Army Materials Center of Excellence Program, contract W911NF-06-2-0014.

2.13 *References*

(1) Voet, D.; Voet, J. G. *Biochemistry*; 3rd ed.; John Wiley & Sons, Inc.: Hoboken, NJ, 2004.
(2) Watson, J. D.; Crick, F. H. C. *Nature (London, U. K.)* **1953**, *171*, 737.
(3) Watson, J. D.; Crick, F. H. C. *Nature* **1953**, *171*, 964.
(4) Macgregor, R. B.; Poon, G. M. K. *Computational Biology and Chemistry* **2003**, *27*, 461.
(5) Baker, E. S.; Bowers, M. T. *Journal of the American Society for Mass Spectrometry* **2007**, *18*, 1188.
(6) Saenger, W. *Principles of Nucleic Acid Structure*; Springer-Verlag: New York, New York, 1984.
(7) Arnott, S. *Trends in Biochemical Sciences* **2006**, *31*, 349.
(8) *Oxford Handbook of Nucleic Acid Structure*; Neidle, S., Ed.; Oxford University Press Inc.: New York, 1999.
(9) Brumovská, E.; Sychrovský, V.; Vokáčová, Z.; Šponer, J.; Schneider, B.; Trantírek, L. *Journal of Biomolecular NMR* **2008**, *42*, 209.
(10) Rich, A. In *RNA Towards Medicine*; Erdmann, V., Barciszewski, J., Brosius, J., Eds.; Springer Berlin Heidelberg: 2006; Vol. 173, p 1.
(11) Schneider, B.; Neidle, S.; Berman, H. M. *Biopolymers* **1997**, *42*, 113.
(12) Ott, R.; Krämer, R. *Applied Microbiology and Biotechnology* **1999**, *52*, 761.
(13) Zhang, J.; Shao, Y.; Wei, L.; Li, Y.; Sheng, X.; Liu, F.; Lu, G. *Science in China Series B: Chemistry* **2009**, *52*, 402.
(14) Germann, M. W.; Kalisch, B. W.; van de Sande, J. H. *Biochemistry* **1988**, *27*, 8302.

(15) Fonseca Guerra, C.; Bickelhaupt, F. M.; Snijders, J. G.; Baerends, E. J. *Journal of the American Chemical Society* **2000**, *122*, 4117.
(16) Fonseca Guerra, C.; Bickelhaupt, F. M.; Snijders, J. G.; Baerends, E. J. *Chemistry – A European Journal* **1999**, *5*, 3581.
(17) Raspaud, E.; Olvera de la Cruz, M.; Sikorav, J. L.; Livolant, F. *Biophysical Journal* **1998**, *74*, 381.
(18) Anderson, C. F.; Record, M. T. *Annual Review of Physical Chemistry* **1982**, *33*, 191.
(19) Wang, L.; Bloomfield, V. A. *Macromolecules* **1991**, *24*, 5791.
(20) Hunter, C. A.; Sanders, J. K. M. *Journal of the American Chemical Society* **1990**, *112*, 5525.
(21) Mignon, P.; Loverix, S.; Steyaert, J.; Geerlings, P. *Nucleic Acids Research* **2005**, *33*, 1779.
(22) Hunter, C. A. *Journal of Molecular Biology* **1993**, *230*, 1025.
(23) Fathalla, M.; Lawrence, C. M.; Zhang, N.; Sessler, J. L.; Jayawickramarajah, J. *Chem. Soc. Rev.* **2009**, *38*, 1608.
(24) Schweitzer, B. A.; Kool, E. T. *Journal of the American Chemical Society* **1995**, *117*, 1863.
(25) Matray, T. J.; Kool, E. T. *Journal of the American Chemical Society* **1998**, *120*, 6191.
(26) Bloomfield, V. A.; Crothers, D. M.; Tinoco, I. *Nucleic Acids: Structures, Properties, and Functions*; University Science Books: Sausalito, 2000.
(27) Yakovchuk, P.; Protozanova, E.; Frank-Kamenetskii, M. D. *Nucleic Acids Research*, *34*, 564.
(28) Hobza, P.; Šponer, J. *Journal of the American Chemical Society* **2002**, *124*, 11802.
(29) McKee, M. G.; Hunley, M. T.; Layman, J. M.; Long, T. E. *Macromolecules* **2006**, *39*, 575.
(30) Tan, Z.-J.; Chen, S.-J. *Biophysical Journal* **2006**, *90*, 1175.
(31) Bosnian, A. W.; Brunsveld, L.; Folmer, B. J. B.; Sijbesma, R. P.; Meijer, E. W. *Macromolecular Symposia* **2003**, *201*, 143.
(32) Brunsveld, L.; Folmer, B. J. B.; Meijer, E. W.; Sijbesma, R. P. *Chemical Reviews* **2001**, *101*, 4071.
(33) Shimizu, L. S. *Polymer International* **2007**, *56*, 444.
(34) Fox, J. D.; Rowan, S. J. *Macromolecules* **2009**, *42*, 6823.
(35) Sijbesma, R. P.; Beijer, F. H.; Brunsveld, L.; Folmer, B. J. B.; Hirschberg, J. H. K. K.; Lange, R. F. M.; Lowe, J. K. L.; Meijer, E. W. *Science (Washington, D. C.)* **1997**, *278*, 1601.
(36) Adam, D.; Schuhmacher, P.; Simmerer, J.; Haussling, L.; Siemensmeyer, K.; Etzbachi, K. H.; Ringsdorf, H.; Haarer, D. *Nature* **1994**, *371*, 141.
(37) Michelsen, U.; Hunter, C. A. *Angewandte Chemie International Edition* **2000**, *39*, 764.
(38) Pollino, J. M.; Weck, M. *Chemical Society Reviews* **2005**, *34*, 193.
(39) Sedlak, M.; Simunek, P.; Antonietti, M. *Journal of Heterocyclic Chemistry* **2003**, *40*, 671.
(40) Lutz, J.-F.; Pfeifer, S.; Chanana, M.; Thünemann, A. F.; Bienert, R. *Langmuir* **2006**, *22*, 7411.
(41) Lutz, J.-F.; Thünemann, A. F.; Nehring, R. *Journal of Polymer Science Part A: Polymer Chemistry* **2005**, *43*, 4805.
(42) Lutz, J.-F.; Thunemann, A. F.; Rurack, K. *Macromolecules* **2005**, *38*, 8124.

(43) Cheng, C.-C.; Huang, C.-F.; Yen, Y.-C.; Chang, F.-C. *Journal of Polymer Science Part A: Polymer Chemistry* **2008**, *46*, 6416.
(44) Cheng, C.-C.; Yen, Y.-C.; Ye, Y.-S.; Chang, F.-C. *Journal of Polymer Science Part A: Polymer Chemistry* **2009**, *47*, 6388.
(45) Mather, B. D.; Baker, M. B.; Beyer, F. L.; Berg, M. A. G.; Green, M. D.; Long, T. E. *Macromolecules* **2007**, *40*, 6834.
(46) Marsh, A.; Khan, A.; Haddleton, D. M.; Hannon, M. J. *Macromolecules* **1999**, *32*, 8725.
(47) Marsh, A.; Khan, A.; Garcia, M.; Haddleton, D. M. *Chemical Communications* **2000**, 2083.
(48) Spijker, H. J.; van Delft, F. L.; van Hest, J. C. M. *Macromolecules* **2007**, *40*, 12.
(49) Spijker, H. J.; Dirks, A. J.; Van Hest, J. C. M. *Journal of Polymer Science, Part A: Polymer Chemistry* **2006**, *44*, 4242.
(50) Zhang, X.; He, Z.; Li, G.; Zhang, Y.; Li, G. *Journal of Polymer Research* **2010**, *17*, 255.
(51) Hurduc, N.; Enea, R.; Scutaru, D.; Sacarescu, L.; Donose, B. C.; Nguyen, A. V. *Journal of Polymer Science Part A: Polymer Chemistry* **2007**, *45*, 4240.
(52) Epure, E.-L.; Moleavin, I.; Taran, E.; Nguyen, A.; Nichita, N.; Hurduc, N. *Polymer Bulletin* **2011**, *67*, 467.
(53) Lisa, G.; Enea, R.; Hurduc, N.; Hurduc, N. *High Performance Polymers* **2009**, *21*, 340.
(54) Enea, R.; Resmerita, A.-M.; Petraru, L.; Grigoras, C.; Scutaru, D.; Simionescu, C. I.; Hurduc, N. *Central European Journal of Chemistry* **2007**, *5*, 981.
(55) Alesi, S.; Brancolini, G.; Viola, I.; Capobianco, M.; Venturini, A.; Camaioni, N.; Gigli, G.; Melucci, M.; Barbarella, G. *Chemistry – A European Journal* **2009**, *15*, 1876.
(56) Navacchia, M. L.; Favaretto, L.; Treossi, E.; Palermo, V.; Barbarella, G. *Macromolecular Rapid Communications* **2010**, *31*, 351.
(57) Jatsch, A.; Kopyshev, A.; Mena-Osteritz, E.; Bauerle, P. *Organic Letters* **2008**, *10*, 961.
(58) Alesi, S.; Brancolini, G.; Melucci, M.; Capobianco, M. L.; Venturini, A.; Camaioni, N.; Barbarella, G. *Chemistry – A European Journal* **2008**, *14*, 513.
(59) Bäuerle, P.; Emge, A. *Advanced Materials* **1998**, *10*, 324.
(60) Tang, Y.; He, F.; Yu, M.; Feng, F.; An, L.; Sun, H.; Wang, S.; Li, Y.; Zhu, D. *Macromolecular Rapid Communications* **2006**, *27*, 389.
(61) Wang, Z.; Zhang, D.; Zhu, D. *Analytica Chimica Acta* **2005**, *549*, 10.
(62) Miyake, Y.; Ono, A. *Tetrahedron Letters* **2005**, *46*, 2441.
(63) Ono, A.; Togashi, H. *Angewandte Chemie, International Edition* **2004**, *43*, 4300.
(64) Rowan, S. J.; Suwanmala, P.; Sivakova, S. *Journal of Polymer Science Part A: Polymer Chemistry* **2003**, *41*, 3589.
(65) Sivakova, S.; Bohnsack, D. A.; Mackay, M. E.; Suwanmala, P.; Rowan, S. J. *Journal of the American Chemical Society* **2005**, *127*, 18202.
(66) Lin, I. H.; Cheng, C.-C.; Yen, Y.-C.; Chang, F.-C. *Macromolecules* **2010**, *43*, 1245.
(67) Yamauchi, K.; Kanomata, A.; Inoue, T.; Long, T. E. *Macromolecules* **2004**, *37*, 3519.
(68) Karikari, A. S.; Mather, B. D.; Long, T. E. *Biomacromolecules* **2006**, *8*, 302.
(69) Hunley, M. T.; Karikari, A. S.; McKee, M. G.; Mather, B. D.; Layman, J. M.; Fornof, A. R.; Long, T. E. *Macromolecular Symposia* **2008**, *270*, 1.
(70) Takemoto, K.; Inaki, Y.; Akashi, M. *Journal of Macromolecular Science, Chemistry* **1979**, *A13*, 519.
(71) Inaki, Y. *Prog. Polym. Sci.* **1992**, *17*, 515.

(72) Akashi, M.; Takada, H.; Inaki, Y.; Takemoto, K. *Journal of Polymer Science, Polymer Chemistry Edition* **1979**, *17*, 747.
(73) Inaki, Y.; Ebisutani, K.; Takemoto, K. *Journal of Polymer Science Part A: Polymer Chemistry* **1986**, *24*, 3249.
(74) Spijker, H. J.; Dirks, A. J.; van Hest, J. C. M. *Polymer* **2005**, *46*, 8528.
(75) South, C. R.; Weck, M. *Macromolecules* **2007**, *40*, 1386.
(76) Lo, P. K.; Sleiman, H. F. *Journal of the American Chemical Society* **2009**, *131*, 4182.
(77) Tao, Y.; Satoh, K.; Kamigaito, M. *Macromolecular Rapid Communications* **2011**, *32*, 226.
(78) Li, C.; Salditt, T. *Biophysical Journal* **2006**, *91*, 3285.
(79) Mehrnejad, F.; Naderi-Manesh, H.; Ranjbar, B. *Proteins: Structure, Function, and Bioinformatics* **2007**, *67*, 931.
(80) Gregory, S. M.; Pokorny, A.; Almeida, P. F. F. *Biophysical Journal* **2009**, *96*, 116.
(81) Zasloff, M. *Proc. Natl. Acad. Sci. U. S. A.* **1987**, *84*, 5449.
(82) Nair, K. P.; Weck, M. *Macromolecules* **2006**, *40*, 211.
(83) Mather, B. D.; Baker, M. B.; Beyer, F. L.; Green, M. D.; Berg, M. A. G.; Long, T. E. *Macromolecules* **2007**, *40*, 4396.

Chapter 3: Synthesis and Solution Rheology of Adenine-Containing Polyelectrolytes for Electrospinning

(Published in *Polymer* **2012,** *53* (7), 1437-1443.)

*Sean T. Hemp, Matthew T. Hunley,[1] Shijing Cheng, Kerry C. DeMella, and Timothy E. Long**

Department of Chemistry, Macromolecules and Interfaces Institute, Virginia Tech, Blacksburg, VA 24061-0344

[1]Currently at Polymers Division, National Institute of Standards and Technology, Gaithersburg, MD 20899-8541.

*To whom correspondence should be addressed. E-mail: telong@vt.edu. TEL: (540)231-2480. FAX: (540)231-8517.

Keywords: electrospinning; polyelectrolytes; nucleobases

3.1 *Abstract*

Conventional free radical copolymerization of 9-vinylbenzyladenine (VBA) and 2-(dimethylamino)ethyl methacrylate (DMAEMA) with subsequent protonation afforded the synthesis of adenine-containing polyelectrolytes. All adenine-containing polyelectrolytes exhibited classical polyelectrolyte solution rheological behavior with scaling factors near 0.6 and 1.6 in the semidilute unentangled and semidilute entangled regimes, respectively. However, the adenine-containing polyelectrolytes deviated from polyelectrolyte behavior in the concentrated regime with increasing scaling factors as adenine-incorporation increased due to intermolecular association. The electrospinning behavior exhibited a strong dependence on adenine incorporation. Higher adenine-incorporation decreased the normalized concentration for fiber formation from $4.5C_e$ for PDMAEMA•HCl to $2.9C_e$ for 35 mol% VBA. The required zero-shear

viscosities for electrospinning were 312 cP for PDMAEMA•HCl and 116 cP for the 35 mol% VBA copolymer. Increasing the adenine concentration also increased the fiber diameters presumably due to adenine-adenine interactions. These adenine-decorated electrospun mats exhibit potential in a variety of applications including filtration, purification, and tissue scaffolding.

3.2 *Introduction*

Polyelectrolytes typically are macromolecules containing high charge densities including sulfonated polystyrene,[1,2] poly(acrylic acid),[3,4] poly (diallyldimethylammonium chloride),[5,6] and nucleic acids;[7,8] the resulting high concentration of charge on the polymer backbone generates unique solution properties.[9] In dilute aqueous solution, polyelectrolytes expand into an extended conformation instead of a random coil due to electrostatic repulsion of like charges on the polymeric backbone.[10] Upon the addition of salt or increased concentrations of polyelectrolyte in solution, the polyelectrolyte approaches a random coil conformation due to charge screening.[9,11,12] Solution rheology is sensitive to these conformational changes and the scaling factors for polyelectrolytes in the semi-dilute unentangled, semi-dilute entangled, and concentrated regimes differ from neutral, non-associating polymers.[9] Salt addition returns the polyelectrolytes' scaling factors to the neutral, non-associating polymers.[13] Polymer solutions shift from the dilute to semi-dilute unentangled regimes at the overlap concentration (C*).[14] The semi-dilute entangled regime onset occurs at the entanglement concentration (C_e) while the concentrated regime begins at C_D. Specifically, **Table 3.1**

Table 3.1 summarizes the scaling factors of specific viscosity (n_{sp}) *versus* concentration for polyelectrolytes and neutral, non-associating polymers.

Table 3.1. Specific Viscosity Scaling Factors ($n_{sp} \sim C^x$) for Neutral Polymers and Polyelectrolytes in the Semi-Dilute Unentangled, Semi-Dilute Entangled, and Concentration Regimes.[14]

	$C^* < C < C_e$	$C_e < C < C_D$	$C > C_D$
Neutral	1.25	3.75	4.6
Polyelectrolyte	0.5	1.5	3.8

Polyelectrolytes also display different electrospinning properties compared to neutral, non-associating polymers. Long et. al.[15] correlated solution rheological properties to the electrospinning of neutral, non-associating linear and branched polyesters and derived two semi-empirical power law relationships for fiber diameter *versus* normalized concentration (C/C_e) or zero-shear viscosity (η_0) as follows:

$$D[\mu m] = 0.18\left(\frac{C}{C_e}\right)^{2.7} \quad (1)$$

$$D[\mu m] = 0.05[\eta_0]^{0.8} \quad (2)$$

Long et. al.[15] also discovered that neutral, non-associating polymers only required the presence of entanglements ($C/C_e >$ 1) for the onset of fiber formation (> 2 for uniform fibers) and η_0 values greater than 30 cP. In contrast, PDMAEMA•HCl, a polyelectrolyte, required a significantly higher C/C_e and η_0 to sufficiently stabilize the electrospinning jet and generate fibers.[16,17] Polyelectrolyte charge repulsion in the electrospinning jet caused bending instabilities and jet break-up, requiring higher concentrations and zero-shear viscosities to stabilize the electrospinning jet for the generation of uniform fibers.

Successful electrospinning requires optimizing a wide range of parameters[18,19] including voltage,[20] distance to target,[21] molecular weight,[22] solution concentration,[23] and intermolecular

forces[24] to sufficiently stabilize the electrospinning jet to obtain electrospun fibers and mats. Previously, Long et. al.[25,26] investigated the influence of self-complementary hydrogen bonding groups, 2-ureido-4[1*H*]-pyrimidone, on the electrospinning of poly(alkyl methacrylates). They found self-complementary hydrogen bonding groups led to polymer-polymer associations in the jet resulting in a significant increase in fiber diameter normalized with C/C_e. Wnek et. al.[27] also found a significant decrease in the required concentration to successful electrospin polyamides compared to other polymers without inter-chain hydrogen bonding. Long et. al.[28] demonstrated melt electrospinning of four-armed star-shaped poly(D,L-lactide) terminally functionalized with adenine and thymine. Upon blending of the adenine- and thymine-functionalized four-armed stars, complementary hydrogen bonding between the nucleobases occurred. The resulting fiber diameters doubled in size compared to the individual nucleobase four-armed stars confirming intermolecular interactions during electrospinning.

Nucleobase-containing polymers are widespread throughout the literature and give rise to elastomers,[29] supramolecular assemblies,[30] and thermoresponsive materials.[31] Researchers have synthesized nucleobase-containing homopolymers,[32-34] random copolymers,[35] alternating copolymers,[36] and block copolymers,[37] and they investigated complementary hydrogen bonding influences on solution and solid-state properties. Weck et. al.[38] pioneered the synthesis of random copolymers containing both complementary hydrogen bonding and electrostatics through the ROMP of 2,6-diaminopyridine (DAP)- and ammonium-functionalized norbornenes. They investigated the non-covalent functionalization of these random copolymers through supramolecular assembly of *n*-butyl thymine to DAP through complementary hydrogen bonding and anion-exchange. Both functionalizations were orthogonal and performed simultaneously to achieve widely varied macromolecular structures from a "universal polymer backbone." Long et.

al.[29] also synthesized adenine-containing triblock copolymers with adenine-containing outer blocks and an *n*-butyl acrylate center block which demonstrated elastomeric behavior and they successfully associated the adenine outer blocks selectively with a uracil-containing phosphonium salt.[39]

In this report, we focus on the synthesis and characterization of water-soluble, adenine-containing polyelectrolytes through the conventional free radical copolymerization of 2-(dimethylamino)ethyl methacrylate (DMAEMA) and 9-vinylbenzyl adenine (VBA) with subsequent protonation. We examined the copolymerization kinetics using *in situ* FTIR spectroscopy and determined the reactivity ratios for the copolymer system. Solution rheology elucidated the influence of adenine incorporation on the solution behavior of the adenine-containing copolymers. We also successfully electrospun the adenine-containing polyelectrolytes and elucidated the influence of hydrogen bonding on electrospinning. For the first time, electrospinning produced cationic, adenine-containing sub-micron fibers and the resulting adenine-decorated electrospun mats will find applications in filtration and biological applications.

3.3 *Experimental Section*

3.3.1 Materials

Adenine (99%), 6-(chloromethyl)uracil (98%), trioctylphosphine (97%), and 4-vinylbenzyl chloride (≥90%) were purchased from Sigma Aldrich and used as received. *2,2′*-Azobis(isobutyronitrile) (AIBN) (98%) was purchased from Sigma Aldrich and recrystallized from methanol. 2-(dimethylamino)ethyl methacrylate (DMAEMA) (98%) was purchased from Sigma Aldrich and passed through a neutral alumina column to remove the inhibitor. All

solvents were purchased from commercial sources and used as received. 4-vinylbenzyl adenine (VBA)[40] and 6-(trioctylphosphonium methyl)uracil chloride (UP+)[39] were synthesized according to previous literature procedures.

3.3.2 Synthesis of PDMAEMA•HCl

49.8 mg of AIBN (0.30 mmol, 0.5 mol%) and 40 mL DMF were added to a 100-mL round-bottomed flask with stir bar. The solution was purged with Ar and then 10 mL of degassed DMAEMA (59.3 mmol) was added using a syringe. The solution was heated at 65 °C for 24 h and then the polymer was precipitated into 75:25 hexanes:THF. The polymer was dried *in vacuo* and subsequently redissolved in an HCl/dH_2O (distilled water) solution at a pH of the 3. After complete dissolution, the polymer was precipitated into acetone. The polymer was dried *in vacuo* and then redissolved in dH_2O and lyophilized to obtain a white powder. ^{1}H NMR spectroscopy confirmed the absence of polymer degradation and successful protonation.

3.3.3 Synthesis of adenine-containing polyelectrolytes

In a typical copolymerization targeting 30 mol% incorporation of VBA, 3.0113 g of VBA (12.0 mmol, 30 mol%) was added to a 100-mL round-bottomed flask with stir bar, and the flask was purged with Ar for 15 min. 4.7 mL of degassed DMAEMA (27.9 mmol, 70 mol%) and 27 mL of degassed DMSO was added to the sealed flask with a syringe. The reaction flask was heated to 65 °C to fully dissolve the VBA. After complete dissolution, 0.52 mL of a degassed AIBN solution (0.20 mmol, 0.5 mol%, 62.8 mg/mL in DMSO) was added to initiate the polymerization; the polymerization occurred at 65 °C for 24 h. The polymer was precipitated into 75:25 hexanes:THF and dried *in vacuo*. The polymer was then dissolved in HCl/dH_2O at a

pH of 3 and precipitated into acetonitrile. The polymer was dried *in vacuo* and subsequently redissolved in dH_2O and lyophilized to obtain a white powder.

3.3.4 Analytical methods

^1H NMR spectroscopy was performed on a 400 MHz Varian Unity spectrometer in DMSO-d_6. *In situ* FTIR spectroscopy was conducted using a Mettler-Toledo ReactIR 45m system with an attenuated total reflectance (ATR) flexible silicon composite (SiComp) probe. Aqueous SEC was performed using a Waters 1515 Isocratic HPLC pump, Waters 717plus autosampler, Waters 2414 refractive index detector, and Wyatt MiniDAWN MALLs detector at a flow rate of 0.8 mL/min in an aqueous mobile phase of 54/23/23 (v/v/v) H_2O/MeOH/AcOH with 0.1 M sodium nitrate. A Wyatt Optilab T-rEX differential refractometer operating at 35 °C and 698 nm was used to obtain offline d*n*/d*c* values for absolute molecular weight determination. Dynamic light scattering (DLS) was performed using a Malvern Zetasizer Nano at 25 °C and at concentrations of 1 mg/mL. X-ray photoelectron spectroscopy (XPS) was performed using a Perkin-Elmer 5300 with a Mg anode at 13 kV and 250 watts. Field-emission scanning electron microscopy (FESEM) was performed on a Leo Zeiss 1550 with an accelerating voltage of 5 keV. Prior to FESEM, the electrospun fibers were sputter coated with 10 nm of 60/40 Au/Pt.

3.3.5 Solution rheology and electrospinning

Polymers were dissolved in dH_2O at varying concentrations and stirred mechanically overnight for equilibration. Solution rheology was performed on a TA AR G-2 rheometer with either a concentric cylinder or cone geometry depending on the viscosity. Strain rate sweeps were performed on each solution and the zero-shear viscosity was determined from the Newtonian plateau. To remain consistent with the solution rheology, electrospinning was also

performed from dH_2O polymer solutions. The polymer solution was loaded into a 3 mL syringe with an 18 gauge needle and the syringe was loaded into a syringe pump. The voltage potential was set to 25 kV and the polymer solution was delivered at 3 mL/h. The electrospun fibers were collected on a ¼ in. by ¼ in. grounded wire mesh target 15 cm from the syringe and FESEM was utilized to examine fiber diameters. A total of 20 fiber diameters were measured to determine the average fiber diameter and standard deviation.

3.4 *Results and Discussion*

3.4.1 Polymer synthesis

Conventional free-radical copolymerization of 9-vinylbenzyladenine (VBA) and 2-(dimethylamino)ethyl methacrylate (DMAEMA) with subsequent protonation achieved water-soluble adenine-containing polyelectrolytes as shown in Scheme 3.1. Nucleobase-containing monomers typically only dissolve in polar, aprotic solvents (DMF, DMSO, NMP, for example) at low concentrations, and the homopolymers typically exhibit poor solubility. The homopolymerizations of VBA in DMSO remained homogenous while all other solvents produced heterogeneous polymerization conditions. Conversely, DMAEMA homopolymerizations in DMSO become heterogeneous during the polymerization; however, the copolymerizations of VBA and DMAEMA remained homogenous throughout the polymerization in DMSO, including low mol% incorporations of VBA. DMAEMA homogenously polymerized in DMF, a similar polar aprotic solvent to DMSO, to maintain similar polymerization conditions. Protonation of DMAEMA with HCl (pH = 3) generated water-soluble polyelectrolytes from the neutral polymers. We precipitated the adenine-containing polyelectrolytes into acetonitrile, redissolved in dH_2O, and lyophilized to remove

excess HCl. ^{1}H NMR spectroscopy in DMSO-d_6 confirmed successful protonation of the DMAEMA without protonation of the adenine units in the copolymers (pKa ≈ 4, N^1 position).[41]

Scheme 3.1. Free-radical copolymerization of VBA and DMAEMA to synthesize adenine-containing polyelectrolytes upon subsequent protonation.

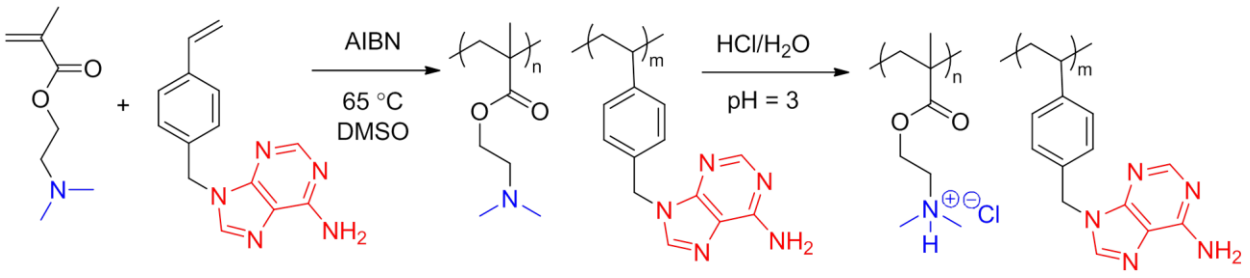

In situ FTIR spectroscopy monitored the copolymerization kinetics to determine the reactivity ratios for the VBA/DMAEMA copolymer system. Previously, our research group demonstrated the efficacy of *in situ* FTIR analysis to accurately determine the reactivity ratios for copolymerization.[42] During the polymerization, IR absorbances corresponding to the vinyl functionality of each monomer (746 cm^{-1} and 817 cm^{-1} for VBA and DMAEMA, respectively, shown in **Figure 3.1** as waterfall plots) decreased due to monomer conversion. The kinetic data obtained at low monomer conversions enabled the determination of the relative rate of monomer consumption, d[VBA]/d[DMAEMA]. Utilizing both the Mayo-Lewis and Fineman-Ross analyses, we determined the reactivity ratios for the VBA/DMAEMA copolymerization using five reactions with different monomer feeds and subsequently different relative rates of monomer consumption. The Mayo-Lewis equation solved for one reactivity ratio and the Fineman-Ross analysis equations are:

$$r_{VBA} = \frac{[M_{DMAEMA}]}{[M_{VBA}]}\left[\frac{d[M_{VBA}]}{d[M_{DMAEMA}]}\left(1+\frac{r_{DMAEMA}[M_{DMAEMA}]}{[M_{VBA}]}\right)-1\right] \quad \text{Mayo-Lewis Equation} \qquad (3)$$

$$G = r_{DMAEMA}F - r_{VBA}, \text{ where}$$

$$F = \frac{X^2}{Y} \quad G = \frac{X(Y-1)}{Y} \quad X = \frac{[M_{DMAEMA}]}{[M_{VBA}]} \quad Y = \frac{d[M_{DMAEMA}]}{d[M_{VBA}]} \text{ Fineman-Ross Analysis} \qquad (4)$$

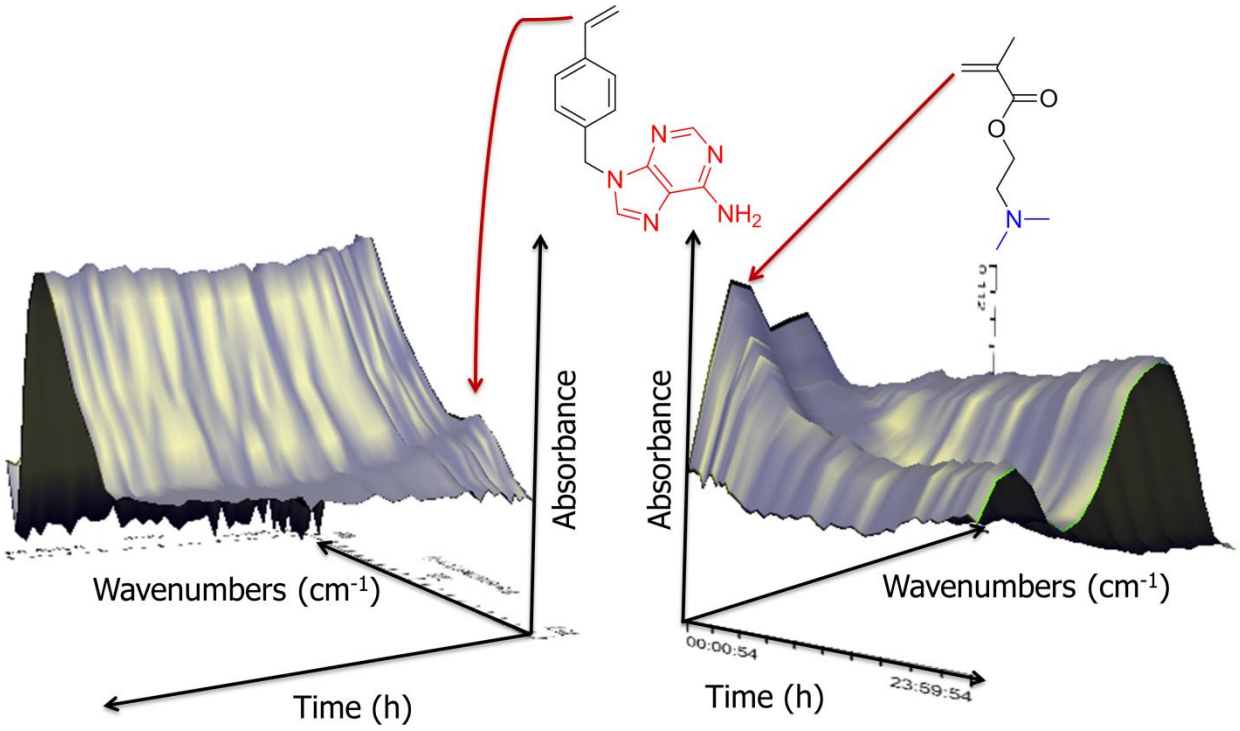

Figure 3.1. *In situ* FTIR waterfall plots depicting decreases in the vinyl peaks of each monomer due to monomer conversion.

Figure 3.2 shows the Mayo-Lewis plot for the copolymerization and depicts the intersection of all five lines corresponding to each molar feed ratio for copolymerization. Through extrapolation of the intersection to the x and y intercepts, the reactivity ratios for DMAEMA and VBA were 0.98 ± 0.04 and 1.19 ± 0.04, respectively. We calculated each reactivity ratio and error using the average and standard deviation for the intersection of all lines.

Fineman-Ross analysis shown in **Figure 3.3** enabled the determination of the reactivity ratios and their standard error more accurately based on the slope and y-intercept of the linear regression. Fineman-Ross analysis determined the reactivity ratios of DMAEMA and VBA as 0.97 ± 0.02 and 1.19 ± 0.02, respectively. Both Mayo-Lewis and Fineman-Ross analysis determined similar reactivity ratios for the VBA/DMAEMA copolymerization and the resulting reactivity ratios confirmed the statistical random copolymerization of VBA and DMAEMA with nearly ideal character ($r_{DMAEMA} \times r_{VBA} = 1.15$).

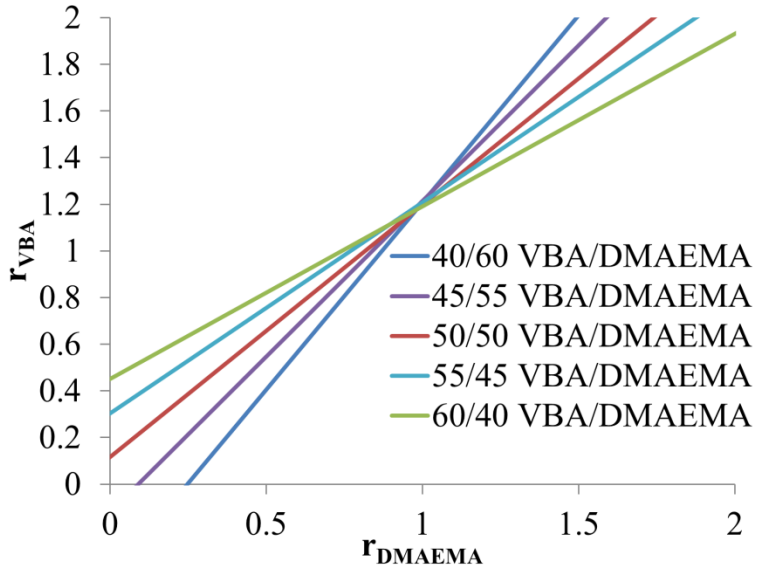

Figure 3.2. Mayo-Lewis analysis showing the linear crossover and the resulting reactivity ratios derived from the plot.

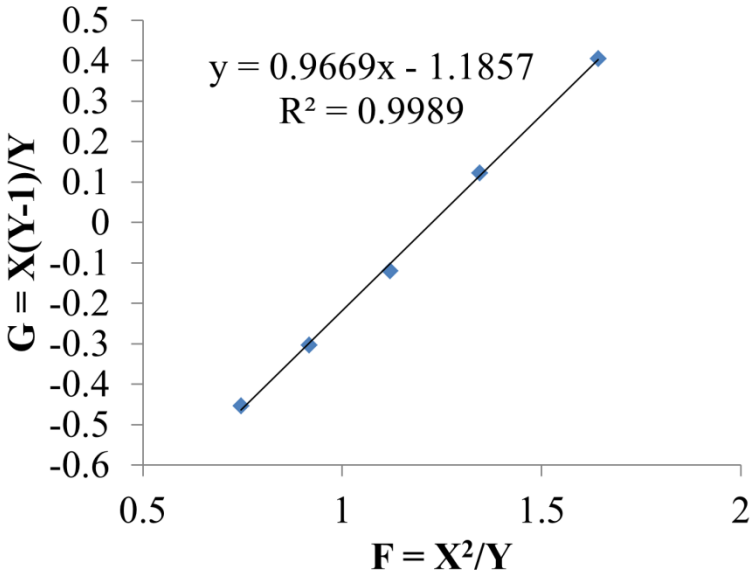

Figure 3.3. Fineman-Ross analysis of the copolymerization kinetics to determine the reactivity ratios and their standard error.

Typically, nucleobase-containing polymers lead to problematic SEC analysis due to poor polymer solubility, polymer aggregation, and polymer-column interactions. We successfully minimized polymer aggregation and polymer-column interactions with aqueous solvents modified with salts and organic co-solvents. Specifically, the adenine-containing polyelectrolytes dissolved without aggregation in 54/23/23 (v/v/v) dH2O/MeOH/AcOH with 0.1 M $NaNO_3$ as shown using DLS (Supporting Information Figure S1). Absolute molecular weight characterization using aqueous SEC in this mobile phase successfully determined molecular weights of both PDMAEMA•HCl and adenine-containing polyelectrolytes. **Figure 3.4** shows the monomodal aqueous SEC traces confirming the absence of polymer-column interactions. As shown in **Table 3.2**, the adenine-containing polyelectrolytes displayed similar molecular weights while PDMAEMA•HCl exhibited significantly lower molecular weight. This molecular weight difference was attributed to the change of solvent from DMSO to DMF which has a higher chain transfer constant.[43]

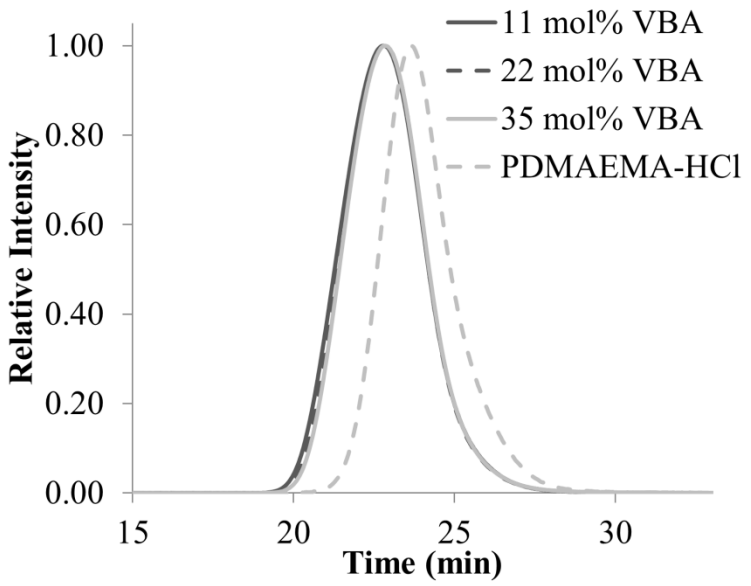

Figure 3.4. Aqueous SEC MALLs traces for the adenine-containing polyelectrolytes. The three adenine-containing polyelectrolytes eluted at similar retention times therefore their aqueous SEC MALLs traces overlapped significantly.

Table 3.2. Molecular weight characterization of the adenine-containing polyelectrolytes.

VBA content (mol %)[a]	$\overline{M}_n$ **(kg/mol)[b]**	$\overline{M}_w$ **(kg/mol)[b]**	$\overline{M}_w / \overline{M}_n$
0	91	136	1.49
11	237	403	1.70
22	253	408	1.61
35	238	395	1.66

[a]^{1}H NMR analysis, [b]Aqueous SEC analysis

3.4.2 Solution rheology

Solution rheology of the adenine-containing polyelectrolytes revealed their solution behavior and dynamics in dH_2O. The copolymers with higher VBA content (>35 mol%) produced poorly water-soluble copolymers for solution rheology and electrospinning. Therefore, we only investigated PDMAEMA•HCl and three adenine-containing polyelectrolytes with varying mol% VBA (11, 22, and 35 mol%) using solution rheology and electrospinning. **Figure**

3.5 depicts the dependence of specific viscosity (η_{sp}) on concentration (wt. %) for both the PDMAEMA•HCl homopolymer and the 35 mol% VBA polyelectrolyte. **Table 3.3** summarizes the steady-shear experiments performed on the copolymers. C* was defined as the concentration when n_{sp} equaled 1 cP.[14] C_e and C_D were determined from the intersection of the linear regressions as shown in **Figure 3.5**; the concentration for C_e was also confirmed from a plot of reduced viscosity *versus* concentration where the minimum corresponded to C_e.[9] The adenine-containing polyelectrolytes exhibited similar C^*, C_e, and C_D transitions due to their similar molecular weights. PDMAEMA•HCl and the adenine-containing polyelectrolytes exhibited extended semidilute regimes with $C_e/C^* > 40$, often observed in polyelectrolyte rheology.[14]

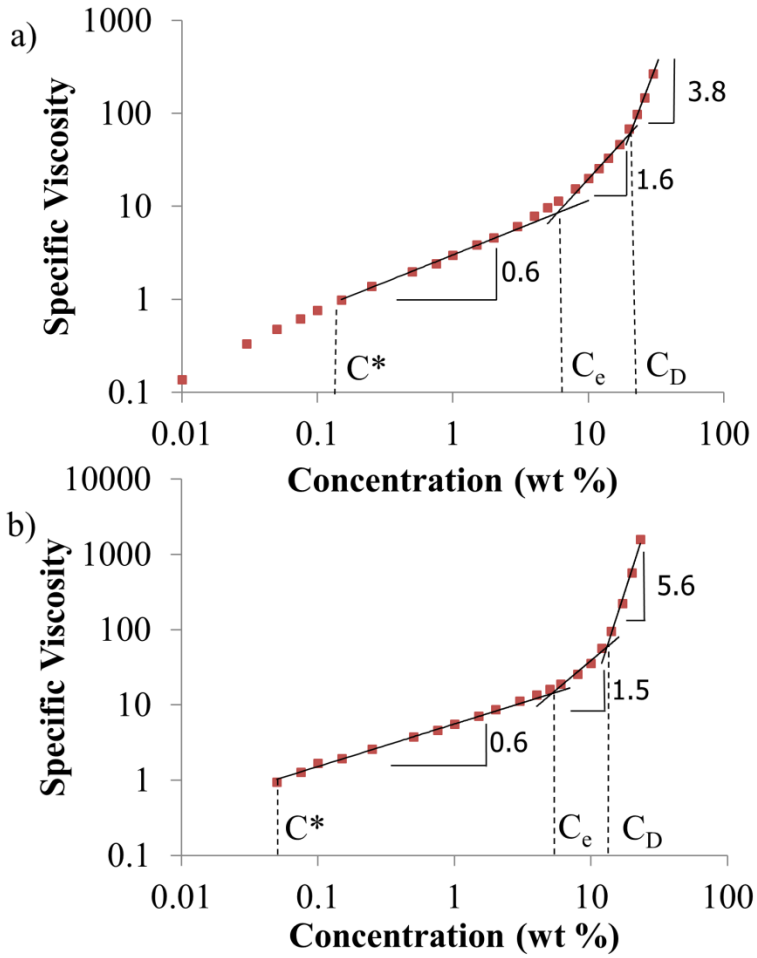

Figure 3.5. Solution rheology analysis for (a) PDMAEMA•HCl and (b) 35 mol% VBA copolymer. PDMAEMA•HCl and the adenine-containing polyelectrolytes exhibited typical polyelectrolyte behavior in dH_2O; adenine-incorporation systematically increased the scaling factor in the concentrated regime.

Table 3.3. Summary of solution rheology and scaling factors for theoretical and adenine-containing polyelectrolytes.

VBA (mol %)	C^* (wt %)	C_e (wt %)	C_D (wt %)	C_e / C^*	Scaling factors		
					$C^* < C < C_e$	$C_e < C < C_D$	$C_D < C$
Polyelectrolyte[14]	--	--	--	>10	0.50	1.50	3.75
Neutral[14]	--	--	--	~10	1.25	3.75	4.60
0	0.17	7.1	20.5	42	0.7	1.6	3.8
11	0.03	5.3	16.4	157	0.6	1.6	4.1
22	0.05	4.5	17.7	93	0.6	1.6	4.9
35	0.05	5.2	13.2	108	0.6	1.5	5.6

PDMAEMA•HCl exhibits strong polyelectrolyte behavior in solution and the scaling factors reported in **Table 3.3** confirmed the polyelectrolyte behavior in all concentration regimes. The adenine-containing polyelectrolytes exhibited polyelectrolyte behavior in the semidilute unentangled and semidilute entangled regimes with scaling factors corresponding to polyelectrolyte theory. In the concentrated regime, the adenine-containing PDMAEMA•HCl copolymers deviated from polyelectrolyte behavior with increasing scaling factors as VBA incorporation increased. Intermolecular hydrogen bonds between polymer chains increased the apparent molecular weight, therefore the solution viscosity increased. In the dilute and semidilute regimes, intramolecular hydrogen bonds likely predominated due to the lower polymer concentration, decreasing the influence of hydrogen bonding on the solution viscosity. In addition, dH_2O competitively hydrogen bonds with adenine decreasing the overall influence of hydrogen bonding on the solution viscosity.

3.4.3 Electrospinning

The polymers were electrospun from dH_2O solutions to draw comparisons between the solution rheology and electrospinning. All electrospinning conditions were maintained constant

allowing comparisons between the different copolymers. Electrospinning of all polyelectrolytes created non-woven mats with uniform fibers. FESEM determined the average fiber diameter of the electrospun fibers at various polymer concentrations. **Figure 3.6** shows exemplary FESEM images for the uniform electrospun fibers of PDMAEMA•HCl and two adenine-containing polyelectrolytes (22 and 35 mol% VBA). For all polymers, the average fiber diameters increased according to a power law relationship with normalized concentration (C/C_e) and with zero-shear viscosity (η_0). **Figure 3.7** depicts the average fiber diameters *versus* normalized concentration for all polyelectrolytes. The semi-empirical power law relationship for neutral, non-associating polymers determined previously in our research group is also shown.[15] **Figure 3.8** shows the average fiber diameters *versus* zero-shear viscosity with the semi-empirical equation for neutral, non-associating polymers.[15] The adenine-containing polyelectrolytes and PDMAEMA•HCl generated smaller fiber diameters compared to neutral, non-associating polymers due to charge repulsion in the jet leading to stretching and thinning of the jet.[17]

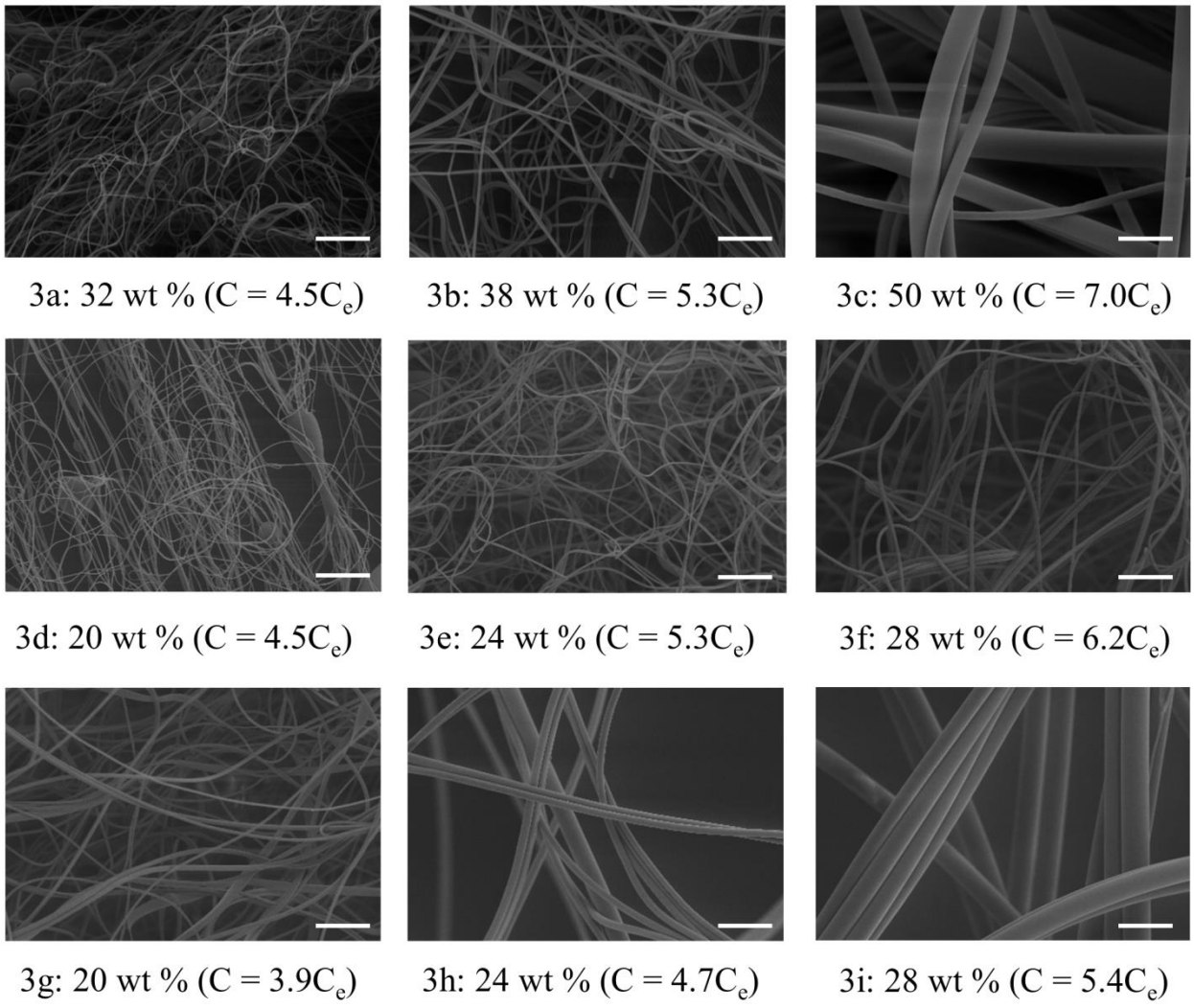

Figure 3.6. FESEM of adenine-containing polyelectrolyte electrospun fibers: (a-c) PDMAEMA•HCl, (d-f) 22 mol% VBA copolymer, and (g-i) 35 mol% VBA copolymer. Scale bar = 10 μm.

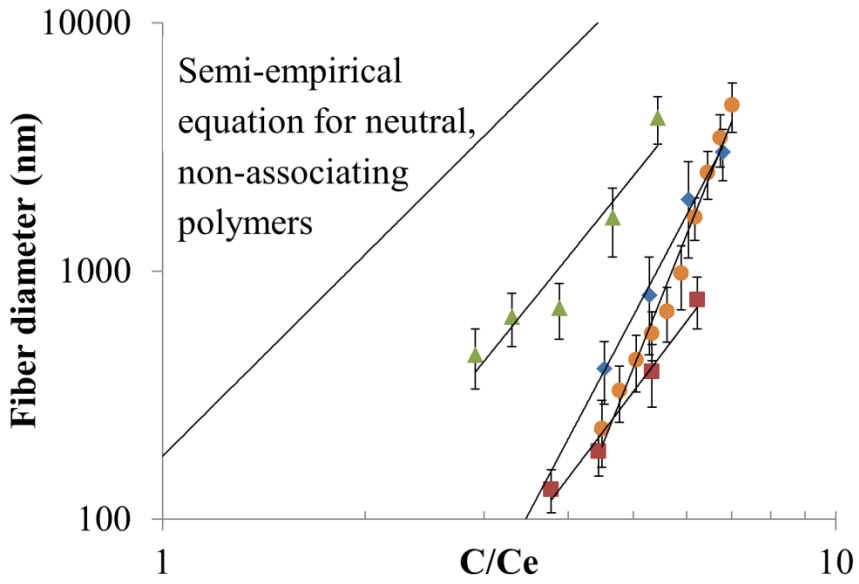

Figure 3.7. C/C_e electrospun fiber analysis of PDMAEMA•HCl and adenine-containing polyelectrolytes: PDMAEMA•HCl (circles), 11 mol% VBA copolymer (diamonds), 22 mol% VBA copolymer (squares), and 35 mol% VBA copolymer (triangles). Semi-empirical equation for neutral, non-associating polymers plotted as bold line.[15]

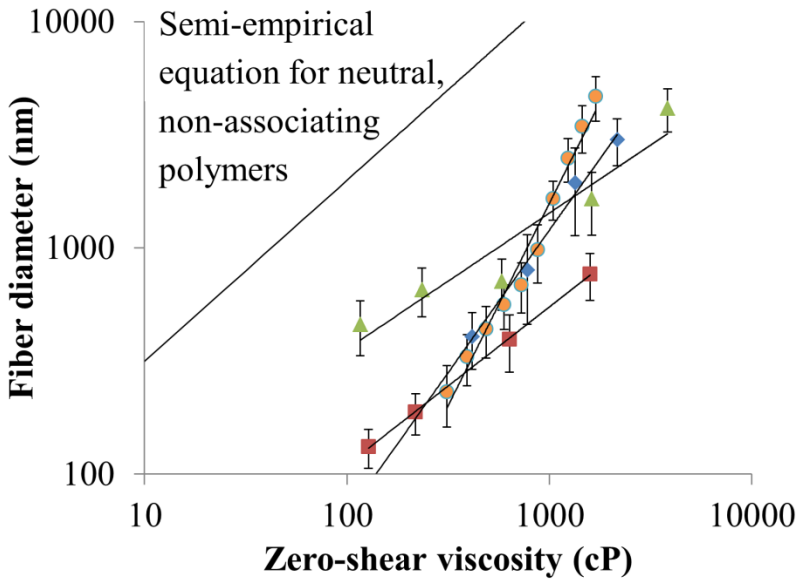

Figure 3.8. Zero-shear viscosity (cP) electrospun fiber analysis of PDMAEMA•HCl and adenine-containing polyelectrolytes: PDMAEMA•HCl (circles), 11 mol% VBA copolymer (diamonds), 22 mol% VBA copolymer (squares), and 35 mol% VBA copolymer (triangles). Semi-empirical equation for neutral, non-associating polymers plotted as bold line.[15]

The fiber diameter scaling factors decreased continuously as the fraction of VBA in the copolymers increased; however, fiber diameters remained dramatically below those expected for neutral polymers at the same normalized concentrations and viscosities. However, at 35 mol% VBA, fiber diameters increased significantly, as the impact of hydrogen bonding became more pronounced. The FESEM images of the 22 and 35 mol% VBA in Figure 3.6 highlight the increase in fiber diameter as the VBA content increased. At similar C/C_e values (4.5 and 4.7 for 22 mol% VBA and 35 mol% VBA copolymers, respectively), significantly larger fibers formed for the 35 mol% VBA copolymer (188 ± 39 nm for 22 mol% VBA and 1648 ± 511 nm for 35 mol% VBA). The resulting larger fibers for 35 mol% VBA occurred presumably due to increased intermolecular hydrogen bonding, which resulted in larger fiber diameters.

We expected larger changes to the fiber diameters as the VBA content increased due to self-association of the adenine in the copolymers. Due to the large shifts in the scaling factors (slopes in the power fit) for both fiber diameter *versus* normalized concentration and fiber diameter *versus* zero-shear viscosities, the influence of hydrogen bonding on the fiber diameters was difficult to correlate for lower VBA incorporation. **Table 3.4** summarizes the scaling factors for all polyelectrolytes and the data shows a decreasing trend as VBA incorporation increased, nearing the semi-empirical scaling factors for neutral, non-associating polymers of 2.7 for normalized concentration and 0.8 for zero-shear viscosity. The influence of VBA on fiber diameter was only easily recognized for 22 mol% and 35 mol% VBA copolymers since their scaling factors were similar. **Table 3.4** summarizes the normalized concentrations and zero-shear viscosities required for uniform fiber formation. As the VBA incorporation increased, the required C/C_e and zero-shear viscosity to achieve a stable electrospinning jet and the formation of uniform fibers decreased. Presumably, the increase in VBA content reduced the instabilities caused by the polyelectrolyte in the electrospinning jet, allowing fiber formation at significantly reduced viscosities and normalized concentrations. Also, the higher mol% VBA copolymers potentially required lower C/C_e's and zero-shear viscosities to electrospin due to the lower overall charge on the polyelectrolytes minimizing charge repulsion.

Table 3.4. Onset of electrospinning and scaling factors for PDMAEMA•HCl and the adenine-containing polyelectrolytes.

VBA (mol %)	C/C_e at onset of fiber formation	η_0 (cP) at onset of fiber formation	Scaling factor for fiber diameter *versus* C/C_e	Scaling factor for fiber diameter *versus* zero-shear viscosity
0	4.5	312	6.8	1.8
11	4.5	415	5.1	1.3
22	3.8	128	3.6	0.7
35	2.9	116	3.4	0.6

3.5 *Conclusions*

Conventional free-radical copolymerization and acidification successfully synthesized adenine-containing polyelectrolytes and we probed the influence of hydrogen bonding on their solution and electrospinning properties. All of the adenine-containing polyelectrolytes exhibited polyelectrolyte behavior in the semidilute unentangled and semidilute entangled regimes but deviated from polyelectrolyte theory in the concentrated regime. Their scaling factors in the concentrated regime increased with VBA incorporation most likely due to the onset of intermolecular hydrogen bonding causing larger increases in the solution viscosity. Higher incorporations of VBA significantly influenced the electrospinning of the adenine-containing polyelectrolytes with higher VBA content lowering the normalized concentrations and zero-shear viscosities required for the onset of electrospinning. Adenine incorporation also increased the fiber sizes approaching neutral, non-associating electrospinning fiber diameters and the adenine-containing copolymers exhibited a shift to decreased scaling factors for the fiber diameter *versus* normalized concentration or zero-shear viscosity, approaching the scaling factors for semi-empirical relationships for neutral, non-associating polymers. The adenine-decorated

electrospun mats will find applications in filtration and biological applications such as tissue scaffolding due to their adenine surface functionality.

3.6 *Acknowledgements*

This material is based upon work supported in part by the U.S. Army Research Office under grant number W911NF-07-1-0452 Ionic Liquids in Electro-Active Devices (ILEAD) MURI. This material is based upon work supported in part by the U.S. Army Research Laboratory and the U.S. Army Research Office under the Army Materials Center of Excellence Program, contract W911NF-06-2-0014. This material is based upon work supported in part by the Army Research Office (ARO) under Award No. W911NF-10-1-0307.

3.7 *References*

(1) Boris, D. C.; Colby, R. H. *Macromolecules* **1998**, *31*, 5746.
(2) Schlenoff, J. B.; Ly, H.; Li, M. *Journal of the American Chemical Society* **1998**, *120*, 7626.
(3) Smitha, B.; Sridhar, S.; Khan, A. A. *Macromolecules* **2004**, *37*, 2233.
(4) Mori, H.; Seng, D. C.; Lechner, H.; Zhang, M.; Müller, A. H. E. *Macromolecules* **2002**, *35*, 9270.
(5) Yeh, F.; Sokolov, E. L.; Khokhlov, A. R.; Chu, B. *Journal of the American Chemical Society* **1996**, *118*, 6615.
(6) Dautzenberg, H.; Görnitz, E.; Jaeger, W. *Macromolecular Chemistry and Physics* **1998**, *199*, 1561.
(7) Wang, L.; Bloomfield, V. A. *Macromolecules* **1991**, *24*, 5791.
(8) Shen, G.; Tercero, N.; Gaspar, M. A.; Varughese, B.; Shepard, K.; Levicky, R. *Journal of the American Chemical Society* **2006**, *128*, 8427.
(9) Rubinstein, M.; Colby, R. H.; Dobrynin, A. V. *Physical Review Letters* **1994**, *73*, 2776.
(10) Dobrynin, A. V.; Colby, R. H.; Rubinstein, M. *Macromolecules* **1995**, *28*, 1859.
(11) Yamaguchi, M.; Wakutsu, M.; Takahashi, Y.; Noda, I. *Macromolecules* **1992**, *25*, 475.
(12) Yamaguchi, M.; Wakutsu, M.; Takahashi, Y.; Noda, I. *Macromolecules* **1992**, *25*, 470.
(13) Lauten, R. A.; Nyström, B. *Macromolecular Chemistry and Physics* **2000**, *201*, 677.
(14) Colby, R. *Rheologica Acta* **2010**, *49*, 425.
(15) McKee, M. G.; Wilkes, G. L.; Colby, R. H.; Long, T. E. *Macromolecules* **2004**, *37*, 1760.
(16) McKee, M. G.; Hunley, M. T.; Layman, J. M.; Long, T. E. *Macromolecules* **2005**, *39*, 575.
(17) Hunley, M. T.; England, J. P.; Long, T. E. *Macromolecules* **2010**, *43*, 9998.
(18) Reneker, D. H.; Yarin, A. L. *Polymer* **2008**, *49*, 2387.
(19) McKee, M. G.; Layman, J. M.; Cashion, M. P.; Long, T. E. *Science* **2006**, *311*, 353.
(20) Deitzel, J. M.; Kleinmeyer, J.; Harris, D.; Beck Tan, N. C. *Polymer* **2001**, *42*, 261.
(21) Geng, X.; Kwon, O.-H.; Jang, J. *Biomaterials* **2005**, *26*, 5427.
(22) Gupta, P.; Elkins, C.; Long, T. E.; Wilkes, G. L. *Polymer* **2005**, *46*, 4799.
(23) Yang, Q.; Li, Z.; Hong, Y.; Zhao, Y.; Qiu, S.; Wang, C.; Wei, Y. *Journal of Polymer Science Part B: Polymer Physics* **2004**, *42*, 3721.
(24) Talwar, S.; Hinestroza, J.; Pourdeyhimi, B.; Khan, S. A. *Macromolecules* **2008**, *41*, 4275.
(25) McKee, M. G.; Elkins, C. L.; Long, T. E. *Polymer* **2004**, *45*, 8705.
(26) Hunley, M. T.; Long, T. E. *Polymer International* **2008**, *57*, 385.
(27) Shenoy, S. L.; Bates, W. D.; Frisch, H. L.; Wnek, G. E. *Polymer* **2005**, *46*, 3372.
(28) Hunley, M. T.; Karikari, A. S.; McKee, M. G.; Mather, B. D.; Layman, J. M.; Fornof, A. R.; Long, T. E. *Macromolecular Symposia* **2008**, *270*, 1.
(29) Mather, B. D.; Baker, M. B.; Beyer, F. L.; Berg, M. A. G.; Green, M. D.; Long, T. E. *Macromolecules* **2007**, *40*, 6834.
(30) Rowan, S. J.; Suwanmala, P.; Sivakova, S. *Journal of Polymer Science Part A: Polymer Chemistry* **2003**, *41*, 3589.
(31) Yamauchi, K.; Lizotte, J. R.; Long, T. E. *Macromolecules* **2002**, *35*, 8745.
(32) Cheng, C.-C.; Yen, Y.-C.; Ye, Y.-S.; Chang, F.-C. *Journal of Polymer Science Part A: Polymer Chemistry* **2009**, *47*, 6388.

(33) Spijker, H. J.; van Delft, F. L.; van Hest, J. C. M. *Macromolecules* **2007**, *40*, 12.
(34) Dahman, Y.; Puskas, J. E.; Margaritis, A.; Merali, Z.; Cunningham, M. *Macromolecules* **2003**, *36*, 2198.
(35) Lutz, J.-F.; Thunemann, A. F.; Rurack, K. *Macromolecules* **2005**, *38*, 8124.
(36) Han, M. J.; Lee, C. W.; Kim, K. H.; Lee, S. H. *Macromolecules* **1992**, *25*, 3528.
(37) Lo, P. K.; Sleiman, H. F. *Journal of the American Chemical Society* **2009**, *131*, 4182.
(38) Nair, K. P.; Weck, M. *Macromolecules* **2006**, *40*, 211.
(39) Mather, B. D.; Baker, M. B.; Beyer, F. L.; Green, M. D.; Berg, M. A. G.; Long, T. E. *Macromolecules* **2007**, *40*, 4396.
(40) Sedlak, M.; Simunek, P.; Antonietti, M. *Journal of Heterocyclic Chemistry* **2003**, *40*, 671.
(41) Christensen, J. J.; Rytting, J. H.; Izatt, R. M. *Biochemistry* **1970**, *9*, 4907.
(42) Pasquale, A. J.; Long, T. E. *Journal of Applied Polymer Science* **2004**, *92*, 3240.
(43) Tan, S.; Li, J.; Zhang, Z. *Macromolecules* **2011**, *44*, 7911.

Chapter 4: From N to P: Utilizing Phosphonium-Based Materials for Emerging Biomedical Applications

(*In preparation* as part of a chapter in a book titled "Handbook of Ionic Liquids and Polymers – properties and applications" published by Springer)

Sean T. Hemp, Michael H. Allen, Jr., and Timothy E. Long*

Macromolecules and Interfaces Institute, Department of Chemistry, Virginia Tech, Blacksburg, VA 24061
*To whom correspondence should be addressed. E-mail: telong@vt.edu. TEL: (540)231-2480 FAX: (540)231-8517

4.1 *Abstract*

Polymerized ionic liquids and polyelectrolytes play a major role in a broad range of biological applications including antimicrobials, nonviral gene delivery, synthetic enzymes, metal chelation, and drug delivery. Ammonium- and phosphonium-containing macromolecules will be reviewed focusing on literature examining structure-property relationships of these polyelectrolytes for biological applications. Phosphonium-containing macromolecules display a broad range of improved properties compared to ammonium macromolecules. For instance, phosphonium macromolecules exhibited enhanced antimicrobial activity and higher nucleic acid delivery compared to ammonium analogs. Finally, a perspective covers other potential cationic macromolecules including sulfonium and arsenium cations, which remain a rich area of potential research within the polymer field.

4.2 *Introduction*

Ionic liquids typically consist of an ammonium, phosphonium, or imidazolium cation with a bulky, fluorinated counterion, which sufficiently depresses the T_m of the ionic compounds to below 100 °C (**Figure 4.1**).[1] Literature typically directly compares ammonium and

phosphonium ionic liquids.[2] Imidazolium ionic liquids are the most common ionic liquids with a broad range of structural diversity through substituent control and counterion structure.[3] Ionic liquids that contain polymerizable functionality enable the generation of polymerized ionic liquids upon polymerization.[4] Typically, researchers examine structure-property relationships of ammonium- and phosphonium-containing polymerized ionic liquids to examine the impact of cation structure on macromolecular properties. This chapter will focus in part on the synthesis, characterization, and biological applications of ammonium and phosphonium polyelectrolytes with a focus on literature that directly compares ammonium and phosphonium polyelectrolytes.

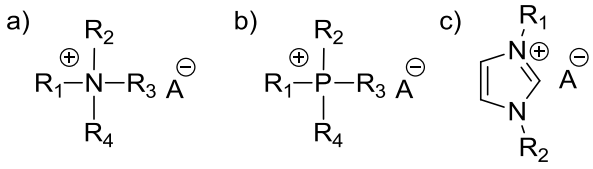

Figure 4.1. Example structures of ionic liquids: a) ammonium, b) phosphonium, and c) imidazolium.

Polyelectrolytes containing ammonium or phosphonium cations are widespread in the literature. They are typically synthesized utilizing two different approaches: a functional monomer route[5] or post-polymerization functionalization.[6] The synthesis of ammonium and phosphonium monomers typically relies on a simple nucleophilic substitution between a haloalkane and a tertiary amine or tertiary phosphine to generate the desired cationic monomer.[5] Monomer stability tends to be the limiting factor in whether a functional monomer route can be approached. Post-polymerization functionalization avoids potential monomer stability issues or polymerization hurdles, but it remains at a disadvantage to achieve 100% functionalization due to steric and neighboring group effects. Halide-containing macromolecules subjected to excess tertiary amines or tertiary phosphines readily generates ammonium and phosphonium

macromolecules.[6] Tertiary amine-containing monomers are also common in the literature and after polymerization, subsequent alkylation using a haloalkane will generate the desired ammonium polyelectrolyte.[7] Tertiary phosphine-containing monomers are rare due to their propensity for oxidation, but 4-(diphenylphosphino)styrene is readily used in the literature.[8,9]

4.3 *Structural Differences of Ammonium and Phosphonium Cations*

Nitrogen is a row 2 element in the periodic table with an atomic weight of 14.01 g/mol while phosphorus is a row 3 element below nitrogen in the periodic table with an atomic weight of 30.97 g/mol. Atomic radii and electronegativities directly impact the overall structure of the ammonium and phosphonium cations. Phosphorus exhibits a larger atomic radius than nitrogen.[10] Electronegativity differences result in a different charge distribution within the cation. Colby et al.[11] performed *ab initio* calculations to determine the specific charges found upon each atom within the ammonium and phosphonium cation. Since nitrogen is more electronegative than carbon, the nitrogen in ammonium cations displayed a slightly negative partial charge of -0.5 eV while the surrounding alpha carbons exhibited a slightly positive charge of 0.3 eV. Conversely, phosphonium cations contained a reversed charge density because phosphorus is less electronegative than carbon; therefore, the phosphorus atom displayed a positive charge of +1.1 eV and the adjacent carbon atoms exhibited a negative charge of -0.2 eV. Ultimately, both atomic radii and electronegativity differences of nitrogen and phosphorus leads to widely different cation structures.

4.4 *Thermal Stability and Base Stability*

Ammonium and phosphonium ionic liquids exhibit significantly different thermal and chemical stabilities. Ammonium ionic liquids typically display poor thermal stability compared

to phosphonium ionic liquids.[12] Hoffman elimination is one of the primary degradation pathways for ammonium ionic liquids that leads to this lower thermal stability. Both ammonium and phosphonium ionic liquids also degrade through reverse Menschutkin reactions wherein the halide counterion displaces the tertiary amine or phosphine.[12] Ammonium and phosphonium polymerized ionic liquids exhibit similar trends in thermal stability to their ionic liquid counterparts. Long et al.[13] performed a broad structure-property relationship study focused on poly(vinyl benzyl ammonium)s and poly(vinyl benzyl phosphonium)s. All phosphonium polymerized ionic liquids displayed dramatically higher thermal stabilities than ammonium analogs (**Figure 4.2**); longer alkyl substituent lengths also dramatically decreased the thermal stabilities of poly(vinyl benzyl ammonium)s. Thermogravimetric analysis (TGA) studies confirmed the primary degradation pathway of poly(vinyl benzyl ammonium)s was reverse Menschutkin degradation. Ammonium and phosphonium ionic liquids degrade through two different pathways under alkaline conditions.[2] Ammonium ionic liquids degrade through Hoffman elimination while phosphonium ionic liquids degrade into tertiary phosphine oxides and alkanes. The overall structure of the ammonium or phosphonium cation largely impacts its overall base stability with examples in the literature of alkaline stable ammonium[14] and phosphonium[15,16] macromolecules.

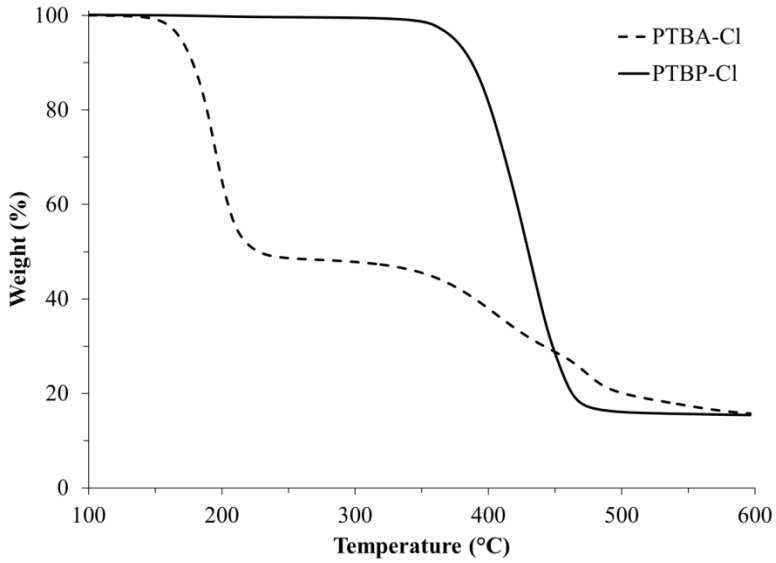

Figure 4.2. Thermogravimetric analysis of poly(tributylvinylbenzylammonium chloride) (PTBA-Cl) and poly(tributylvinylbenzylphosphonium chloride) (PTBP-Cl). Reprinted with permission from Ref. 13. ©2013 John Wiley and Sons, Inc.

4.5 *Antimicrobials*

Cationic macromolecules electrostatically associate non-specifically to the negatively-charged microbial cell membrane.[17] Upon association to the microbial cell membrane, the lipophilic portions of the cationic macromolecules insert into the cellular membrane, leading to rupture and cell death. Typical bacteria utilized during efficacy studies include Escherichia coli (E. coli) and Staphylococcus aureus (S. aureus). E. coli are the prototypical Gram-negative bacteria[18] while S. aureus are a representative Gram-positive bacteria.[19] Gram-positive bacteria contain a cell wall consisting of a single cellular membrane with an outer rigid, thick peptidoglycan layer.[19] The peptidoglycan layer consists of a broad mix of peptidoglycans and contains pores, which allow nutrients and particles to reach the inner cell membrane.[20] Cell walls of Gram-negative bacteria include an inner cell membrane, a thin peptidoglycan layer, and

then another outer cell membrane.[18] The outer cell membrane protects the integrity of the inner cell membrane, increasing the antimicrobial resistance of Gram-negative bacteria.[21]

Endo and coworkers pioneered structure-property analyses of ammonium- and phosphonium-containing polyelectrolytes for antimicrobial applications. They directly probed the antimicrobial efficacy of ammonium- and phosphonium-containing monomers and polymers against E. coli and S. aureus.[22] All polyelectrolytes displayed improved antimicrobial activity compared to their respective monomers. Also, phosphonium polyelectrolytes displayed enhanced antimicrobial properties compared to ammonium analogs (**Figure 4.3**). Ultimately, longer alkyl substituents attached to the cation resulted in the highest antimicrobial activity with n-octyl chains being the most effective at killing both E. coli and S. aureus. Endo and coworkers also examined ammonium and phosphonium random copolymers and polymer blends.[23] Polymer blends of ammonium and phosphonium polyelectrolytes exhibited a synergistic bactericidal effect, which resulted in improved efficacy. Interestingly, ammonium and phosphonium random copolymers failed to display any synergistic effect and higher phosphonium concentrations in the random copolymers resulted in higher antimicrobial efficacies.

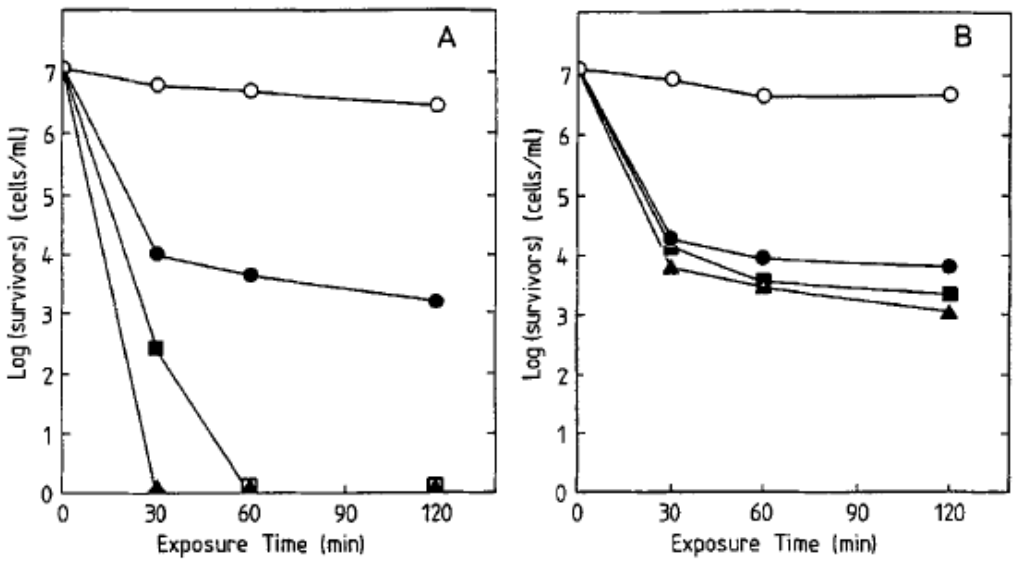

Figure 4.3. Antimicrobial activity of a) PTBP-Cl and b) PTBA-Cl demonstrating the enhanced efficacy of phosphonium macromolecules. Polymer concentrations: 0 μM (open circle), 280 μM (filled triangle), 28 μM (filled square), and 2.8 μM (filled circle). Reprinted with permission from Ref. 22. ©1993 John Wiley and Sons, Inc.

Kenawy and coworkers also extensively examined structure-property relationships of ammonium- and phosphonium-containing polyelectrolytes as antimicrobial agents. They typically generated halide-containing macromolecules and then subsequently performed post-polymerization functionalizations using tertiary amines or phosphines to generate the desired polyelectrolytes. Tartrate-based polyamides with pendant ammonium and phosphonium groups displayed high antibacterial activity, with tributylphosphonium cations exhibiting the highest efficacy (**Figure 4.4**).[24] Cationic poly(glycidyl methacrylate-*co*-hydroxyethyl methacrylate) random copolymers also showed the highest antibacterial and antifungal activity with tributylphosphonium cations attached to the polymer backbone.[25] Kenawy and coworkers also examined crosslinked cationic materials wherein triphenylphosphonium cations displayed the highest antimicrobial efficiency.[26] Finally, they controlled the charge density of ammonium- and

phosphonium-containing copolymers, which elucidated improved antmicrobial activity for phosphonium cations and higher charge densities.[27]

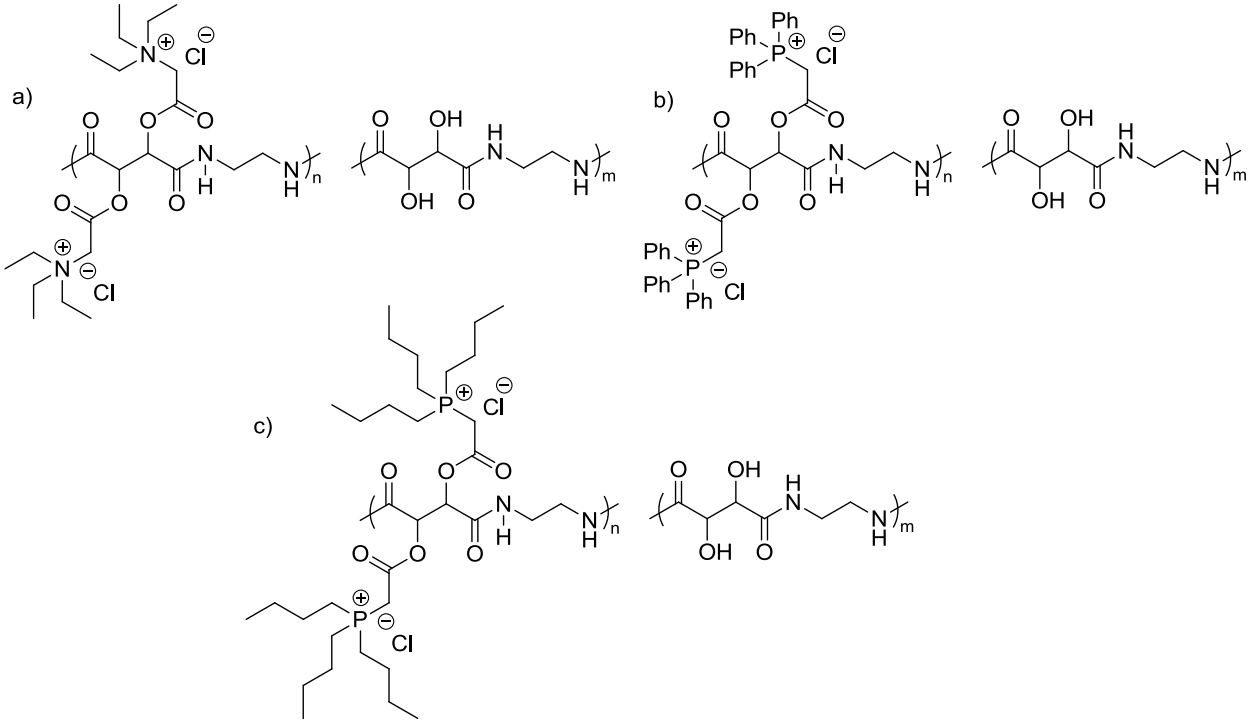

Figure 4.4. Tartrate-containing polyamides functionalized with a) triethylammonium, b) triphenylphosphonium, and c) tributylphosphonium substituents.[24]

4.6 *Nonviral Nucleic Acid Delivery*

Nitrogen-based cations such as ammonium, imidazolium, and pyridinium cations are utilized throughout literature to electrostatically complex nucleic acids and delivery them to cells *in vitro* and *in vivo* (**Figure 4.5**).[28] Typical cationic nitrogen-containing macromolecules examined for nonviral nucleic acid delivery include polyethyleneimine,[29] poly(amido amine) dendrimers,[30] chitosan,[31] poly(vinyl imidazolium)s,[32,33] poly(2-dimethylamino)ethyl methacrylate,[34] and poly(vinyl pyridinium)s.[35] Nitrogen-based cationic systems also display the advantageous property of typically containing protonatable nitrogens.[36] These protonatable sites

provide buffering capacity to the macromolecule, enabling endosomal escape. Endosomal escape is one of the major barriers to nucleic acid delivery. Delivery vehicles that buffer during endosomal acidification enable polyplex escape through the proton-sponge effect, wherein endosomal acidification and polymeric buffering capacity induces an influx of chloride anions.[36] Subsequent osmotic pressure ruptures the endosome. Prior to 2012, researchers failed to examine phosphonium-containing macromolecules for nonviral nucleic acid delivery.

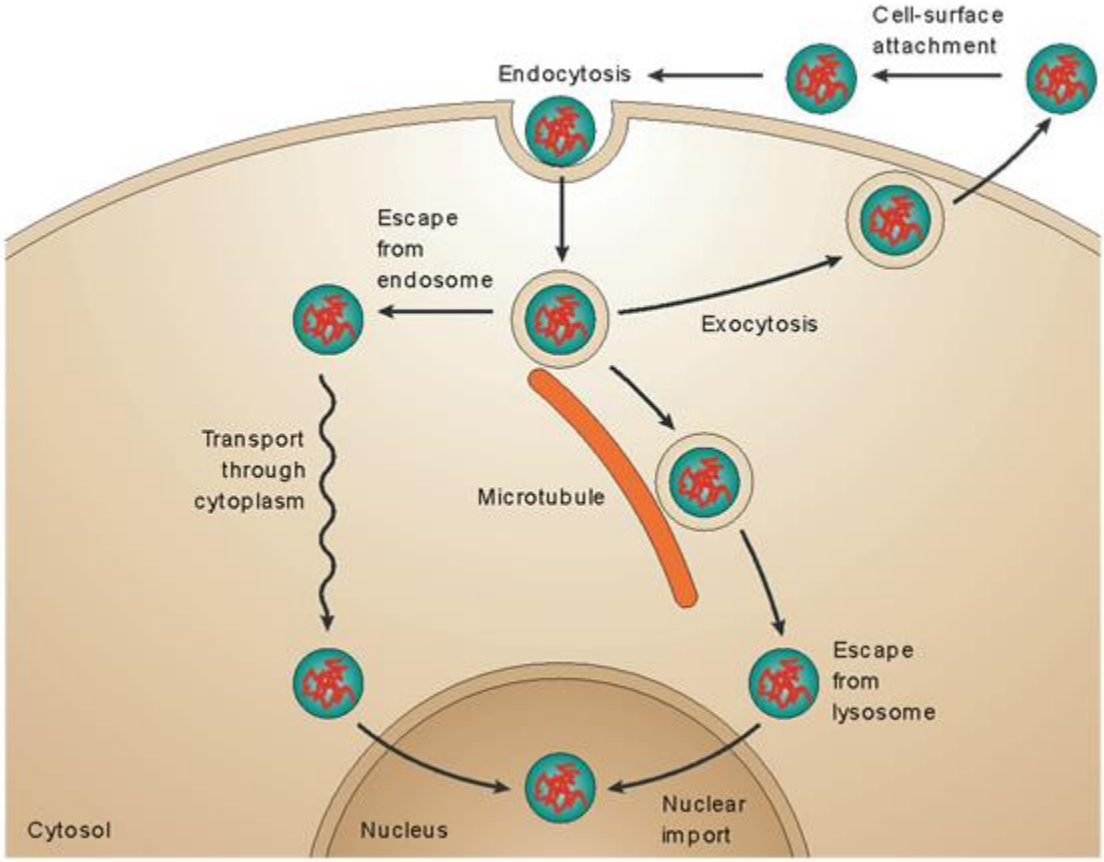

Figure 4.5. Nonviral gene delivery pathway demonstrating the necessary steps to achieve successful delivery. Reprinted with permission from Ref. 37. ©2005 Nature Publishing Group.

Long et. al.[38] pioneered the utilization of phosphonium macromolecules for nonviral nucleic acid delivery. They examined similar poly(vinyl benzyl ammonium)s and poly(vinyl

benzyl phosphonium)s that Endo et. al. previously used to highlight the improved antimicrobial properties of phosphonium macromolecules. Phosphonium-containing polystyrenes bound nucleic acids more effectively than ammonium analogs, completely complexing nucleic acids at charge ratios of 2 compared to charge ratios of 4 for ammonium analogs. Luciferase expression assays performed in serum-free media demonstrated improved nucleic acid delivery for phosphonium polystyrenes compared to ammonium polystyrenes (**Figure 4.6**). Unfortunately, ammonium and phosphonium polystyrenes performed poorly in serum-containing media, presumably due to aggregation with serum proteins. They also posed significant cytotoxicity *in vitro*, which resulted from their high charge density.

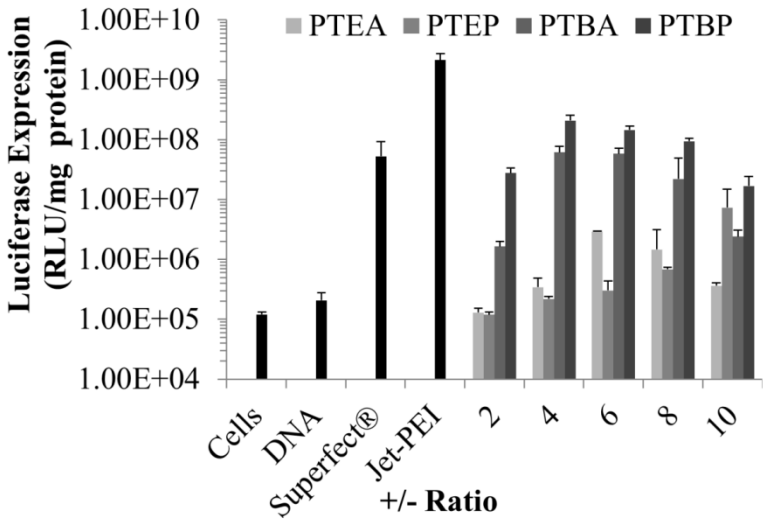

Figure 4.6. Luciferase transfection assay in serum-free media demonstrating improved efficacy for phosphonium-containing macromolecules. Reprinted with permission from Ref. 38. ©2012 American Chemical Society.

Long et. al.[39] aimed to improve nucleic acid delivery under serum-containing conditions and minimize cytotoxicity through the synthesis of phosphonium-containing AB diblock copolymers. The A block consisted of either an oligo(ethylene glycol) methyl ether methacrylate (OEG) or methacryloxyphosphoryl choline (MPC) block. Previous literature on OEG and MPC

blocks demonstrated their efficacy for enhancing nanoparticle colloidal stability. The B block composed of 4-(vinylbenzyltributyl)phosphonium chloride efficiently bound and compacted nucleic acids, as demonstrated previously. The authors targeted similar molecular weights for the A block (25 kg/mol) and varied the B block DP (25, 50, or 75). They found all diblock copolymers bound pDNA at charge ratios of 1. Phosphonium diblock copolymer polyplexes also displayed excellent colloidal stability, remaining similar diameters over 24 h under salt or serum conditions. These delivery vehicles delivery pDNA inefficiently to HeLa and COS-7 cells under serum conditions, likely due to the steric stabilizing A block minimizing cellular uptake. In HepaRG cells, a predictive cell line for *in vivo* studies, all phosphonium diblock copolymers delivered pDNA efficiently on the same order of magnitude as Jet-PEI with minimal cytotoxicity.

siRNA delivery is a rapidly expanding field focused on therapeutic treatment through the siRNA pathway, wherein delivered siRNA induces silencing of a specific protein through cellular machinery.[40] Protein silencing enables treatment of various diseases, including cancer and genetic diseases. Fréchet et. al.[41] first examined phosphonium polyacrylates for siRNA delivery and compared them to ammonium polyacrylates. Phosphonium polyacrylates displayed improved gene knockdown and higher cell viabilities compared to ammonium analogs. They also found a significant impact of alkyl substituent on toxicity and transfection efficiency. Finally, Kumar and coworkers[42] reported the elegant design and synthesis of triphenylphosphonium-modified PEI, which displayed improved pDNA and siRNA delivery compared to a linear PEI analog.

4.7 *Other Cations*

Traditionally, polymerized ionic liquids rely primarily on phosphonium cations and nitrogen-based cations such as ammonium and imidazolium cations. Alternative cations with a

broad potential for research include arsenium and sulfonium cations. Arsenium ionic liquids and polyelectrolytes are completely absent from the literature to our knowledge primarily due to the low commercial availability of suitable tertiary arsines. Triphenylarsine is the most available tertiary arsine, which unfortunately displays poor nucleophilicity in comparison to triphenylphosphine.[43] Sulfonium cations are widely important in biological systems with the most important sulfonium cation being S-adenosylmethionine.[44] S-adenosylmethionine acts as a methylating agent in a broad range of biological process such as nucleic acid methylation. Multiple reports of sulfonium ionic liquids are widespread in the literature.[45-47] Examples of sulfonium macromolecules exist in the literature with a primary focus on post-polymerization functionalization.[48-50] Endo et al.[51] examined the antimicrobial activity of a sulfonium-containing polystyrene and its monomer; they revealed improved antimicrobial activity of the sulfonium polymer compared to the sulfonium monomer. Deming et al.[52] demonstrated a wide range of sulfonium poly(L-methionine)s utilizing different alkyl halides and alkylation procedures to generate functional sulfonium-containing polyelectrolytes. Activated halides such as methyl iodide or other strategies were necessary to achieve high alkylation efficiencies. Long et al.[53] utilized similar procedures to Deming and coworkers to alkylate poly(2-methylthioethyl methacrylate) with methyl iodide to generate poly(2-dimethylsulfoniumethyl methacrylate). For the first time, sulfonium macromolecules bound nucleic acids effectively and delivered nucleic acids to HeLa cells more effectively than cells and DNA only negative controls.[53]

4.8 *Conclusions*

Ammonium and phosphonium polyelectrolytes display a broad range of properties suitable for many biological applications including antimicrobials and nonviral nucleic acid delivery. Atomic radii and electronegatives dramatically alter the cation structure when the

cationic atom is nitrogen or phosphorus. Monomer synthesis and post-polymerization functionalization are the two primary methods to generate ammonium and phosphonium poylelectrolytes. Phosphonium polyelectrolytes displayed enhanced thermal stability due to their resistance to Hoffman elimination. Cationic macromolecules exhibit significant antimicrobial activity and researchers found phosphonium macromolecules generally displayed higher antimicrobial efficiency. Ammonium and phosphonium macromolecules also effectively bound and delivered nucleic acids to cells; phosphonium polyelectrolytes displayed enhanced nucleic acid binding and delivery efficiency compared to ammonium analogs.

4.9 *Acknowledgements*

This material is based upon work supported in part by the U.S. Army Research Laboratory and the U.S. Army Research Office under the Army Materials Center of Excellence Program, contract W911NF-06-2-0014. This material is based upon work supported in part by the Macromolecular Interfaces with Life Sciences (MILES) Integrative Graduate Education and Research Traineeship (IGERT) of the National Science Foundation under Agreement No. DGE-0333378. This material is also based upon work supported in part by the US Army Research Office under Grant No. W911NF-07-1-0452 Ionic Liquids in Electro-Active Devices (ILEAD) MURI.

4.10 *References*

(1) Welton, T. *Chemical Reviews* **1999**, *99*, 2071.
(2) Fraser, K. J.; MacFarlane, D. R. *Australian Journal of Chemistry* **2009**, *62*, 309.
(3) Huddleston, J. G.; Visser, A. E.; Reichert, W. M.; Willauer, H. D.; Broker, G. A.; Rogers, R. D. *Green Chemistry* **2001**, *3*, 156.
(4) Mecerreyes, D. *Progress in Polymer Science* **2011**, *36*, 1629.
(5) Hatakeyama, E. S.; Ju, H.; Gabriel, C. J.; Lohr, J. L.; Bara, J. E.; Noble, R. D.; Freeman, B. D.; Gin, D. L. *Journal of Membrane Science* **2009**, *330*, 104.

(6) Parent, J. S.; Penciu, A.; Guillen-Castellanos, S. A.; Liskova, A.; Whitney, R. A. *Macromolecules* **2004**, *37*, 7477.
(7) Bütün, V.; Armes, S. P.; Billingham, N. C. *Macromolecules* **2001**, *34*, 1148.
(8) Choi, M. K. W.; He, H. S.; Toy, P. H. *The Journal of Organic Chemistry* **2003**, *68*, 9831.
(9) Guino, M.; Hii, K. K. *Chemical Society Reviews* **2007**, *36*, 608.
(10) Bondi, A. *The Journal of Physical Chemistry* **1964**, *68*, 441.
(11) Wang, S.-W.; Liu, W.; Colby, R. H. *Chemistry of Materials* **2011**, *23*, 1862.
(12) Bradaric, C. J.; Downard, A.; Kennedy, C.; Robertson, A. J.; Zhou, Y. *Green Chemistry* **2003**, *5*, 143.
(13) Hemp, S. T.; Zhang, M.; Allen, M. H.; Cheng, S.; Moore, R. B.; Long, T. E. *Macromolecular Chemistry and Physics* **2013**, *ASAP*.
(14) Bauer, B.; Strathmann, H.; Effenberger, F. *Desalination* **1990**, *79*, 125.
(15) Noonan, K. J. T.; Hugar, K. M.; Kostalik, H. A.; Lobkovsky, E. B.; Abruña, H. D.; Coates, G. W. *Journal of the American Chemical Society* **2012**, *134*, 18161.
(16) Hemp, S. T.; Zhang, M.; Tamami, M.; Long, T. E. *Polymer Chemistry* **2013**, *4*, 3582.
(17) Kenawy, E.-R.; Worley, S. D.; Broughton, R. *Biomacromolecules* **2007**, *8*, 1359.
(18) Decad, G. M.; Nikaido, H. *Journal of Bacteriology* **1976**, *128*, 325.
(19) Sutcliffe, I. C.; Russell, R. *Journal of Bacteriology* **1995**, *177*, 1123.
(20) Meroueh, S. O.; Bencze, K. Z.; Hesek, D.; Lee, M.; Fisher, J. F.; Stemmler, T. L.; Mobashery, S. *Proceedings of the National Academy of Sciences of the United States of America* **2006**, *103*, 4404.
(21) Vaara, M. *Microbiological Reviews* **1992**, *56*, 395.
(22) Kanazawa, A.; Ikeda, T.; Endo, T. *J. Polym. Sci., Part A: Polym. Chem.* **1993**, *31*, 335.
(23) Kanazawa, A.; Ikeda, T.; Endo, T. *J. Appl. Polym. Sci.* **1994**, *53*, 1245.
(24) Kenawy, E.-R.; Abdel-Hay, F. I.; Shahada, L.; El-Raheem, A.; El-Shanshoury, R.; El-Newehy, M. H. *J. Appl. Polym. Sci.* **2006**, *102*, 4780.
(25) Kenawy, E.-R.; Abdel-Hay, F. I.; El-Shanshoury, A. E.-R. R.; El-Newehy, M. H. *J. Polym. Sci., Part A: Polym. Chem.* **2002**, *40*, 2384.
(26) Kenawy, E.-R.; Abdel-Hay, F. I.; Abou, E.-M. A.; Mahmoud, Y. *React. Funct. Polym.* **2006**, *66*, 419.
(27) Kenawy, E.-R.; Mahmoud, Y. A. G. *Macromol. Biosci.* **2003**, *3*, 107.
(28) Mintzer, M. A.; Simanek, E. E. *Chemical Reviews* **2009**, *109*, 259.
(29) Ahn, H. H.; Lee, J. H.; Kim, K. S.; Lee, J. Y.; Kim, M. S.; Khang, G.; Lee, I. W.; Lee, H. B. *Biomaterials* **2008**, *29*, 2415.
(30) Dufès, C.; Uchegbu, I. F.; Schätzlein, A. G. *Advanced Drug Delivery Reviews* **2005**, *57*, 2177.
(31) Koping-Hoggard, M.; Tubulekas, I.; Guan, H.; Edwards, K.; Nilsson, M.; Varum, K. M.; Artursson, P. *Gene Therapy* **2001**, *8*, 1108.
(32) Allen, M. H.; Day, K. N.; Hemp, S. T.; Long, T. E. *Macromolecular Chemistry and Physics* **2013**, *214*, 797.
(33) Allen, M. H.; Green, M. D.; Getaneh, H. K.; Miller, K. M.; Long, T. E. *Biomacromolecules* **2011**, *12*, 2243.
(34) Layman, J. M.; Ramirez, S. M.; Green, M. D.; Long, T. E. *Biomacromolecules* **2009**, *10*, 1244.
(35) San Juan, A.; Letourneur, D.; Izumrudov, V. A. *Bioconjugate Chemistry* **2007**, *18*, 922.
(36) Behr, J.-P. *CHIMIA International Journal for Chemistry* **1997**, *51*, 34.

(37) Pack, D. W.; Hoffman, A. S.; Pun, S.; Stayton, P. S. *Nat Rev Drug Discov* **2005**, *4*, 581.
(38) Hemp, S. T.; Allen, M. H.; Green, M. D.; Long, T. E. *Biomacromolecules* **2012**, *13*, 231.
(39) Hemp, S. T.; Smith, A. E.; Bryson, J. M.; Allen, M. H.; Long, T. E. *Biomacromolecules* **2012**, *13*, 2439.
(40) Whitehead, K. A.; Langer, R.; Anderson, D. G. *Nat Rev Drug Discov* **2009**, *8*, 129.
(41) Ornelas-Megiatto, C.; Wich, P. R.; Fréchet, J. M. J. *Journal of the American Chemical Society* **2012**, *134*, 1902.
(42) Bansal, R.; Tripathi, S. K.; Gupta, K. C.; Kumar, P. *Journal of Materials Chemistry* **2012**, *22*, 25427.
(43) THORSTENSON, T.; SONGSTAD, J. *Acta Chcmica Scandinavia A* **1976**, *30*, 724.
(44) Lu, S. C. *The International Journal of Biochemistry & Cell Biology* **2000**, *32*, 391.
(45) Matsumoto, H.; Matsuda, T.; Miyazaki, Y. *Chemistry Letters* **2000**, *29*, 1430.
(46) Matsumoto, H.; Sakaebe, H.; Tatsumi, K. *Journal of Power Sources* **2005**, *146*, 45.
(47) Fang, S.; Yang, L.; Wei, C.; Peng, C.; Tachibana, K.; Kamijima, K. *Electrochemistry Communications* **2007**, *9*, 2696.
(48) Bailey, F. E.; La Combe, E. M. *Journal of Macromolecular Science: Part A - Chemistry* **1970**, *4*, 1293.
(49) Novak, B. M.; Hagen, E.; Hoff, S.; Viswanathan, A. *Macromolecules* **1994**, *27*, 1985.
(50) Hatch, M. J.; Meyer, F. J.; Lloyd, W. D. *Journal of Applied Polymer Science* **1969**, *13*, 721.
(51) Kanazawa, A.; Ikeda, T.; Endo, T. *Journal of Polymer Science Part A: Polymer Chemistry* **1993**, *31*, 2873.
(52) Kramer, J. R.; Deming, T. J. *Biomacromolecules* **2012**, *13*, 1719.
(53) Hemp, S. T.; Allen, M. H.; Smith, A. E.; Long, T. E. *ACS Macro Letters* **2013**, 731.

Chapter 5: Comparing Ammonium and Phosphonium Polymerized Ionic Liquids: Thermal Analysis, Conductivity, and Morphology

(Published in *Macromolecular Chemistry and Physics* **2013**, *ASAP*)

Sean T. Hemp, Mingqiang Zhang, Michael H. Allen, Jr., Shijing Cheng, Robert B. Moore, and Timothy E. Long*

Macromolecules and Interfaces Institute, Department of Chemistry, Virginia Tech, Blacksburg, VA 24061
*To whom correspondence should be addressed. E-mail: telong@vt.edu. TEL: (540)231-2480 FAX: (540)231-8517

Keywords: phosphonium, ammonium, polymerized ionic liquids, ionic conductivity

5.1 *Abstract*

Conventional free radical polymerization and anion metathesis of ammonium and phosphonium styrenics successfully generated high molecular weight polymerized ionic liquids (PILs). Phosphonium polyelectrolytes containing Cl^- counterions displayed significantly higher thermal stabilities (>370 °C) compared to ammonium analogs (<220 °C). Anion exchange to BF_4^-, TfO^-, and Tf_2N^- improved the thermal stability of all PILs due to decreased basicity of the anions. Larger anions depressed the T_g of PILs with all Tf_2N^- containing PILs displaying T_g's below 100 °C. Longer alkyl substituent lengths led to decreased thermal stabilities and lower T_g's. Impedance spectroscopy probed ionic conductivities of PILs containing Tf_2N^-, and phosphonium PILs exhibited higher ionic conductivities than ammonium analogs. T_g-independent ionic conductivity demonstrated increased alkyl substituent lengths led to lower ionic conductivities. Phosphonium PILs continued to exhibit higher ionic conductivities than respective ammonium analogs. Wide-angle x-ray diffraction (WAXD) showed changes in morphology, which was dependent only on alkyl substituent length with minimal influence of the

cationic center on morphology. Phosphonium PILs displayed many advantages over ammonium PILs for emerging applications that demand higher thermal stabilities and ionic conductivities.

5.2 *Introduction*

Phosphorus-containing macromolecules contain main-chain or pendant phosphorus atoms in a wide range of oxidation states (phosphates, phosphines, phosphine oxides, and phosphoniums), and many compositions are suitable for a variety of applications including electronic and biomedical applications. Many researchers observed enhanced thermal stability[1] and flame retardency[2] of phosphorus-containing macromolecules, which are ideal for high temperature aerospace and transportation applications. Also, their natural occurrence (nucleic acids) and their widespread use in biological applications highlights the importance of these phosphorus-containing macromolecules.[3] Cationic phosphonium-containing macromolecules include homopolymers,[4,5] random copolymers,[6,7] and block copolymers.[8,9] Ammonium- and phosphonium-containing macromolecules typically exhibit widely different physical properties due to the minor structural change from a cationic nitrogen to cationic phosphorus. Kenawy et. al.[10-12] and Endo et. al.[13,14] demonstrated improved antimicrobial activity for phosphonium-containing polyelectrolytes compared to ammonium-containing polyelectrolytes. Long et. al.[15,16] also recently highlighted improved nucleic acid binding and delivery of phosphonium-containing vehicles over ammonium analogs. Gin and coworkers[17] synthesized a wide range of ammonium- and phosphonium-functionalized polystyrenes and examined the efficacy of ammonium and phosphonium coatings on the antifouling properties of water purification membranes.

Many ammonium- and phosphonium-containing monomers are classified as ionic liquid monomers.[18] Ionic liquids are salts that exhibit a melting point (T_m) below 100 °C.[19] Ionic liquid structure variation enables the generation of designer solvents,[20] and ionic liquids display

high thermal stabilities,[21] low vapor pressures,[22] high conductivities,[23] and variable solubility.[24] Many common ionic liquids typically consist of an imidazolium cation with a bulky, asymmetric counterion to sufficiently suppress the T_m below 100 °C. Ammonium ionic liquids are less popular, primarily arising from their poor thermal stability. Ammonium ionic liquids typically degrade through a reverse nucleophilic substitution mechanism or Hoffman elimination mechanism, where the counterion abstracts a β-hydrogen, in the first step of an elimination reaction.[25] Phosphonium ionic liquids exhibit significantly improved thermal stabilities over the ammonium analogs.[26] Initially, the poor commercial availability of phosphines limited the number of phosphonium ionic liquids, however, a broader commercial phosphine library recently enabled the synthesis of low viscosity, high conductivity phosphonium ILs.[27]

Ionic liquids containing a polymerizable functional group enable the formation of polymerized ionic liquids (PILs).[18] Polymerization of IL monomers typically results in reduced ionic conductivities due to immobilization of the cation and a higher T_g,[28] but PILs result in single-ion conductors suitable for electromechanical actuators,[29] gas separation membranes,[30] and ion exchange membranes.[31] Researchers typically focus on imidazolium-containing PILs. Recent work on poly(vinylimidazolium)s summarized structure-property relationships of alkyl substituent length and counterion selection on thermal properties, ionic conductivity, and morphology.[32,33] Mahesh et. al. probed ionic conductivities of poly(vinylbenzyl imidazolium)s with different alkyl substituent lengths and counterions;[34] they also examined the influence of morphology on ionic conductivity of well-defined poly(styrene-*b*-vinylbenzyl imidazolium) diblock copolymers.[35] Commonly investigated ammonium PILs include protonated/quaternized poly(2-dimethylaminoethyl methacrylate),[36] poly(vinylbenzyl

ammonium)s,[37] and poly(diallyldimethylammonium chloride).[38] Similar to ammonium ILs, they typically exhibit poor thermal stabilities with basic counterions due to Hoffman elimination.

The earlier literature lacks a systematic comparison and understanding of the thermal properties and ionic conductivities of polymerized ammonium- and phosphonium-containing ionic liquids. Herein, we report a detailed structure-property relationship study that examines ammonium and phosphonium polymerized ionic liquids. Monomer design and post-polymerization anion metathesis successfully generated a library of ammonium and phosphonium PILs to examine the influence of cation selection, alkyl substituent length, and counterion on thermal properties, ionic conductivities, and morphologies of ammonium and phosphonium PILs. Thermogravimetric analysis and differential scanning calorimetry elucidated thermal stabilities and thermal transitions of ammonium and phosphonium PILs. Impedance spectroscopy probed the influence of minor structural changes on PIL conductivity. Finally, wide-angle x-ray diffraction (WAXD) elucidated the impact of polymer morphology on ionic conductivity. PILs will continue to play a major role in emerging applications and a fundamental understanding of the influence of macromolecular structure on resulting properties will aid in development of these advanced polymers.

5.3 *Experimental Section*

5.3.1 Materials

α,α′-Azoisobutyronitrile (AIBN) was obtained from Sigma Aldrich and recrystallized from methanol twice. Trimethylphosphine (1.0 M in THF), triethylphosphine (99%), tripropylphosphine (97%), tributylphosphine (99%), trimethylamine (~4.2 M in ethanol), triethylamine (≥99.5%), tripropylamine (≥99), tributylamine (≥98.5%), 4-vinylbenzyl chloride

(≥90%), sodium tetrafluoroborate (98%), sodium triflate (98%), lithium bis(trifluoromethane)sulfonamide (≥99%), and silver nitrate (≥99%) were obtained from Sigma Aldrich and used as received. All solvents were obtained from Fisher Scientific and used as received. Triethyl-(4-vinylbenzyl)ammonium chloride, tripropyl-(4-vinylbenzyl)ammonium chloride, tributyl-(4-vinylbenzyl)ammonium chloride, trimethyl-(4-vinylbenzyl)phosphonium chloride, triethyl-(4-vinylbenzyl)phosphonium chloride, tripropyl-(4-vinylbenzyl)phosphonium chloride and tributyl-(4-vinylbenzyl)phosphonium chloride were synthesized as reported earlier.[7,17]

5.3.2 Synthesis of trimethyl-(4-vinylbenzyl)ammonium chloride

Trimethylamine (17.0 mL, 71.4 mmol), 4-vinylbenzyl chloride (10 mL, 120.6 mmol), and acetonitrile (30 mL) were added to a 250-mL, round-bottomed flask with stir bar. The resulting solution was heated at 50 °C for 48 h and then subsequently concentrated *in vacuo*. The viscous solution was added dropwise to 4 L ethyl acetate to precipitate the TMA-Cl monomer. The white solid was suction filtered and rinsed with ethyl acetate. The resulting white solid was dried *in vacuo* at 23 °C (13.73 g, 91% yield). ^{1}H NMR (400 MHz, $CDCl_3$) δ 7.57 (d, J = 8.2 Hz, 2H), 7.37 (d, J = 8.2 Hz, 2H), 6.64 (dd, J = 17.6, 10.9 Hz, 1H), 5.74 (d, J = 17.6 Hz, 1H), 5.29 (d, J = 11.0 Hz, 1H), 5.01 (s, 2H), 3.36 (s, 9H). ^{13}C NMR (101 MHz, $CDCl_3$) δ 139.88, 135.68, 133.38, 126.92, 126.40, 115.48, 68.51, 52.55. Mass Spectrometry: Theoretical, m/z 176.1434; Experimental, m/z 176.1423.

5.3.3 Polymer synthesis

All polyelectrolytes were synthesized following a similar procedure and the synthesis of poly(trimethyl-(4-vinylbenzyl)ammonium chloride) follows as an example. Trimethyl-(4-

vinylbenzyl)ammonium chloride (5.99 g, 28.3 mmol), AIBN (23.3 mg, 0.142 mmol), and 50/50 v/v DMF/H_2O (54 mL) were added to a 100-mL round-bottomed flask. The solution was purged with Ar for 30 min and then heated at 65 °C for 24 h. The resulting solution was dialyzed against water and lyophilized to obtain a white powder (5.62 g, 94% yield)

5.3.4 Anion metathesis

All polyelectrolytes were anion exchanged to various anions utilizing a similar anion metathesis reaction. An example procedure follows detailing the anion exchange of poly[trimethyl-(4-vinylbenzyl)phosphonium chloride] to poly[trimethyl-(4-vinylbenzyl)phosphonium bis(trifluoromethane)sulfonimide)]. Poly[trimethyl-(4-vinylbenzyl)phosphonium chloride] (535 mg, 2.3 mmol) was dissolved in 10 mL water and lithium bis(trifluoromethane)sulfonimide (3.50 g, 12.2 mmol) was dissolved in another 10 mL aliquot of water. The resulting polymer solution was added dropwise to the salt solution to yield a white precipitate. The solution was stirred for 16 h. The white precipitate was washed exhaustively with water until the filtrate was chloride free determined using a silver nitrate test. The white precipitate was dried *in vacuo* at 60 °C (1.02 g, 92% yield). XPS analysis showed minimal residual chloride (<1%), which confirmed complete conversion to the desired anion.

5.3.5 Instrumentation

NMR spectroscopy was performed using a Varian Unity 400 operating at 400 MHz and 23 °C. Thermogravimetric analysis was completed using a TA Instruments TGA Hi-Res 2950 under N_2 at 10 °C/min. Differential scanning calorimetry (DSC) was executed using a TA Instruments DSC Q2000 under N_2 using a heat/cool/heat cycle at 10 °C/min. All T_g's were obtained from the second heat. Aqueous size-exclusion chromatography (SEC) was performed

in a ternary solvent mixture consisting of 54/23/23 v/v/v water/methanol/acetic acid with 0.1 M sodium acetate. Aqueous SEC was implemented using a Waters 1515 isocratic HPLC pump and Waters 717plus autosampler with a Waters 2414 differential refractive index (DRI) detector (35 °C, 880 nm) and a Wyatt Minidawn multi-angle laser light scattering (MALLS) detector (690 nm). The columns consisted of two Waters Ultrahydrogel linear columns and one Waters Ultrahydrogel 250 column maintained at 30 °C. d*n*/d*c* values were obtained offline using a Wyatt Optilab T-rEX differential refractometer (35 °C, 658 nm). Absolute molecular weights were therefore reported using the DRI and MALLS detectors on the aqueous SEC.

Impedance spectroscopy was obtained using a Metrohm Autolab 302N with a 4-point in-plane cell (BekkTeck, Inc.) and an ESPEC BTL-433 environmental chamber, which controlled the temperature from 95 °C to 135 °C under a dry environment. Polymer solutions (30 wt% in acetone) were cast onto glass slides. The resulting film was air dried for 4 h and then subsequently annealed at 135 °C in the environmental chamber for 16 h prior to measurements. The alternating voltage set point was 0.2 V and the frequency was varied from 0.1 Hz to 1 MHz. Each measurement was the average of 5 measurements and measurements were performed in 10 °C/step from 135 °C to 95 °C. The sample was equilibrated at each temperature for at least 2 h prior to measurement. The resistance was calculated from the x-intercept of the Nyquist plot in the Autolab Nova software suite and subsequently converted to conductivity using $\sigma = L/AR$ where L is the length between the inner electrodes, A is the area between the electrodes, and R is the measured resistance.

The Vogel-Fulcher-Tamman (VFT) equation is a three-parameter equation with the variables infinite conductivity (σ_0), the Vogel temperature (T_0) where ion motion stops, and a

constant related to the activation temperature or Arrhenius activation energy (B). The 3-parameter VFT equation is as follows:

$$\sigma(T) = \sigma_0 \exp\left(\frac{-B}{T - T_0}\right) \quad (1)$$

Due to the difficulty of fitting a three-parameter equation, Elabd et. al. modified the VFT equation using a reference conductivity ($\sigma(T_r)$) and a reference temperature (T_r) to reduce the VFT equation to two parameters (T_0 and B).[39] They demonstrated the efficacy of this modification, and the 2-parameter VFT equation results in more reliable fitting due to only two variables. Their modified VFT equation is:

$$\sigma(T) = \sigma(T_r) \exp\left(-B\left(\frac{1}{T - T_0} - \frac{1}{T_r - T_0}\right)\right) \quad (2)$$

The Origin Lab 7 software suite was utilized to fit ammonium and phosphonium PIL conductivity data using three- and two-parameter VFT equations.

Wide-angle x-ray diffraction (WAXD) was performed using a Rigaku S-Max 3000 3 pinhole SAXS system, equipped with a rotating anode emitting X-rays with a wavelength of 0.154 nm (Cu Kα). Scattering from a silver behenate standard was used to calibrate the sample-to-detector distance (80 mm). WAXD two-dimensional diffraction patterns were obtained using an image plate with an exposure time of 1 h. All WAXD two-dimensional diffraction patterns were analyzed using the SAXSGUI software package to obtain radially integrated WAXD intensity versus 2θ profiles, where θ is one half of the scattering angle. WAXD profiles were vertically shifted to facilitate a comparison of the peak positions.

5.4 *Results and Discussion*

5.4.1 Polymer synthesis

The ammonium and phosphonium PILs library enabled an examination of the influence of cationic site, alkyl substituent length, and counterion on thermal properties, ionic conductivity, and morphology. Conventional free radical polymerization of ammonium or phosphonium styrenics with variable alkyl substituent lengths generated ammonium and phosphonium polyelectrolytes (**Scheme 5.1**). The polyelectrolytes included: poly[trimethyl-(4-vinylbenzyl)phosphonium chloride] (PTMP-Cl), poly[triethyl-(4-vinylbenzyl)phosphonium chloride] (PTEP-Cl), poly[tripropyl-(4-vinylbenzyl)phosphonium chloride] (PTPP-Cl), poly[tributyl-(4-vinylbenzyl)phosphonium chloride] (PTBP-Cl), poly[trimethyl-(4-vinylbenzyl)ammonium chloride] (PTMA-Cl), poly[triethyl-(4-vinylbenzyl)ammonium chloride] (PTEA-Cl), poly[tripropyl-(4-vinylbenzyl)ammonium chloride] (PTPA-Cl), and poly[tributyl-(4-vinylbenzyl)ammonium chloride] (PTBA-Cl).

Scheme 5.1. Synthesis of ammonium- and phosphonium-containing polymerized ionic liquids using conventional free radical polymerization and anion-exchange.

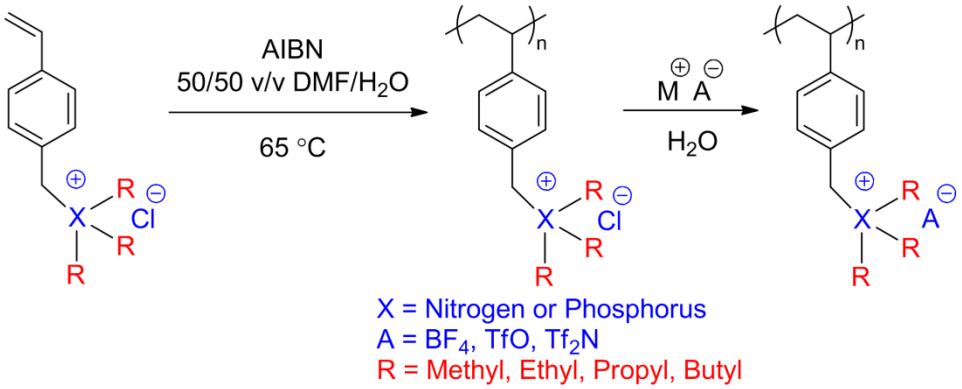

SEC analysis of highly charged polyelectrolytes remains challenging due to a multitude of issues, including polymer aggregation, column interactions, and poor solubility.[40] All polyelectrolytes were water-soluble, and consequently, an aqueous SEC solvent, which contained organic cosolvents and salt to minimize polymer aggregation and column interactions, was suitable for these polyelectrolytes. The aqueous SEC solvent consisted of 54/23/23 v/v/v water/methanol/acetic acid with 0.1 M sodium acetate. Our earlier literature demonstrated that this ternary mixture prevents polymer aggregation and enabled reliable aqueous SEC analysis of ammonium- and phosphonium-functionalized polystyrenes.[16] A differential refractometer determined d*n*/dc values offline for each polyelectrolyte in the aqueous SEC solvent, enabling *absolute* molecular weight determination using RI and MALLS detectors. **Table 5.1** summarizes *absolute* molecular weight analysis of ammonium and phosphonium polyelectrolytes. Conventional free radical polymerization generated high molecular weight homopolymers (150-350 kg/mol) with polydispersities expected for conventional free radical polymerization.

Table 5.1. Absolute molecular weight characterization of ammonium- and phosphonium-containing polyelectrolytes.

Polymer	d*n*/d*c* (mL/g)	M_n (kg/mol)	M_w (kg/mol)	PDI	X_n
PTMA	0.203	225	311	1.38	1063
PTEA	0.179	251	395	1.57	989
PTPA	0.197	167	238	1.43	564
PTBA	0.165	250	391	1.56	740
PTMP	0.185	235	292	1.25	1028
PTEP	0.190	270	388	1.44	999
PTPP	0.189	342	553	1.62	1093
PTBP	0.195	314	499	1.59	885

Aqueous SEC: 54/23/23 v/v/v H_2O/MeOH/AcOH with 0.1 M sodium acetate, MALLS

Anion metathesis in water with an excess of the desired metal salt allowed facile anion exchange. The polyelectrolytes contained four different counterion structures: Cl^-, BF_4^-, TfO^-, and Tf_2N^-. All polyelectrolytes with a Cl^- counterion were water soluble and upon anion exchange, the resulting PILs precipitated from solution as a white solid. After isolating and washing the white precipitates, the silver nitrate test assessed the filtrate for residual Cl^- anions. A precipitate did not form upon addition of silver nitrate to aqueous filtrates confirming complete anion exchange and removal of residual Cl^- anions from PILs. Furthermore, XPS analysis on anion-exchanged PILs demonstrated the absence of residual Cl^- anions (<1%).

5.4.2 Thermal analysis

Cationic site, alkyl substituent length, and counterion structural changes influenced the thermal stability and thermal transitions of PILs. Ammonium and phosphonium polyelectrolytes with Cl^- counterions exhibited significant differences in their thermal stability (**Figure 5.1**).

PTBA-Cl showed a multi-step degradation profile with the initial step occurring at a $T_{d,\ 5\%}$ of 169 °C. In sharp contrast, PTBP-Cl displayed a single step degradation with a $T_{d,\ 5\%}$ of 374 °C, greater than 200 °C more stable than the ammonium analog PTBA-Cl. **Table 5.2** summarizes the thermal properties for all PILs. Ammonium polyelectrolytes with Cl^- counterions exhibited thermal stabilities 200 °C lower than their respective phosphonium analog.

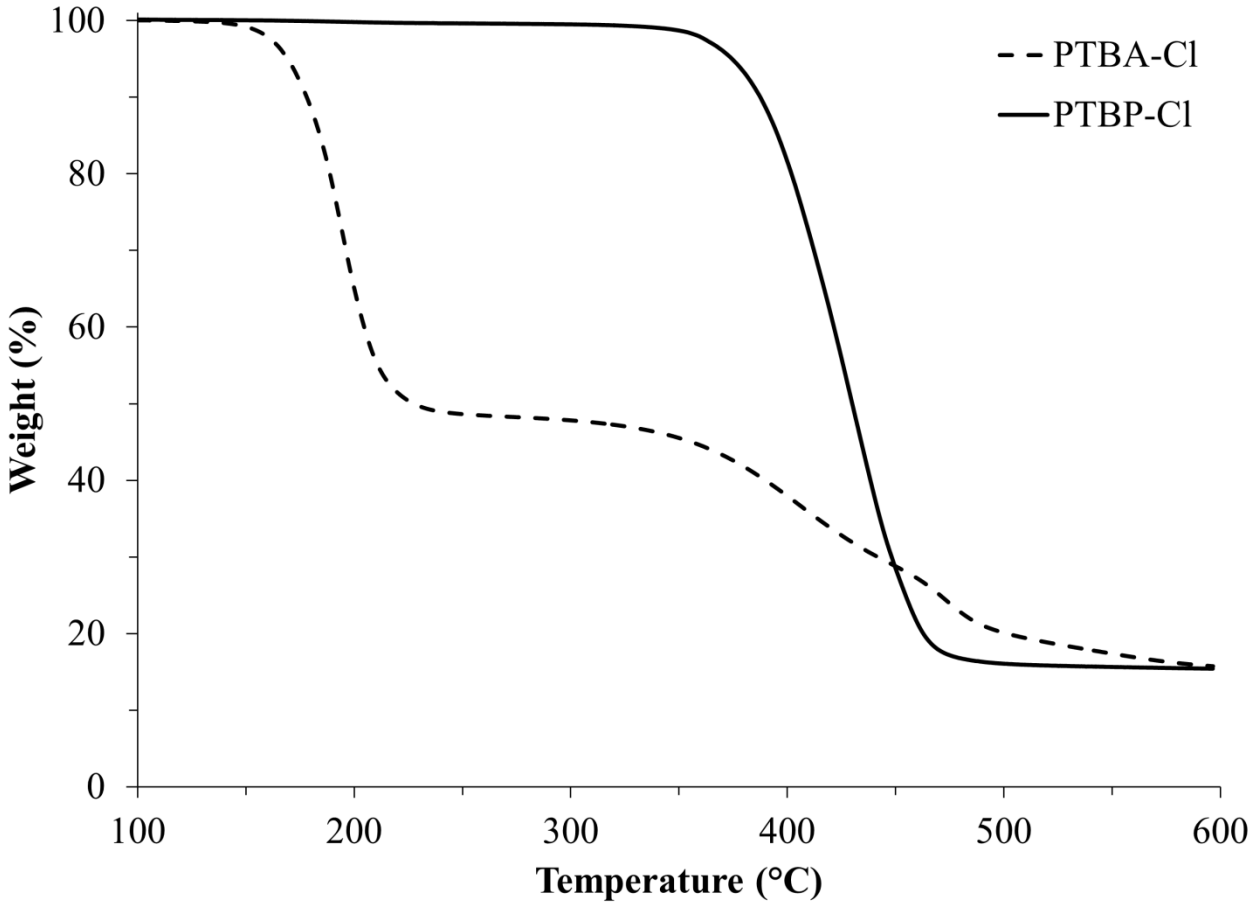

Figure 5.1. Thermogravimetric analysis of PTBA-Cl and PTBP-Cl showing the enhanced thermal stability of phosphonium-based polyelectrolytes. TGA performed at 10 °C/min under a N_2 atmosphere.

Table 5.2. Thermal analysis of ammonium- and phosphonium-containing polymerized ionic liquids.

	$T_{d,\,5\%}$ (°C)[a]				T_g (°C)[b]			
Polymer	Cl^-	BF_4^-	TfO^-	Tf_2N^-	Cl^-	BF_4^-	TfO^-	Tf_2N^-
PTMA	220	345	351	371	ND	240	182	91
PTEA	200	321	331	341	ND	195	138	70
PTPA	177	298	324	341	ND	171	130	82
PTBA	169	301	315	330	ND	147	119	62
PTMP	421	437	462	465	284	230	167	91
PTEP	393	417	462	462	240	195	132	68
PTPP	377	422	457	452	195	167	128	71
PTBP	374	427	450	437	177	143	117	66

[a]TGA, 10 °C/min, N_2 atmosphere; [b]DSC, 10 °C/min, second heat, N_2 atmosphere

Ammonium-containing macromolecules exhibit poor thermal stability due two typically invoked pathways: Hoffman elimination or reverse Menschutkin (nucleophilic) degradation (**Scheme 5.2**).[41] Hoffman elimination occurs when the counterion abstracts a hydrogen from the β-carbon causing subsequent elimination. For PTBA-Cl, Hoffman byproducts are HCl and 1-butene. Reverse Menschutkin degradation corresponds to nucleophilic attack of the Cl^- counterion at the benzylic position, which liberates tributylamine for PTBA-Cl. Mahesh et al. reported that poly(vinylbenzyl imidazolium)s initially degrade through this nucleophilic substitution pathway.[42]

Table 5.3 summarizes theoretical % weight loss for Hoffman and nucleophilic degradation pathways with experimental % weight loss attributed to the initial first degradation step in ammonium polyelectrolytes containing a Cl^- counterion. PTMA-Cl fails to undergo Hoffman elimination due to the absence of β-hydrogens. **Table 5.3** clearly shows that ammonium polyelectrolytes predominately undergo nucleophilic degradation since their experimental weight loss compared closely to theoretical weight loss for nucleophilic degradation. Additionally, longer alkyl substituent lengths on ammonium polyelectrolytes with Cl^- counterions exhibited lower thermal stabilities, which correlated with initial nucleophilicity of the tertiary amine.

Scheme 5.2. Thermal degradation of ammonium polyelectrolytes through either a Hoffman elimination or reverse nucleophilic substitution mechanism.

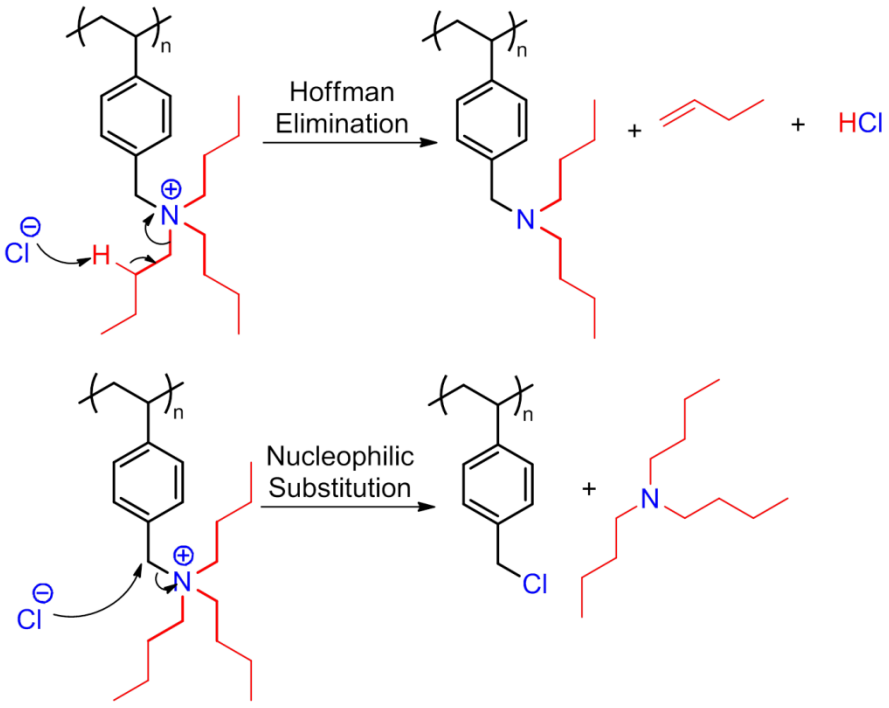

Table 5.3. Correlation of initial degradation of ammonium polyelectrolytes to degradation pathway.

Polymer	Experimental Weight Loss (%)	Theoretical Weight Loss Hoffman (%)	Theoretical Weight Loss Nuc. (%)
PTMA-Cl	32	--	28
PTEA-Cl	41	25	40
PTPA-Cl	49	27	48
PTBA-Cl	51	27	55

TGA, 10 °C/min, N_2 atmosphere

Anion exchange to BF_4^-, TfO^-, and Tf_2N^- improved the thermal stability of both ammonium and phosphonium polyelectrolytes (**Table 5.2**). Previous reports detailed similar results for other PILs where exchange to less basic anions improved thermal stability.[36] In this case, ammonium PILs exhibited significantly higher thermal stabilities (>300 °C) and phosphonium PILs also displayed improved thermal stabilities (>400 °C). Overall, as the basicity of the counterion decreased, thermal stabilities of PILs increased in the order $Tf_2N^- > TfO^- > BF_4^- > Cl^-$. The propensity for ammonium PILs to degrade through the reverse Menschutkin pathway decreased as counterion nucleophilicity decreased, correlating to our proposed degradation pathway for ammonium polyelectrolytes with Cl^- counterions (**Figure 5.2**).

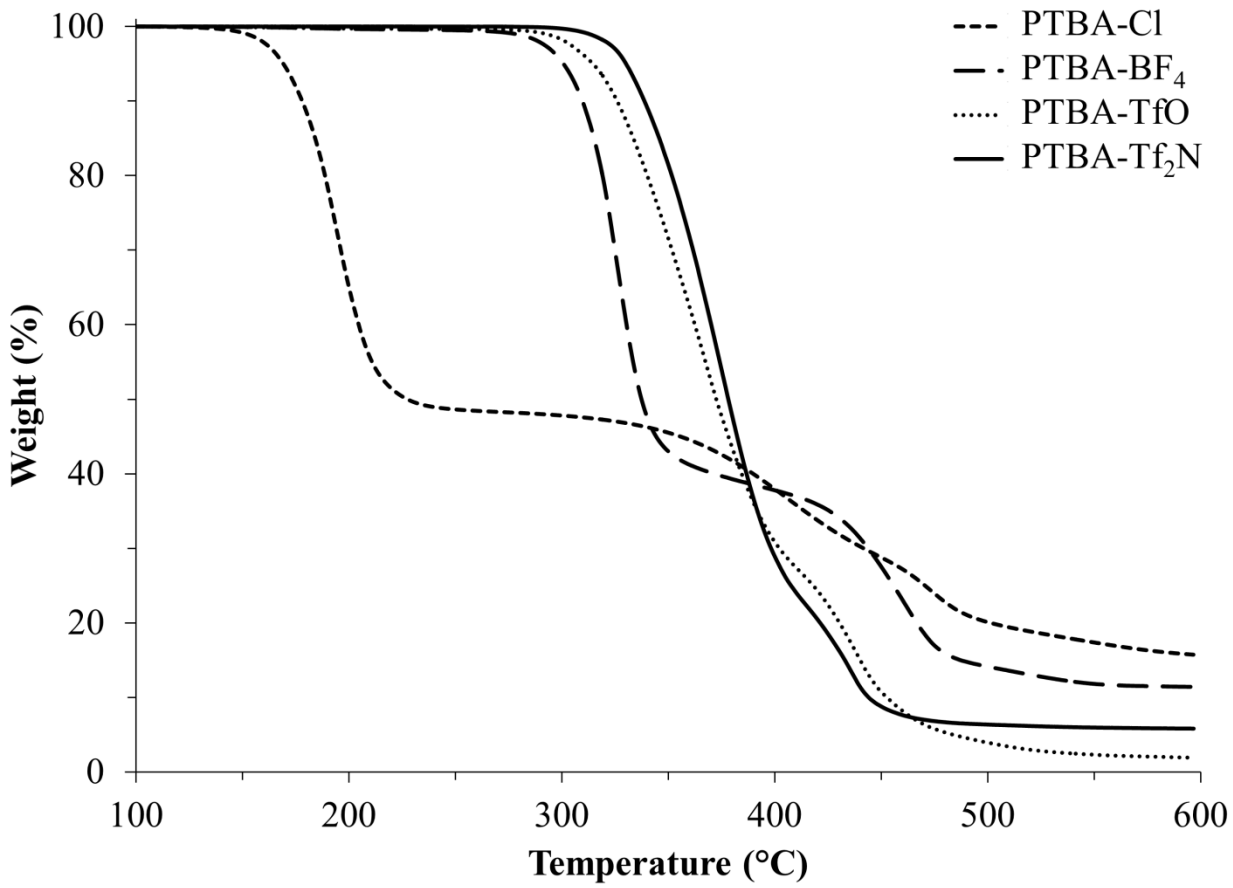

Figure 5.2. Thermogravimetric analysis of PTBA with four different anions: Cl^-, BF_4^-, TfO^-, and Tf_2N^-. Anion-exchange to bulkier, less basic anions improved the overall thermal stability of polymerized ionic liquids. TGA performed at 10 °C/min under a N_2 atmosphere.

Due to the poor thermal stability of ammonium polyelectrolytes with Cl^- counterions, glass transition temperatures (T_g) were not detected below degradation. Conversely, phosphonium polyelectrolytes with Cl^- counterions exhibited excellent thermal stabilities, enabling the determination of the T_g for each phosphonium polyelectrolyte. Longer alkyl substituent lengths on the phosphonium cation depressed the T_g of the polyelectrolytes from 240 °C for PTMP-Cl to 177 °C for PTBP-Cl. The T_g decreased as alkyl substituent length increased due to the bulkier alkyl chains, which presumably increased free volume. Similarly, anion

exchange to larger counterions depressed the T_g's of PILs in the order of Cl^- > BF_4^- > TfO^- > Tf_2N^-. Ultimately, Tf_2N^- containing PILs exhibited the lowest T_g's (<100 °C). Upon anion exchange of ammonium PILs, the thermal stabilities increased and the T_g's decreased, enabling the determination of the T_g's prior to the onset of polymer degradation. Interestingly, different cationic atoms displayed negligible differences in T_g.

5.4.3 Ionic Conductivity

Impedance spectroscopy probed the influence of alkyl substituent length and cationic center on ionic conductivity of Tf_2N-containing PILs. **Figure 5.3** reports ionic conductivities of ammonium and phosphonium PILs with Tf_2N^- counterions. All phosphonium PILs displayed higher ionic conductivities than ammonium PILs. Within the alkyl series, ethyl-containing PILs exhibited the highest ionic conductivities while butyl-containing PILs displayed the lowest ionic conductivities. Ionic conductivity is highly T_g dependent,[43] and therefore **Figure 5.4** reports ionic conductivities of PILs normalized with T_g. All phosphonium PILs displayed higher T_g–independent ionic conductivities than their ammonium analog. Comparisons of T_g–independent ionic conductivities also highlighted a significant trend between each ammonium and phosphonium PIL series, where shorter alkyl substituent lengths exhibited higher ionic conductivities (methyl > ethyl > propyl > butyl).

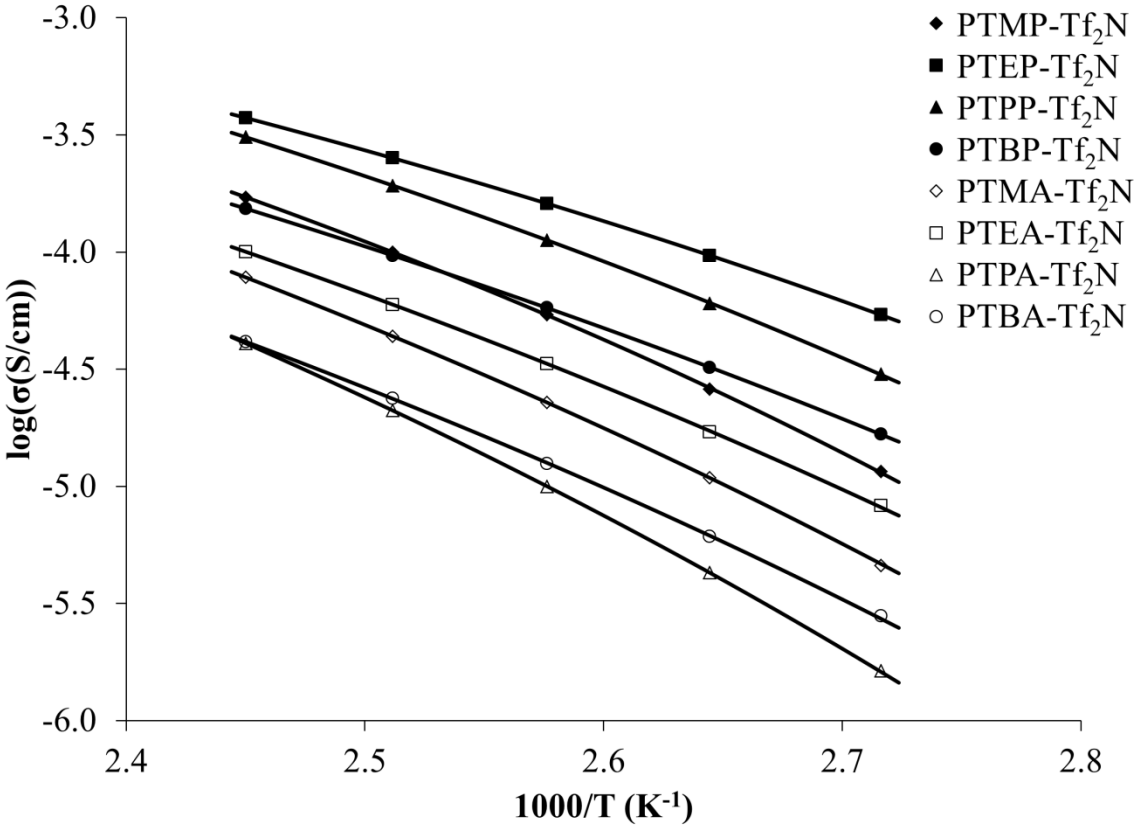

Figure 5.3. Ionic conductivity of ammonium- and phosphonium-containing polymerized ionic liquids. Phosphonium polymerized ionic liquids exhibited higher ionic conductivities than ammonium analogs. Impedance spectroscopy performed from 135°C to 95 °C in 10 °C/step using a 4-point in-plane cell.

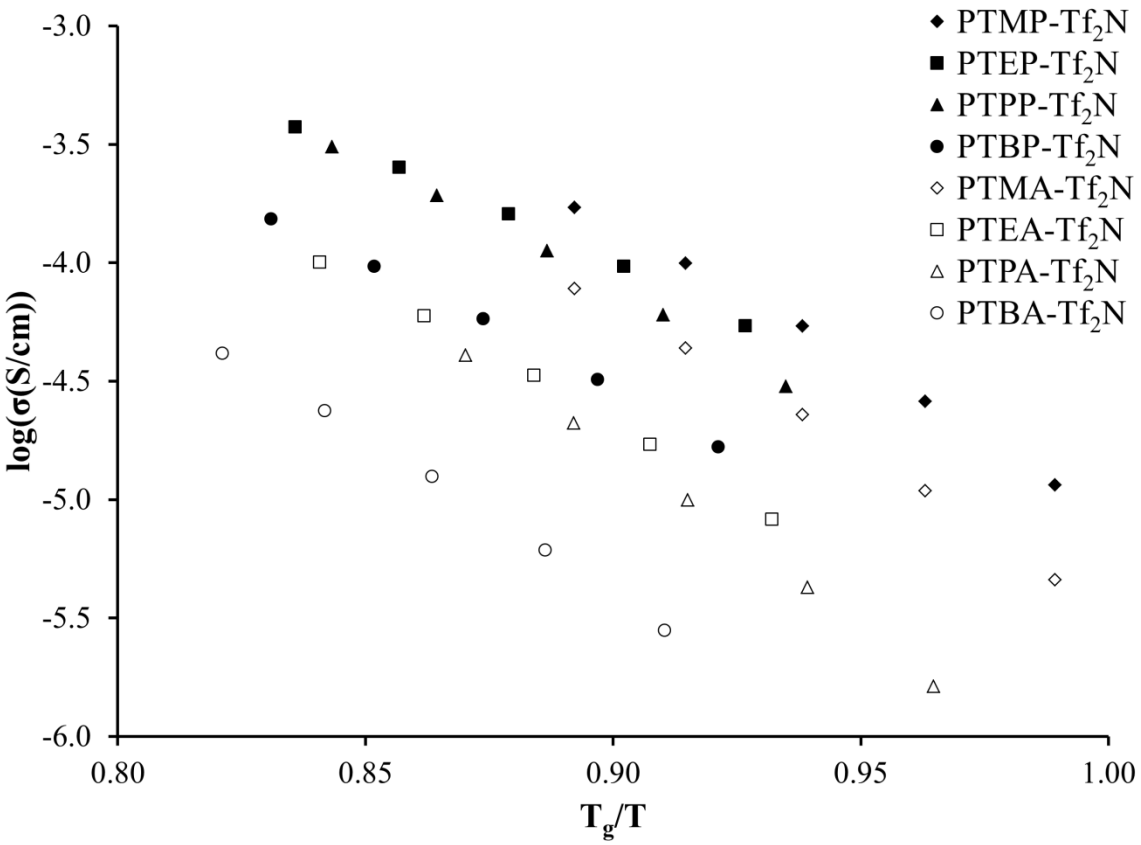

Figure 5.4. Ionic conductivity of ammonium- and phosphonium-containing polymerized ionic liquids after normalization with T_g. After T_g normalization, shorter alkyl substituent lengths demonstrated the highest ionic conductivities while phosphonium polymerized ionic liquids exhibited higher ionic conductivities than their ammonium analog. Impedance spectroscopy performed from 135°C to 95 °C in 10 °C/step at using a 4-point in-plane cell.

Three-parameter and two-parameter VFT equations were fitted to ammonium and phosphonium PILs' ionic conductivity data to extract information regarding the B value and T_0. Three-parameter VFT fits depicted as solid lines in **Figure 5.3** demonstrate acceptable fitting behavior of the data to VFT equations. Fitting the ionic conductivity data to three-parameter and

two-parameter VFT equations resulted in similar σ_{inf}, T_0, and B values. For ionic liquids, $T_g - T_0$ typically is near 50 K.[44] As shown in **Table 5.4**, all PILs exhibited significantly higher $T_g - T_0$'s from 106 to 134 K. Mahesh et. al.[42] and Elabd et. al.[39] previously reported similar findings for their PILs where $T_g - T_0$'s were greater than 50 K for PILs. VFT fitting also provided evidence for the improved ionic conductivity of phosphonium PILs compared to ammonium PILs. Specifically, B values, which correspond to an activation temperature or energy, for phosphonium PILs remained significantly lower than B values for ammonium analogs. Lower activation energies for phosphonium PILs likely relates to cationic structural differences between ammonium and phosphonium cations. Specifically, a partial negative charge lies on the nitrogen atom with a partial positive charge on the adjacent carbon atoms for the ammonium cation.[45] Conversely, the phosphorus atom bears more of the positive charge in a phosphonium cation with slightly negative adjacent carbon atoms. The slightly negative carbons presumably shield the positive charge on the phosphonium cation, minimizing ion-pairing to the counterion, decreasing the energy necessary for ion motion and conduction. Future dielectric relaxation spectroscopy experiments will aim to examine ion mobility in ammonium and phosphonium PILs.

Table 5.4. VFT and WLF fitting and analysis of PIL conductivity data.

PIL	VFT 3-Parameter (VFT 2-Parameter)			
	σ_{inf} (S/cm)	B (K)	T_0 (K)	T_g–T_0 (K)
PTMA	1.29 (1.18)	1727 (1702)	230 (231)	134 (133)
PTEA	0.75 (0.70)	1623 (1602)	226 (227)	117 (116)
PTPA	2.07 (2.10)	1888 (1889)	234 (234)	121 (121)
PTBA	0.54 (0.54)	1697 (1751)	229 (227)	106 (108)
PTMP	0.53 (0.47)	1276 (1244)	249 (251)	115 (113)
PTEP	0.23 (0.25)	1112 (1135)	235 (234)	106 (107)
PTPP	0.65 (0.59)	1307 (1280)	237 (239)	107 (105)
PTBP	0.50 (0.43)	1504 (1455)	222 (225)	117 (114)

5.4.4 Morphology

Morphology plays a major role in ion conduction and numerous reports detail the influence of morphology on ionic conductivity for block copolymers,[35] random copolymers,[46] and homopolymers.[33] **Figure 5.5** depicts WAXD profiles for ammonium and phosphonium PILs, respectively. Initial examination shows only minor changes in PIL morphology based on the cationic atom; thus, morphology played a minor role in the improved conductivity of phosphonium PILs. However, PIL morphology changed dramatically based on alkyl substituent length. Methyl- and ethyl-containing PILs displayed similar morphologies while propyl- and butyl-containing PILs exhibited comparable morphologies.

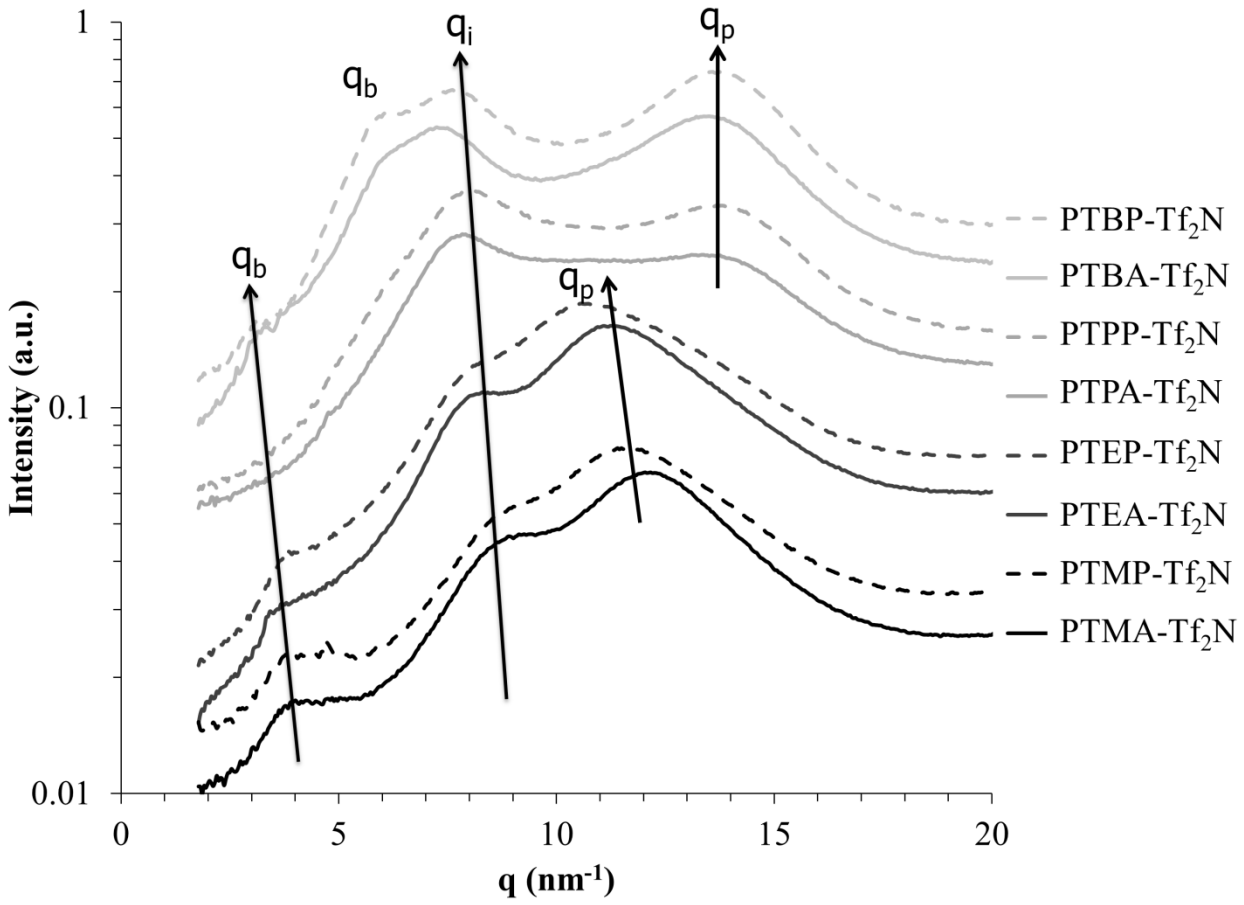

Figure 5.5. WAXD of Tf_2N-containing PILs. Alkyl substituent length dramatically impacted PIL morphology while substitution of the cationic atom resulted in similar morphologies.

Winey et al.[33,47] extensively detailed the morphology of poly(vinyl imidazolium)s and they examined the impact of anion selection and alkyl substituent length on the WAXD profiles of poly(vinyl imidazolium)s. Winey et al. defined a pendant-to-pendant spacing (q_p) between 12 – 16 nm^{-1}, which corresponded to the spacing of pendant alkyl substituents attached to the imidazolium ring. TfO^- and Tf_2N^- counterions also resulted in an additional correlation peak between 8 – 11 nm^{-1}, presumably from ion-ion correlation distances (q_i). **Figure 5.5** summarizes the defined correlations for the ammonium- and phosphonium-containing PILs with Tf_2N^-

counterions. Previously, our group reported the WAXD of PTBP-Tf_2N and PTOP-Tf_2N homopolymers; the PILs displayed two significant correlations between 3 – 8 nm^{-1}, which corresponded to non-interdigitated and interdigitated backbone-to-backbone spacings (q_b).[6] PILs with alkyl substituent lengths shorter than butyl chains displayed only a single q_b, presumably due to the inability of the shorter alkyl substituent lengths to sufficiently interdigitate. Supporting Information Figure S1 highlights the appearance of the q_i peak upon anion exchange of PTMA-Cl to PTMA-Tf_2N, which enabled the q_i peak to be defined for all Tf_2N^- PILs. The q_p peak occurred between 10 – 15 nm^{-1}, similar to q_p values for poly(vinyl imidazolium)s. Interestingly, a significant shift for q_p occured between ethyl- and propyl-containing PILs, wherein densification occurred due to the longer alkyl substituent lengths for propyl- and butyl-containing PILs resulting in larger q_p values. Overall, both q_b and q_i shifted to smaller q values as alkyl substituent lengths increased. Thus, longer alkyl substituent lengths increased the distances between both backbone-to-backbone and ion-to-ion spacings, presumably the cause of lower ionic conductivities for longer alkyl substituent lengths.

5.5 *Conclusions*

Ammonium and phosphonium polymerized ionic liquids synthesized using conventional free radical polymerization and anion metathesis displayed significantly different thermal properties and ionic conductivities. Ammonium polyelectrolytes containing Cl^- counterions displayed reduced thermal stability due to a nucleophilic degradation pathway. Phosphonium PILs displayed higher thermal stabilities than ammonium analogs, and phosphonium PILs exhibited only a single step degradation profile. Anion exchange to bulkier, less basic anions improved the thermal stability of all PILs and depressed the T_g's of PILs. Impedance spectroscopy determined ionic conductivities of Tf_2N^- containing PILs, and phosphonium PILs

displayed higher ionic conductivities than their ammonium analogs. WAXD analyzed the morphology of PILs and found no cation-dependent morphological changes while morphology varied based on alkyl substituent length. Ultimately, phosphonium PILs displayed higher thermal stabilities and ionic conductivities than their ammonium analogs, highlighting the advantageous use of phosphonium PILs for high temperature, conductive applications.

5.6 *Acknowledgements*

This material is based upon work supported in part by the U.S. Army Research Office under grant number W911NF-07-1-0452 Ionic Liquids in Electro-Active Devices (ILEAD) MURI. This material is based upon work supported in part by the U.S. Army Research Laboratory and the U.S. Army Research Office under the Army Materials Center of Excellence Program, contract W911NF-06-2-0014. This material is partially based upon work supported by the National Science Foundation under Grant No. DMR-0923107. We acknowledge funding from NSF (CHE-0722638) for the acquisition of our Agilent 6220 LC-TOF-MS. This material is based upon work supported by the Army Research Office (ARO) under Award No. W911NF-10-1-0307 (DURIP). The authors also acknowledge the Institute for Critical Technology and Applied Science (ICTAS) at Virginia Tech for facility support.

5.7 *References*

(1) Xie, W.; Xie, R.; Pan, W.-P.; Hunter, D.; Koene, B.; Tan, L.-S.; Vaia, R. *Chemistry of Materials* **2002**, *14*, 4837.
(2) Moreno, M.; Lligadas, G.; Ronda, J. C.; Galià, M.; Cádiz, V. *Journal of Polymer Science Part A: Polymer Chemistry* **2012**, *50*, 3206.
(3) Monge, S.; Canniccioni, B.; Graillot, A.; Robin, J.-J. *Biomacromolecules* **2011**, *12*, 1973.
(4) Godeau, G.; Navailles, L.; Nallet, F.; Lin, X.; McIntosh, T. J.; Grinstaff, M. W. *Macromolecules* **2012**, *45*, 2509.
(5) Ghassemi, H.; Riley, D. J.; Curtis, M.; Bonaplata, E.; McGrath, J. E. *Applied Organometallic Chemistry* **1998**, *12*, 781.
(6) Cheng, S.; Zhang, M.; Wu, T.; Hemp, S. T.; Mather, B. D.; Moore, R. B.; Long, T. E. *J. Polym. Sci., Part A: Polym. Chem.* **2012**, *50*, 166.
(7) Wang, R.; Lowe, A. B. *Journal of Polymer Science Part A: Polymer Chemistry* **2007**, *45*, 2468.
(8) Cheng, S.; Beyer, F. L.; Mather, B. D.; Moore, R. B.; Long, T. E. *Macromolecules* **2011**, *44*, 6509.
(9) Williams, S. R.; Wang, W.; Winey, K. I.; Long, T. E. *Macromolecules* **2008**, *41*, 9072.
(10) Kenawy, E.-R.; Mahmoud, Y. A. G. *Macromolecular Bioscience* **2003**, *3*, 107.
(11) Kenawy, E.-R.; Abdel-Hay, F. I.; El-Shanshoury, A. E.-R. R.; El-Newehy, M. H. *Journal of Controlled Release* **1998**, *50*, 145.
(12) Kenawy, E.-R.; Abdel-Hay, F. I.; El-Shanshoury, A. E.-R. R.; El-Newehy, M. H. *Journal of Polymer Science Part A: Polymer Chemistry* **2002**, *40*, 2384.
(13) Kanazawa, A.; Ikeda, T.; Endo, T. *Journal of Applied Polymer Science* **1994**, *53*, 1245.
(14) Kanazawa, A.; Ikeda, T.; Endo, T. *Journal of Polymer Science Part A: Polymer Chemistry* **1993**, *31*, 335.
(15) Hemp, S. T.; Smith, A. E.; Bryson, J. M.; Allen, M. H.; Long, T. E. *Biomacromolecules* **2012**, *13*, 2439.
(16) Hemp, S. T.; Allen, M. H.; Green, M. D.; Long, T. E. *Biomacromolecules* **2012**, *13*, 231.
(17) Hatakeyama, E. S.; Ju, H.; Gabriel, C. J.; Lohr, J. L.; Bara, J. E.; Noble, R. D.; Freeman, B. D.; Gin, D. L. *Journal of Membrane Science* **2009**, *330*, 104.
(18) Mecerreyes, D. *Progress in Polymer Science* **2011**, *36*, 1629.
(19) Forsyth, S. A.; Pringle, J. M.; MacFarlane, D. R. *Australian Journal of Chemistry* **2004**, *57*, 113.
(20) Smiglak, M.; Metlen, A.; Rogers, R. D. *Accounts of Chemical Research* **2007**, *40*, 1182.
(21) Huddleston, J. G.; Visser, A. E.; Reichert, W. M.; Willauer, H. D.; Broker, G. A.; Rogers, R. D. *Green Chemistry* **2001**, *3*, 156.
(22) G. Huddleston, J.; D. Rogers, R. *Chemical Communications* **1998**, 1765.
(23) Armand, M.; Endres, F.; MacFarlane, D. R.; Ohno, H.; Scrosati, B. *Nat Mater* **2009**, *8*, 621.
(24) Welton, T. *Chemical Reviews* **1999**, *99*, 2071.
(25) Scammells, P. J.; Scott, J. L.; Singer, R. D. *Australian Journal of Chemistry* **2005**, *58*, 155.
(26) Bradaric, C. J.; Downard, A.; Kennedy, C.; Robertson, A. J.; Zhou, Y. *Green Chemistry* **2003**, *5*, 143.
(27) Fraser, K. J.; MacFarlane, D. R. *Australian Journal of Chemistry* **2009**, *62*, 309.

(28) Lu, J.; Yan, F.; Texter, J. *Progress in Polymer Science* **2009**, *34*, 431.
(29) Ricks-Laskoski, H. L.; Snow, A. W. *Journal of the American Chemical Society* **2006**, *128*, 12402.
(30) Bara, J. E.; Gabriel, C. J.; Hatakeyama, E. S.; Carlisle, T. K.; Lessmann, S.; Noble, R. D.; Gin, D. L. *Journal of Membrane Science* **2008**, *321*, 3.
(31) Ye, Y.; Elabd, Y. A. *Macromolecules* **2011**, *44*, 8494.
(32) Green, M. D.; Salas‐de la Cruz, D.; Ye, Y.; Layman, J. M.; Elabd, Y. A.; Winey, K. I.; Long, T. E. *Macromolecular Chemistry and Physics* **2011**.
(33) la Cruz, D. S.; Green, M. D.; Ye, Y.; Elabd, Y. A.; Long, T. E.; Winey, K. I. *Journal of Polymer Science Part B: Polymer Physics* **2012**.
(34) Weber, R. L.; Ye, Y.; Banik, S. M.; Elabd, Y. A.; Hickner, M. A.; Mahanthappa, M. K. *Journal of Polymer Science Part B: Polymer Physics* **2011**.
(35) Weber, R. L.; Ye, Y.; Schmitt, A. L.; Banik, S. M.; Elabd, Y. A.; Mahanthappa, M. K. *Macromolecules* **2011**, *44*, 5727.
(36) Hunley, M. T.; England, J. P.; Long, T. E. *Macromolecules* **2010**, *43*, 9998.
(37) Blasig, A.; Tang, J.; Hu, X.; Shen, Y.; Radosz, M. *Fluid Phase Equilibria* **2007**, *256*, 75.
(38) Valade, D.; Boschet, F.; Roualdès, S.; Ameduri, B. *Journal of Polymer Science Part A: Polymer Chemistry* **2009**, *47*, 2043.
(39) Ye, Y.; Elabd, Y. A. *Polymer* **2011**, *52*, 1309.
(40) Layman, J. M.; Borgerding, E. M.; Williams, S. R.; Heath, W. H.; Long, T. E. *Macromolecules* **2008**, *41*, 4635.
(41) Williams, S. R.; Borgerding, E. M.; Layman, J. M.; Wang, W.; Winey, K. I.; Long, T. E. *Macromolecules* **2008**, *41*, 5216.
(42) Weber, R. L.; Ye, Y.; Banik, S. M.; Elabd, Y. A.; Hickner, M. A.; Mahanthappa, M. K. *Journal of Polymer Science Part B: Polymer Physics* **2011**, *49*, 1287.
(43) Fukumoto, K.; Yoshizawa, M.; Ohno, H. *Journal of the American Chemical Society* **2005**, *127*, 2398.
(44) Williams, M. L.; Landel, R. F.; Ferry, J. D. *Journal of the American Chemical Society* **1955**, *77*, 3701.
(45) Wang, S.-W.; Liu, W.; Colby, R. H. *Chemistry of Materials* **2011**, *23*, 1862.
(46) Mauritz, K. A.; Moore, R. B. *Chemical Reviews* **2004**, *104*, 4535.
(47) Allen, M. H.; Wang, S.; Hemp, S. T.; Chen, Y.; Madsen, L. A.; Winey, K. I.; Long, T. E. *Macromolecules* **2013**.

Chapter 6: Phosphonium-Containing Polyelectrolytes for Nonviral Gene Delivery

(Published in *Biomacromolecules* **2012,** *13* (1), 231-238.)

Sean T. Hemp, Michael H. Allen, Jr., Matthew D. Green,[‡] and Timothy E. Long*

Departments of Chemistry, Macromolecules and Interfaces Institute, and Chemical Engineering,[‡] Virginia Tech, Blacksburg, VA 24061

*To whom correspondence should be addressed. E-mail: telong@vt.edu. TEL: (540)231-2480 FAX: (540)231-8517

Keywords: nonviral gene delivery, polyelectrolytes, phosphonium, ammonium

6.1 *Abstract*

Nonviral gene therapy focuses intensely on nitrogen-containing macromolecules and lipids to condense and deliver DNA as a therapeutic for genetic human diseases. For the first time, DNA binding and gene transfection experiments compared phosphonium-containing macromolecules to their respective ammonium analogs. Conventional free radical polymerization of quaternized 4-vinylbenzyl chloride monomers afforded phosphonium- and ammonium-containing homopolymers for gene transfection experiments of HeLa cells. Aqueous size exclusion chromatography confirmed similar absolute molecular weights for all polyelectrolytes. DNA gel shift assays and luciferase expression assays revealed phosphonium-containing polymers bound DNA at lower charge ratios and displayed improved luciferase expression relative to the ammonium analogs. The triethyl-based vectors for both cations failed to transfect HeLa cells while tributyl-based vectors successfully transfected HeLa cells similar to Superfect® demonstrating the influence of the alkyl substituent lengths on the efficacy of the gene delivery vehicle. Cellular uptake of Cy5-labeled DNA highlighted successful cellular

uptake of triethyl-based polyplexes showing that intracellular mechanisms presumably prevented luciferase expression. Endocytic inhibition studies using genistein, methyl β-cyclodextrin, or amantadine demonstrated the caveolae-mediated pathway as the preferred cellular uptake mechanism for the delivery vehicles examined. Our studies demonstrated changing the polymeric cation from ammonium to phosphonium enables an unexplored array of synthetic vectors for enhanced DNA binding and transfection that may transform the field of nonviral gene delivery.

6.2 *Introduction*

Nonviral gene delivery is a rapidly growing field of biomedical research for polymer chemistry focused on the therapeutic delivery of DNA to treat and potentially cure various genetic diseases.[1-3] Cationic polymers or lipids electrostatically complex and compact DNA to form a polyplex or lipoplex, respectively, to effectively deliver DNA to cells.[4,5] These nanoparticles inhibit cellular enzymatic degradation of DNA during delivery to the nucleus[6] and also provide an avenue for cellular uptake,[7] endosomal escape,[8] and trafficking to the nucleus with subsequent release of the DNA.[9] The cationic polymers and lipids of major focus commercially and academically for gene delivery include polyethyleneimine (PEI),[10,11] Lipofectamine™,[12,13] Superfect®,[14,15] and chitosan.[16,17] Currently, numerous researchers concentrate primarily on modifying the chemical composition and architecture of nitrogen-containing polymers including ammonium and imidazolium cations for gene delivery to investigate various structure-property relationships including acetylation,[18,19] PEGylation,[20-22] attachment of targeting ligands,[23,24] controlling charge density,[25,26] incorporating hydrogen bonding,[26,27] and topology.[28,29]

Phosphorus-containing macromolecules are widely studied in a variety of fields and applications due to their improved thermal stability,[30] flame retardency,[31] and biocompatibility.[32] Substitution of cationic phospholipid head groups from ammonium to phosphonium or arsenium in antitumor lipids decreased cytotoxicity while maintaining efficacy.[33] Few references concentrate on the structure-property relationship between different cationic centers for nonviral gene delivery. Clément et al. first successfully synthesized and examined ammonium-, phosphonium-, and arsenium-containing lipids for nonviral gene delivery.[34-36] In these lipid-based gene delivery vectors, they found modifying the cationic head group from ammonium to phosphonium or arsenium improved gene delivery *in vivo* and *in vitro* and decreased cytotoxicity. The phosphonium and arsenium lipid-based vectors also displayed improved solution stability. Tang et. al. functionalized chitosan through amidation to generate a chitosan with roughly 3-4 mol% incorporation of a phosphonium substituent and they found the water-soluble chitosan displayed negligible cytotoxicity but did not investigate gene transfection with these polymers.[37]

Cellular uptake of polyplexes predominately occurs through either clathrin- or caveolae-mediated endocytosis.[38] Clathrin and dynamin cause invagination and pinching-off of vesicles respectively in the clathrin pathway.[39] Vesicles originating from clathrin-mediated endocytosis undergo acidification to form an endosome (pH ~ 5-6) and eventually fuse with lysosomes (pH ~5) where enzymatic degradation occurs. The proton sponge hypothesis is often invoked throughout the literature as an avenue for polymers with large buffering capacity to display increased transfection efficiency.[40-43] The proton sponge hypothesis relies on protonatable sites on cationic vectors that buffer the endosome during acidification causing the influx of Cl^- ions with the increased osmotic pressure rupturing the endosome. Caveolae-mediated endocytosis requires a high concentration of caveolin (a protein) and cholesterol on the cell membrane

surface to generate a caveosome.[44] The resulting caveosome undergoes an indirect pathway to the lysosome enabling more efficient transfection.[38,45-47]

Herein, we report for the first time to our knowledge the synthesis and characterization of phosphonium-containing macromolecules for nonviral gene delivery. We directly compared phosphonium-containing macromolecules to ammonium-containing analogs to elucidate the influence of the cationic site on transfection efficiency. We also demonstrated the effect of varying alkyl substituent length on DNA delivery. These vectors did not contain protonatable sites pointing to a different endosomal escape mechanism other than the proton sponge effect. The polyelectrolytes were examined for their ability to bind and deliver DNA to HeLa cells using DNA binding assays, dynamic light scattering (DLS), cytotoxicity assays, luciferase expression assays, and wide-field fluorescence optical microscopy. We found both substitutions (cation and alkyl substituent lengths) greatly influenced transfection efficiency of the vectors. Endocytic inhibition studies determined the preferred endocytic pathway for these polyelectrolytes.

6.3 *Experimental Section*

6.3.1 Materials

Triethylamine (99.5%), tributylamine (≥98.5%), triethylphosphine (99%), tributylphosphine (≥93.5%), and 4-vinylbenzyl chloride (≥90%) were purchased from Sigma Aldrich and used as received. α,α'-Azoisobutyronitrile (AIBN) was purchased from Sigma Aldrich and recrystallized from methanol. Triethyl-(4-vinylbenzyl)ammonium chloride, tributyl-(4-vinylbenzyl)ammonium chloride, and tributyl-(4-vinylbenzyl)phosphonium chloride were

synthesized as previously reported in the literature.[48] All solvents were obtained from Sigma Aldrich and used as received.

6.3.2 Analytical Methods

^{1}H NMR spectroscopy was performed on a Varian Unity 400 at 400 MHz in $CDCl_3$ or D_2O. Mass spectrometry was performed with an Agilent 6220 LC-TOF-MS system. Aqueous size-exclusion chromatography (SEC) was performed using a Waters 1515 Isocratic HPLC Pump and Waters 717plus Autosampler with Waters 2414 Refractive Index and Wyatt MiniDAWN MALLS detectors at a flow rate of 0.8 mL/min. Two Waters Ultrahydrogel Linear and one Waters Ultrahydrogel 250 columns were utilized. The aqueous solvent was composed of 54/23/23 (v/v/v %) water/methanol/acetic acid with 0.1 M sodium acetate. DLS confirmed the absence of polymer aggregates in the aqueous SEC solvent. Absolute molecular weights were obtained from the MALLS detector after determining the d*n*/d*c* offline using a Wyatt Optilab T-rEX Differential Refractometer at 658 nm and 35 °C. Statistical analysis of the transfection experiments was performed using the Student's t-test.

6.3.3 Monomer Synthesis

All monomers were synthesized following similar procedures in the earlier literature.[48] The synthesis of triethyl-(4-vinylbenzyl)phosphonium chloride follows as an example. Dry acetonitrile (30 mL) was added to a flame-dried 100-mL round-bottomed flask, containing a magnetic stir bar, using a cannula. 6.0 mL 4-vinylbenzyl chloride (42.6 mmol) and 5.4 mL triethylphosphine (36.7 mmol) were added to the flask. The yellow solution was heated to 40 °C for 24 h and the monomer was precipitated into 1 L of a 75:25 hexanes:ethyl acetate mixture. The solid was vacuum filtered and washed with hexanes. The resulting white crystals were dried

at reduced pressure (0.5 mmHg) to obtain a final yield of 9.4 g (95% yield). ^{1}H NMR (400 MHz, $CDCl_3$, 25 °C) (δ, ppm): 1.21 (m, CH_3-, 9H), 2.46 (m, -CH_2-, 6H), 4.24 (d, -Ar-CH_2-P-, 2H), 5.26 (d, CH_2=, 1H), 5.73 (d, CH_2=, 1H), 6.63 (dd, =CH, 1H), 7.34 (d, ArH, 2H), 7.41 (dd, ArH, 2H). ^{13}C NMR: 6.11 (d, CH_3-), 12.27 (d, -PCH_2-), 26.14 (d, $ArCH_2P$), 115.05 (d, CH_2=), 127.21 (d, Ar), 127.89 (d, Ar), 130.49 (d, Ar), 135.87 (d, Ar), 137.74 (d, Ar). ^{31}P NMR: 36.79. Mass Spectrometry: Theoretical m/z 270.1304 Experimental m/z 270.1296.

6.3.4 Polymer Synthesis

In a typical polymerization, 1.0032 g of triethyl-(4-vinylbenzyl)ammonium chloride monomer was added to a 25-mL, round-bottomed flask with 50/50 (v/v %) DMF/dH_2O, 3.2 mg of AIBN (0.02 mmol, 0.5 mol%), and stir bar at a concentration of 10 wt% solids. The flask was sealed and purged with argon for 30 min to remove oxygen. The polymerization was then conducted at 65 °C for 24 h. The resulting polymer solution was dialyzed against dH_2O for 2 days to remove monomer and DMF and then lyophilized to obtain a white powder in 60-80% yield.

6.3.5 DNA Binding Assay

Agarose gels were prepared with 0.6 g of agarose in 60 mL of 1X Tris-acetate-EDTA (TAE, Sigma Aldrich) buffer and 6 µL of SYBR Green I (Sigma Aldrich) as a fluorescent stain for DNA. Polyplexes were prepared using 0.2 µL of gWiz-Luc plasmid DNA (1 µg/µL in H_2O, Aldevron) and the required amount of polymer to obtain a desired +/- ratio (positively charged cation in the polymeric vector to negatively charged phosphate in DNA) in a 1X TAE buffer solution (28 µL total volume). The polyplexes were incubated for 30 min at 23 °C and then 7 µL of gel loading buffer (Sigma Aldrich) was added. The polyplexes were loaded onto the gel and

metered at 70 V for 90 min. The gels were imaged using a MultiDoc-it™ Digital Imaging System (UVP).

6.3.6 Dynamic Light Scattering

Dynamic light scattering (DLS) was performed on a Malvern Zetasizer Nano ZS utilizing disposable zeta potential cells to obtain both polyplex diameter and zeta potential. 2.0 µg of gWiz-Luc DNA was added to 0.5 mL of Opti-MEM (Invitrogen) while the appropriate amount of polymer required to reach a desired +/- ratio was added to another vial of 0.5 mL Opti-MEM. The polymer Opti-MEM solution was added to the DNA Opti-MEM solution and incubated for 30 min prior to measurement. All size and zeta potential measurements were repeated in triplicate at 25 °C.

6.3.7 Cell Culture

Human cervical cancer (HeLa) cells were obtained from ATCC (Manassas, VA) and incubated in Dulbecco's modified Eagle's media (DMEM) supplemented with 10% fetal bovine serum (FBS), 100 U/mL of penicillin, and 100 µg/mL of streptomycin. Cells were incubated at 37 °C in 95% humidity with 5% CO_2. All components were obtained from Mediatech.

6.3.8 Cytotoxicity Assay

The 3-[4,5-dimethylthiazol-2-yl]2,5-diphenyltetrazolium bromide (MTT, Sigma Aldrich) colorimetric assay was utilized to determine polymer cytotoxicity. 100 µL of a 50,000 HeLa cells/mL solution was added to each well of a 96-well plate. The cells were incubated for 24 h at 37 °C with 5% CO_2. Each well was aspirated and rinsed with DMEM prior to application of polymer solutions. Polymer solutions were prepared containing varying amounts of polymer and Opti-MEM to obtain a range of polymer concentrations. Polymer solutions were applied and the

cells were incubated for 24 h. After incubation, the polymer solutions were removed and the cells rinsed with 100 µL of DMEM. 100 µL of a 0.5 mg/mL MTT solution in DMEM was added to each well and the cells were incubated for 4 h. The MTT solution was removed using suction and then 100 µL of DMSO was added to dissolve the formazan product. A Molecular Devices SpectraMax M2 was utilized to measure the resulting solutions absorbance at 570 nm. Cell viabilities were compared to control wells containing no polymer to determine the cytotoxicity of the polymers. For polyplex cytotoxicity, 100 µL of a 50,000 HeLa cells/mL solution was added to each well of a 96-well plate and allowed to incubate for 24 h. After aspirating and rinsing with 100 µL of Hank's buffered salt solution (HBSS), 100 µL of the polyplex solution (2 µg DNA/mL and the required polymer amount to obtain the desired +/- ratio in Opti-MEM) were applied and the cells were incubated for 4 h. The polyplex solutions were removed and 100 µL of complete media was added to each well. After 48 h of incubation, the complete media was aspirated and the cells were rinsed with 100 µL of DMEM. The above procedure involving the addition and incubation of the MTT solution was performed, and the cell viability was analyzed in the same manner as the free polymer MTT cytotoxicity assay.

6.3.9 Luciferase Expression Assay

Polyplexes were formed in Opti-MEM with final gWiz-Luc concentrations of 2.0 µg/mL and the appropriate amount of polymer required to reach the desired +/- ratio. Superfect® and Jet-PEI polyplexes were prepared and applied to cells according to manufacturer specifications. Upon addition of the polymer, the polyplexes were incubated for 30 min prior to application to the cells. Wells in a 24-well plate were seeded with 100,000 HeLa cells 24 h prior to transfection and the cells were rinsed with 300 µL HBSS before polyplex application. 500 µL of each polyplex solution corresponding to 1 µg DNA/well was applied to each well. After 4 h of

incubation, the polyplex solutions were aspirated and 500 µL of complete media was added. The cells were incubated for a total of 48 h after transfection. The media was aspirated at 48 h, the cells were rinsed with 300 µL of PBS, and then 120 µL of a 1 X lysis buffer (Promega) was added. The cells were incubated for 30 min at 37 °C then subjected to multiple freeze-thaw cycles to fully lyse the cells. A Promega luciferase assay kit was utilized according to the manufacturer's protocol to determine the luciferase activity. Protein concentration was determined using a Pierce BCA Protein Assay kit according to the enclosed directions. Gene expression was reported as relative light units per mg of cell protein lysate (RLU/mg). Experiments were repeated twice in quadruplicate. Serum transfections were performed similarly to the above except 400 µL of complete media was added to each well and then 100 µL of the polyplex solutions (10 µg DNA/mL) in Opti-MEM were added for a total of 1 µg DNA/well.

The endocytic inhibition luciferase assay followed the same procedure as the above serum-free luciferase transfection except for the initial pre-incubation of the cells with the inhibitory drugs. Prior to polyplex addition, 500 µL of genistein (100 µg/mL in Opti-MEM), methyl β-cyclodextrin (20 mg/mL in Opti-MEM), and amantadine (2 mM in Opti-MEM) solutions were applied to individual wells. After 1 h incubation, 500 µL of the polyplex solution (+/- ratio of 4, 2µg DNA/mL in Opti-MEM) was applied to each well for a total transfection volume of 1 mL and half the initial inhibitory drug concentrations. The serum-free luciferase transfection protocol was then followed from the point of the polyplex incubation. Luciferase expressions from each drug inhibition were compared to control transfection wells with no drug inhibition.

6.3.10 Wide-Field Fluorescence Optical Microscopy

6.3.10.1 Polyplex Uptake

Cy5-labeled gWiz-Luc plasmid (0.1 μg/μL in H_2O) was diluted in Opti-MEM to a concentration of 4.0 μg/mL. Simultaneously, the polyelectrolytes were diluted in Opti-MEM to a final concentration corresponding to a +/- ratio of 4. These solutions were incubated for 10 min before adding the polymer to the pDNA and then incubated at 23 ^{o}C for 30 min. HeLa cells were plated into 24 well plates at a cell density of 100,000 cells/well 24 h prior to polyplex exposure. The cells were rinsed with HBSS and 0.5 mL of transfection solution was added to each well. The cells were incubated at 37 ^{o}C and 5% CO_2 for 2 h. Cellular nuclei were stained through the addition of 1 μL of 4',6-diamidino-2-phenylindole (DAPI, 1 μg/μL in PBS) to the transfection solution and incubated for 10 min at 37 ^{o}C. The cells were then rinsed twice with PBS, fixed with 0.5 mL paraformaldehyde (2 wt% in PBS) for 10 min at 37 ^{o}C, and cellular membranes were permeabilized with 0.5 mL TritonX-100 (0.1 vol% in PBS) for 10 min at 37 ^{o}C. The cells were rinsed with PBS, and the cellular F-Actin were stained with 0.5 mL of Alexa Fluor 488 phalloidin (5 U/mL in PBS) for 10 min at 37 ^{o}C. The cells were rinsed with PBS, and then stored in PBS. Images were acquired using Cy5, UV-2EC, and F/EGFP fluorescence filters using a Nikon Eclipse TE2000-U inverted microscope equipped with a Nikon C-HGFI Intensilight light source and Nikon DS-Qi,Mc B&W CCD camera.

6.3.10.2 GFP Expression

gWiz-GFP plasmid (1 μg/μL in H_2O) was diluted in Opti-MEM to a concentration of 4.0 μg/mL. Simultaneously, the vectors were diluted in Opti-MEM to a final concentration corresponding to a +/- ratio of 4. These solutions were incubated for 10 min before adding the

polymer to the pDNA and then incubated at 23 ^{o}C for 30 min. Superfect® and Jet-PEI polyplexes were prepared according to the manufacturer's suggestion. HeLa cells were plated into 24 well plates at a cell density of 100,000 cells/well 24 h prior to polyplex exposure. The cells were rinsed with HBSS and 0.5 mL of transfection solution was added to each well. The cells were incubated at 37 ^{o}C and 5% CO_2 for 4 h. The transfection media was then removed and replaced with complete DMEM, and the cells were incubated at 37 ^{o}C, 5% CO_2 for 48 h. After 48 h, cellular nuclei were stained through the addition of 1 μL DAPI (1 μg/μL in PBS) to the transfection solution and incubated for 10 min at 37 ^{o}C. The cells were then rinsed twice with PBS, fixed with 0.5 mL paraformaldehyde (2 wt% in PBS) for 10 min at 37 ^{o}C, and the cellular membrane was permeabilized with 0.5 mL TritonX-100 (0.1 vol% in PBS) for 10 min at 37 ^{o}C. The cells were rinsed with PBS, and the cellular F-Actin was stained with 12.5 μL Alexa Fluor 647 phalloidin (200 U/mL in methanol) for 10 min at 37 ^{o}C. The cells were rinsed with PBS, and then stored in PBS. Images were acquired using Cy5, UV-2EC, and F/EGFP fluorescence filters using a Nikon Eclipse TE2000-U inverted microscope equipped with a Nikon C-HGFI Intensilight light source and Nikon DS-Qi,Mc B&W CCD camera.

6.4 *Results and Discussion*

6.4.1 Polymer Synthesis and Characterization

Conventional free radical polymerization of styrenic-based ammonium and phosphonium monomers afforded the opportunity to evaluate the influence of cation structure on nonviral gene delivery (**Scheme 6.1**). Varying the length of the alkyl substituent attached to the cation also provided additional control over macromolecular structure to give a better understanding of the impact of structure on DNA delivery. Polymerization of functional monomers enabled the

synthesis of a fully quaternized polyelectrolyte in contrast to post-polymerization quaternization of poly(4-vinylbenzyl chloride) that does not ensure quantitative functionalization. The ammonium- and phosphonium-containing polyelectrolytes included poly(triethyl-(4-vinylbenzyl)ammonium chloride) (PTEA), poly(tributyl-(4-vinylbenzyl)ammonium chloride) (PTBA), poly(triethyl-(4-vinylbenzyl)phosphonium chloride) (PTEP), and poly(tributyl-(4-vinylbenzyl)phosphonium chloride) (PTBP).

Scheme 6.1. Conventional free-radical polymerization of ammonium- and phosphonium-containing styrenic homopolymers to afford gene delivery vectors with different alkyl substituent lengths.

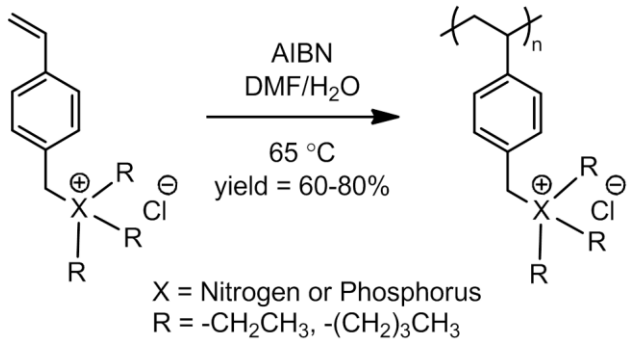

Aqueous SEC-MALLS determined the absolute molecular weights of all the ammonium- and phosphonium-containing styrenic-based polymers. The aqueous SEC solvent, i.e. 54/23/23 (v/v/v/ %) water/methanol/acetic acid with 0.1 M sodium acetate,[49] dissolved the polyelectrolytes without aggregation, and the polyelectrolytes successfully eluted from the SEC columns shown in **Figure 6.1**. **Table 6.1** summarizes the absolute molecular weights for the ammonium and phosphonium polyelectrolytes. Long et al. showed previously that molecular weight variance influences transfection as higher molecular weight PDMAEMA-HCl samples improved gene delivery compared to lower molecular weight PDMAEMA-HCl.[50] All polymers displayed similar absolute number-average molecular weights ($\overline{M}_n$) with typical polydispersities

for conventional free-radical polymerization, therefore, minimizing the influence of molecular weight on transfection efficiency.

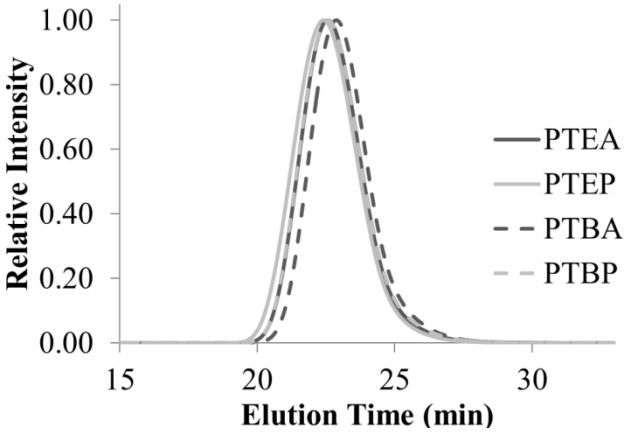

Figure 6.1. Aqueous SEC curves for the ammonium- and phosphonium-containing polyelectrolytes. MALLS detector traces are shown highlighting the similarity in absolute molecular weights of all the samples.

Table 6.1. Absolute molecular weight analysis of the ammonium- and phosphonium-containing gene delivery vectors.

Sample	$\overline{M}_n$ (kg/mol)	$\overline{M}_w$ (kg/mol)	$\overline{M}_w / \overline{M}_n$
PTEA	230	384	1.67
PTBA	224	389	1.74
PTEP	304	484	1.59
PTBP	254	462	1.82

6.4.2 DNA Binding and DLS Analysis

DNA gel shift assays examined the affinity of all four polymers for DNA: PTEA, PTBA, PTEP, and PTBP (**Figure 6.2**). Typically, researchers utilize N/P ratios to create different polyplexes where N corresponds to protonated/protonatable nitrogens and P corresponds to negatively charged phosphates in the DNA backbone.[23] We defined a similar ratio called a +/- ratio (charge ratio) where + corresponds to quaternized cationic charges and - corresponds to

negatively charged phosphates in the DNA backbone. The ammonium polyelectrolytes bound DNA at a +/- ratio of 4 while the phosphonium polyelectrolytes bound DNA at a +/- ratio of 2, which suggested improved DNA binding of phosphonium cations over ammonium cations. Phosphorus, structurally a larger and less electronegative atom than nitrogen, forms larger cations with different electron density distributions compared to ammonium cations.[51] Colby et. al. reported *ab initio* calculations of the charge distribution on the cationic atom and the surrounding carbons for tetrabutylphosphonium and tetrabutylammonium cations.[51] Since nitrogen has a higher electronegativity than carbon, the positive charge was distributed on the adjacent carbons (+0.375e for each carbon) while the nitrogen atom had a negative charge (-0.5e). For the tetrabutylphosphonium cation, the charge distribution was reversed with a positive charge on the phosphorus (+1.1e) and a negative charge on the adjacent carbons (-0.025e for each carbon). We propose that a combination of different charge densities and cation sizes influenced the DNA binding affinity of the polyelectrolytes causing the phosphonium polyelectrolytes with a larger cation and less diffuse positive charge to bind DNA more effectively.

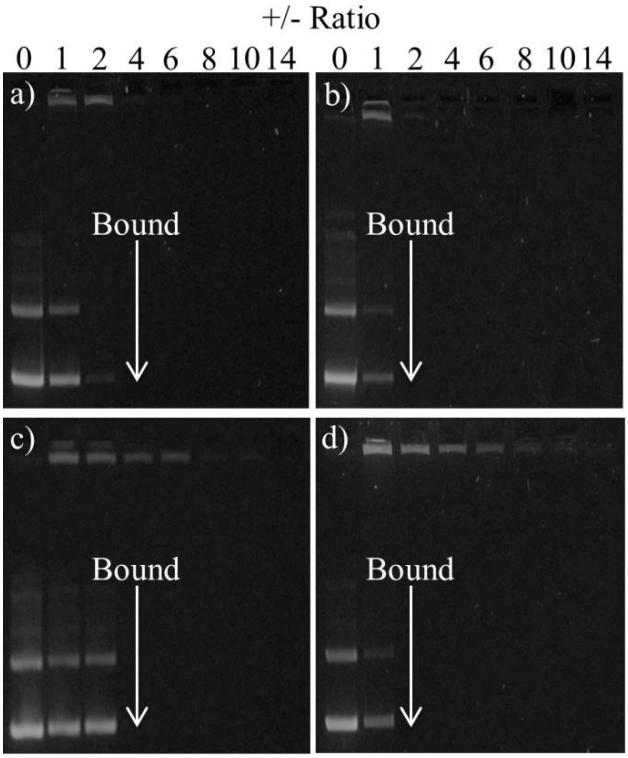

Figure 6.2. DNA binding assays for the ammonium- and phosphonium-containing polyelectrolytes: a) PTEA b) PTEP c) PTBA d) PTBP.

The DNA gel shift assay also showed differences between the triethyl- and tributyl-based polyelectrolytes. Upon complete DNA binding, the triethyl-containing polyelectrolytes quenched SYBR Green I fluorescence while the tributyl-containing polyelectrolytes required higher +/- ratios to fully quench fluorescence. SYBR Green I must bind to dsDNA to fluoresce green;[52] therefore, the absence of fluorescence indicated tight polyplex formation blocking access to the DNA strands for binding. While not quantitative, the DNA binding gel highlighted an improved DNA binding ability for shorter alkyl substituent lengths due to either lower steric hindrance or hydrophobicity than the longer alkyl substituent length polyelectrolytes.[53]

DLS determined the polyplex diameter and zeta potential for the ammonium and phosphonium polyelectrolytes (**Figure 6.3**). All polyelectrolytes except for PTBP condensed DNA into polyplexes near 200 nm or less at +/- ratios of 4 or higher. These polyelectrolytes also

exhibited a plateau in their zeta potential without significant change from a +/- ratio of 2 to 10. PTBP polyplexes generated at a +/- ratio of 2 had zeta potentials near neutral, and the polyplexes were greater than 300 nm until a +/- ratio of 6, which was significantly different from the other polyelectrolytes. The zeta potentials of the triethyl-based polyplexes were more positive than the tributyl-based polyplexes due to hydrophobic screening of the cationic charge with longer alkyl chains.[54] Zeta potentials of the free polymers in Opti-MEM (1 mg/mL) showed a similar trend of higher zeta potentials for the triethyl-containing polyelectrolytes. The polyplex diameter and zeta potential for all polyelectrolytes plateaued at higher +/- ratios suggesting that additional polymer remained as free polymer in solution uncomplexed to DNA.

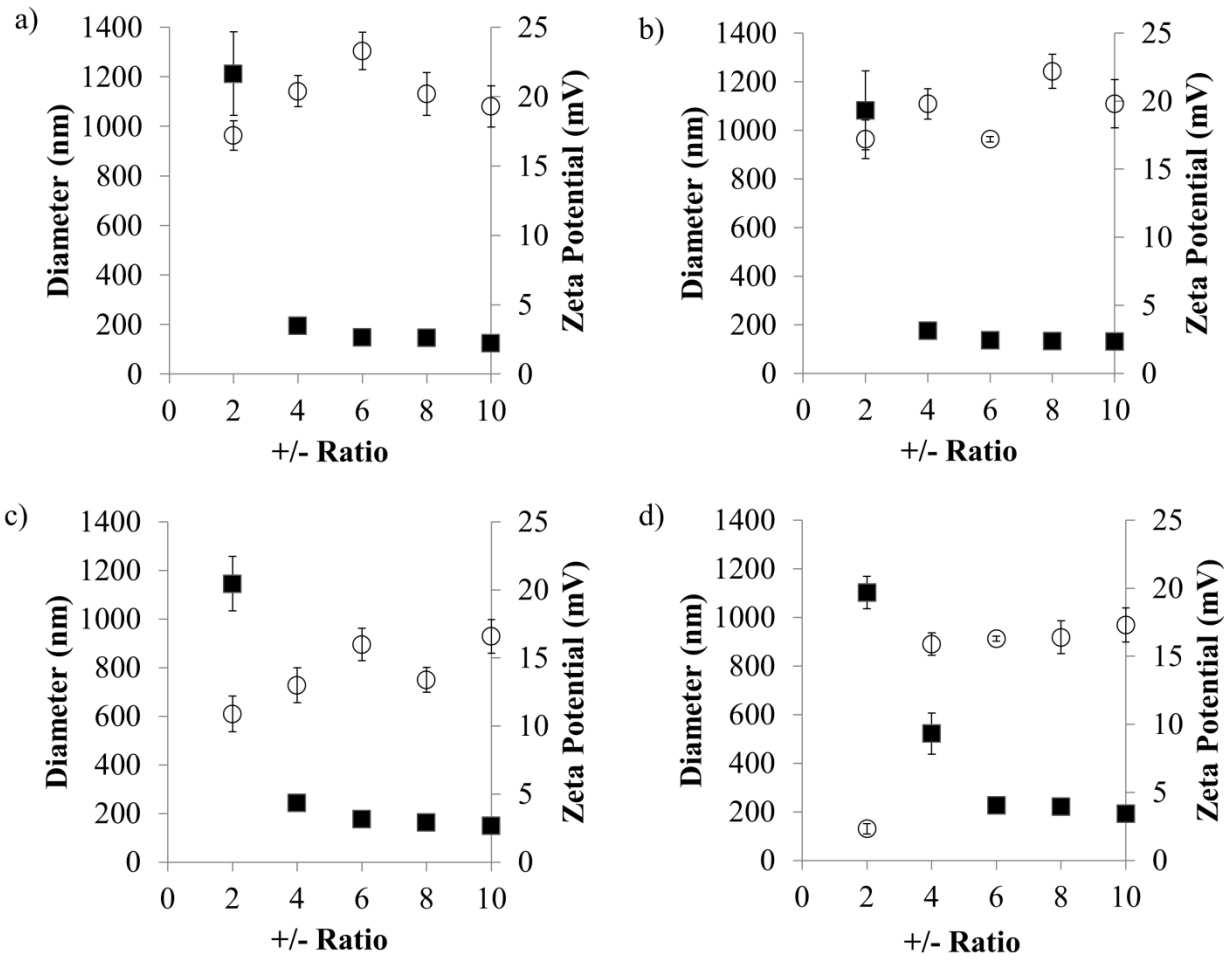

Figure 6.3. Polyplex diameter (squares) and zeta potential (circles) of the various ammonium- and phosphonium-containing polyplexes: a) PTEA b) PTEP c) PTBA d) PTBP.

6.4.3 Cytotoxicity and Transfection Assays

MTT colorimetric assays determined the cytotoxicity of both free polymer and polyplexes in HeLa cells (**Figure 6.4**). These polyelectrolytes demonstrated high toxicity to HeLa cells primarily due to their high charge density.[55] All polyelectrolytes exhibited similar cytotoxicities and were non-toxic to 3 µg/mL with significant toxicity occurring at 5 µg/mL. The polyplexes with these polyelectrolytes were also toxic at the +/- ratio of 2 as shown in **Figure 6.5**. Their polyplex cytotoxicity approximately equaled Jet-PEI's cytotoxicity at a +/-

ratio of 2. Ammonium- and phosphonium-containing polyplexes exhibited similar cytotoxicities. DLS analysis suggests that cytotoxicity at higher +/- ratios may result from free polymer in solution.

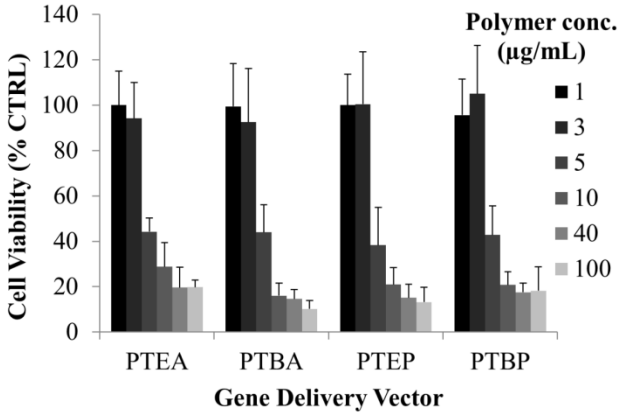

Figure 6.4. Cytotoxicities of the ammonium- and phosphonium-containing gene delivery vectors (n = 8). All polymers exhibited similar toxicities due to their 100% charge density.

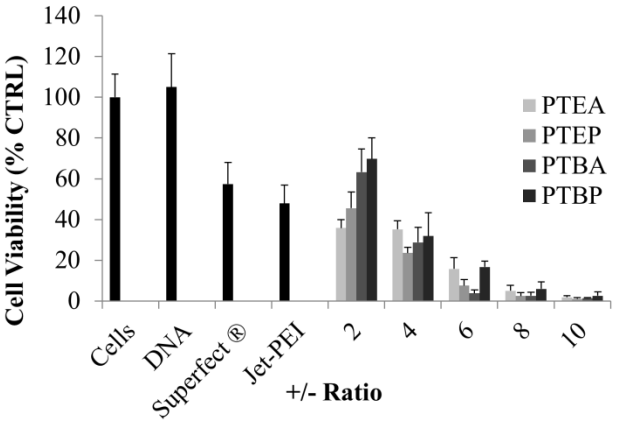

Figure 6.5. Polyplex cytotoxicities of the ammonium- and phosphonium-containing gene delivery vectors (n = 8).

Serum-free luciferase expression for each styrenic polyelectrolyte compared to negative and positive controls determined their efficacy for gene transfection and protein expression (**Figure 6.6**). Both PTEA and PTEP displayed poor transfection efficiency compared to Superfect® and Jet-PEI while PTBA and PTBP exhibited excellent transfection efficiency

similar to Superfect®. In fact, PTBP showed higher transfection efficiency than PTBA and Superfect® ($p < 0.05$). Stayton et al. focused on the synthesis of diblock copolymers containing a cationic block for siRNA condensation and a terpolymer amphiphilic block for endosomal release.[56,57] When Stayton incorporated higher mol% of n-butyl methacrylate into the endosomolytic block, siRNA delivery improved and the hemolytic activity of the diblock copolymers increased. Upon endocytosis and endosomal acidification, the terpolymer block became cationic enabling the block to presumably electrostatically associate with the endosome membrane. Upon association, the hydrophobic n-butyl methacrylate in the endosomolytic block inserted into the hydrophobic membrane ultimately disrupting and lysing the endosome membrane achieving polyplex escape. Both PTEP and PTBP polyplexes (+/- ratio of 4) successfully entered the cell as determined using Cy5-labeled DNA and wide-field fluorescence optical microscopy (**Figure 6.7**). The larger and higher intensity polyplexes presumably correlated to aggregated intracellular polyplexes. Since the triethyl-based polyplexes were successfully taken up into HeLa cells, their poor transfection resulted from other intracellular mechanisms preventing transfection such as endosomal escape or DNA release. In our polyelectrolytes, we propose that the tributyl-containing polyelectrolytes with longer, more hydrophobic, alkyl chains aided in membrane destabilization and endosomal release similar to Stayton's endosomolytic block. Additionally, the DNA gel shift assays demonstrated tighter DNA binding potentially leading to reduced DNA release and transfection for the triethyl-based polyplexes.[58]

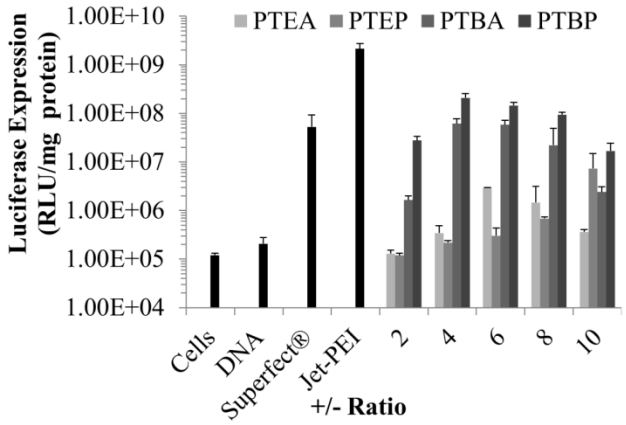

Figure 6.6. Serum-free luciferase expression of the ammonium- and phosphonium-containing polyelectrolytes (n = 4).

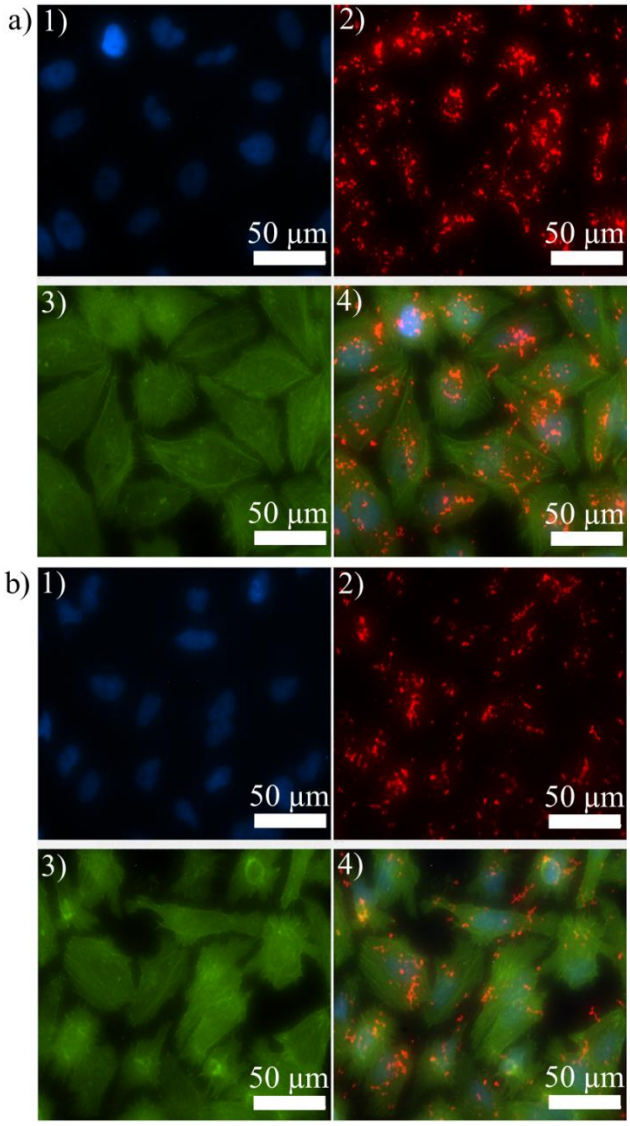

Figure 6.7. Cellular uptake of Cy5-labeled DNA for the phosphonium polyelectrolytes (+/- ratio of 4) showing successful cellular uptake of polyplexes into the HeLa cells: a) PTEP b) PTBP. Channels: 1) DAPI stained nuclei, 2) Cy5-labeled DNA showing polyplexes, 3) Alexa Fluor® 488 Phalloidin stained F-actin, and 4) Overlay of all three channels highlighting cellular uptake of polyplexes. Scale bar = 50 µm.

When comparing PTBA and PTBP, PTBP showed enhanced DNA delivery over PTBA at all +/- ratios ($p < 0.05$). PTBP also exhibited significantly improved gene transfection over Superfect® at +/- ratios of 4 and 6 ($p < 0.05$). GFP transfection microscopy results (+/- ratio of 4)

qualitatively correlated with the quantitative luciferase expression results. Our results demonstrated a marked improvement in nonviral gene delivery upon modification of the cationic center from an ammonium to a phosphonium. Endo et al. focused on the investigation of the antibacterial properties of PTBA and PTBP and the influence of the cation on antibiotic activity.[59,60] Cationic polymeric biocides primarily function through cellular membrane destabilization resulting in cellular death. PTBP exhibited improved antibiotic activity over PTBA presumably due to improved cellular membrane destabilization. Our results comparing the triethyl-based and tributyl-based polyelectrolytes also point to the importance of endosomolytic activity and the improved transfection of PTBP over PTBA may result from improved endosomolytic activity.

As expected, all polyelectrolytes exhibited poor transfection in serum-containing media as shown in **Figure 6.8**. Since the vectors are fully charged, they generated polyplexes with large, positive zeta potentials causing significant protein aggregation rendering the vectors ineffective as transfection agents in serum.[61] Future publications from our group will present ameliorating serum aggregation through PEGylation, changes in charge density, hydrogen bonding incorporation, and other structural modifications to provide salt and serum stability while minimizing cytotoxicity.

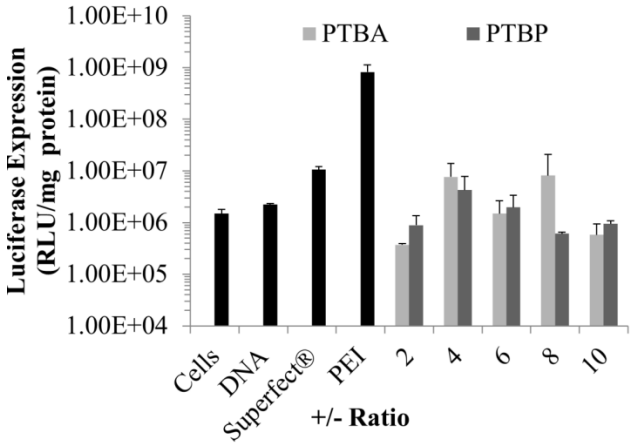

Figure 6.8. Serum-containing luciferase expression of the ammonium- and phosphonium-containing polyelectrolytes (n = 4).

Endocytic inhibition of either clathrin-mediated or caveolae-mediated endocytosis elucidated the preferred method of cellular uptake for both PTBA and PTBP. Pack et al. previously utilized the same endocytic inhibitors (genistein, methyl β-cyclodextrin, and amantadine) to elucidate the preferred endocytic pathway for PEI.[46] They showed that PEI's primary avenue of effective delivery was caveolae-mediated endocytosis. We followed a similar procedure as Pack et al. with some modifications to inhibit caveolae-mediated endocytosis using genistein or methyl β-cyclodextrin and clathrin-mediated endocytosis using amantadine. Relative luciferase expressions were compared to a positive control with the polyelectrolyte vector in the absence of endocytic inhibition (**Figure 6.9**). Genistein and methyl β-cyclodextrin (caveolae-mediated endocytosis inhibitors) knocked down luciferase expression showing PTBA and PTBP efficiently delivered through caveolae-mediated endocytosis ($p < 0.05$) while amantadine (clathrin-mediated endocytosis inhibitor) improved gene transfection compared to the control ($p < 0.05$). Improved transfection during inhibition of clathrin-mediated endocytosis resulted from increased cellular uptake of polyplexes through more efficient endocytic pathways such as caveolae-mediated endocytosis. PTBA and PTBP more efficiently transfected HeLa

cells when cellular uptake occurred through caveolae-mediated endocytosis versus clathrin-mediated endocytosis.

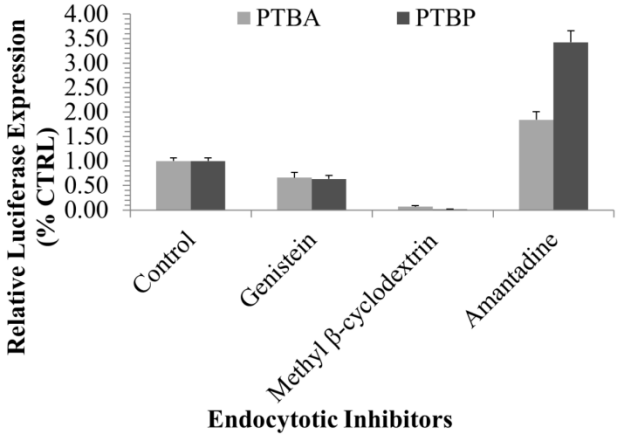

Figure 6.9. Relative luciferase expression for PTBA and PTBP with various endocytic inhibitors (n = 4). Genistein and methyl β-cyclodextrin inhibited caveolae-mediated endocytosis while amantadine inhibited clathrin-mediated endocytosis.

6.5 *Conclusions*

We investigated the gene delivery of phosphonium-containing macromolecules, which has led to a novel class of nonviral gene delivery vectors. We also elucidated structure-property relationships between alkyl substituent lengths on the cationic center. PTEA and PTEP, triethyl-based vectors, failed to deliver DNA effectively to HeLa cells while PTBA and PTBP, tributyl-based vectors, successfully induced protein expression in HeLa cells at similar levels as Superfect®. Cellular uptake of Cy5-labeled DNA showed the poor transfection of the triethyl-based polyelectrolytes resulted from intracellular mechanisms, e.g. poor endosomal escape or DNA release, since both triethyl-based and tributyl-based polyplexes entered the HeLa cells. Future studies will further examine the cellular uptake mechanism and intracellular mechanisms of endosomal escape and DNA release using flow cytometry. PTBP exhibited significantly

higher transfection efficiency relative to PTBA at all +/- ratios and Superfect® at +/- ratios of 4 and 6 ($p < 0.05$). An endocytic inhibition study ascertained the preferred efficient DNA delivery method for PTBA and PTBP was caveolae-mediated endocytosis. Our work expands upon the potential synthetic nonviral gene delivery vectors through substitution of traditional nitrogen-based cationic centers with phosphorus. We plan to further investigate the utility of phosphonium cations for nonviral gene delivery through the synthesis of phosphonium-containing random and block copolymers to minimize cytotoxicity, charge density, and serum aggregation while improving gene transfection. These novel vectors will also exhibit suitable properties for siRNA delivery due to their high affinity for nucleic acids. Controlled radical polymerization will enable the synthesis of a diblock copolymer with a PEG-containing block for serum stability and a cationic ammonium- or phosphonium-containing block for DNA condensation.

6.6 *Acknowledgements*

This material is based upon work supported in part by the U.S. Army Research Office under grant number W911NF-07-1-0452 Ionic Liquids in Electro-Active Devices (ILEAD) MURI. This material is based upon work supported in part by the U.S. Army Research Laboratory and the U.S. Army Research Office under the Army Materials Center of Excellence Program, contract W911NF-06-2-0014. We acknowledge funding from NSF (CHE-0722638) for the acquisition of our Agilent 6220 LC-TOF-MS. We also thank Dr. Adam Smith in our research group for helpful discussions.

6.7 *References*

(1) Mintzer, M. A.; Simanek, E. E. *Chemical Reviews* **2009**, *109*, 259.
(2) Li, S. D.; Huang, L. *Gene Therapy* **2006**, *13*, 1313.

(3) Heath, W. H.; Senyurt, A. F.; Layman, J.; Long, T. E. *Macromolecular Chemistry and Physics* **2007**, *208*, 1243.
(4) Lai, E.; van Zanten, J. H. *Journal of Controlled Release* **2002**, *82*, 149.
(5) Lai, E.; van Zanten, J. H. *Biophysical Journal* **2001**, *80*, 864.
(6) Richardson, S. C. W.; Kolbe, H. V. J.; Duncan, R. *International Journal of Pharmaceutics* **1999**, *178*, 231.
(7) Ruponen, M.; Rönkkö, S.; Honkakoski, P.; Pelkonen, J.; Tammi, M.; Urtti, A. *Journal of Biological Chemistry* **2001**, *276*, 33875.
(8) Funhoff, A. M.; van Nostrum, C. F.; Koning, G. A.; Schuurmans-Nieuwenbroek, N. M. E.; Crommelin, D. J. A.; Hennink, W. E. *Biomacromolecules* **2003**, *5*, 32.
(9) Forrest, M. L.; Pack, D. W. *Molecular Therapy* **2002**, *6*, 57.
(10) Ahn, H. H.; Lee, J. H.; Kim, K. S.; Lee, J. Y.; Kim, M. S.; Khang, G.; Lee, I. W.; Lee, H. B. *Biomaterials* **2008**, *29*, 2415.
(11) Godbey, W. T.; Wu, K. K.; Mikos, A. G. *Proceedings of the National Academy of Sciences* **1999**, *96*, 5177.
(12) Dalby, B.; Cates, S.; Harris, A.; Ohki, E. C.; Tilkins, M. L.; Price, P. J.; Ciccarone, V. C. *Methods* **2004**, *33*, 95.
(13) Hardy, J. G.; Love, C. S.; Gabrielson, N. P.; Pack, D. W.; Smith, D. K. *Organic & Biomolecular Chemistry* **2009**, *7*, 789.
(14) Dufès, C.; Uchegbu, I. F.; Schätzlein, A. G. *Advanced Drug Delivery Reviews* **2005**, *57*, 2177.
(15) Luo, D.; Haverstick, K.; Belcheva, N.; Han, E.; Saltzman, W. M. *Macromolecules* **2002**, *35*, 3456.
(16) Koping-Hoggard, M.; Tubulekas, I.; Guan, H.; Edwards, K.; Nilsson, M.; Varum, K. M.; Artursson, P. *Gene Therapy* **2001**, *8*, 1108.
(17) Strand, S. P.; Lelu, S.; Reitan, N. K.; de Lange Davies, C.; Artursson, P.; Vårum, K. M. *Biomaterials* **2010**, *31*, 975.
(18) Nimesh, S.; Aggarwal, A.; Kumar, P.; Singh, Y.; Gupta, K. C.; Chandra, R. *International Journal of Pharmaceutics* **2007**, *337*, 265.
(19) Gabrielson, N. P.; Pack, D. W. *Biomacromolecules* **2006**, *7*, 2427.
(20) Tang, G. P.; Zeng, J. M.; Gao, S. J.; Ma, Y. X.; Shi, L.; Li, Y.; Too, H. P.; Wang, S. *Biomaterials* **2003**, *24*, 2351.
(21) Brumbach, J. H.; Lin, C.; Yockman, J.; Kim, W. J.; Blevins, K. S.; Engbersen, J. F. J.; Feijen, J.; Kim, S. W. *Bioconjugate Chemistry* **2010**, *21*, 1753.
(22) Ramirez, S. M.; Layman, J. M.; Bissel, P.; Long, T. E. *Macromolecules* **2009**, *42*, 8010.
(23) Chan, P.; Kurisawa, M.; Chung, J. E.; Yang, Y.-Y. *Biomaterials* **2007**, *28*, 540.
(24) Kursa, M.; Walker, G. F.; Roessler, V.; Ogris, M.; Roedl, W.; Kircheis, R.; Wagner, E. *Bioconjugate Chemistry* **2002**, *14*, 222.
(25) Rungsardthong, U.; Ehtezazi, T.; Bailey, L.; Armes, S. P.; Garnett, M. C.; Stolnik, S. *Biomacromolecules* **2003**, *4*, 683.
(26) Allen, M. H.; Green, M. D.; Getaneh, H. K.; Miller, K. M.; Long, T. E. *Biomacromolecules* **2011**, *12*, 2243.
(27) Prevette, L. E.; Kodger, T. E.; Reineke, T. M.; Lynch, M. L. *Langmuir* **2007**, *23*, 9773.
(28) Georgiou, T. K.; Vamvakaki, M.; Patrickios, C. S.; Yamasaki, E. N.; Phylactou, L. A. *Biomacromolecules* **2004**, *5*, 2221.

(29) Deshpande, M. C.; Garnett, M. C.; Vamvakaki, M.; Bailey, L.; Armes, S. P.; Stolnik, S. *Journal of Controlled Release* **2002**, *81*, 185.
(30) Xie, W.; Xie, R.; Pan, W.-P.; Hunter, D.; Koene, B.; Tan, L.-S.; Vaia, R. *Chemistry of Materials* **2002**, *14*, 4837.
(31) Ren, H.; Sun, J.; Wu, B.; Zhou, Q. *Polymer Degradation and Stability* **2007**, *92*, 956.
(32) Monge, S.; Canniccioni, B.; Graillot, A.; Robin, J.-J. *Biomacromolecules* **2011**, *12*, 1973.
(33) Stekar, J.; Nössner, G.; Kutscher, B.; Engel, J.; Hilgard, P. *Angewandte Chemie International Edition in English* **1995**, *34*, 238.
(34) Picquet, E.; Le Ny, K.; Delépine, P.; Montier, T.; Yaouanc, J.-J.; Cartier, D.; des Abbayes, H.; Férec, C.; Clément, J.-C. *Bioconjugate Chemistry* **2005**, *16*, 1051.
(35) Floch, V.; Loisel, S.; Guenin, E.; Hervé, A. C.; Clément, J. C.; Yaouanc, J. J.; des Abbayes, H.; Férec, C. *Journal of Medicinal Chemistry* **2000**, *43*, 4617.
(36) Guénin, E.; Hervé, A.-C.; Floch, V.; Loisel, S.; Yaouanc, J.-J.; Clément, J.-C.; Férec, C.; des Abbayes, H. *Angewandte Chemie International Edition* **2000**, *39*, 629.
(37) Wang, L.; Xu, X.; Guo, S.; Peng, Z.; Tang, T. *International Journal of Biological Macromolecules* **2011**, *48*, 375.
(38) van der Aa, M.; Huth, U.; Häfele, S.; Schubert, R.; Oosting, R.; Mastrobattista, E.; Hennink, W.; Peschka-Süss, R.; Koning, G.; Crommelin, D. *Pharmaceutical Research* **2007**, *24*, 1590.
(39) Khalil, I. A.; Kogure, K.; Akita, H.; Harashima, H. *Pharmacological Reviews* **2006**, *58*, 32.
(40) Boussif, O.; Lezoualc'h, F.; Zanta, M. A.; Mergny, M. D.; Scherman, D.; Demeneix, B.; Behr, J. P. *Proceedings of the National Academy of Sciences* **1995**, *92*, 7297.
(41) Ramirez, S. M.; Layman, J. M.; Long, T. E. *Macromolecular Bioscience* **2009**, *9*, 1127.
(42) Dai, J.; Zou, S.; Pei, Y.; Cheng, D.; Ai, H.; Shuai, X. *Biomaterials* **2011**, *32*, 1694.
(43) Behr, J.-P. *CHIMIA International Journal for Chemistry* **1997**, *51*, 34.
(44) Pelkmans, L.; Helenius, A. *Traffic* **2002**, *3*, 311.
(45) Rejman, J.; Bragonzi, A.; Conese, M. *Molecular Therapy* **2005**, *12*, 468.
(46) Gabrielson, N. P.; Pack, D. W. *Journal of Controlled Release* **2009**, *136*, 54.
(47) McLendon, P. M.; Fichter, K. M.; Reineke, T. M. *Molecular Pharmaceutics* **2010**, *7*, 738.
(48) Hatakeyama, E. S.; Ju, H.; Gabriel, C. J.; Lohr, J. L.; Bara, J. E.; Noble, R. D.; Freeman, B. D.; Gin, D. L. *Journal of Membrane Science* **2009**, *330*, 104.
(49) Layman, J. M.; Borgerding, E. M.; Williams, S. R.; Heath, W. H.; Long, T. E. *Macromolecules* **2008**, *41*, 4635.
(50) Layman, J. M.; Ramirez, S. M.; Green, M. D.; Long, T. E. *Biomacromolecules* **2009**, *10*, 1244.
(51) Wang, S.-W.; Liu, W.; Colby, R. H. *Chemistry of Materials* **2011**, *23*, 1862.
(52) Simpson, D. A.; Feeney, S.; Boyle, C.; Stitt, A. W. *Molecular Vision* **2000**, *6*, 178.
(53) Yang, Y.; Lee, J.; Cho, M.; Sheares, V. V. *Macromolecules* **2006**, *39*, 8625.
(54) Santos, J. L.; Oliveira, H.; Pandita, D.; Rodrigues, J.; Pêgo, A. P.; Granja, P. L.; Tomás, H. *Journal of Controlled Release* **2010**, *144*, 55.
(55) Fischer, D.; Li, Y.; Ahlemeyer, B.; Krieglstein, J.; Kissel, T. *Biomaterials* **2003**, *24*, 1121.
(56) Convertine, A. J.; Diab, C.; Prieve, M.; Paschal, A.; Hoffman, A. S.; Johnson, P. H.; Stayton, P. S. *Biomacromolecules* **2010**, *11*, 2904.
(57) Convertine, A. J.; Benoit, D. S. W.; Duvall, C. L.; Hoffman, A. S.; Stayton, P. S. *Journal of Controlled Release* **2009**, *133*, 221.

(58) Song, Y.; Wang, H.; Zeng, X.; Sun, Y.; Zhang, X.; Zhou, J.; Zhang, L. *Bioconjugate Chemistry* **2010**, *21*, 1271.
(59) Kanazawa, A.; Ikeda, T.; Endo, T. *Journal of Polymer Science Part A: Polymer Chemistry* **1993**, *31*, 335.
(60) Kanazawa, A.; Ikeda, T.; Endo, T. *Journal of Applied Polymer Science* **1994**, *53*, 1245.
(61) Dash, P. R.; Read, M. L.; Barrett, L. B.; Wolfert, M. A.; Seymour, L. W. *Gene Therapy* **1999**, *6*, 643.

Chapter 7: Phosphonium-Containing Diblock Copolymers for Enhanced Colloidal Stability and Efficient Nucleic Acid Delivery

(Published in *Biomacromolecules* **2012,** *13* (8), 2439-2445.)

Sean T. Hemp,[§] Adam E. Smith,[§] Joshua M. Bryson,[†] Michael H. Allen, Jr.,[§] and Timothy E. Long*[,§]

[§]*Department of Chemistry and Macromolecules and Interfaces Institute, Virginia Tech, Blacksburg, VA 24061*

[†]*Techulon, Inc., Blacksburg, VA 24060*

*To whom correspondence should be addressed. E-mail: telong@vt.edu. TEL: (540)231-2480 FAX: (540)231-8517

Keywords: nonviral gene delivery, phosphonium, colloidal stability, RAFT, block copolymers

7.1 *Abstract*

RAFT polymerization successfully controlled the synthesis of phosphonium-based AB diblock copolymers for nonviral gene delivery. A stabilizing block of either oligo(ethylene glycol$_9$) methyl ether methacrylate or 2-(methacryloxy)ethyl phosphorylcholine provided colloidal stability, and the phosphonium-containing cationic block of 4-vinylbenzyltributylphosphonium chloride induced electrostatic nucleic acid complexation. RAFT polymerization generated well-defined stabilizing blocks (M_n = 25,000 g/mol) and subsequent chain extension synthesized diblock copolymers with DPs of 25, 50, and 75 for the phosphonium-containing block. All diblock copolymers bound DNA efficiently at +/- ratios of 1.0 in H_2O, and polyplexes generated at +/- ratios of 2.0 displayed hydrodynamic diameters between 100 to 200 nm. The resulting polyplexes exhibited excellent colloidal stability under

physiological salt or serum conditions, and they maintained constant hydrodynamic diameters over 24 h. Cellular uptake studies using Cy5-labeled DNA confirmed reduced cellular uptake in COS-7 and HeLa cells, and consequently, resulted in low transfection in these cell lines. Serum transfection in HepaRG cells, which are a predictive cell line for *in vivo* transfection studies, showed successful transfection using all diblock copolymers with luciferase expression on the same order of magnitude as Jet-PEI. All diblock copolymers exhibited low cytotoxicity (>80% cell viability). Promising *in vitro* transfection and cytotoxicity results suggest future studies involving the *in vivo* applicability of these phosphonium-based diblock copolymer delivery vehicles.

7.2 *Introduction*

The promise of gene delivery strives to treat many genetic diseases through the delivery of exogenous DNA for successful transcription and translation into therapeutic proteins.[1-3] Viral vectors exhibit a number of significant drawbacks (deleterious immuno-response, lack of cell specificity, and high manufacturing costs) that limit their widespread clinical impact despite their efficient delivery of therapeutics.[4] These shortcomings of viral vectors and the advent of controlled, modular synthetic strategies have stimulated the development of nonviral vectors for the successful delivery of nucleic therapeutics to a cell. Cationic macromolecular delivery vehicles bind and compact nucleic acids into nanoparticles termed "polyplexes."[5,6] Cationic polymers reversibly bind nucleic acids to offer protection from enzymatic degradation and facilitate cellular uptake through various endocytic mechanisms.[7] Common cationic macromolecules include poly(ethylene imine) (PEI),[8,9] Superfect,[10,11] poly(2-dimethylaminoethyl methacrylate) (PDMAEMA),[12,13] and chitosan.[14,15]

Multiple barriers exist for the *in vivo* delivery of nucleic acids, including colloidal instability, rapid renal clearance, and insufficient biodistribution to the target organ.[16] In addition, many nonviral gene delivery vehicles, such as PEI, exhibit poor colloidal stability in serum-containing media. Salt induces polyplex aggregation through charge neutralization,[17] and negatively-charged serum proteins associate to the positively-charged polyplexes, which induces aggregation that causes inefficient cellular uptake and delivery of the nucleic acid payload.[18] The inclusion of a neutral, hydrophilic segment that provides steric shielding prevents salt- and serum-induced aggregation for many cationic homopolymers.[19] Additionally, the incorporation of a hydrophilic stabilizing block reduces opsonization and reticuloendothelial system clearance leading to increased blood circulation time.[20-22]

Conventional nonviral gene therapy almost exclusively focuses on nitrogen-containing macromolecules and lipids to condense and deliver nucleic acids. Macromolecules containing phosphorus typically exhibit enhanced biocompatibility,[23] flame retardancy,[24] thermal stability,[25] ionic aggregation,[26] and molecular recognition in block and random copolymers.[27] Clément et al. first established the utility of phosphonium and arsenium cations in lipid-based delivery systems.[28-30] They showed that phosphonium- and arsenium-containing lipids mediated higher gene transfection with lower cytotoxicity compared to the ammonium-based analogs *in vitro* and *in vivo*. For the first time, our research group disclosed the utility of phosphonium-containing macromolecules for nonviral gene delivery.[31] Specifically, we directly compared ammonium- and phosphonium-containing polystyrene homopolymers with variable alkyl substituent lengths attached to the cationic center. Phosphonium vectors mediated higher gene transfection than ammonium analogs; the longer tributyl alkyl substituent lengths attached to the cationic center also imparted enhanced pDNA delivery relative to triethyl-based analogs. Subsequently, Fréchet

et al. recently demonstrated the improved siRNA delivery of phosphonium-containing polyacrylate homopolymers compared to ammonium-containing polyacrylates.[32]

Herein, we report the first phosphonium-containing AB diblock copolymers for enhanced nucleic acid delivery where the A block provides colloidal stability and the phosphonium-based B block efficiently complexes pDNA to generate core-shell nanoparticles. The A block consisted of either oligo(ethylene glycol$_9$) methyl ether methacrylate (OEG) or 2-methacryloyloxyethyl phosphorylcholine (MPC) since both polymeric units exhibit protein resistance and extended circulation times due to steric shielding of the nanoparticles.[23,33] RAFT polymerization controlled OEG and MPC to yield macroCTAs with similar number-average molecular weights, and subsequent chain extension with 4-vinylbenzyltributylphosphonium chloride (TBP) provided AB diblock structures with variable block lengths. DNA binding studies probed the effective nucleic acid binding of the TBP block, and dynamic light scattering (DLS) examined the colloidal stability of the polyplexes under physiological salt and serum conditions. Transfection studies assessed the ability of the diblock copolymer polyplexes to deliver DNA to three cell lines (COS-7, HeLa, and HepaRG cells) and elucidated the cytotoxicities of the diblock copolymer polyplexes.

7.3 *Experimental Section*

7.3.1 Materials

OEG (485 g/mol) was purchased from Sigma Aldrich and purified using a basic alumina column prior to use. MPC was purchased from Polysciences, dissolved in water, and washed with diethyl ether to remove the inhibitor. 4,4'-Azobis(4-cyanopentanoic acid) (V-501) was purchased from Sigma Aldrich and recrystallized twice from methanol prior to use. TBP and 4-

cyano-4-(propylsulfanylthiocarbonyl)sulfanylpentanoic acid (CPP) were synthesized as previously reported in literature.[34] All solvents were obtained from Sigma Aldrich and used as received.

7.3.2 Analytical Methods

^{1}H NMR spectroscopy was performed on a Varian Inova 400 in D_2O. Aqueous size exclusion chromatography (SEC) was utilized to determine the number-average molecular weight (M_n) and polydispersity indices (PDIs) for the macroCTAs and the diblock copolymers using an aqueous eluent of 54/23/23 (v/v/v %) water/methanol/acetic acid with 0.1 M sodium acetate at a flow rate of 0.8 mL/min, a Waters 1515 isocratic HPLC pump, a Waters 717plus autosampler, two Waters ultrahydrogel linear columns, one Waters ultrahydrogel 250 column, a Wyatt MiniDAWN, and a Waters 2414 refractive index detector. An Optilab T-rEX refractometer (λ = 658 nm) was used to measure d*n*/dc values offline for determination of absolute molecular weights.

7.3.3 Polymer Synthesis

A solution of CPP (82.3 mg, 0.297 mmol), OEG (10.8 g, 22.3 mmol), and V-501 (16.8 mg, 0.060 mmol) in 90 mL of DMSO was added to a 250-mL, round-bottomed flask equipped with a magnetic stir bar to synthesize the OEG_{52} macroCTA. The solution was sparged with nitrogen for 30 min and subsequently placed in a preheated oil bath at 70 °C for 3 h. The OEG_{52} macroCTA was recovered as viscous yellow oil after dialysis against water (pH 4 - 5) and lyophilization.

The MPC_{87} macroCTA was synthesized according to a similar procedure as above. Briefly, MPC (5.52 g, 18.7 mmol), CPP (51.8 mg, 0.187 mmol), and V-501 (5.2 mg, 0.019 mmol)

were dissolved in 70 mL of 4:1 acetate buffer (pH 5.2)/DMSO in a 250-mL, round-bottomed flask equipped with a magnetic stir bar. The solution was sparged with nitrogen for 30 min and subsequently placed in a preheated oil bath at 70 °C for 3.5 h. After dialysis against water (pH 4 - 5) and lyophilization, the MPC_{87} macroCTA was recovered as a white powder.

The two macroCTAs were subsequently chain extended with TBP to yield diblock copolymers following a similar procedure. The polymerizations were performed using a target DP of 100 for TBP and aliquots were removed to follow polymerization kinetics and yield the six diblock copolymers. As an example, TBP (0.350 g, 0.986 mmol), OEG_{52} (0.250 g), and V-501 (2.8 mg, 9.86 x 10^{-3} mmol) were dissolved in 4 mL of 1:1 acetate buffer (pH 5.2)/DMSO and was added to a 10-mL, round-bottomed flask equipped with a magnetic stir bar. After sparging with nitrogen for 30 min, the reaction was allowed to proceed at 70 °C for 2.5 h. The product was dialyzed against DI water (pH 4 - 5), lyophilized, and recovered as a white powder.

7.3.4 DNA Binding Assay

gWiz-Luc plasmid DNA (0.2 μL of 1 μg/μL in H_2O, Aldevron) was mixed with the required amount of polymer to obtain the desired +/- ratio (ratio of positively charged phosphonium cation on the polymeric vector to negatively charged phosphate on DNA) in H_2O (28 μL total volume). After an incubation time of 30 min at room temperature, 7 μL of gel loading buffer (30% glycerol in H_2O) was added. The polyplex solution (20 μL) was loaded onto an agarose gel (0.6 g of agarose and 6 μL of SYBR Green I (Sigma Aldrich) in 60 mL of 1× Tris-acetate-EDTA) and electrophoresed at 70 V for 30 min. A MultiDoc-it Digital Imaging System (UVP) was utilized to image the agarose gels.

7.3.5 Dynamic Light Scattering

A Malvern Instruments Zetasizer Nano ZS (633 nm) was used to measure the polyplex sizes. gWiz-Luc DNA (2 μg in 100 μL of H_2O) was incubated for 30 min at room temperature with the required amount of each diblock copolymer in 200 μL of H_2O to give a +/- ratio of 2.0. After the incubation period, 800 μL of H_2O, Dulbecco's modified Eagle's media (DMEM), or DMEM supplemented with 10% fetal bovine serum (FBS) was added to assess the colloidal stability of the polyplexes in salt- and serum-containing media. The particle sizes were then measured at time intervals of 0, 1, 2, 4, and 24 h after dilution. The zeta potential measurements were also performed on the samples diluted with H_2O using a Malvern Instruments Zetasizer Nano ZS. All measurements were performed in triplicate and the data are represented as the mean ± the standard deviation.

7.3.6 Cell Culture

HepaRG cells (Life Technologies, Carlsbad, CA) were maintained in supplemented Williams Medium E (65 mL HepaRG maintenance supplement, 5 mL GlutaMAX-I™, and 500 mL Williams Medium E) (Invitrogen). Cells were incubated in 95% humidity with 5% CO_2 at 37 °C.

7.3.7 Luciferase Expression and Cytotoxicity Assay

Prior to transfection, HepaRG cells were plated on 24-well plates at a density of 100,000 cells per well, approximately 95% confluency. Cells were incubated in 400 μL of supplemented Williams Medium E for 24 h at 37 °C in a 5% CO_2 environment. Control reagents were formulated with pDNA based upon their recommended protocols. Polymers were formulated with pDNA at a +/- ratio of 2.0 in 100 μL of Williams Medium E (no supplements). Solutions of

pDNA (gWiz-Luciferase, Aldevron, Fargo, ND) complexes for each polymer were added in triplicate to corresponding wells (1.5 µg pDNA per well, V_t=500 µL). After 48 h of incubation, the media was evacuated from wells and cells were lysed in 100 µL Cell Lysis Buffer (Promega, Madison, WI). Cell lysates were deposited on 96-well plates and analyzed for luciferase activity on a luminometer plate reader (Promega GloMax® 96 Microplate Luminometer). Protein lysates were stained using a Pierce BCA Protein Assay kit according to manufacturer protocols. Cell viability was determined from sample absorbance relative to the cells only control. Student's t test analysis of the luciferase transfection results was performed to determine statistical significance ($p < 0.02$).

7.3.8 Wide-Field Fluorescence Optical Microscopy

HepaRG cells were plated at a density of 500,000 cells per well on 6-well plates 24 h prior to transfection and polyplexes were formed using the same methods reported above in the luciferase assay instead using a plasmid encoding enhanced green florescent protein (EGFP-C1, 7.5 µg total per well). Transfection conditions were consistent with those reported above. After 48 h, cells were directly imaged on an AMG Evos-Fl microscope for both differential interference contrast images and for GFP florescence (ex. 488 nm, em. 509 nm).

7.4 *Results and Discussion*

7.4.1 Polymer Synthesis and Characterization

Controlled radical polymerization enables the synthesis of well-defined block copolymers where each block serves a specific function in nucleic acid delivery.[35,36] Chain transfer agents, such as dithioesters and trithiocarbonates, utilized in RAFT polymerization enable controlled free radical polymerization through degenerative chain transfer.[37] RAFT polymerization allows

a modular design in block chemical composition, block molecular weight, and end group functionality to optimize delivery vehicles.[38-40] We initially aimed to examine the influence of two A block structures on colloidal stability and ultimately gene transfection for a series of diblock copolymers. The A block structures included a PEG brush block (OEG) and a zwitterionic block (MPC). We synthesized similar A block molecular weights which resulted in different degrees of polymerization (DP) due to the disparity in repeat unit molecular weight for each monomer. RAFT polymerization successfully controlled the molecular weights using a trithiocarbonate chain transfer agent (CTA) and V-501 (an azo initiator) to achieve M_n = 25,000 g/mol and PDIs < 1.10 for each macroCTA as shown in **Table 7.1**.

Table 7.1. Molecular weight analysis of the initial macroCTAs and the final diblock copolymers.

Polymer	M_n (g/mol)	M_w/M_n	DP of A block	DP of B Block
TBP_{61}	21,700	1.24	0	61
OEG_{52}	25,400	1.02	52	0
$OEG_{52}TBP_{27}$	34,900	1.05	52	27
$OEG_{52}TBP_{56}$	45,100	1.10	52	56
$OEG_{52}TBP_{78}$	53,100	1.13	52	78
MPC_{87}	25,600	1.02	87	0
$MPC_{87}TBP_{23}$	33,800	1.04	87	23
$MPC_{87}TBP_{59}$	46,500	1.05	87	59
$MPC_{87}TBP_{81}$	54,400	1.09	87	81

Currently, a majority of researchers intensely focus on nitrogen-containing monomers for the B block to condense and package nucleic acids for delivery.[1] Our research group previously demonstrated the effectiveness of 4-vinylbenzyltributylphosphonium chloride (TBP) homopolymers for DNA complexation and delivery.[31] Subsequent chain extension of the macroCTAs with TBP, as shown in **Scheme 7.1**, achieved the desired AB diblock copolymers.

We varied the TBP block DP to investigate the influence of the A/B block ratio on gene transfection. **Figure 7.1** highlights the monotonic shift in elution time for each peak as the molecular weight of the TBP block increased for the $OEG_{52}TBP_y$ and $MPC_{87}TBP_y$ diblock copolymers. **Table 7.1** summarizes the *absolute* molecular weights from aqueous SEC for the final diblock copolymer compositions. All diblock copolymers exhibited PDIs < 1.20 demonstrating polymerization control using the RAFT process. Three DPs (25, 50, and 75) of the TBP block were targeted and the resulting OEG- and MPC-based diblock copolymers closely matched the target DPs. In addition, RAFT polymerization allowed the controlled synthesis of a TBP_{61} homopolymer to achieve a DP similar to the $OEG_{52}TBP_{56}$ and $MPC_{87}TBP_{59}$ diblock copolymers as a control for DNA binding and colloidal stability assays.

Scheme 7.1. RAFT polymerization of OEG and MPC with subsequent chain extension using TBP to synthesize phosphonium-containing diblock copolymers OEG_xTBP_y and MPC_xTBP_y.

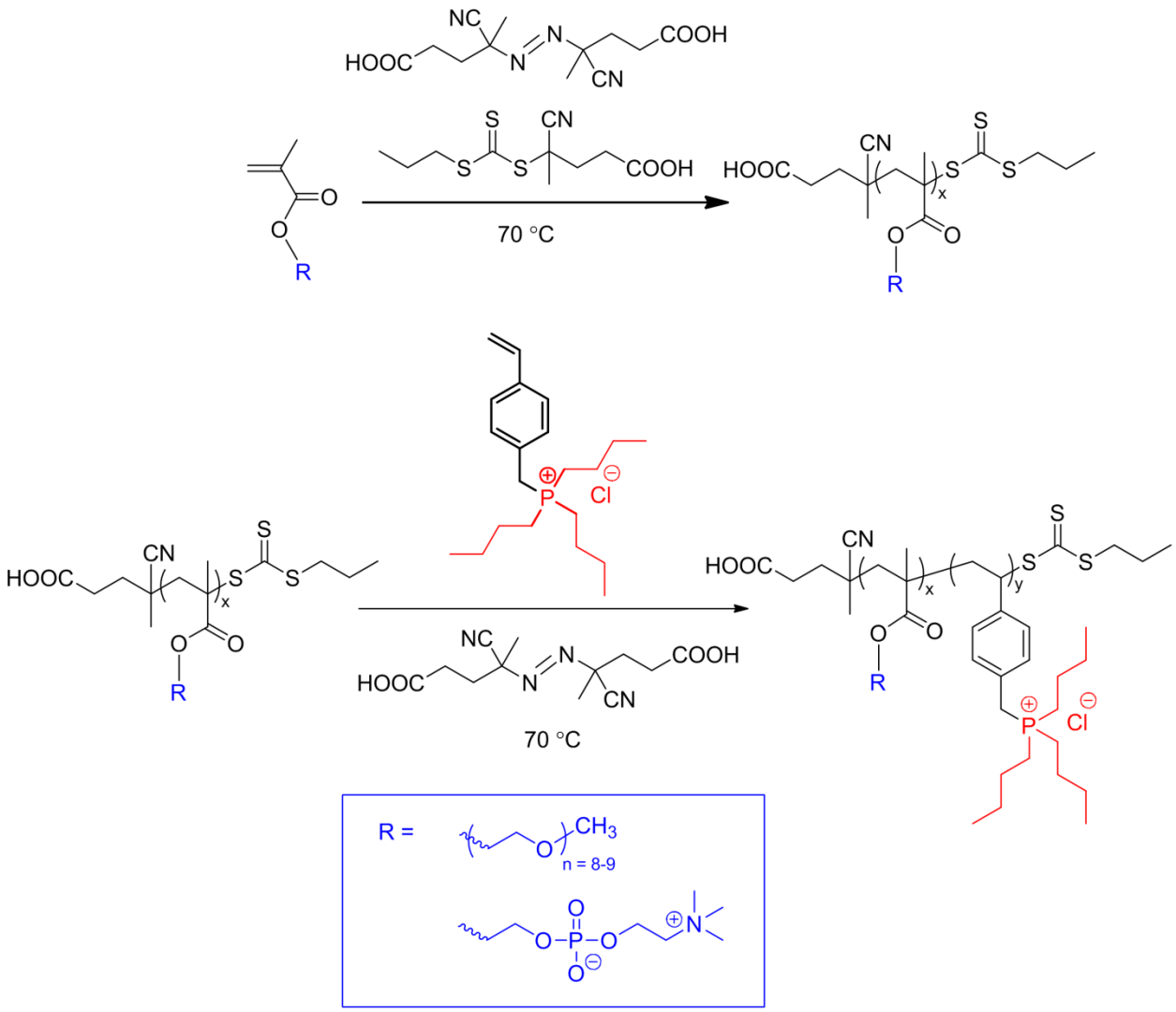

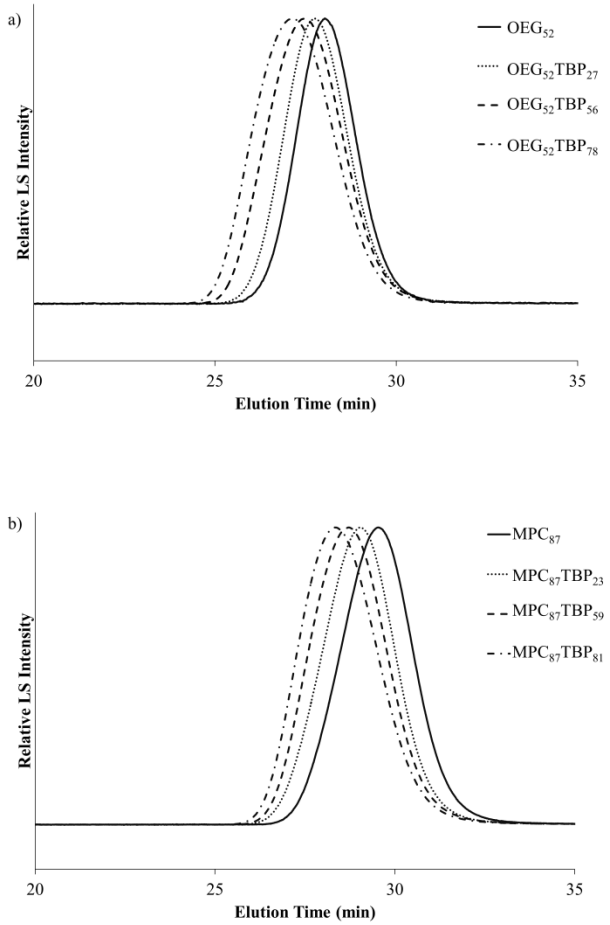

Figure 7.1. Aqueous SEC LS curves for: a) the initial OEG_{52} macroCTA and the final $OEG_{52}TBP_y$ diblock copolymers and b) the initial MPC_{87} macroCTA and the resulting $MPC_{87}TBP_y$ diblock copolymers.

7.4.2 DNA Binding and Colloidal Stability

Initial studies focused on the DNA complexation and compaction of these novel diblock copolymers using DNA gel shift assays and DLS. Due to the absence of protonatable and positively charged nitrogens in our system, we utilized a charge ratio (+/- ratio) of positively charged phosphonium cations in the diblock copolymers to negatively charged phosphate anions in the DNA backbone instead of the typical N/P ratio. TBP_{61} and all the diblock copolymers

bound DNA completely at a +/- ratio of 1.0 (**Figure 7.2**). There was not a detectable effect on the onset of DNA binding as a function of the A block composition or TBP block length. DLS confirmed DNA binding and compaction, forming polyplexes (sizes of 100 – 200 nm) in water at +/- ratios of 2.0 for all diblock copolymers. Zeta potentials for all diblock copolymers except $MPC_{87}TBP_{23}$ exhibited positive values between 20 – 35 mV; $MPC_{87}TBP_{23}$ demonstrated a slightly negative zeta potential of -3 mV presumably due to the shorter TBP block and zwitterionic nature of the MPC block.

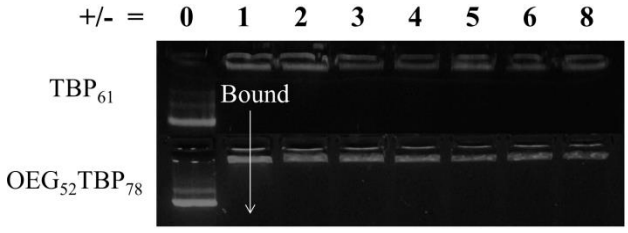

Figure 7.2. DNA gel shift assays of TBP_{61} and $OEG_{52}TBP_{78}$ as a representative DNA gel shift assay for the diblock copolymers demonstrating complete DNA binding at a +/- ratio of 1.0.

In vivo nucleic acid delivery requires a sufficiently small polyplex (< 200 nm) to enable long circulation times and cellular uptake.[41] In addition, polyplexes must resist salt and serum induced aggregation. In sharp contrast, nonviral gene delivery vehicles for *in vitro* applications typically rely on poor colloidal stability to induce polyplex aggregation and sedimentation onto the cell monolayer, which enables efficient cellular uptake and transfection.[42] DLS enabled kinetic analysis of the polyplex aggregation in serum-free and serum-containing media conditions to investigate the colloidal stability of the diblock copolymers, TBP_{61}, and Jet-PEI.[43] Serum-free DMEM effectively mimics the physiological salt and nutrient conditions required for cell growth, and serum-containing media contains anionic proteins similar to those found in blood, which may electrostatically associate with polyplexes and induce aggregation.[44]

Physiological salt conditions induce polyplex aggregation through neutralization of the polyplex surface charge resulting in neutral polyplexes that aggregate.[17] **Figure 7.3** depicts the hydrodynamic diameter of each polyplex prepared using the diblock copolymers (+/- ratio of 2.0), TBP_{61} (+/- ratio of 2.0), and Jet-PEI (N/P = 5.0). TBP_{61} initially produced polyplexes with sizes of 77 nm in water; upon dilution into serum-free DMEM, the TBP_{61} polyplexes rapidly increased 1300% in size to 1051 nm after 2 h under physiological salt conditions. TBP_{61} polyplexes precipitated from serum-free DMEM conditions after 2 h. In contrast, the phosphonium-based diblock copolymers generated polyplexes (~110 nm in size), which remained colloidally stable without aggregation under physiological salt conditions for 24 h suggesting the efficiency of the A block to generate stable polyplex colloids. Neither A block composition nor TBP block length significantly influenced the polyplex colloidal stability under physiological salt conditions. Jet-PEI, a popular positive control for nonviral gene delivery, demonstrated reduced colloidal stability, increasing in size from 63 nm to 606 nm over 2 h in serum-free DMEM.

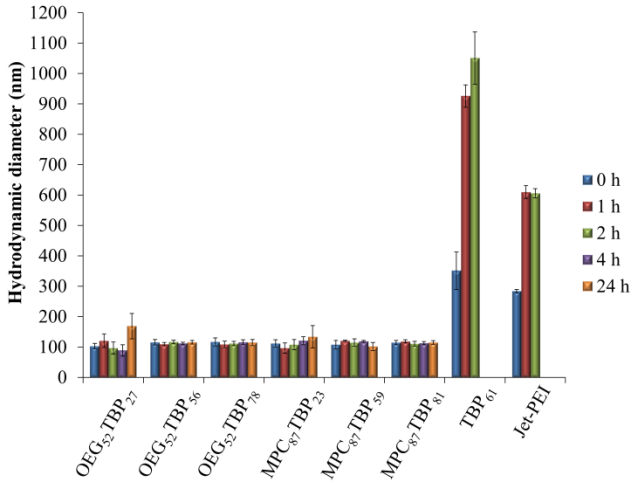

Figure 7.3. Hydrodynamic diameter of the polyplexes formed using the phosphonium-based diblock copolymers, TBP_{61}, and Jet-PEI challenged under serum-free media conditions for 24 h to probe their colloidal stability. Polyplexes prepared in water at +/- ratios of 2.0 for the phosphonium-based vehicles and N/P ratio of 5 for Jet-PEI with subsequent dilution into serum-free DMEM. Error bars represent the standard deviation of three measurements.

Colloidal stability assays also probed the diblock copolymer polyplexes' resistance to serum-induced polyplex aggregation. Anionic serum proteins stimulate polyplex aggregation through electrostatic association to the polyplex surface causing charge neutralization and consequently polyplex aggregation.[18] **Figure 7.4** highlights the change in the hydrodynamic diameters of the diblock copolymer (+/- ratio of 2.0), TBP_{61} (+/- ratio of 2.0), and Jet-PEI (N/P = 5.0) polyplexes after dilution into serum-containing DMEM. TBP_{61} polyplexes rapidly increased 250% in hydrodynamic diameter to 190 nm and remained ~190 nm in size over 24 h. Substantial increase in polyplex size did not occur after the initial growth, presumably due to anionic protein association to the TBP_{61} polyplex surface providing an overall negative surface charge and therefore providing colloidal stability.[45] All diblock copolymer polyplexes resisted serum-induced polyplex aggregation and remained a similar size over a 24 h period without an obvious

difference in the efficacy of the A block composition or TBP block length on serum colloidal stability. Both OEG and MPC stabilizing blocks prevented polyplex aggregation presumably through steric repulsion of the brush PEG block or zwitterionic block, respectively. Jet-PEI exhibited diminished colloidal stability under serum-containing DMEM conditions with a rapid 1200% growth in polyplex size over 2 h to 744 nm.

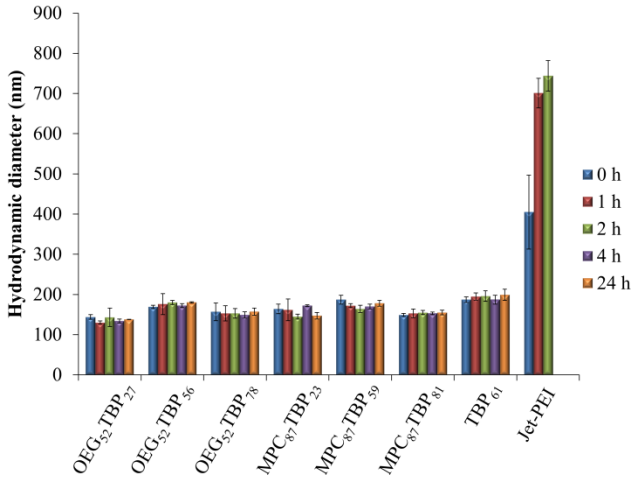

Figure 7.4. Hydrodynamic diameter of the polyplexes prepared with the phosphonium-based diblock copolymers, TBP_{61}, and Jet-PEI challenged under serum-containing media conditions for 24 h to probe their colloidal stability. Polyplexes prepared in water at +/- ratios of 2.0 for the phosphonium-based vehicles and N/P ratio of 5 for Jet-PEI and then diluted into serum-containing DMEM. Error bars represent the standard deviation of three measurements.

7.4.3 Cytotoxicity and Transfection

We focused on three different cell lines (COS-7, HeLa, and HepaRG) to investigate the transfection efficiency and cytotoxicity of the phosphonium-based diblock copolymers. COS-7 (African green monkey kidney fibroblasts) and HeLa (Human cervical cancer epithelia) cells are two typical cell lines utilized in the nonviral gene delivery field to elucidate the *in vitro* transfection capabilities of novel delivery vehicles.[46] HepaRG cells are terminally differentiated

human hepatocytes, which grow with similar hepatic morphologies and enzymatic activity.[47] *In vitro* drug metabolism studies typically utilize HepaRG cells as a predictive metric for drug metabolism and hepatic toxicity concerns preceding *in vivo* testing.[48] We therefore also investigated the cytotoxicity and transfection efficacy of the diblock copolymers in HepaRG cells to provide justification for future *in vivo* administration.[49]

Initial transfection experiments focused on the delivery of luciferase-encoded pDNA (1 μg/well) to HeLa and COS-7 cells at low +/- ratios of 2.0 and 4.0. Ideally, *in vivo* nucleic acid delivery vehicles must bind and deliver DNA efficiently under serum conditions at low charge ratios to minimize cytotoxicity and noncomplexed polymer in solution. All diblock copolymers failed to efficiently deliver pDNA to HeLa and COS-7 cells at +/- ratios of 2.0 and 4.0 compared to the positive control Jet-PEI. Wide-field optical fluorescence microscopy studies focused on the cellular uptake of Cy5-labeled DNA under serum-free conditions did not show cellular uptake of diblock copolymer polyplexes after 4 h; however, TBP_{61} and Jet-PEI polyplexes demonstrated cellular uptake within 4 h. While steric stabilizing blocks such as OEG and MPC provide superior colloidal stability, these functionalities also hinder cellular uptake through screening of the cationic charge and steric repulsion against the cellular membrane.[50,51] The poor colloidal stability of TBP_{61} and Jet-PEI compared to the diblock copolymers also presumably aided in cellular uptake through aggregation and sedimentation of the polyplexes onto the cell monolayer inducing cellular uptake.[45,52,53]

Dose-dependent GFP expression studies performed in HepaRG cells elucidated the optimal DNA/well concentration required for successful transfection in serum-containing HepaRG media. HepaRG cells were dosed at various GFP-encoded pDNA concentrations (0.35 μg DNA/mL to 14 μg DNA/mL) using the diblock copolymers (+/- ratios of 2.0). **Figure 7.5**

shows representative wide-field fluorescence optical microscopy for all the diblock copolymers at a dosage of 1.4 μg/well, which revealed the largest proportion of GFP expressing HepaRG cells compared to other DNA dosages. Therefore, we performed luciferase transfections at 1.5 μg DNA/mL to quantify nucleic acid delivery compared to the GFP expression.

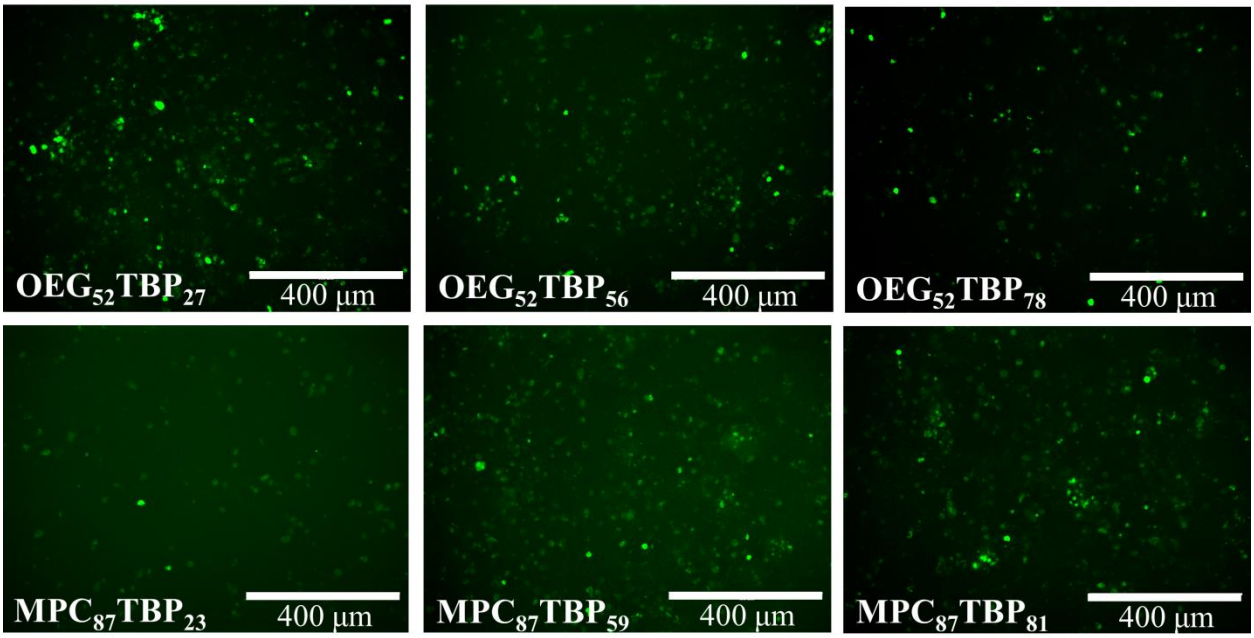

Figure 7.5. GFP expression of successfully transfected HepaRG cells using the phosphonium-containing diblock copolymers at a +/- ratio of 2.0 and dosages of 1.4 μg DNA/well.

HepaRG luciferase transfections established a significant influence of cell type on the transfection results for the diblock copolymers. Although the diblock copolymers failed to transfect COS-7 and HeLa cells, the diblock copolymers (+/- ratio of 2.0) delivered DNA effectively on the same order of magnitude as Jet-PEI (N/P = 5) in HepaRG cells (**Figure 7.6**). The diblock copolymers all performed statistically higher than cells and DNA only ($p < 0.02$), however, the diblock copolymers did not demonstrate a statistically significant trend in transfection capability for different A block compositions or TBP block lengths. **Figure 7.6** summarizes the polyplex cytotoxicities of the diblock copolymers in HepaRG cells. The

$OEG_{52}TBP_y$ diblock copolymers showed an unexpected trend of increasing cell viability as the TBP block length increased (from ~80% for $OEG_{52}TBP_{27}$ to ~100% for $OEG_{52}TBP_{78}$) while the cell viability for the $MPC_{87}TBP_x$ copolymers remained unchanged across the various TBP DPs (>80%). Overall, the diblock copolymers demonstrated selective *in vitro* transfection in HepaRG cells with minimal cytotoxicity. Future *in vivo* assays for biodistribution, pharmacokinetics, and efficacy will highlight the capabilities of these novel phosphonium-based diblock copolymers for nonviral nucleic acid delivery.

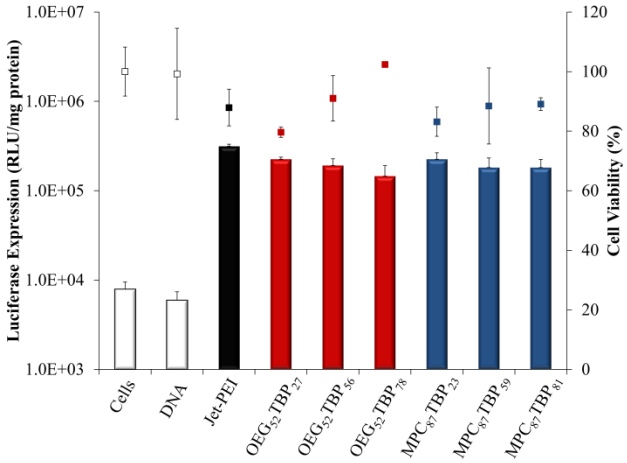

Figure 7.6. Luciferase expression and cell viability of transfected HepaRG cells using the phosphonium-containing diblock copolymers (+/- ratios of 2.0) and Jet-PEI (N/P = 5.0). The histogram bars correlate to the luciferase expression and the individual points correspond to the cell viability. Error bars represent the standard deviation of three measurements. All delivery vehicles transfected statistically higher than the negative controls, cells and DNA only ($p < 0.02$).

7.5 *Conclusions*

The manuscript describes the first synthesis and characterization of phosphonium-based diblock copolymers for nonviral nucleic acid delivery. RAFT polymerization successfully controlled the synthesis of $OEG_{52}TBP_y$ and $MPC_{87}TBP_y$ diblock copolymers with M_n's of

25,000 g/mol for the stabilizing A block and variable DPs of the TBP block (25, 50, and 75). All diblock copolymers and the TBP_{61} homopolymer initially bound DNA at a +/- ratio of 1.0. The $OEG_{52}TBP_y$ and $MPC_{87}TBP_y$ diblock copolymers at +/- ratios of 2.0 exhibited enhanced colloidal stability compared to TBP_{61} (+/- ratio of 2.0) and Jet-PEI (N/P = 5.0) under physiological salt and serum conditions due to the stabilizing A block. Serum transfections in COS-7, HeLa, and HepaRG cells demonstrated cell specificity for cellular uptake and transfection. Cellular uptake studies demonstrated poor cellular uptake for the diblock copolymers, which led to inadequate transfection in HeLa and COS-7 cells. GFP microscopy studies in HepaRG cells showed successful transfection in a dose-dependent manner and all diblock copolymers delivered pDNA on the same order of magnitude as Jet-PEI with minimal cytotoxicity. Future studies will focus on the *in vivo* biodistribution, pharmacokinetics, and efficacy of the diblock copolymers for nonviral nucleic acid delivery. Different A block molecular weights will optimize colloidal stability and improve cellular uptake to improve transfection across multiple cell lines.

7.6 *Acknowledgements*

The authors gratefully thank Techulon, Inc. for financial and material support. This material is based upon work supported by the Army Research Office (ARO) under Award No. W911NF-10-1-0307 (DURIP).

7.7 *References*

(1) Mintzer, M. A.; Simanek, E. E. *Chemical Reviews* **2009**, *109*, 259.
(2) Li, S. D.; Huang, L. *Gene Therapy* **2006**, *13*, 1313.
(3) Heath, W. H.; Senyurt, A. F.; Layman, J.; Long, T. E. *Macromolecular Chemistry and Physics* **2007**, *208*, 1243.
(4) Yue, X.; Qiao, Y.; Qiao, N.; Guo, S.; Xing, J.; Deng, L.; Xu, J.; Dong, A. *Biomacromolecules* **2010**, *11*, 2306.

(5) Lai, E.; van Zanten, J. H. *Journal of Controlled Release* **2002**, *82*, 149.
(6) Allen, M. H.; Green, M. D.; Getaneh, H. K.; Miller, K. M.; Long, T. E. *Biomacromolecules* **2011**, *12*, 2243.
(7) Reineke, T. M. *J. Polym. Sci., Part A: Polym. Chem.* **2006**, *44*, 6895.
(8) Ahn, H. H.; Lee, J. H.; Kim, K. S.; Lee, J. Y.; Kim, M. S.; Khang, G.; Lee, I. W.; Lee, H. B. *Biomaterials* **2008**, *29*, 2415.
(9) Godbey, W. T.; Wu, K. K.; Mikos, A. G. *Proceedings of the National Academy of Sciences* **1999**, *96*, 5177.
(10) Dufès, C.; Uchegbu, I. F.; Schätzlein, A. G. *Advanced Drug Delivery Reviews* **2005**, *57*, 2177.
(11) Luo, D.; Haverstick, K.; Belcheva, N.; Han, E.; Saltzman, W. M. *Macromolecules* **2002**, *35*, 3456.
(12) Layman, J. M.; Ramirez, S. M.; Green, M. D.; Long, T. E. *Biomacromolecules* **2009**, *10*, 1244.
(13) Synatschke, C. V.; Schallon, A.; Jérôme, V.; Freitag, R.; Müller, A. H. E. *Biomacromolecules* **2011**, *12*, 4247.
(14) Koping-Hoggard, M.; Tubulekas, I.; Guan, H.; Edwards, K.; Nilsson, M.; Varum, K. M.; Artursson, P. *Gene Therapy* **2001**, *8*, 1108.
(15) Strand, S. P.; Lelu, S.; Reitan, N. K.; de Lange Davies, C.; Artursson, P.; Vårum, K. M. *Biomaterials* **2010**, *31*, 975.
(16) Davis, M. E.; Chen, Z. G.; Shin, D. M. *Nat. Rev. Drug Discovery* **2008**, *7*, 771.
(17) Prevette, L. E.; Lynch, M. L.; Kizjakina, K.; Reineke, T. M. *Langmuir* **2008**, *24*, 8090.
(18) de Wolf, H. K.; Luten, J.; Snel, C. J.; Oussoren, C.; Hennink, W. E.; Storm, G. *Journal of Controlled Release* **2005**, *109*, 275.
(19) Neu, M.; Fischer, D.; Kissel, T. *The Journal of Gene Medicine* **2005**, *7*, 992.
(20) Hwang, S. J.; Davis, M. E. *Curr. Opin. Mol. Ther.* **2001**, *3*, 183.
(21) Kakizawa, Y.; Kataoka, K. *Adv. Drug Delivery Rev.* **2002**, *54*, 203.
(22) Knop, K.; Hoogenboom, R.; Fischer, D.; Schubert, U. S. *Angew. Chem. Int. Ed.* **2010**, *49*, 6288.
(23) Monge, S.; Canniccioni, B.; Graillot, A.; Robin, J.-J. *Biomacromolecules* **2011**, *12*, 1973.
(24) Ren, H.; Sun, J.; Wu, B.; Zhou, Q. *Polymer Degradation and Stability* **2007**, *92*, 956.
(25) Xie, W.; Xie, R.; Pan, W.-P.; Hunter, D.; Koene, B.; Tan, L.-S.; Vaia, R. *Chemistry of Materials* **2002**, *14*, 4837.
(26) Cheng, S.; Zhang, M.; Wu, T.; Hemp, S. T.; Mather, B. D.; Moore, R. B.; Long, T. E. *J. Polym. Sci., Part A: Polym. Chem.* **2012**, *50*, 166.
(27) Mather, B. D.; Baker, M. B.; Beyer, F. L.; Green, M. D.; Berg, M. A. G.; Long, T. E. *Macromolecules* **2007**, *40*, 4396.
(28) Floch, V.; Loisel, S.; Guenin, E.; Hervé, A. C.; Clément, J. C.; Yaouanc, J. J.; des Abbayes, H.; Férec, C. *Journal of Medicinal Chemistry* **2000**, *43*, 4617.
(29) Guénin, E.; Hervé, A.-C.; Floch, V.; Loisel, S.; Yaouanc, J.-J.; Clément, J.-C.; Férec, C.; des Abbayes, H. *Angewandte Chemie International Edition* **2000**, *39*, 629.
(30) Picquet, E.; Le Ny, K.; Delépine, P.; Montier, T.; Yaouanc, J.-J.; Cartier, D.; des Abbayes, H.; Férec, C.; Clément, J.-C. *Bioconjugate Chemistry* **2005**, *16*, 1051.
(31) Hemp, S. T.; Allen, M. H.; Green, M. D.; Long, T. E. *Biomacromolecules* **2012**, *13*, 231.
(32) Ornelas-Megiatto, C.; Wich, P. R.; Fréchet, J. M. J. *Journal of the American Chemical Society* **2012**, *134*, 1902.

(33) Knop, K.; Hoogenboom, R.; Fischer, D.; Schubert, U. S. *Angew. Chem. Int. Ed.* **2010**, *49*, 6288.
(34) Hatakeyama, E. S.; Ju, H.; Gabriel, C. J.; Lohr, J. L.; Bara, J. E.; Noble, R. D.; Freeman, B. D.; Gin, D. L. *Journal of Membrane Science* **2009**, *330*, 104.
(35) Chu, D. S. H.; Schellinger, J. G.; Shi, J.; Convertine, A. J.; Stayton, P. S.; Pun, S. H. *Accounts of Chemical Research* **2012**, *ASAP*, DOI: 10.1021/ar200242z.
(36) Xu, F. J.; Yang, W. T. *Progress in Polymer Science* **2011**, *36*, 1099.
(37) Moad, G.; Rizzardo, E.; Thang, S. H. *Australian Journal of Chemistry* **2009**, *62*, 1402.
(38) York, A. W.; Kirkland, S. E.; McCormick, C. L. *Advanced Drug Delivery Reviews* **2008**, *60*, 1018.
(39) Scales, C. W.; Huang, F.; Li, N.; Vasilieva, Y. A.; Ray, J.; Convertine, A. J.; McCormick, C. L. *Macromolecules* **2006**, *39*, 6871.
(40) York, A. W.; Zhang, Y.; Holley, A. C.; Guo, Y.; Huang, F.; McCormick, C. L. *Biomacromolecules* **2009**, *10*, 936.
(41) Scholz, C.; Wagner, E. *Journal of Controlled Release* **2012**, *161*, 554.
(42) Nguyen, J.; Szoka, F. C. *Accounts of Chemical Research* **2012**, *ASAP*, DOI: 10.1021/ar3000162.
(43) Smith, A. E.; Sizovs, A.; Grandinetti, G.; Xue, L.; Reineke, T. M. *Biomacromolecules* **2011**, *12*, 3015.
(44) Jeong, J.; Park, T.; Kim, S. *Pharmaceutical Research* **2011**, *28*, 2072.
(45) Ogris, M.; Steinlein, P.; Kursa, M.; Mechtler, K.; Kircheis, R.; Wagner, E. *Gene Ther.* **1998**, *5*, 1425.
(46) Boussif, O.; Lezoualc'h, F.; Zanta, M. A.; Mergny, M. D.; Scherman, D.; Demeneix, B.; Behr, J. P. *Proceedings of the National Academy of Sciences* **1995**, *92*, 7297.
(47) Kanebratt, K. P.; Andersson, T. B. *Drug Metabolism and Disposition* **2008**, *36*, 137.
(48) Kanebratt, K. P.; Andersson, T. B. *Drug Metabolism and Disposition* **2008**, *36*, 1444.
(49) McGill, M. R.; Yan, H.-M.; Ramachandran, A.; Murray, G. J.; Rollins, D. E.; Jaeschke, H. *Hepatology* **2011**, *53*, 974.
(50) Zhang, X.; Pan, S.-R.; Hu, H.-M.; Wu, G.-F.; Feng, M.; Zhang, W.; Luo, X. *Journal of Biomedical Materials Research Part A* **2008**, *84A*, 795.
(51) Georgiou, T. K.; Vamvakaki, M.; Phylactou, L. A.; Patrickios, C. S. *Biomacromolecules* **2005**, *6*, 2990.
(52) De Smedt, S. C.; Demeester, J.; Hennink, W. E. *Pharmaceutical Research* **2000**, *17*, 113.
(53) Luo, D.; Saltzman, W. M. *Nat Biotech* **2000**, *18*, 893.

Chapter 8: Phosphonium Ionenes from Well-Defined Step-Growth Polymerization: Thermal and Melt Rheological Properties

(Published in *Polymer Chemistry* **2013,** *4* (12), 3582-3590.)

Sean T. Hemp, Musan Zhang, Mana Tamami, and Timothy E. Long*

Macromolecules and Interfaces Institute, Department of Chemistry, Virginia Tech, Blacksburg, VA 24061
*To whom correspondence should be addressed. E-mail: telong@vt.edu. TEL: (540)231-2480 FAX: (540)231-8517
Keywords: phosphonium, ionenes, melt rheology, polyelectrolytes

8.1 *Abstract*

Step-growth polymerization of ditertiary phosphines with dibromoalkanes enabled the synthesis of a novel family of phosphonium ionenes. *In situ* FTIR spectroscopy monitored the increase in absorbance as a function of time at 1116 cm^{-1}, which corresponded to the polymeric P^+–Ph stretch. Aqueous size-exclusion chromatography (SEC) provided absolute molecular weights and confirmed expected molecular weight growth for difunctional step-growth polymerization. Phosphonium ionenes exhibited improved thermal and base stability compared to ammonium ionenes, which was attributed to the propensity of the ammonium cation towards Hofmann elimination. Melt rheology examined phosphonium ionene viscous flow and the influence of charge density on melt viscosity as a function of shear rate and temperature. Time-temperature superposition (TTS) resulted in both master curves and pseudomaster curves depending on phosphonium ionene composition. Two primary relaxations occurred at these time scales: (1) onset of long-range segmental motion at T_g, and (2) relaxation attributed to electrostatic interactions. Higher charge densities shifted these two relaxations to longer time scales and increased flow activation energies. Phosphonium ionenes also readily bound pDNA effectively (+/- ratios of 1), and base stability suggested applications in energy generation.

8.2 *Introduction*

Cationic polyelectrolytes continue to receive significant attention in the literature due to their intriguing physical properties and opportunity to impact emerging technologies. Typical cationic polyelectrolytes include poly[2-(dimethylamino)ethyl methacrylate],[1] poly(diallyldimethylammonium chloride),[2] poly(vinyl imidazolium)s,[3] and cationic polystyrenes.[4] Polyelectrolytes have an extended coil conformation in solution, termed the polyelectrolyte effect, resulting from electrostatic repulsion in dilute solution.[5] They also exhibit high ionic conductivities due to their high charge density.[6] Recently, counterion exchange to fluorinated, bulky anions broadened the library of polyelectrolytes, leading to improved thermal stabilities, lower glass transition temperatures, and higher solid-state conductivity. Applications for polyelectrolytes include flocculation,[7] antimicrobials,[8] nonviral nucleic acid delivery,[9] and thin films.[10]

Ionenes are a unique class of polyelectrolytes with the cationic charges incorporated directly into the polymer backbone.[11] Due to a vast array of difunctional monomers, ionenes enable a thorough fundamental structure-property understanding of the influence of charge density, charge placement, and polymer architecture on polyelectrolyte behavior. Marvel et. al. initially reported the step-growth polymerization of ammonium ionenes utilizing AB monomers, which consisted of a tertiary amine and a halide.[12,13] Ditertiary amines and dihaloalkanes also undergo a Menschutkin reaction, which readily yields ammonium ionenes with varied alkylene spacers.[11] Ammonium ionenes are typically named x,y-ionenes wherein x and y correspond to the number of methylenes that space the tertiary amines and halides in each monomer, respectively. Long and coworkers previously reported on imidazolium ionenes, which contained

imidazolium cations within the macromolecular backbone.[14] These segmented ionenes displayed elastomeric behavior with improved thermal stabilities compared to ammonium analogs.

Phosphonium-containing macromolecules exhibit vastly improved properties compared to ammonium analogs. Endo and coworkers synthesized poly(vinylbenzyl phosphonium)s that displayed improved antimicrobial activity over poly(vinylbenzyl ammonium)s.[15,16] Kenawy et. al. also examined a broad range of phosphonium polyelectrolytes and demonstrated enhanced antimicrobial properties compared to ammonium polymers.[17-19] Our group recently reported the potential of phosphonium-containing macromolecules in nonviral nucleic acid delivery.[20,21] Subsequently, other groups also reinforced the efficacy of phosphonium delivery vehicles.[22,23] Phosphonium-containing macromolecules also show improved thermal and chemical stabilities in alkaline environments compared to ammonium analogs, which suggests impact on energy generation and storage devices. Therefore, many phosphonium-based materials are suitable for alkaline fuel cells[24] and anion-exchange membranes.[25]

We report the unprecedented synthesis of phosphonium ionenes utilizing ditertiary phosphines and dibromoalkanes to generate high molecular weight ionenes. *In situ* FTIR spectroscopy elucidated monomer conversion, and aqueous SEC provided absolute molecular weight growth values as a function of monomer conversion. Phosphonium ionene synthesis adhered to step-growth polymerization behavior, and high molecular weight phosphonium ionenes were achieved within 24 h at 100 °C. Monomer variation enabled a thorough study of the influence of charge density on thermal properties. pH stability studies confirmed the suitability of phosphonium ionenes for highly alkaline applications. Melt rheology directly probed the impact of charge density on phosphonium ionene melt flow, elucidating flow

activation energies and two primary relaxations. Finally, DNA gel shift assays examined the potential of phosphonium ionenes for nonviral nucleic acid delivery.

8.3 *Experimental Section*

8.3.1 Materials

1,2-bis(diphenylphosphino)ethane (97%), 1,4-bis(diphenylphosphino)butane (98%), and 1,6-bis(diphenylphosphino)hexane (97%) were purchased from Sigma-Aldrich and recrystallized from chloroform/methanol. 1,2-dibromoethane (98%), 1,4-dibromobutane (99%), and 1,6-dibromohexane (96%) were obtained from Sigma-Aldrich and distilled under reduced pressure. 1,12-dibromododecane (98%) was acquired from Sigma-Aldrich and recrystallized from ethanol. Potassium diphenylphosphide (0.5 M in THF) was purchased from Sigma-Aldrich and used as received. All solvents were obtained from Sigma-Aldrich and used as received. 1,12-bis(diphenylphosphino)dodecane was synthesized according to prior literature.[26]

8.3.2 Analytical Methods

Nuclear magnetic resonance (NMR) spectroscopy was completed in D_2O or CD_3OD at 23 °C using a Varian Unity 400 spectrometer. Thermogravimetric analysis (TGA) was performed using a TA Instruments TGA Q50 from 25 °C to 600 °C at a heating rate of 10 °C/min. Differential scanning calorimetry (DSC) was accomplished using a TA Instruments DSC Q1000 under a N_2 atmosphere with a heat/cool/heat cycle performed at 10 °C/min. Aqueous size-exclusion chromatography (SEC) utilized a ternary solution of 54/23/23 (v/v/v %) water/methanol/acetic acid with 0.1 M sodium acetate. The aqueous SEC included a Waters 717plus autosampler, a Waters 1515 isocratic HPLC pump, two Waters ultrahydrogel linear columns, and one Waters ultrahydrogel 250 column. The flow rate was 0.8 mL/min and a two

detector system consisting of a Waters 2414 refractive index (RI) detector and Wyatt MiniDAWN light scattering (LS) detector enabled the determination of absolute molecular weights. Offline d*n*/d*c* measurements were performed using a Wyatt Opti-lab T-rEX refractometer (λ = 658 nm).

Melt rheology was performed using a TA Instruments DHR-2 rheometer with an 8 mm parallel plate geometry. Initial strain sweep experiments (0.004 to 4.0 % oscillatory strain at 1 Hz) determined the linear viscoelastic region for phosphonium ionenes. The samples were subjected to temperature step, frequency sweep experiments at 10 °C/step (1.25% oscillatory strain, 0.1 – 100 rad/s). The resulting storage and loss moduli for each polymer were shifted using the TA Instruments TRIOS software package and horizontal shift factors (a_T). Master curves based on shifting and overlapping both storage and loss moduli generated horizontal shift factors, which were fitted to the WLF equation using TA Instruments TRIOS software package. Pseudomaster curves[27] based on fitting only loss modulus data resulted in suitable horizontal shift factors to fit an Arrhenius analysis to horizontal shift factors in the terminal flow region to obtain melt flow activation energies (E_a).

8.3.3 2P,2-cyclic Synthesis

A Schlenk tube with a magnetic stir bar was charged with 1,2-dibromoethane (223 μL, 2.59 mmol), 1,2-bis(diphenylphosphino)ethane (1.0283 g, 2.58 mmol), and DMF (4.54 mL). The resulting heterogeneous solution was degassed using three freeze-pump-thaw cycles and then heated to 100 °C for 2 h. The solution became homogeneous at 100 °C until the cyclic product precipitated. After 2 h, the resulting heterogeneous solution was poured into 500 mL ethyl acetate, and the resulting white solid was collected using filtration. The white solid was dried *in vacuo* at 60 °C for 24 h. ^{1}H NMR (400 MHz, D_2O, 23 °C) (δ, ppm): 7.66 (m, 12 H),

7.79 (m, 16 h). ^{13}C NMR: 136.74, 132.94, 131.34, 115.34, 114.43. ^{31}P NMR: 14.55. Mass spectrometry: theoretical m/z 425.1583, experimental m/z 425.1564.

8.3.4 Phosphonium Ionene Synthesis

All ionene polymerizations were accomplished utilizing a similar procedure, and the synthesis of 4P,12-ionene follows as an example. 1,4-bis(diphenylphosphino)butane (2.5494 g, 5.98 mmol), 1,12-dibromododecane (1.9612 g, 5.98 mmol), and DMF (14.3 mL) were added to a 25-mL, round-bottomed flask with a magnetic stir bar. After purging with Ar, the resulting heterogeneous solution was heated to 100 °C to obtain a homogenous solution and the polymerization was performed for 24 h at 100 °C. The resulting polymer solution was diluted with methanol and subsequently dialyzed against methanol (MWCO = 3500 g/mol) for 3 d. The polymer solution was concentrated *in vacuo*, and the solid polymer was dried *in vacuo* at 80 °C for 24 h (59% yield).

8.3.5 Monomer Conversion and Molecular Weight Growth Studies

In situ FTIR spectroscopy was implemented using a Mettler-Toledo ReactIR 4000 with a K6 DiComp conduit probe to monitor the polymerization. A 25-mL, two-necked, round-bottomed flask equipped with a stir bar was charged with 1,4-bis(diphenylphosphino)butane (2.00 g, 4.69 mmol) and DMF (10.0 mL). The two-necked flask was attached to the DiComp probe using a Teflon adapter and the second neck was sealed with a rubber septum. The resulting heterogeneous solution was purged with Ar and then equilibrated at 100 °C for 30 min to obtain a homogenous solution. The *in situ* FTIR spectroscopy was initiated, and 0.72 mL of 1,6-dibromohexane (4.69 mmol) was added using a syringe. The polymerization was monitored for 25 h at 100 °C.

Analysis using aqueous SEC to monitor the evolution of molecular weight growth was performed in a similar fashion using a 10-mL, one-necked, round-bottomed flask. 1,4-bis(diphenylphosphino)butane (1.1763 g, 2.76 mmol), 1,6-dibromohexane (424 μL, 2.76 mmol), and DMF (5.9 mL) were added to the flask, which was subsequently purged with Ar. The solution was heated to 100 °C for 24 h. Aliquots of the polymerization solution were removed using a syringe at different times in the polymerization. A portion of each aliquot was directly diluted into the aqueous SEC mobile phase to obtain a concentration of 5 mg polymer/mL, and this solution was injected to obtain absolute molecular weights as a function of time.

8.3.6 Base Stability of Phosphonium Ionenes

A solution of 4P,4-ionene (105.8 mg) in methanol (1.6 mL) was added to a 10-mL, round-bottomed flask. Subsequently, 10 M NaOH (0.4 mL) was added to the ionene solution to achieve a methanolic 2 M NaOH solution. After stirring for 24 h at 23 °C, an aliquot was removed and diluted into the aqueous SEC solvent to achieve a polymer concentration of 5 mg mg/mL. The resulting solution was injected on the aqueous SEC system to examine the change in molecular weight of 4P,4-ionene.

8.3.7 DNA Binding of Phosphonium Ionenes

Due to limited water solubility of phosphonium ionenes, phosphonium ionenes were placed into 10-mL, round-bottomed flasks with corresponding amount of water to obtain 1 mg polymer/mL solutions. The flasks were sealed with a rubber septum and then heated to 100 °C for 1 h. Upon cooling, the phosphonium ionenes remained in solution, enabling the examination of DNA binding using gel shift assays. gWiz-Luc plasmid DNA (0.2 μL, 1μg/μL in dH_2O, Aldevron) was complexed with the necessary amount of polymer solution (1 mg/mL) to obtain

various +/- ratios (positively charged phosphonium groups on polymer to negatively charged phosphate groups on DNA) in a total volume of 28 μL dH_2O. The resulting solutions were incubated for 30 min and then 2 μL loading buffer (30 wt% glycerol in H_2O) was added. Each solution (20 μL) was loaded onto a 1 wt% agarose gel stained with 6 μL of SYBR Green I (Sigma Aldrich) and the gel was metered at 70 V for 30 min. A MultiDoc-it Digital Imaging System (UVP) imaged the agarose gels to examine DNA complexation.

8.4 *Results and Discussion*

8.4.1 Monomer and Polymer Synthesis

Synthesis of ammonium ionenes relies upon the quantitative Menschutkin reaction of a ditertiary amine with a dihalide. Typically, ditertiary amines contain four methyl substituents and a longer alkyl spacer between the two tertiary amines. Larger substituents attached to the tertiary amine other than methyl groups decrease the nucleophilicity of the tertiary amine, resulting in insufficient conversions. Substitution of the methyls with phenyls further limits the nucleophilicity of the tertiary amine due to sterics and resonance delocalization of the lone pair across the phenyl rings. Conversely, tertiary phosphines consisting of three alkyl substituents are more prone to oxidation, therefore limiting the commercial availability of ditertiary phosphines to compounds with two phenyls and a single alkyl substituent attached to the tertiary phosphorus. In this case, the tertiary phosphine remains nucleophilic due to the polarizable electron pair and larger atomic radius of phosphorus.[28]

Scheme 8.1 displays the synthesis of phosphonium ionenes with primarily commercially available bis(diphenyl)phosphinoalkanes and dibromoalkanes. Control of the alkyl spacer between the phosphines or bromides generated a broad range of phosphonium ionenes with

controlled alkyl spacing between cationic sites. Phosphonium ionenes were labeled xP,y-ionene similar to ammonium ionene nomenclature wherein x corresponds to the length of the methylene spacer in the ditertiary phosphine, and y corresponds to the length of the methylene spacer in the dihaloalkane. All dibromoalkanes and bis(diphenyl)phosphinoalkanes were commercially available with the exception of 1,12-bis(diphenylphosphino)dodecane, which was synthesized according to previous literature.[26] Aqueous SEC utilizing a ternary mixture of 54/23/23 (v/v/v %) water/methanol/acetic acid with 0.1 M sodium acetate sufficiently screened polymer aggregation and column interactions to achieve reliable absolute molecular weight determination with light scattering detection of phosphonium ionenes.

Scheme 8.1. Step-growth polymerization of bis(diphenyl)phosphines and dibromides to synthesize phosphonium ionenes.

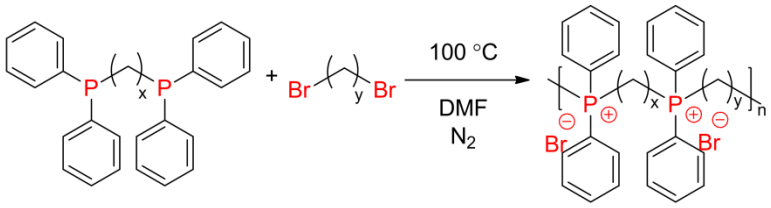

Initial syntheses focused on short alkyl spacers with the aim to create polyethyleneimine mimics containing phosphonium cations for nonviral nucleic acid delivery. Reaction of 1,2-bis(diphenylphosphino)ethane and 1,2-dibromoethane subsequently led to quantitative conversion to the six-membered cyclic shown in **Scheme 8.2**. ^{1}H NMR spectorscopy showed multiple overlapping signals from 7.6 – 7.9 ppm, and ^{31}P NMR showed a single peak at 14.6 ppm corresponding to a phosphonium oxidation state. High-resolution MS confirmed the cyclic structure. Previously, Noguchi and Rembaum probed the impact of alkyl spacer length on the formation of macromolecules or oligomers/cyclics during the synthesis of ammonium ionenes.[29]

They found alkyl spacers shorter than three primarily led to cyclic product formation, similar to our results with 1,2-dibromoethane and 1,2-bis(diphenylphosphino)ethane.

Scheme 8.2. Quantitative cyclization of 1,2-bis(diphenylphosphino)ethane and 1,2-dibromoethane.

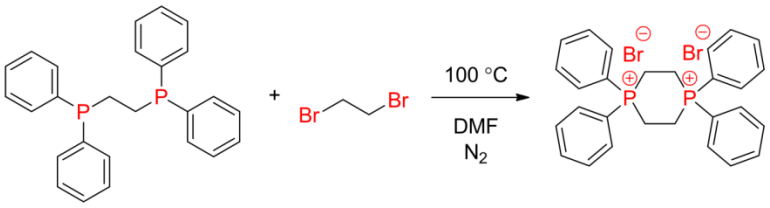

While quantitative cyclization occured during the synthesis of 2P,2-ionene, all other xP,y-phosphonium ionenes where x and y varied from 2, 4, 6, and 12 resulted in high molecular weight ionenes (M_n's ranging from 10.7 to 23.6 kg/mol) as shown in **Table 8.1**. Polydispersities (PDI) from the MALLS detector were relatively narrow compared to broader PDIs determined from a relative calibration to poly(ethylene glycol) standards. Our group previously reported similar findings for ammonium ionenes.[30] Aqueous SEC elucidated the presence of oligomeric cyclics in crude phosphonium ionene products. **Figure 8.1** displays aqueous SEC dRI traces for 2P,2-cyclic and 6P,4-ionene before and after dialysis (MWCO = 3,500 g/mol). Aqueous SEC of 6P,4-ionene prior to dialysis displayed a bimodal distribution where one peak corresponded to high molecular weight macromolecules (24-30 min elution time). The low molecular weight peak (32-34 min elution time) corresponded closely to 2P,2-cyclic, presumably corresponding to oligomeric cyclics formed during polymerization of 6P,4-ionene. Interestingly, formation of oligomeric cyclics did not result in a stoichiometric imbalance, enabling the synthesis of high molecular weight 6P,4-ionenes. xP,y-ionenes with alkyl spacers ≥6 exhibited a monomodal SEC trace, suggesting the absence of oligomeric cyclics. Dialysis against a 3,500 g/mol MWCO enabled purification of oligomeric cyclics from phosphonium ionene macromolecules as shown

in **Figure 8.1**. Further characterization of phosphonium ionenes were performed on dialyzed phosphonium ionenes to remove the influence of cyclics on macromolecular properties.

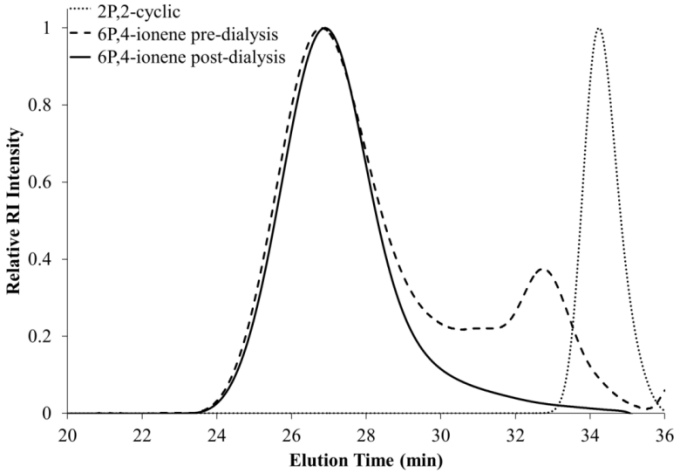

Figure 8.1. Aqueous SEC analysis of 2P,2-cyclic and 6P,4-ionene before and after dialysis highlighting the initial presence of cyclics in 6P,4-ionene prior to dialysis.

Table 8.1. Absolute molecular weight analysis of phosphonium ionenes.

Ionene	M_n (kg/mol)[a]	M_w (kg/mol)[a]	PDI[a]	PDI[b]	d*n*/d*c* (mL/g)[c]	Cyclics?[b]
4P,4	17.9	24.0	1.34	2.36	0.225	Yes (10 ring)
4P,6	15.3	18.2	1.19	2.34	0.224	Yes (12 ring)
6P,4	16.1	18.6	1.16	2.00	0.224	Yes (12 ring)
6P,6	20.6	27.2	1.32	2.51	0.213	No (14 ring)
2P,12	10.7	12.4	1.16	1.84	0.210	No (16 ring)
4P,12	23.6	28.4	1.20	2.07	0.205	No (18 ring)
6P,12	15.3	19.6	1.28	2.05	0.201	No (20 ring)
12P,12	18.8	19.5	1.04	1.31	0.191	No (26 ring)

[a]Aq. SEC MALLS, 54/23/23 H_2O/MeOH/AcOH 0.1 M NaAc; [b]Aq. SEC RI, Relative to PEO standards; [c]Wyatt Opti-lab T-rEX dRI, 35 °C

8.4.2 Monomer Conversion and Molecular Weight Growth

In situ FTIR spectroscopy and aqueous SEC probed the phosphonium ionene polymerization where *in situ* FTIR monitored monomer conversion and aqueous SEC followed absolute molecular weight growth during polymerization. Our group previously utilized *in situ* FTIR spectroscopy and aqueous SEC to examine ammonium ionene polymerization kinetics.[30] *In situ* FTIR spectroscopy specifically monitored the P^+–Ph stretch[31] at 1116 cm^{-1}, which increased as ditertiary phosphine monomers reacted with dibromoalkanes during polymerization. **Figure 8.2** depicts the *in situ* FTIR waterfall plot and the normalized P^+–Ph absorbance *versus* time plot over a 25 h period. Rapid monomer conversion and oligomerization occurred during the first 6 h of polymerization with very slow peak growth over the remaining 19 h. Due to the necessity of achieving high conversion (>99%) to obtain high molecular weights in a step-growth polymerization, aqueous SEC probed molecular weight growth throughout the polymerization.

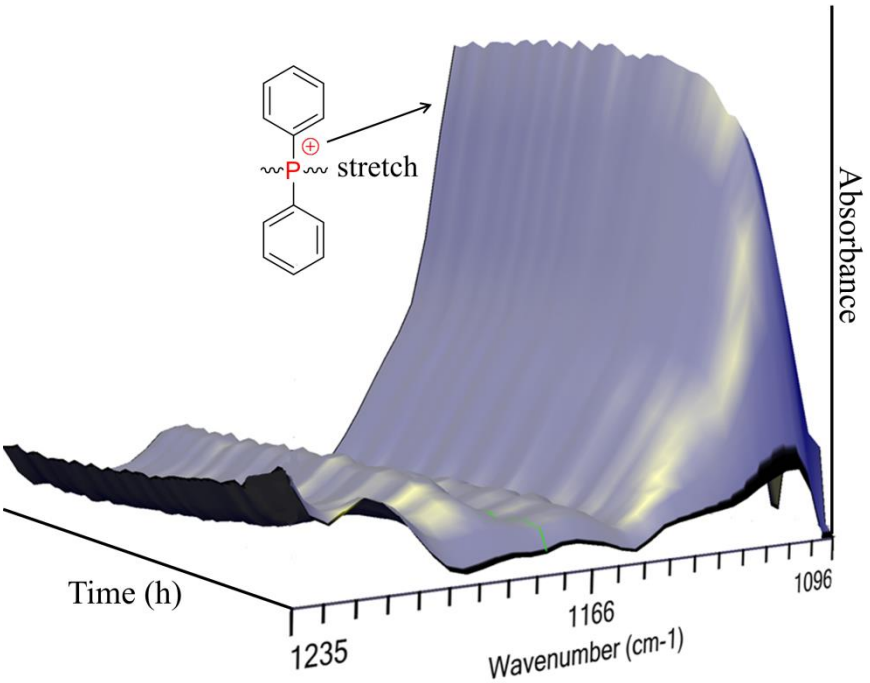

a)

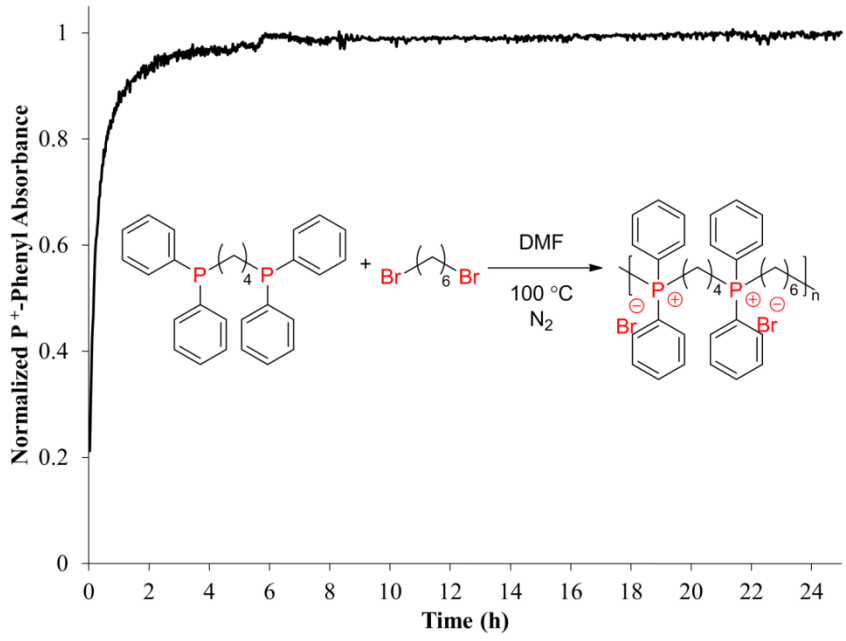

b)

Figure 8.2. *in situ* FTIR spectroscopy of 4P,6-ionene polymerization: a) *in situ* FTIR waterfall plot and b) absorbance increase of the P^{+}-C stretch at 1116 cm^{-1} during polymerization.

Figure 8.3 displays the evolution of molecular weight during 4P,6-ionene polymerization. Aliquots were removed at various times and injected onto the aqueous SEC to monitor molecular weight growth. The peak in the LS traces clearly exhibited a monotonic shift to shorter elution times and higher intensities corresponding to higher molecular weights. Correlation of absolute molecular weights to the normalized P^+–Ph absorbance confirmed expected molecular weight growth for a step-growth polymerization (**Figure 8.4**) with high molecular weights only achieved at high monomer conversions. Monomer stoichiometric imbalance enabled control of molecular weights to further confirm step-growth polymerization. Specifically, 4P,6-ionene polymerization with 5 mol% excess ditertiary phosphine or dibromoalkane resulted in a M_w of 12.7 kg/mol compared to 18.2 kg/mol for a 1:1 stoichiometry polymerization. The theoretical molecular weight calculated from the modified Carothers' equation was 13.7 kg/mol, which agreed well with the experimental M_w of 12.7 kg/mol.

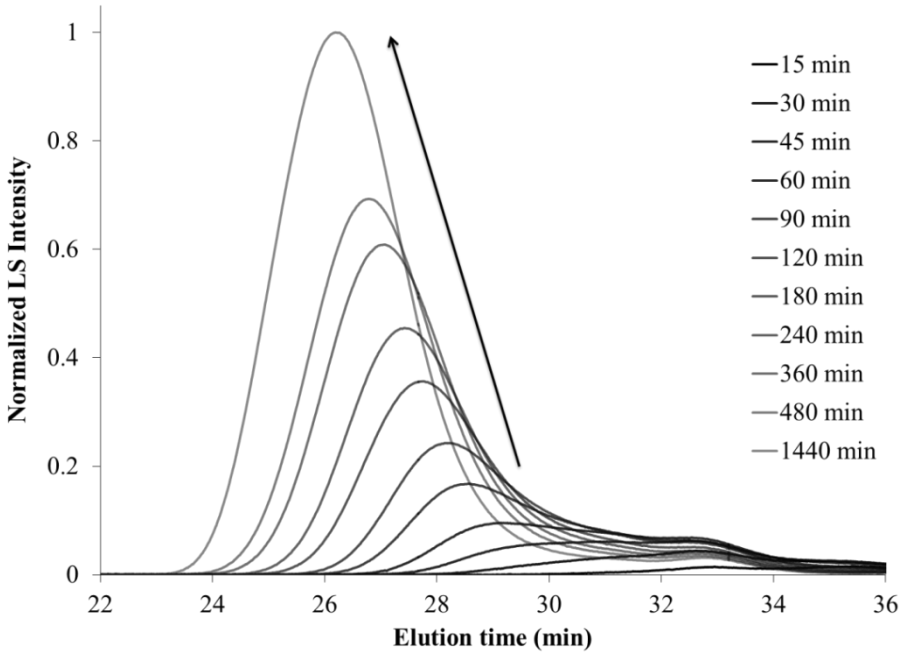

Figure 8.3. Molecular weight growth during 4P,6-ionene polymerization.

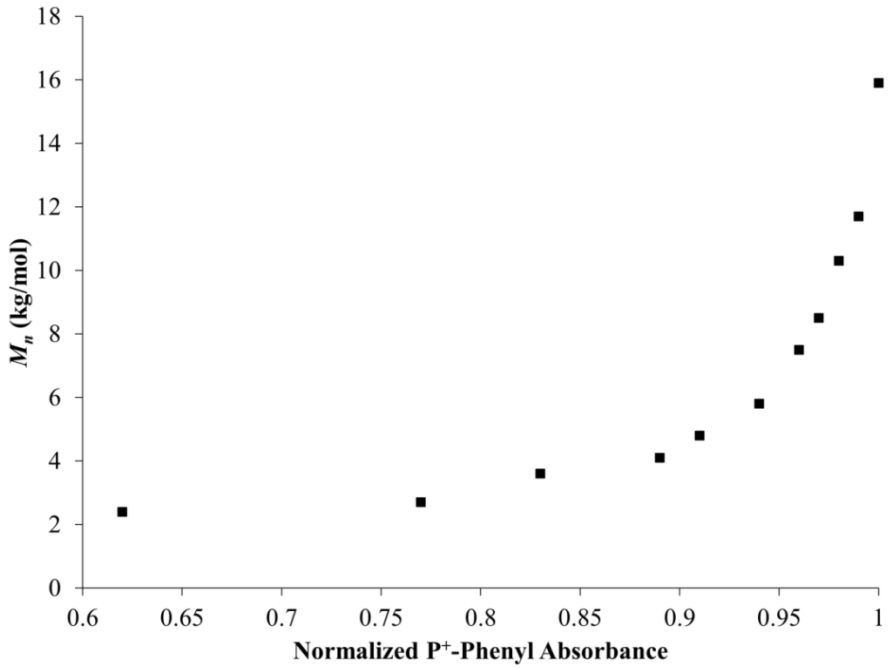

Figure 8.4. 4P,6-ionene molecular weight growth *versus* normalized absorbance demonstrating expected molecular weight growth in a step-growth polymerization.

8.4.3 Thermal Properties and Chemical Stability

Thermogravimetric analysis (TGA) probed the thermal stability of phosphonium ionenes (**Table 8.2**) and **Figure 8.5** shows the TGA curves for 6P,12-ionene and 6N,12-ionene. All phosphonium ionenes displayed thermal stabilities ≥300 °C, which were significantly more stable than ammonium ionenes previously reported (225 °C).[32] Phosphonium cations typically exhibit higher thermal stabilities compared to ammonium cations.[33] Literature suggests multiple different degradative pathways for ammonium polyelectrolytes, primarily Hofmann elimination and reverse Menschutkin degradation.[11] Hofmann elimination involves β-hydrogen abstraction to generate an alkene and liberate the tertiary amine. Reverse Menschutkin degradation occurs when the counterion (typically a halide) attacks the α-carbon, regenerating the original haloalkane and tertiary amine. Phosphonium cations typically resist reverse Menschutkin

degradation and Hofmann elimination, leading to improved thermal stabilities.[28] Variation of alkyl spacers in ditertiary phosphine and dibromoalkane monomers elucidated the impact of charge density on phosphonium ionene glass transition temperatures (T_g). Electrostatic associations from ionic substituents, which hinder molecular motion, typically result in increased T_g's for macromolecules.[34] Phosphonium ionenes exhibited lower T_g's as charge density decreased, presumably due to fewer ionic interactions. Specifically, the shortest alkyl spacer 4P,4-ionene displayed the highest T_g of 172 °C while the longest alkyl spacer 12P,12-ionene displayed the lowest T_g of 76 °C (**Table 8.2)**.

Table 8.2. Thermal properties of phosphonium ionenes.

Ionene	**T_g (°C)[a]**	**$T_{d,\ 5\%}$ (°C)[b]**
2P,2 (cyclic)	n.d.	302
4P,4	172	339
6P,6	n.d.	328
4P,6	155	334
6P,4	154	329
2P,12	148	300
4P,12	123	322
6P,12	104	314
12P,12	76	309

[a]TA DSC Q1000, 10 °C/min; [b]TA TGA Q50, 10 °C/min

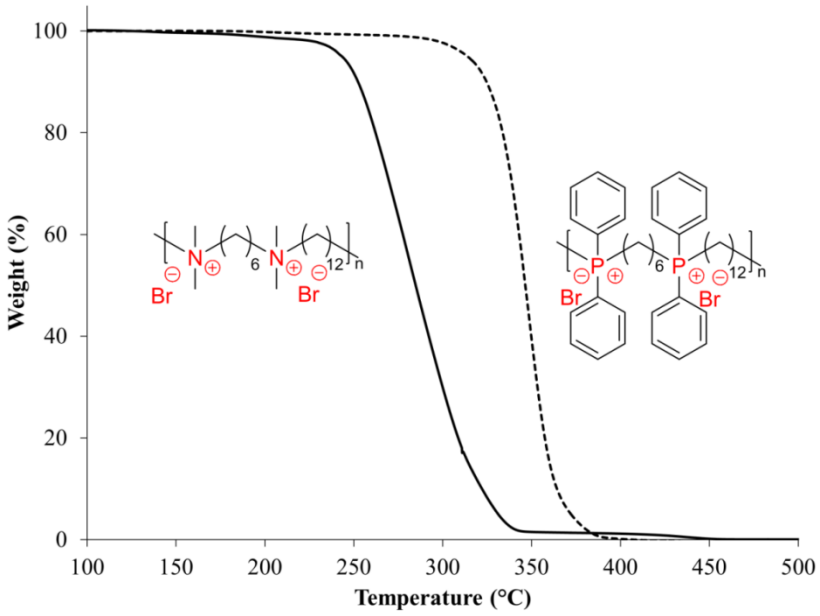

Figure 8.5. Weight (%) *versus* temperature of 6N,12-ionene and 6P,12-ionene demonstrating enhanced thermal stability of phosphonium ionenes compared to ammonium ionenes.

Previously, our group reported the base degradation of ammonium ionenes, wherein ammonium ionenes degraded through Hofmann elimination in the presence of 1M NaOH.[32] After 24 h in 1M NaOH at 23 °C, aqueous SEC showed a decrease in molecular weight with a multimodal and asymmetric molecular weight distribution, confirming base degradation of 12N,12-ionene. Phosphonium cations have less propensity for Hofmann elimination in the presence of strong bases and preferentially degrade into a tertiary phosphine oxide and alkane.[28] Due to limited solubility of phosphonium ionenes in water, phosphonium ionene base stability was probed in a methanolic 2M NaOH solution at 23 °C for 24 h (**Scheme 8.3)**. Phosphonium ionenes displayed enhanced base stability compared to ammonium ionenes. **Figure 8.6** shows the aqueous SEC traces for 4P,4-ionene before and after exposure to 2M NaOH. The molecular weight and molecular weight distribution remained unchanged after base treatment, which confirmed the improved base stability of phosphonium ionenes. Cation structure impacts

alkaline stability and the literature reports both ammonium[25,35] and phosphonium[24,36] macromolecules that exhibit alkaline stability. We aim to investigate further the improved alkaline stability of phosphonium ionenes compared to ammonium ionenes for applications in alkaline environments.

Scheme 8.3. Base stability study of phosphonium ionenes.

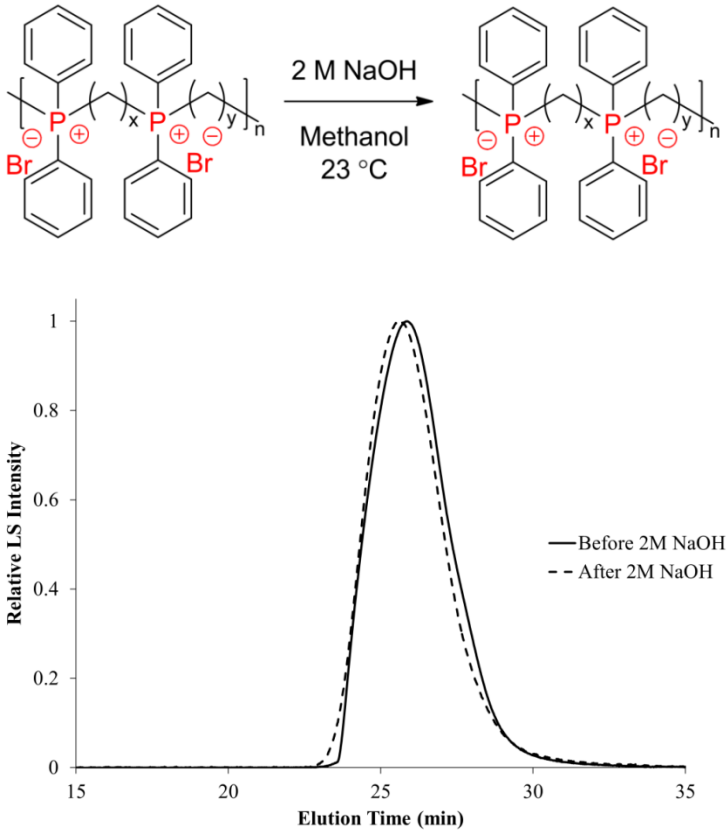

Figure 8.6. Base stability of 4P,4-ionene. Aqueous SEC MALLS confirmed absence of degradation after 1 d in a methanolic 2M NaOH solution at 23 °C. The M_n values before and after exposure to 2M NaOH were 23.0 kg/mol and 22.6 kg/mol, respectively.

8.4.4 Melt Rheology of Phosphonium Ionenes

Previous literature reports of the melt rheology of polyelectrolytes is relatively scarce,[37] predominately due to relatively high T_g's or low thermal stabilities of polyelectrolytes that

prevent a suitable thermal window to examine melt characteristics. High thermal stabilities (>300 °C) and relatively low T_g's (<172 °C) of phosphonium ionenes facilitated dynamic melt rheological studies to examine the impact of charge density on polyelectrolyte flow characteristics. Melt rheology of xP,12-ionenes directly explored the impact of alkyl spacer and charge density in a systematic fashion within the linear viscoelastic region. Frequency sweeps at 1.25% oscillatory strain were performed in 10 °C temperature steps to examine a broad viscoelastic region for time-temperature superposition (TTS).

Figure 8.7a highlights storage (G') and loss moduli (G'') master curves while **Figure 8.7b** depicts pseudomaster curves of complex viscosity generated from exclusively loss moduli. All phosphonium ionenes shared a similar reference temperature (T_r) of 170 °C for TTS. xP,12-ionenes obeyed TTS as seen in **Figure 8.7a** since both storage and loss moduli exhibited reasonable overlap across a frequency range of 8 decades leading to terminal flow. Master curves of phosphonium ionenes demonstrated two key relaxations modes within the polymer melt. The first mode at relatively high frequencies corresponded to the onset of long-range segmental motion at the T_g. The other mode at relatively lower frequencies presumably correlated to relaxation of electrostatic interactions, which agrees with similar relaxations in ionomers.[38] Overall, charge density impacted phosphonium ionene flow characteristics significantly with longer relaxation times for both relaxation modes as charge density increased from 12P,12-ionene to 2P,12-ionene. Terminal flow typically results in slopes where $G' \sim \omega^2$ and $G'' \sim \omega^1$; terminal slopes for phosphonium ionene loss moduli (0.9) agreed closely with expected slopes while phosphonium ionene terminal slopes for storage moduli (1.3 – 1.7) were lower than expected.

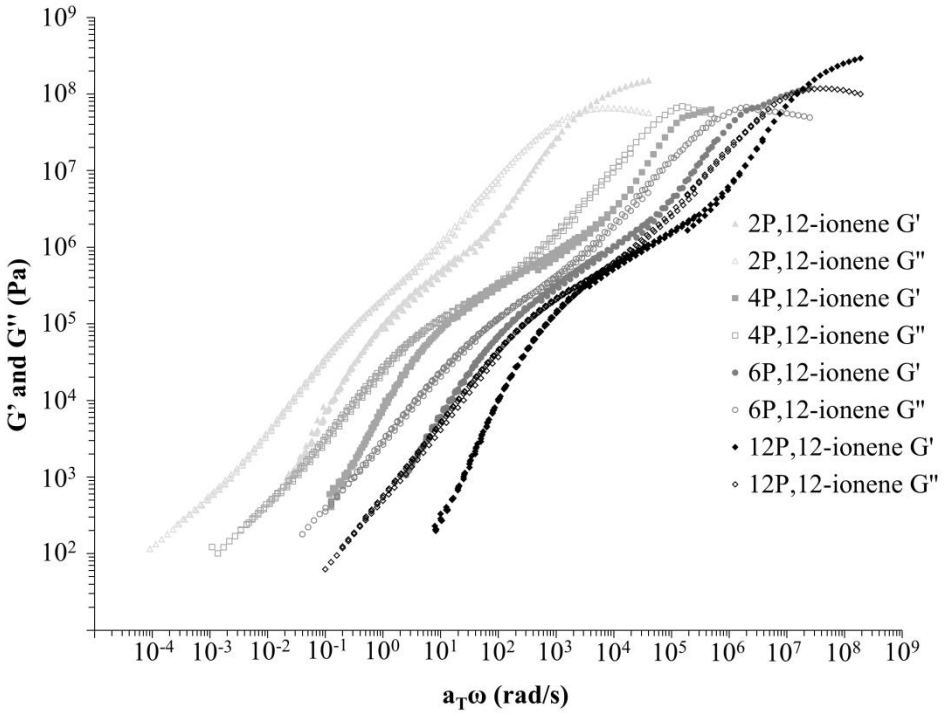

a)

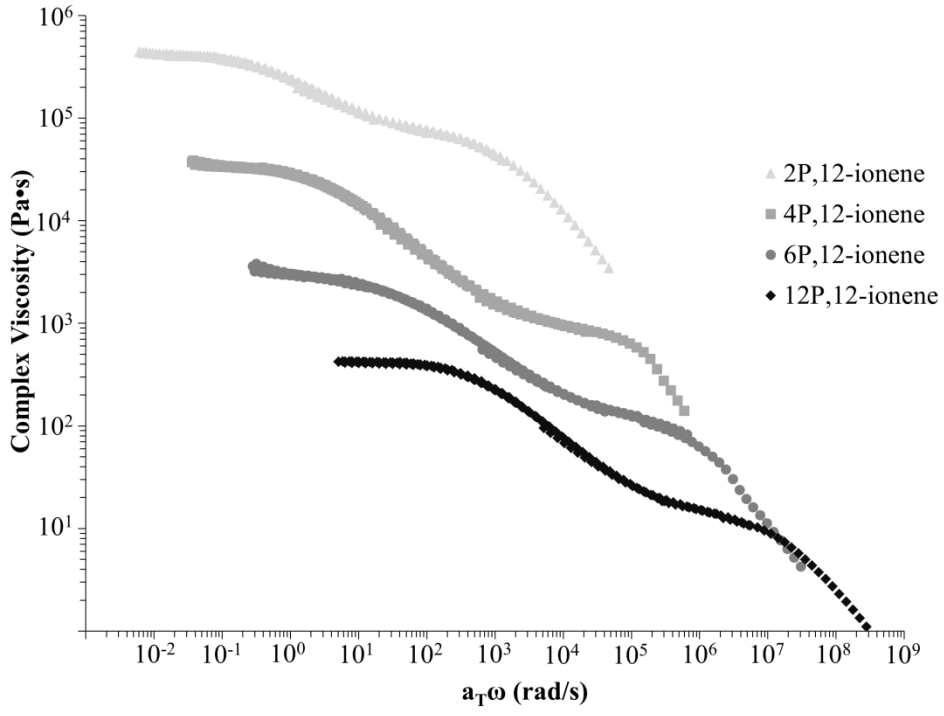

b)

Figure 8.7. Master curves of storage and loss moduli (a) and pseudo-master curves of complex viscosity (b) for xP,12-ionenes (T_r = 170 °C).

Shift factors (a_T) *versus* temperature for all xP,12-ionenes obeyed the Williams-Landel-Ferry equation,[39] which follows:

$$log(a_T) = \frac{-C_1(T - T_r)}{C_2 + (T - T_r)} \quad (1)$$

C_1 and C_2 are polymer-specific constants and T_r corresponds to the reference temperature chosen. **Figure 8.8** shows an exemplary WLF fit of shift factors for 4P,12-ionene. C_1 and C_2 constants depend on the T_r utilized in the TTS; therefore, they were converted to C_1^g and C_2^g values based on T_g using the following equations to enable direct comparisons to other C_1^g and C_2^g values in literature:

$$C_1^g = \frac{C_1 C_2}{C_2 + (T_g - T_r)} \quad (2)$$

$$C_2^g = C_2 + (T_g - T_r) \quad (3)$$

Neutral, non-associating polymers typically display C_1^g and C_2^g values of 16.79 ± 5.43 and 51.6 ± 28.1 K, respectively.[40] **Table 8.3** summaries C_1^g and C_2^g values for xP,12-ionenes. Phosphonium ionene C_1^g and C_2^g values occurred within error of neutral, non-associating polymer constants. WLF constants provide information regarding polymer fractional free volume at T_g (f_g) and the thermal expansion coefficient (α_f) using the following equations:

$$f_g = \frac{B}{2.303 C_1^g} \quad (4)$$

$$\alpha_f = \frac{B}{2.303 C_1^g C_2^g} \quad (5)$$

Doolittle and other researchers typically assume a value of 1 for the B constant.[41,42] Interestingly, f_g for xP,12-ionenes depended significantly on charge density with lower f_g's at lower charge densities, approaching neutral, non-associating polymers. Elabd and coworkers also

demonstrated higher fractional free volumes for polymerized ionic liquids with high charge densities.[40]

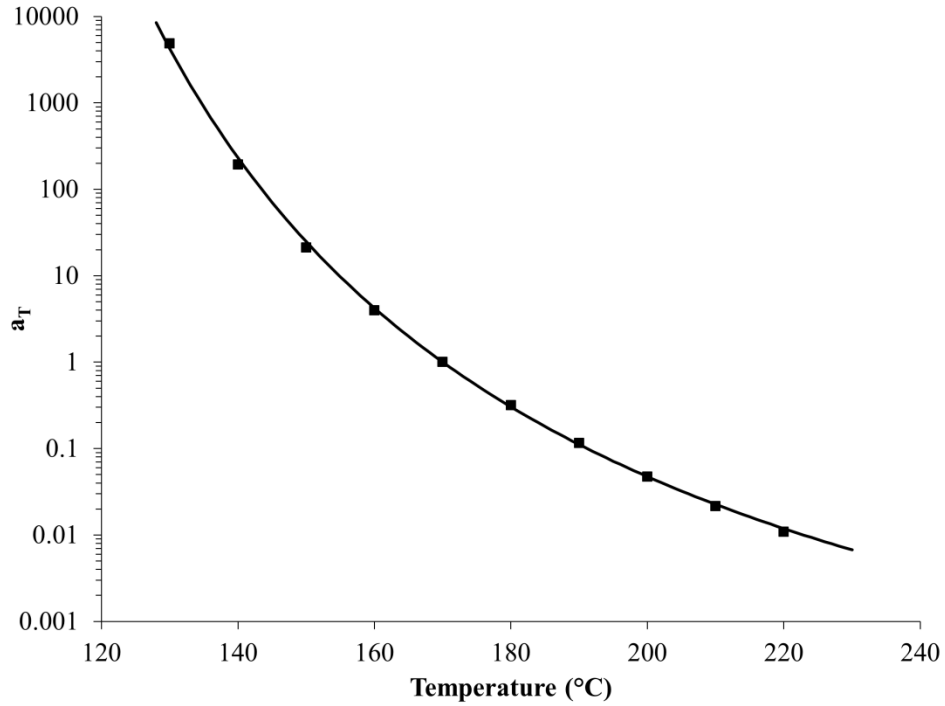

Figure 8.8. Shift factors (a_T) *versus* temperature (°C) for 4P,12-ionene. The WLF equation was fitted to experimental data to extract C_1 and C_2 values for all xP,12-ionenes at T_r = 170 °C. The solid black curve shows excellent fitting of the WLF equation to experimental data.

Table 8.3. WLF parameters, fractional free volumes, thermal expansion coefficients, and melt flow activation energies of xP,12-ionenes.

Ionene	**C_1**	**C_2 (K)**	**C_1^g**	**C_2^g (K)**	**f_g**	**α_f (10^{-4} K^{-1})**	**E_a (kJ/mol)**
2P,12	7.69	80.3	10.59	58.3	0.041	7.03	269
4P,12	6.02	106	10.79	59.4	0.040	6.77	176
6P,12	4.76	113	11.43	47.1	0.038	8.06	174
12P,12	4.17	133	14.15	39.3	0.031	7.81	156

Ionomers extensively studied utilizing melt rheology typically fail TTS principles, especially within rheologically complex regions corresponding to electrostatic relaxations in the storage moduli.[43] In these cases, researchers generate pseudomaster curves where shifts of loss moduli adhere to TTS.[27] These pseudomaster curves provide important information in the terminal flow region for ionomers and allows calculation of melt flow activation energies using the Arrhenius equation, which depends primarily on loss moduli.[44] Rheological complexity in the interim region between the T_g relaxation and electrostatic relaxation of phosphonium ionenes led to poor overlap of the storage moduli in this region. Therefore, pseudomaster curves of only the loss moduli generated shift factors suitable for complex viscosity (**Figure 8.7b**) and Arrhenius analysis of these shift factors provided phosphonium ionene flow activation energies. Flow activation energies shown in **Table 8.3** decreased from 269 kJ/mol to 156 kJ/mol as phosphonium ionene charge density decreased, which demonstrated the importance of electrostatics in the terminal flow region of phosphonium ionenes.

8.4.5 DNA Gel Shift Assay

While phosphonium ionenes exhibited poor water solubility due to phenyl substituents attached to the phosphonium cation, they readily dissolved at 100 °C and remained soluble at room temperature suitable for preliminary DNA binding studies. **Figure 8.9** shows a preliminary DNA gel shift assay for 6P,6-ionene, which readily bound DNA effectively at +/- ratios of 1. Phosphonium ionenes will enable a thorough understanding of how charge placement and charge density impact nucleic acid binding and delivery. Future reports will focus on the biological characterization of phosphonium ionenes and also segmented PEG-containing phosphonium ionenes, which will presumably improve water solubility and colloidal stability while decreasing cytotoxicity.

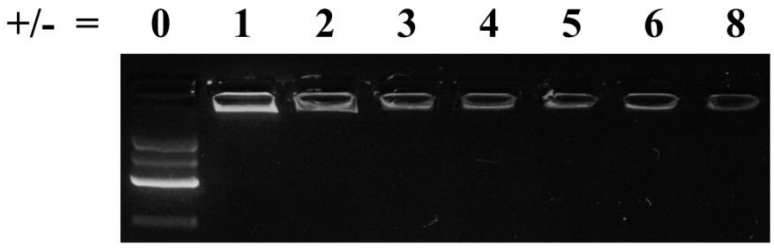

Figure 8.9. DNA gel shift assay for 6P,6-ionene demonstrating DNA binding efficiency of phosphonium ionenes.

8.5 *Conclusions*

The Menschutkin reaction between ditertiary phosphines and dibromoalkanes readily synthesized phosphonium ionenes with controlled charge density. *In situ* FTIR spectroscopy and aqueous SEC monitored the polymerization and confirmed expected step-growth behavior, achieving high molecular weights within 24 h. Phosphonium ionenes demonstrated improved thermal and chemical stabilities compared to ammonium analogs, which resulted from the phosphonium cation's enhanced resistance to degradation through either Hofmann elimination or reverse Menschutkin degradation. Melt rheology directly probed phosphonium ionene flow characteristics. Phosphonium ionenes exhibited two primary relaxations, one based on long-range segmental motion at T_g with short time scales and the other due to electrostatic relaxations at longer time scales. Higher charge densities shifted both relaxations to longer time scales and increased fractional free volumes at T_g. Flow activation energies also depended significantly on charge density, with higher activation energies as charge density increased. Finally, phosphonium ionenes demonstrated sufficient water solubility and 6P,6-ionene effectively bound pDNA at a +/- ratio of 1. Future work will focus on utilizing phosphonium ionenes in a variety of applications including nonviral nucleic acid delivery and alkaline fuel cells due to their advantageous properties.

8.6 *Acknowledgements*

This material is based upon work supported in part by the U.S. Army Research Laboratory and the U.S. Army Research Office under the Army Materials Center of Excellence Program, contract W911NF-06-2-0014. We acknowledge funding from NSF (CHE-0722638) for the acquisition of our Agilent 6220 LC-TOF-MS. This material is based upon work supported by the Army Research Office (ARO) under Award No. W911NF-10-1-0307 (DURIP). The authors also acknowledge the Institute for Critical Technology and Applied Science (ICTAS) at Virginia Tech for facility support.

8.7 *References*

(1) Hunley, M. T.; England, J. P.; Long, T. E. *Macromolecules* **2010**, *43*, 9998.
(2) Assem, Y.; Chaffey-Millar, H.; Barner-Kowollik, C.; Wegner, G.; Agarwal, S. *Macromolecules* **2007**, *40*, 3907.
(3) Green, M. D.; Salas‐de la Cruz, D.; Ye, Y.; Layman, J. M.; Elabd, Y. A.; Winey, K. I.; Long, T. E. *Macromolecular Chemistry and Physics* **2011**.
(4) Hatakeyama, E. S.; Ju, H.; Gabriel, C. J.; Lohr, J. L.; Bara, J. E.; Noble, R. D.; Freeman, B. D.; Gin, D. L. *Journal of Membrane Science* **2009**, *330*, 104.
(5) Dobrynin, A. V.; Colby, R. H.; Rubinstein, M. *Macromolecules* **1995**, *28*, 1859.
(6) Mecerreyes, D. *Progress in Polymer Science* **2011**, *36*, 1629.
(7) Li, D.; Zhu, S.; Pelton, R. H.; Spafford, M. *Colloid Polym Sci* **1999**, *277*, 108.
(8) Paslay, L. C.; Abel, B. A.; Brown, T. D.; Koul, V.; Choudhary, V.; McCormick, C. L.; Morgan, S. E. *Biomacromolecules* **2012**, *13*, 2472.
(9) Mintzer, M. A.; Simanek, E. E. *Chemical Reviews* **2009**, *109*, 259.
(10) Yang, Y.-H.; Haile, M.; Park, Y. T.; Malek, F. A.; Grunlan, J. C. *Macromolecules* **2011**, *44*, 1450.
(11) Williams, S. R.; Long, T. E. *Prog. Polym. Sci.* **2009**, *34*, 762.
(12) Gibbs, C. F.; Littmann, E. R.; Marvel, C. S. *Journal of the American Chemical Society* **1933**, *55*, 753.
(13) Lehman, M. R.; Thompson, C. D.; Marvel, C. S. *Journal of the American Chemical Society* **1933**, *55*, 1977.
(14) Williams, S. R.; Salas-de la Cruz, D.; Winey, K. I.; Long, T. E. *Polymer* **2010**, *51*, 1252.
(15) Kanazawa, A.; Ikeda, T.; Endo, T. *Journal of Applied Polymer Science* **1994**, *53*, 1245.
(16) Kanazawa, A.; Ikeda, T.; Endo, T. *Journal of Polymer Science Part A: Polymer Chemistry* **1993**, *31*, 335.
(17) Kenawy, E.-R.; Abdel-Hay, F. I.; El-Shanshoury, A. E.-R. R.; El-Newehy, M. H. *Journal of Polymer Science Part A: Polymer Chemistry* **2002**, *40*, 2384.

(18) Kenawy, E.-R.; Mahmoud, Y. A. G. *Macromolecular Bioscience* **2003**, *3*, 107.
(19) Kenawy, E.-R.; Abdel-Hay, F. I.; El-Shanshoury, A. E.-R. R.; El-Newehy, M. H. *Journal of Controlled Release* **1998**, *50*, 145.
(20) Hemp, S. T.; Smith, A. E.; Bryson, J. M.; Allen, M. H.; Long, T. E. *Biomacromolecules* **2012**, *13*, 2439.
(21) Hemp, S. T.; Allen, M. H.; Green, M. D.; Long, T. E. *Biomacromolecules* **2012**, *13*, 231.
(22) Ornelas-Megiatto, C.; Wich, P. R.; Fréchet, J. M. J. *Journal of the American Chemical Society* **2012**, *134*, 1902.
(23) Bansal, R.; Tripathi, S. K.; Gupta, K. C.; Kumar, P. *Journal of Materials Chemistry* **2012**, *22*, 25427.
(24) Noonan, K. J. T.; Hugar, K. M.; Kostalik, H. A.; Lobkovsky, E. B.; Abruña, H. D.; Coates, G. W. *Journal of the American Chemical Society* **2012**, *134*, 18161.
(25) Merle, G.; Wessling, M.; Nijmeijer, K. *Journal of Membrane Science* **2011**, *377*, 1.
(26) Paulusse, J. M. J.; Huijbers, J. P. J.; Sijbesma, R. P. *Macromolecules* **2005**, *38*, 6290.
(27) Greener, J.; Gillmor, J. R.; Daly, R. C. *Macromolecules* **1993**, *26*, 6416.
(28) Bradaric, C. J.; Downard, A.; Kennedy, C.; Robertson, A. J.; Zhou, Y. *Green Chemistry* **2003**, *5*, 143.
(29) Noguchi, H.; Rembaum, A. *Journal of Polymer Science Part B: Polymer Letters* **1969**, *7*, 383.
(30) Layman, J. M.; Borgerding, E. M.; Williams, S. R.; Heath, W. H.; Long, T. E. *Macromolecules* **2008**, *41*, 4635.
(31) Witschard, G.; Griffin, C. E. *Spectrochimica Acta* **1963**, *19*, 1905.
(32) Williams, S. R.; Borgerding, E. M.; Layman, J. M.; Wang, W.; Winey, K. I.; Long, T. E. *Macromolecules* **2008**, *41*, 5216.
(33) Fraser, K. J.; MacFarlane, D. R. *Australian Journal of Chemistry* **2009**, *62*, 309.
(34) Wang, F.; Hickner, M.; Kim, Y. S.; Zawodzinski, T. A.; McGrath, J. E. *Journal of Membrane Science* **2002**, *197*, 231.
(35) Bauer, B.; Strathmann, H.; Effenberger, F. *Desalination* **1990**, *79*, 125.
(36) Gu, S.; Cai, R.; Luo, T.; Chen, Z.; Sun, M.; Liu, Y.; He, G.; Yan, Y. *Angewandte Chemie International Edition* **2009**, *48*, 6499.
(37) Nakamura, K.; Saiwaki, T.; Fukao, K.; Inoue, T. *Macromolecules* **2011**, *44*, 7719.
(38) Weiss, R. A.; Fitzgerald, J. J.; Kim, D. *Macromolecules* **1991**, *24*, 1071.
(39) Ferry, J. D. *Viscoelastic properties of polymers*; Wiley: New York, 1980.
(40) Ye, Y.; Elabd, Y. A. *Polymer* **2011**, *52*, 1309.
(41) Doolittle, A. K. *Journal of Applied Physics* **1951**, *22*, 1471.
(42) Ikeda, Y.; Masui, H.; Matoba, Y. *Journal of Applied Polymer Science* **2005**, *95*, 178.
(43) Tierney, N. K.; Register, R. A. *Macromolecules* **2003**, *36*, 1170.
(44) Wu, Q.; Weiss, R. A. *Polymer* **2007**, *48*, 7558.

Chapter 9: Phosphonium Gemini Surfactants: Synthesis, Solution Properties, and Electrospinning

(*In preparation* for submission)

Sean T. Hemp, Amanda G. Hudson, Michael H. Allen, Jr., Sandeep S. Pole, Robert B. Moore,

and Timothy E. Long*

Macromolecules and Interfaces Institute, Department of Chemistry, Virginia Tech, Blacksburg, VA 24061
*To whom correspondence should be addressed. E-mail: telong@vt.edu. TEL: (540)231-2480 FAX: (540)231-8517

Keywords: phosphonium, gemini surfactants, solution rheology, electrospinning

9.1 *Abstract*

Bis(diphenylphosphino)alkanes reacted with excess 1-bromododecane generated novel phosphonium gemini surfactants with controlled spacer lengths from 2-4 methylenes. While dodecyltriphenylphosphonium bromide (DTPP), a monomeric surfactant analog, displayed excellent water solubility, phosphonium gemini surfactants exhibited low water solubility due to the two hydrophobic tails and relatively hydrophobic cationic head groups with phenyl substituents. Isothermal calorimetry showed no measureable critical micelle concentration for 12-2-12 phosphonium gemini surfactant in water at 25 °C. Subsequent experiments in 50/50 v/v water/methanol at 25 °C showed a CMC of 1.0 mM for 12-2-12. All phosphonium gemini surfactants effectively complexed nucleic acids, but they failed to deliver nucleic acids *in vitro* to HeLa cells. The solution behavior of phosphonium gemini surfactants was also probed in chloroform, an organic solvent where reverse micellar structures presumably formed. Solution rheology in chloroform explored the solution behavior of the phosphonium gemini surfactants compared to DTPP. Finally, the 12-2-12 and 12-3-12 gemini surfatants were successfully

electrospun from chloroform to generate uniform fibers while 12-4-12 gemini surfactant and DTPP only electrosprayed, forming droplets.

9.2 *Introduction*

Gemini surfactants have received significant attention in the literature recently due to their unique solution properties.[1] Gemini surfactants are composed of two conventional monomeric surfactants bound together at their head groups covalently through a spacer.[2] The head groups are hydrophilic and composed of ionic[3] or nonionic[4] groups. Common ionic head groups include ammoniums,[5] imidazoliums,[6] sulfonates,[7] and carboxylates.[8] The identity of the spacer directly impacts solution properties[9] and a variety of spacers have been examined including flexible alkyl spacers or rigid aromatic spacers.[10] Gemini surfactants displayed lower critical micelle concentrations (CMCs),[1] enhanced surface active properties,[11] and enhanced solubilization[12] compared to conventional surfactants. The spacer constrains the head groups, forcing more efficient packing of the head groups in supramolecular assemblies.[13] A broad range of supramolecular assemblies are adopted as a result including spherical micelles,[14] worm-like micelles,[15] and vesicles.[16]

Phosphonium gemini surfactants are relatively rare in the literature. To our knowledge, Gin et al.[17,18] demonstrated the only example of a phosphonium gemini surfactant in the literature. Using sophisticated techniques, they synthesized bis(alkyl-1,3-diene)-containing phosphonium gemini surfactants with methyl substituents on the head groups. Alkyl tail lengths and spacer lengths directly impacted the self-assembly of the phosphonium gemini surfactants into lyotropic liquid crystalline phases. The terminal diene groups on each tail enabled the crosslinking of the liquid crystalline materials and the crosslinked gemini surfactants maintained their liquid crystalline phase. Gin and coworkers[18] engineered a crosslinked composite

containing the phosphonium gemini surfactant to generate a highly efficient water purification membrane.

Candau et al.[19] reported on three theoretical concentration regimes for surfactants in solution: (1) a dilute regime with slow micellar growth, (2) a semidilute regime wherein the micelles rapidly grow in size, and (3) a concentrated regime where the net charge on the micelle end-caps directly impacts aggregation number. C* and C** correspond to transitions in the concentration regimes from the dilute to semidilute regime or semidilute to concentrated regime, respectively. Long et al.[20] examined the solution behavior of a common ammonium gemini surfactant called 12-2-12 with methyl substituents on the head groups. In water, the 12-2-12 surfactant displayed all three concentration regimes and cryo-TEM showed a change in micelle structure resulted in the regime changes. The scaling factors increased from the dilute regime to the concentrated regime due to enhanced micelle overlap at higher concentrations, leading to higher viscosities.

Electrospinning of polymers from solution or melt is a widely popular method to generate sub-micron, non-woven fibrous mats suitable for a broad range of applications including filtration and tissue scaffolds.[21] During the electrospinning process, the polymer solution is electrified and extruded from a needle whereupon it accelerates towards a grounded or electrified target.[22] Charge repulsion within the jet results in stretching and thinning of the fluid until it reaches the target where it solidifies.[23] The polymer must sufficiently stabilize the electrospinning jet to achieve uniform fibers.[24] Chain entanglements play a primary role in stabilizing the electrospinning jet and if the polymer concentration is too low to achieve sufficient chain entanglements, electrospraying will occur.[25] Long et al.[26] first reported the successful electrospinning of a low molar mass surfactant. The phospholipid mixture, soy

lecithin, self-assembled into worm-like micelles in organic solution and they sufficiently entangled at higher concentrations similar to polymer chains, stabilizing the electrospinning jet and generating uniform fibers. Long et al.[20] extended electrospinning of low molar molar mass molecules to a common ammonium gemini surfactant called 12-2-12 showing the impact of the supramolecular assembly on electrospinning behavior. Other researchers also have reported the electrospinning of other small molecules.[27-31]

We report herein the synthesis and characterization of novel phosphonium gemini surfactants with phenyl-containing head groups wherein the alkyl spacer between the head groups was varied between 2-4 methylenes. Thermogravimetric analysis and differential scanning calorimetry explored the thermal properties of the phosphonium gemini surfactants. The solution behavior of the phosphonium gemini surfactants was examined in both aqueous and organic solutions. Dynamic light scattering and isothermal calorimetry examined their aqueous solution behavior. Solution rheology probed the solution behavior of the phosphonium gemini surfactants in organic solution across a broad concentration regime and the ability of the phosphonium gemini surfactants to generate electrospun fibers was probed.

9.3 *Experimental Section*

9.3.1 Materials

1,2-bis(diphenylphosphino)ethane (99%), 1,3-bis(diphenylphosphino)propane (97%), 1,4-bis(diphenylphosphino)butane (98%), dodecyltriphenylphosphonium bromide (98%), and 1-bromododecane (97%) were obtained from Sigma-Aldrich and used as received. All solvents were obtained from Sigma-Aldrich and used as received.

9.3.2 Analytical Methods

Nuclear magnetic resonance (NMR) spectroscopy was performed in $CDCl_3$ using a Varian Unity 400 spectrometer operating at 400 MHz. Mass spectrometry was accomplished using an Agilent 6220 LC-TOF Mass Spectrometer. Thermogravimetric analysis (TGA) was completed using a TA Instruments TGA Q50 operating at a 10 °C/min ramp from 25 °C to 600 °C. Differential scanning calorimetry (DSC) was accomplished using a TA Instruments DSC Q1000 with a heat/cool/heat cycle. Solution rheology was performed using a TA Instruments DHR-2 strain-controlled rheometer with a concentric cylinder and solution cup geometry. Zero-shear viscosities were obtained from the Newtonian plateau in shear sweep experiments. Scanning electron microscopy (SEM) was performed using a Nikon Jeol SEM operating at 10 kV under high vacuum. Dynamic light scattering (DLS) was executed using a Malvern Zetasizer Nano operating at 25 °C.

Isothermal titration calorimetry (ITC) measurements were performed with a TA Instruments low volume Nano ITC. The Nano ITC has a gold reference and sample cell, each with a fixed volume of 190 μL, along with a gas tight syringe with a maximum volume of 50 μL. For the first set of experiments, duplicate titrations were performed where the sample cell was filled with ultrapure water and the injection syringe contained a 0.11 mM solution of 12-2-12. The ITC was held at 25 °C with a 350 rpm stir rate and aliquots of 1.43 μL were injected into the sample cell at an interval of 300 s between injections. In a second set of duplicate measurements for a mixed solvent system, the sample cell was filled with a mixture of 50/50 v/v water/methanol. The injection syringe was filled with an 8.05 mM solution of 12-2-12 in the same 50/50 v/v water/methanol mixture. Injections of the surfactant solution were titrated into

the cell in 1.99 μL aliquots with 300 s intervals between each injection. The CMC value was determined from the first derivative plot of interpolated enthalpy values.

9.3.3 Synthesis of 12-2-12 phosphonium gemini surfactant

1,2-bis(diphenylphosphino)ethane (24.85 g, 62.4 mmol), 1-bromododecane (62.65 g, 251.4 mmol), and ethanol (300 mL) were added to a 500-mL, round-bottomed flask with a magnetic stir bar. The solution was purged with argon for 1 h and subsequently heated at 80 °C for 3 d. The solution was concentrated *in vacuo* to obtain a viscous liquid. The viscous liquid was added dropwise to 3 L of hexanes to precipitate the gemini surfactant. The gemini surfactant was filtered and washed with 300 mL hexanes three times. The 12-2-12 surfactant was dried *in vacuo* at 70 °C for 2 d (46.00 g, 82.2% yield). ^{1}H NMR (400 MHz, $CDCl_3$) δ 8.10 (q, 8 H, ArH), 7.72 (t, 4 H, ArH), 7.64 (t, 8 H, ArH), 3.67 (m, 4 H, -PCH_2CH_2P-), 3.58 (m, 4 H, -PCH_2-), 1.43 (m, 4 H, -CH_2-), 1.14 (m, 36 H, -CH_2-), 0.83 (t, 6 H, -CH_3). ^{31}P NMR ($CDCl_3$) δ 30.68. Mass Spectrometry: Theoretical, m/z 368.2627; Experimental, m/z 368.2659.

9.3.4 Synthesis of 12-3-12 phosphonium gemini surfactant

1,3-bis(diphenylphosphino)propane (21.16 g, 51.3 mmol), 1-bromododecane (53.95 g, 216.5 mmol), and ethanol (300 mL) were added to a 500-mL, round-bottomed flask equipped with a magnetic stir bar. After purging the solution with argon for 1 h, the solution was heated at 80 °C for 3d. After concentrating the solution *in vacuo*, the viscous liquid was added to 3 L hexanes to obtain the solid 12-3-12 surfactant. The solid was filtered using suction and rinsed with 300 mL hexanes three times. The 12-3-12 surfactant was dried *in vacuo* at 70 °C for 2 d (42.98 g, 92.0% yield). ^{1}H NMR (400 MHz, $CDCl_3$) δ 7.93 (m, 8 H, ArH), 7.67 (m, 4 H, ArH), 7.61 (m, 8 H, ArH), 3.75 (m, 4 H, -PCH_2), 3.27 (m, 4 H, -PCH_2-), 2.03 (m, 2 H, -CH_2-) 1.44 (m,

8 H, -CH_2-), 1.15 (m, 32 H, -CH_2-), 0.84 (t, 6 H, -CH_3). ^{31}P NMR ($CDCl_3$) δ 27.16. Mass Spectrometry: Theoretical, m/z 375.2706; Experimental, m/z 375.2704.

9.3.5 Synthesis of 12-4-12 phosphonium gemini surfactant

1,4-bis(diphenylphosphino)butane (25.04 g, 58.7 mmol), 1-bromododecane (59.64 g, 239.3 mmol), and ethanol (300 mL) were added to a 500-mL, round-bottomed flask containing a magnetic stir bar. The solution was heated to 80 °C for 3 d after purging with argon for 1 h. The bulk of the ethanol was removed *in vacuo* and the viscous liquid was added dropwise to 3 L hexanes. A resulting yellow oil was obtained, which was washed with 3 L hexanes three times to induce solidification. The resulting solid was filtered to obtain the 12-4-12 surfactant. The surfactant was dried *in vacuo* at 70 °C for 2 d (44.80 g, 82.5% yield). ^{1}H NMR (400 MHz, $CDCl_3$) δ 7.91 (m, 8 H, ArH), 7.70 (m, 4 H, ArH), 7.65 (m, 8 H, ArH), 3.57 (m, 4 H, -PCH_2), 3.12 (m, 4 H, -PCH_2-), 1.93 (m, 4 H, -CH_2-) 1.45 (m, 8 H, -CH_2-), 1.16 (m, 32 H, -CH_2-), 0.84 (t, 6 H, -CH_3). ^{31}P NMR ($CDCl_3$) δ 28.24. Mass Spectrometry: Theoretical, m/z 382.2784; Experimental, m/z 382.2777.

9.3.6 Electrospinning

All phosphonium surfactants were electrospun from solutions of chloroform using a syringe pump to control the flow rate at 1 mL/hr. The surfactant solution was electrified at +20 kV with one power supply while the aluminum foil target was electrified at -15 kV using another power supply to generate an overall potential difference of 35 kV. The target was 15 cm from the syringe needle. After electrospinning, the fibers were imaged using SEM and 20 fibers were measured to obtain the average fiber diameter and standard deviation.

9.3.7 Polyplex Formation and Characterization

Phosphonium gemini surfactants displayed poor water solubility, requiring the dissolution of the surfactants in water at 0.1 mg/mL concentrations. The heterogenous solutions were sealed and heated to 100 °C for 1 h to generate homogenous solutions and then subsequently cooled to room temperature. DNA gel shift assays were performed as follows. Plasmid DNA (gWiz-Luc, Aldevron, 0.2 μg) was complexed with the required amount of phosphonium gemini surfactant to obtain the desired charge ratio in 28 μL total volume of water for 30 min. Loading buffer (30 wt% glycerol in water, 2 μL) was added and then 20 μL of the polyplex solutions was loaded in a 1 wt% agarose gel stained with 6 μL SYBR Green I (Sigma-Aldrich). The gel was metered at 70 V for 30 min and subsequently imaged using a MultiDoc-it Digital Imaging System (UVP).

9.3.8 Cell Culture

Human cervical cancer cells (HeLa) were cultured at 37 °C and 5% CO_2 in a saturated humid environment. The cells were grown in Dulbecco's modified Eagle's media (DMEM) supplemented with 10% fetal bovine serum (FBS), 100 U/mL penicillin, and 100 μg/mL streptomycin. All reagents were obtained from MediaTech and used as received.

9.3.9 Luciferase Assay

Polyplex solutions were prepared as follows for transfection. Plasmid DNA (5 μg) was diluted into H_2O (250 μL total volume). Phosphonium gemini surfactants (250 μL) at the appropriate concentration to generate the desired charge ratio when added to the DNA solution were also prepared. The surfactant solution was added to the pDNA solution and incubated for 30 min.

HeLa cells (500 uL, 100,000 cells/mL) were plated in 24-well plates 24 h prior to transfection. The complete media was aspirated and the cells were rinsed with 300 μL HBSS. After the addition of 400 μL DMEM to each well, 100 μL of the polyplex solution was added to the well (1 μg DNA/well). Lipofectamine 2000 and Jet-PEI formulations followed recommended manufacturer's protocols. The cells were transfected for 4 h and then the transfection media was aspirated. Complete media (500 μL) was added to each well and the cells were incubated for 44 h. Each well was rinsed with 300 μL PBS and the cells were subsequently lysed with 120 μL 1x Promega lysis buffer. The plates were incubated for 30 min and then subjected to two freeze-thaw cycles. A Promega luciferase kit was utilized following manufacturer's instructions to quantify luciferase expression. Luciferase transfection was reported as relative light units (RLU) and the transfections were performed in quadruplicate. Student's t-test was performed to determine statistical significance at a 95% confidence interval.

9.4 *Results and Discussion*

9.4.1 Synthesis

Previously, our group reported the synthesis of high molecular weight phosphonium ionenes from the well-defined step-growth polymerization of bis(diphenylphosphino)alkanes and alkyl dibromide monomers.[32] A logical extension of this research focused on the synthesis of novel phosphonium gemini surfactants wherein a monofunctional alkyl bromide, 1-bromododecane, was utilized to alkylate the bis(diphenylphosphino)alkanes to generate the desired gemini surfactants. **Scheme 9.1** depicts the synthesis utilized to generate phosphonium gemini surfactants. Gemini surfactants are commonly named x-y-x wherein x corresponds to the alkyl length of the tail and y correlates to the spacer length in between the cationic head groups.

12-y-12 phosphonium gemini surfactants were examined with y = 2-4 to examine the impact of the alkyl spacer length on solution behavior. All gemini surfactants were synthesized using a 4 molar excess of 1-bromododecane at 80 °C in ethanol for 3 d to ensure complete alkylation and minimize monoalkylation. Dodecyltriphenylphosphonium bromide (DTPP) served as a monofunctional surfactant control compared to the phosphonium gemini surfactants.

Scheme 9.1. Synthesis of phosphonium gemini surfactants.

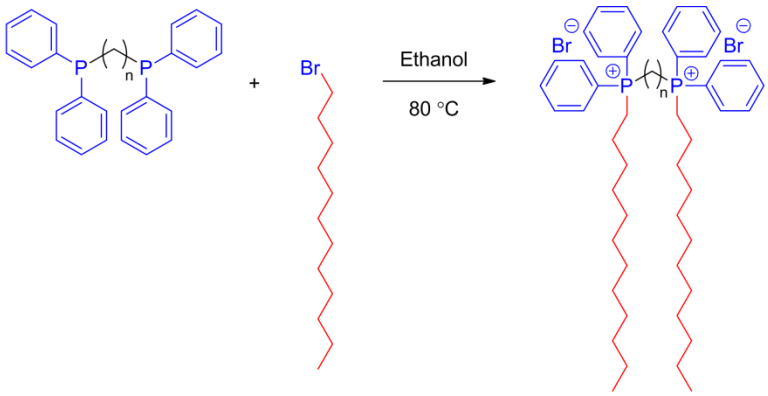

TGA and DSC examined the thermal stability and thermal transitions of the phosphonium gemini surfactants compared to the DTPP control surfactant (**Table 9.1**). 12-2-12 gemini surfactant displayed the lowest thermal stability due to the proximity of the phosphonium head groups decreasing the surfactant stability. Interestingly, 12-3-12 and 12-4-12 gemini surfactants exhibited improved thermal stability compared to DTPP. DSC analysis elucidated both the melting point and glass transition temperature of all surfactants. The melting point was obtained from the first heat while the glass transition temperature was determined from the second heat. The gemini surfactant T_g decreased as the spacer length increased while the T_m increased as the spacer length increased.

Table 9.1. Thermal properties of phosphonium gemini surfactants.

Gemini Surfactant	T_g (°C)	T_m (°C)	$T_{d,5\%}$ (°C)
DTPP	25	102	274
12-2-12	57	64	264
12-3-12	52	109	300
12-4-12	47	135	305

9.4.2 Gemini Surfactants in Water

DTPP is readily water soluble and displays a CMC of 1.80 mM in water.[33] Phosphonium gemini surfactants displayed poor water solubility, presumably due to the hydrophobic nature of the phenyl-containing head groups and the hydrophobic tails attached to the two head groups. Phosphonium gemini surfactants were heated at 100 °C for 1 h to generate stable surfactant solutions (0.1 mg/mL). Dynamic light scattering (DLS) experiments probed the solution structure of the phosphonium gemini surfactants in water at 0.1 mg/mL concentrations. **Figure 9.1** highlights the DLS traces for 12-2-12 and 12-3-12 phosphonium gemini surfactants. The size of the aggregates for 12-2-12 and 12-3-12 were 117 ± 2 nm and 105 ± 8 nm, respectively, with monomodal, narrow distributions. 12-4-12 gemini surfactant failed to display well-defined aggregates in aqueous solution based on DLS analysis.

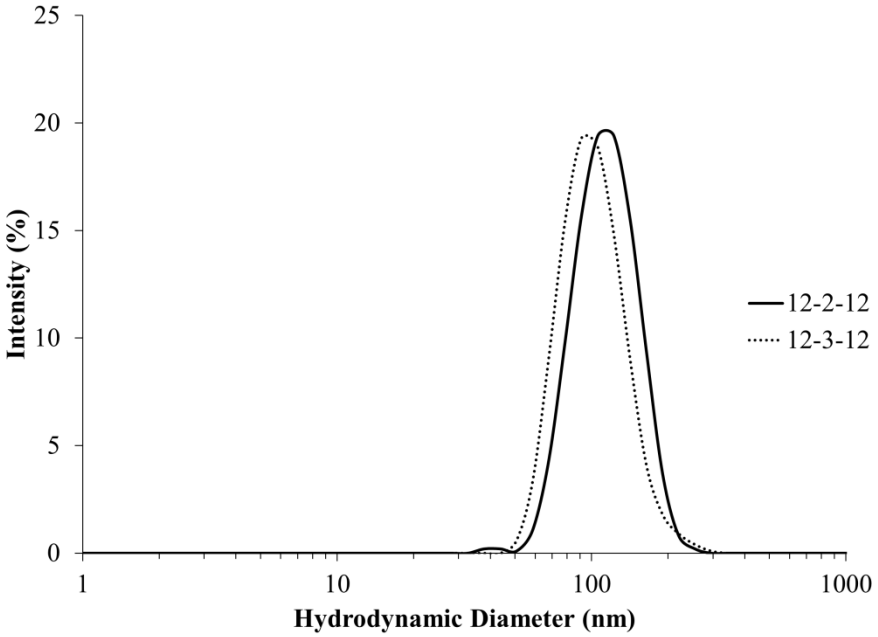

Figure 9.1. Dynamic light scattering of 12-2-12 and 12-3-12 phosphonium gemini surfactants in 0.1 mg/mL aqueous solutions.

Critical micelle concentrations (CMCs) are a critical property of all surfactants and multiple techniques including fluorescence spectroscopy,[34] conductivity,[35] and ITC[36] enable the determination of CMCs accurately. Initial experiments to determine the CMC of phosphonium gemini surfactants focused on fluorescence spectroscopy and conductivity methods to determine CMCs. Unfortunately, phenyl-containing phosphonium surfactants similar to the gemini surfactants have previously been shown to exhibit fluorescence quenching properties,[37] making fluorescence spectroscopy difficult. Conductivity methods also failed to determine the CMC of phosphonium gemini surfactants. The Krafft temperature, also called the critical micellization temperature, corresponds to the temperature necessary for the surfactant to readily dissolve and micellize in solution.[38] Below the Krafft temperature, the surfactant fails to display a CMC and remains in a hydrated crystalline state. The phosphonium gemini surfactants presumably exhibit

a very high Krafft temperature due to the hydrophobic tails and hydrophobic phenyl groups, which would lead to the absence of a CMC when below the Krafft temperature. Further, the solution preparation required 100 °C for 1 h to generate 0.1 mg/mL gemini surfactant solutions, suggesting a high Krafft temperature. Future work will examine the solubility of phosphonium gemini surfactants in aqueous solution further to understand the interplay of the Krafft temperature on micellization behavior.

Isothermal calorimetry (ITC) is one of the most effective methods to calculate the CMC of a surfactant while obtaining other thermodynamic information regarding the micellization behavior.[36] **Figure 9.2** depicts initial ITC experiments performed on 12-2-12 in water and a 50/50 v/v water/methanol solution. The titration of a concentrated 12-2-12 aqueous solution into water resulted in titration curves similar to the titration of water into water suggesting no appreciable demicellization occurring in pure water at 25 °C, also evidence for a high Krafft temperature. Titrations performed in 50/50 v/v water/methanol resulted in reproducible titration curves as shown in **Figure 9.2b**. The CMC for 12-2-12 in 50/50 v/v water/methanol was 1.0 mM at 25 °C. The addition of methanol resulted in improved solubility of the phosphonium gemini surfactants and enabled the determination of the CMC using ITC. Further work will develop a method to extrapolate the CMC of phosphonium gemini surfactants in water through a series of ITC experiments using different concentrations of water/methanol.

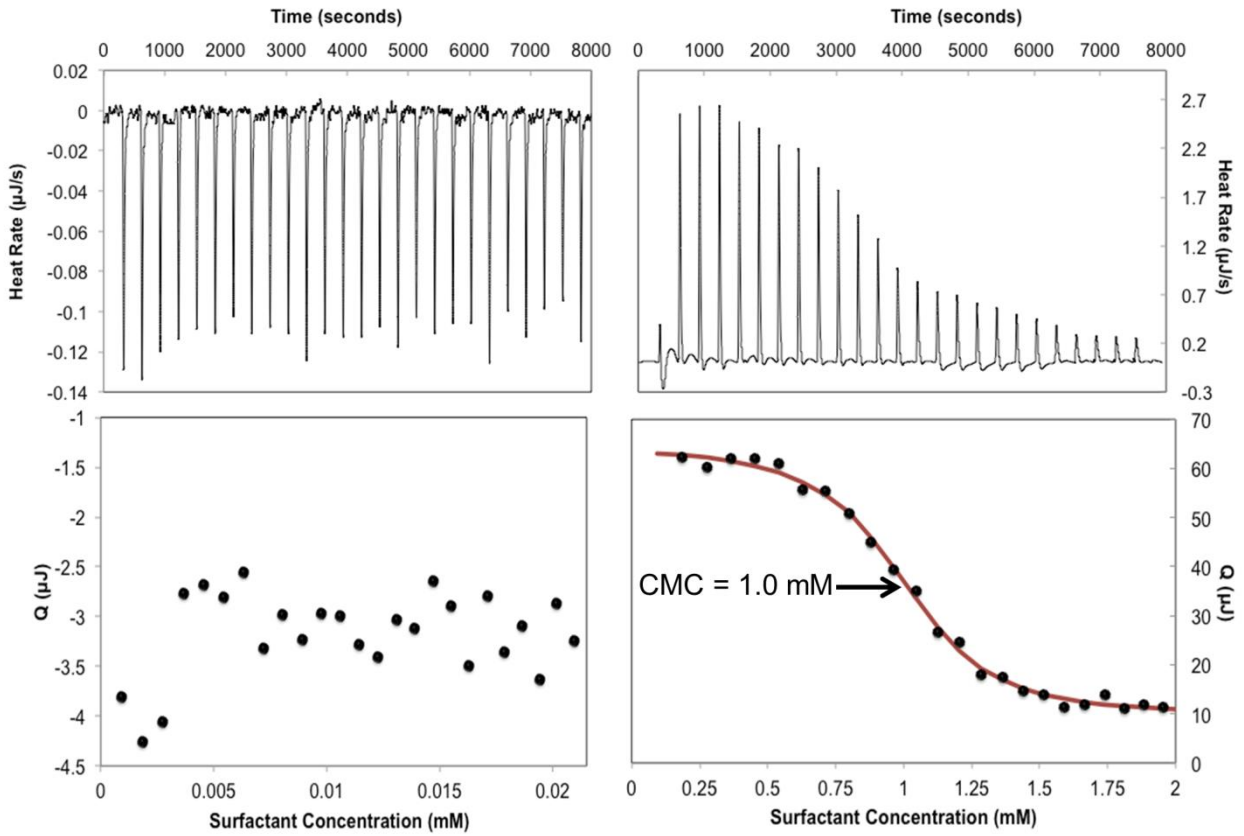

Figure 9.2. Isothermal calorimetry of 12-2-12 gemini surfactant in a) water and b) 50/50 v/v water/methanol.

DNA gel shift assays and luciferase transfection assays examined the suitability of phosphonium gemini surfactants as nonviral nucleic acid delivery agents. The complexation of a cationic surfactant and negatively-charged nucleic acid in solution generates nanoparticles or aggregates called lipoplexes. **Figure 9.3** shows DNA gel shift assays for all phosphonium gemini surfactants, which elucidated the efficacy of phosphonium gemini surfactants to bind nucleic acids. The charge ratio (+/- ratio) was defined as the moles of cationic head groups in the surfactant to the moles of negatively-charged phosphate groups in the plasmid DNA backbone. All phosphonium gemini surfactants bound nucleic acids with 12-2-12, 12-3-12, and 12-4-12 binding plasmid DNA completely at +/- ratios of 3, 2, and 2, respectively. Luciferase

transfection experiments in serum-free media elucidated the low transfection efficiency of phosphonium gemini surfactants compared to common positive controls, Jet-PEI and Lipofectamine 2000 (**Figure 9.4**).

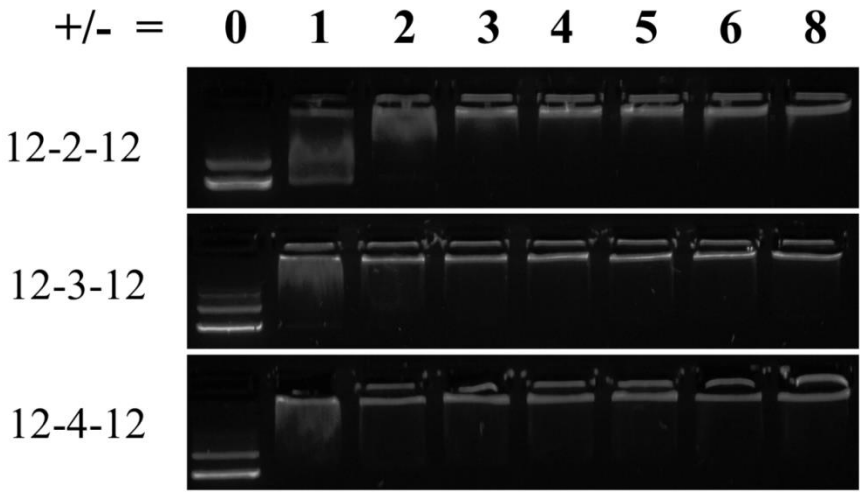

Figure 9.3. DNA gel shift assays for phosphonium gemini surfactants.

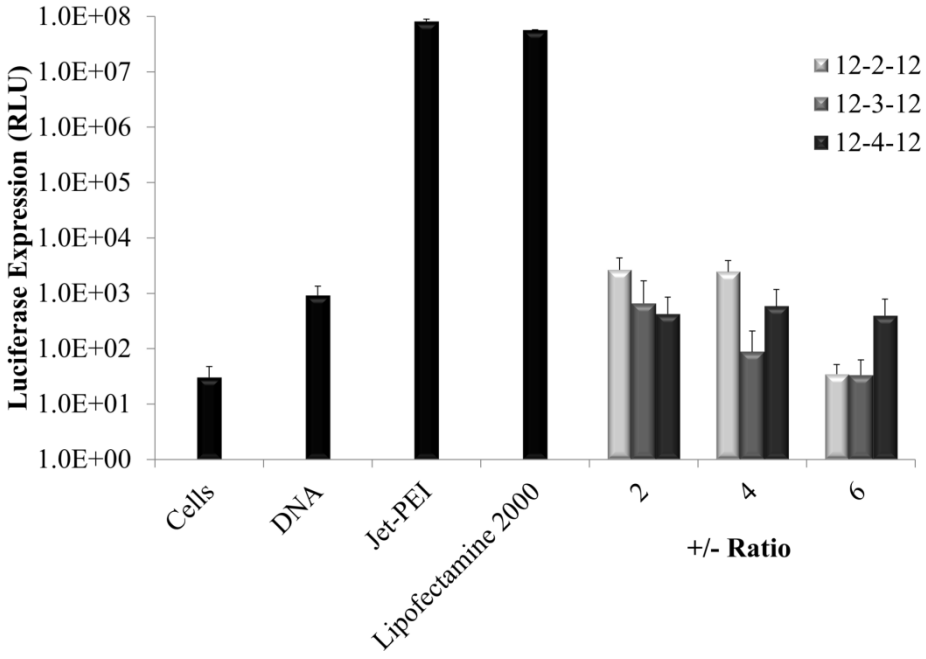

Figure 9.4. Serum-free luciferase assay for phosphonium gemini surfactants.

9.4.3 Gemini Surfactants in Chloroform

With the goal of generating electrospun fibers composed of the phosphonium gemini surfactants, the solution behavior of phosphonium gemini surfactants in organic solutions was examined to provide information necessary for electrospinning. Phosphonium gemini surfactants displayed excellent solubility in organic solvents except for hexanes. Chloroform was chosen as the solvent to examine the solution properties of phosphonium gemini surfactants due to its ability to dissolve the surfactants and its volatility, necessary for an electrospinning application. Surfactants generate reverse micelle and other reverse supramolecular structures in organic solutions.[39,40] Reverse micelles differ from normal micelles in that the head group sequesters itself into the micelle core and the hydrophobic tails reside in the shell of the micelle.

Solution rheology of DTPP and all phosphonium gemini surfactants studied the solution behavior of the surfactants in chloroform. **Figure 9.5** reports the specific viscosity vs. concentration for all surfactants examined. In each graph, three different solution regimes were identified based upon a change in the slope of the data. C* and C** were defined as the crossover points where each power law regression overlaped with the power law regression of the adjacent concentration regime. All surfactants displayed similar C* transitions, occurring at ~19 wt% in chloroform. C** depended significantly on the surfactant with DTPP displaying significantly a higher C** at 39 wt% compared to 30-32 wt% for the phosphonium gemini surfactants. The constraint of the head groups in the gemini surfactants presumably resulted in different supramolecular structures, which resulted in significant overlap of the structures in solution at lower concentrations. Soy lecithin, a phospholipid mixture, displayed a similar C** of 35 wt% in 70/30 v/v chloroform/DMF compared to the phosphonium gemini surfactants.[26]

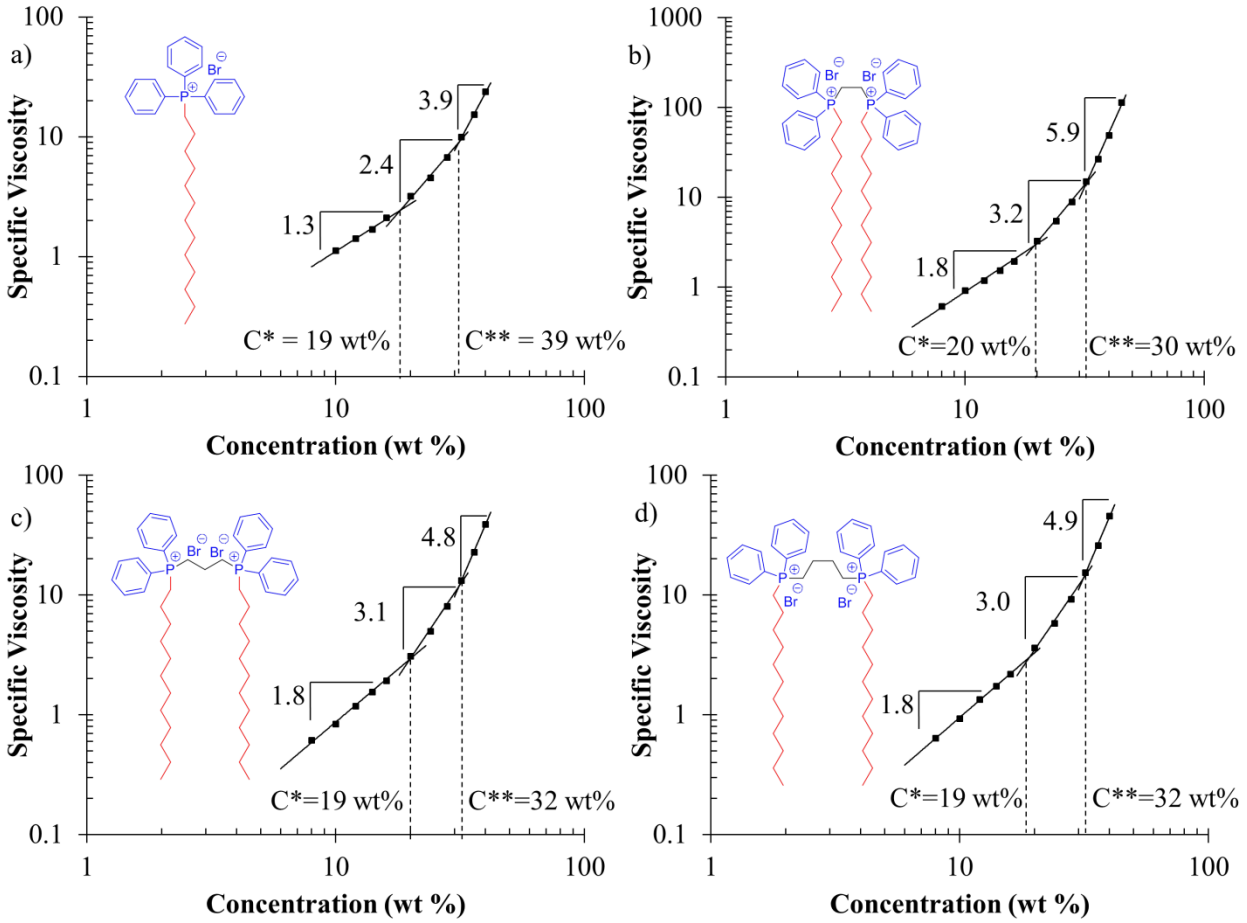

Figure 9.5. Solution rheology of phosphonium control surfactant and phosphonium gemini surfactants in chloroform.

Polymer solution rheology utilizes the scaling parameters in each concentration regime to identify the solution behavior of the polymer. For instance, neutral, non-associating polymers display significantly different scaling factors compared to polyelectrolytes and the scaling factors provide information regarding the polymer solution conformation and solution behavior. All phosphonium gemini surfactants exhibited higher scaling factors compared to the DTPP control, especially in the concentrated regime above C**. 12-2-12 gemini surfactant resulted in the highest scaling factors compared to all surfactants, likely due to the short ethylene spacer

constraining the conformation of the head group. As a comparison, soy lecithin in 70/30 v/v chloroform/DMF displayed scaling factors of 2.4 and 8.4 in the semidilute and concentrated regimes, respectively.[26] The phosphonium gemini surfactants exhibited similar semidilute scaling factors as soy lecithin, but their concentrated scaling factors were significantly lower than the concentrated scaling factor for soy lecithin.

Attempts at electrospinning DTPP and the phosphonium gemini surfactants examined the impact of the surfactant structure on fiber formation. All electrospinning attempts occurred at concentrations of 52 wt% or lower. DTPP and 12-4-12 gemini surfactant failed to generate any electrospun fibers, primarily electrospraying that created droplets. Conversely, 12-2-12 and 12-3-12 gemini surfactants sufficiently stabilized the electrospinning jet to generate electrospun fibers as shown in **Figure 9.6**. Prior to 52 wt%, ill-defined fibers were formed with the incorporation of droplets or beaded fibers. Concentrations of 52 wt% were necessary to generate uniform, well-defined fibers. The 12-2-12 and 12-3-12 gemini surfactants generated fibers diameters of 1.0 ± 0.3 μm and 1.1 ± 0.2 μm, respectively, at 52 wt% in chloroform. As a comparison, aqueous solutions (50/50 v/v water/methanol) of an ammonium gemini surfactant (12-2-12) at concentrations of 42 and 44 wt% generated uniform fibers of 4 and 5 μm diameters, respectively.[20] Ultimately, spacers of 2 or 3 methylenes were necessary to generate a stable electrospinning jet to obtain uniform fibers. The longer alkyl spacer of 4 methylenes and the DTPP surfactant failed to generate electrospun fibers, presumably due to the absence of sufficient supramolecular entanglements.

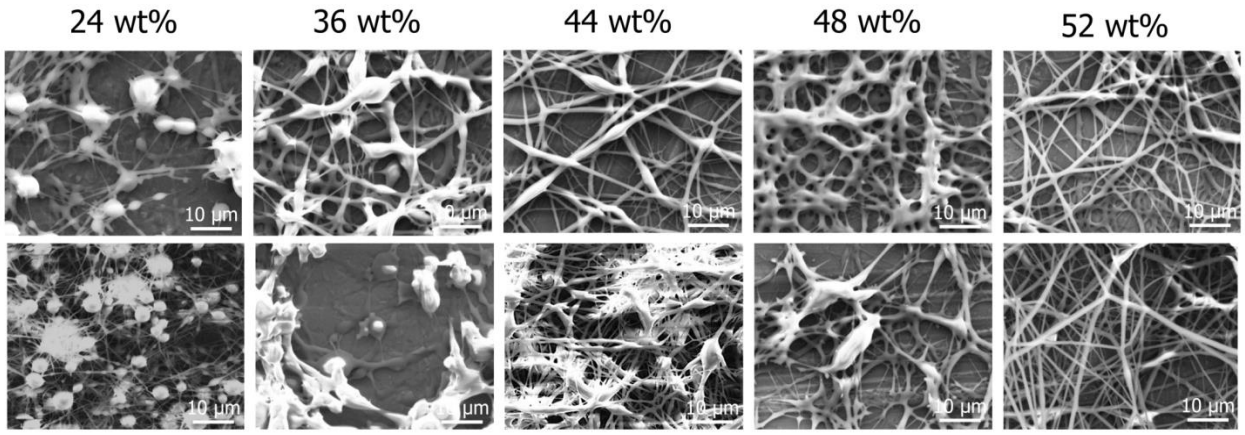

Figure 9.6. SEM of electrospun phosphonium gemini surfactants from chloroform with the top images corresponding to the 12-2-12 gemini surfactant and the bottom images corresponding to the 12-3-12 gemini surfactant.

9.5 *Conclusions*

The alkylation of ditertiary phosphines using 1-bromododecane generated phosphonium gemini surfactants in high yields. The cationic head groups displayed significant hydrophobicity due to the phenyl substituents leading to poor solubility in water. 12-2-12 and 12-3-12 gemini surfactants self-assembled into large supramolecular structures shown using DLS. Isothermal calorimetry confirmed the absence of a CMC for 12-2-12 in pure water at 25 °C while the 12-2-12 gemini surfactant displayed a CMC of 1.0 mM in 50/50 v/v water/methanol solution. Preliminary biological assays focused on nucleic acid complexation and delivery demonstrated efficient nucleic acid binding for phosphonium gemini surfactants. The phosphonium gemini surfactants failed to efficiently deliver nucleic acids *in vitro* to HeLa cells. Phosphonium gemini surfactants were also studied in chloroform, an organic solvent, that promoted reverse micellar structures. Solution rheology elucidated the overall solution behavior of phosphonium gemini surfactants and DTPP in chloroform. Ultimately, electrospinning of 12-2-12 and 12-3-12 gemini

surfactants generated uniform fibers with fiber diameters of ~1 μm while 12-4-12 and DTPP failed to electrospin.

9.6 *Acknowledgements*

This material is based upon work supported in part by the U.S. Army Research Office under grant number W911NF-07-1-0452 Ionic Liquids in Electro-Active Devices (ILEAD) MURI. This material is based upon work supported in part by the U.S. Army Research Laboratory and the U.S. Army Research Office under the Army Materials Center of Excellence Program, contract W911NF-06-2-0014. This material is partially based upon work supported by the National Science Foundation under Grant No. DMR-0923107. We acknowledge funding from NSF (CHE-0722638) for the acquisition of our Agilent 6220 LC-TOF-MS. This material is based upon work supported by the Army Research Office (ARO) under Award No. W911NF-10-1-0307 (DURIP). The authors also acknowledge the Institute for Critical Technology and Applied Science (ICTAS) at Virginia Tech for facility support.

9.7 *References*

(1) Menger, F. M.; Keiper, J. S. *Angewandte Chemie International Edition* **2000**, *39*, 1906.
(2) Menger, F. M.; Littau, C. *Journal of the American Chemical Society* **1991**, *113*, 1451.
(3) Menger, F.; Littau, C. *Journal of the American Chemical Society* **1993**, *115*, 10083.
(4) Castro, M. J.; Kovensky, J.; Fernández Cirelli, A. *Langmuir* **2002**, *18*, 2477.
(5) Wang, X.; Wang, J.; Wang, Y.; Yan, H.; Li, P.; Thomas, R. K. *Langmuir* **2003**, *20*, 53.
(6) Ao, M.; Xu, G.; Zhu, Y.; Bai, Y. *Journal of Colloid and interface science* **2008**, *326*, 490.
(7) Wang, Y.; Han, Y.; Huang, X.; Cao, M.; Wang, Y. *Journal of Colloid and interface science* **2008**, *319*, 534.
(8) Huang, X.; Cao, M.; Wang, J.; Wang, Y. *The Journal of Physical Chemistry B* **2006**, *110*, 19479.
(9) Rosen, M. J.; Song, L. D. *Journal of Colloid and interface science* **1996**, *179*, 261.
(10) Song, L. D.; Rosen, M. J. *Langmuir* **1996**, *12*, 1149.
(11) Rosen, M. J.; Mathias, J. H.; Davenport, L. *Langmuir* **1999**, *15*, 7340.
(12) Dreja, M.; Tieke, B. *Langmuir* **1998**, *14*, 800.
(13) Camesano, T. A.; Nagarajan, R. *Colloids and Surfaces A: Physicochemical and Engineering Aspects* **2000**, *167*, 165.

(14) Bergsma, M.; Fielden, M. L.; Engberts, J. B. F. N. *Journal of Colloid and interface science* **2001**, *243*, 491.
(15) Oda, R.; Panizza, P.; Schmutz, M.; Lequeux, F. *Langmuir* **1997**, *13*, 6407.
(16) Johnsson, M.; Wagenaar, A.; Engberts, J. B. F. N. *Journal of the American Chemical Society* **2002**, *125*, 757.
(17) Pindzola, B. A.; Jin, J.; Gin, D. L. *Journal of the American Chemical Society* **2003**, *125*, 2940.
(18) Zhou, M.; Nemade, P. R.; Lu, X.; Zeng, X.; Hatakeyama, E. S.; Noble, R. D.; Gin, D. L. *Journal of the American Chemical Society* **2007**, *129*, 9574.
(19) Kern, F.; Lequeux, F.; Zana, R.; Candau, S. J. *Langmuir* **1994**, *10*, 1714.
(20) Cashion, M. P.; Li, X.; Geng, Y.; Hunley, M. T.; Long, T. E. *Langmuir* **2009**, *26*, 678.
(21) Huang, Z.-M.; Zhang, Y.-Z.; Kotaki, M.; Ramakrishna, S. *Composites Science and Technology* **2003**, *63*, 2223.
(22) Reneker, D. H.; Yarin, A. L.; Fong, H.; Koombhongse, S. *Journal of Applied Physics* **2000**, *87*, 4531.
(23) McKee, M. G.; Hunley, M. T.; Layman, J. M.; Long, T. E. *Macromolecules* **2005**, *39*, 575.
(24) Shenoy, S. L.; Bates, W. D.; Frisch, H. L.; Wnek, G. E. *Polymer* **2005**, *46*, 3372.
(25) McKee, M. G.; Wilkes, G. L.; Colby, R. H.; Long, T. E. *Macromolecules* **2004**, *37*, 1760.
(26) McKee, M. G.; Layman, J. M.; Cashion, M. P.; Long, T. E. *Science* **2006**, *311*, 353.
(27) Singer, J. C.; Giesa, R.; Schmidt, H.-W. *Soft Matter* **2012**, *8*, 9972.
(28) Chen, M.; Nielsen, S. R.; Uyar, T.; Zhang, S.; Zafar, A.; Dong, M.; Besenbacher, F. *Journal of Materials Chemistry C* **2013**, *1*, 850.
(29) Celebioglu, A.; Uyar, T. *Journal of Colloid and interface science* **2013**, *404*, 1.
(30) Singh, G.; Bittner, A. M.; Loscher, S.; Malinowski, N.; Kern, K. *Advanced Materials* **2008**, *20*, 2332.
(31) Yan, X.; Zhou, M.; Chen, J.; Chi, X.; Dong, S.; Zhang, M.; Ding, X.; Yu, Y.; Shao, S.; Huang, F. *Chemical Communications* **2011**, *47*, 7086.
(32) Hemp, S. T.; Zhang, M.; Tamami, M.; Long, T. E. *Polymer Chemistry* **2013**, *4*, 3582.
(33) Prasad, M.; Moulik, S. P.; MacDonald, A.; Palepu, R. *The Journal of Physical Chemistry B* **2003**, *108*, 355.
(34) Kalyanasundaram, K.; Thomas, J. *Journal of the American Chemical Society* **1977**, *99*, 2039.
(35) Pérez-Rodríguez, M.; Prieto, G.; Rega, C.; Varela, L. M.; Sarmiento, F.; Mosquera, V. *Langmuir* **1998**, *14*, 4422.
(36) Stodghill, S. P.; Smith, A. E.; O'Haver, J. H. *Langmuir* **2004**, *20*, 11387.
(37) Basu Ray, G.; Ghosh, S.; Moulik, S. *J Chem Sci* **2010**, *122*, 109.
(38) Chu, Z.; Feng, Y. *Langmuir* **2011**, *28*, 1175.
(39) Das, P. K.; Chaudhuri, A. *Langmuir* **1999**, *16*, 76.
(40) Schurtenberger, P.; Scartazzini, R.; Magid, L. J.; Leser, M. E.; Luisi, P. L. *The Journal of Physical Chemistry* **1990**, *94*, 3695.

Chapter 10: Synthesis and Properties of Sulfonium Polyelectrolytes for Biological Applications

(Published in *ACS Macro Letters* ***2013****, 731-735*.)

Sean T. Hemp,[†] Michael H. Allen, Jr.,[†] Adam E. Smith,[‡] and Timothy E. Long*[,†]

[†]*Department of Chemistry and Macromolecules and Interfaces Institute, Virginia Tech, Blacksburg, VA 24061*

[‡]*Department of Chemical Engineering, The University of Mississippi, University, MS 38677*

*To whom correspondence should be addressed. E-mail: telong@vt.edu. TEL: (540)231-2480 FAX: (540)231-8517

Keywords: nonviral gene delivery, sulfonium, colloidal stability, RAFT

10.1 *Abstract*

Sulfonium macromolecules displayed for the first time nucleic acid binding and transfection *in vitro*. Conventional and controlled radical polymerization techniques coupled with subsequent alkylation generated a sulfonium homopolymer, poly(DMSEMA), and a sulfonium diblock copolymer, poly(OEG-*b*-DMSEMA). DNA gel shift assays probed the ability of sulfonium macromolecules to complex nucleic acids, and luciferase assays examined the transfection efficiency and cytotoxicity of both sulfonium macromolecules. Poly(DMSEMA) and poly(OEG-*b*-DMSEMA) bound pDNA at a charge ratio of 1 and both induced significant luciferase expression in HeLa cells under serum-free conditions. Colloidal stability studies using dynamic light scattering highlighted the excellent colloidal stability of poly(OEG-*b*-DMSEMA) under salt and serum conditions due to the sterically stabilizing OEG block. Sulfonium macromolecules offer an alternate route to design cationic macromolecules for nonviral nucleic

acid delivery and future work will aim to add functionality to create more efficient delivery vehicles.

10.2 *Introduction*

Prior to 2012, researchers relied solely on nitrogen-based cationic macromolecules for nonviral nucleic acid delivery. Common nitrogen-based cations that were utilized for electrostatic complexation and compaction of negatively charged nucleic acids included ammoniums,[1] pyridiniums,[2] imidazoliums,[3] and guanidiniums.[4] Cationic macromolecules typically examined in the literature include polyethyleneimine (PEI),[5] poly[2-(dimethylamino)ethyl methacrylate],[6] poly(vinyl imidazolium)s,[7] and chitosan.[8] These macromolecules encapsulate nucleic acids to generate nanoparticles called polyplexes and they mediate cellular uptake and endosomal escape to enter the cell.[9] In 2012, Long et al. first described the utilization of phosphonium macromolecules for nonviral nucleic acid delivery.[10] They demonstrated improved nucleic acid binding and transfection using phosphonium macromolecules compared to ammonium analogs. Phosphonium-based diblock copolymers containing a stabilizing block consisting of oligo(ethylene glycol) methyl ether methacrylate (OEG) or 2-methacryloyloxyethyl phosphorylcholine demonstrated enhanced colloidal stability due to steric repulsion of the stabilizing block.[11] Fréchet et al. demonstrated the elegant synthesis of phosphonium acrylates, which displayed excellent siRNA-mediated gene knockdown compared to ammonium acrylates.[12] Kumar et al. also recently reported a triphenylphosphonium-modified PEI that exhibited enhanced pDNA and siRNA delivery compared to linear PEI.[13]

The synthesis of sulfonium cations normally relies on the quaternization of thioethers using activated halides or other techniques to drive quaternization to high conversions.[14]

Sulfonium cations display inherent instability due to the poor nucleophilicity of the initial thioether[15] and there are few reports detailing sulfonium polyelectrolytes. Hatch et al. reported the synthesis of poly(vinylbenzyl sulfonium)s wherein the sulfonium instability resulted in crosslinking during polymerization.[15] Novak et al. alkylated poly(p-phenylene sulfide) to generate poly(p-phenylene sulfonium)s suitable as photoresists.[16] Bailey and Combe examined sulfonium polyacrylates as potential flocculants.[17] S-methylmethionine and S-adenosyl methionine, sulfonium-containing amino acids, occur naturally in biology and have multiple biological functions.[18-20] Kramer and Deming detailed multiple synthetic pathways to quaternize poly(L-methionine) and they reported a library of alkylated poly(L-methionine)s with varying functional groups.[14] Their post-polymerization functionalization led to high quaternization levels and stable, water-soluble sulfonium poly(L-methionine)s.

Herein, we report the unprecedented synthesis and examination of sulfonium macromolecules for nonviral nucleic acid delivery. Conventional and controlled radical polymerization created a thioether-containing homopolymer and diblock copolymer. Post-polymerization alkylation generated a sulfonium homopolymer and sulfonium diblock copolymer suitable for nucleic acid complexation and delivery. DNA gel shift assays and dynamic light scattering studies examined plasmid DNA (pDNA) binding and polyplex colloidal stability. Luciferase transfection assays directly examined transfection efficiency and cytotoxicity of sulfonium macromolecules. Further expansion of cation choice to include sulfonium cations will enable researchers to select from a broader library of delivery vehicles for nonviral nucleic acid delivery.

10.3 *Experimental Section*

10.4 Materials

Methyl iodide (99%), sodium chloride (≥99%), and 2-(methylthio)ethyl methacrylate (96%) were obtained from Sigma-Aldrich and used as received. OEG (485 g/mol) was purchased from Sigma-Aldrich and passed through neutral alumina to remove the inhibitor. α,α'-Azoisobutyronitrile (AIBN) and 4,4'-Azobis(4-cyanopentanoic acid) (V-501) were obtained from Sigma-Aldrich and recrystallized from methanol. 4-cyano-4-(ethylsulfanylthiocarbonyl)sulfanylpentanoic acid (CEP) was synthesized according to previous literature.[21]

10.5 Analytical Methods

^{1}H NMR spectroscopy was performed on a Varian Unity 400 operating at 400 MHz in CD_3OD or $CDCl_3$. The aqueous size-exclusion chromatography (SEC) instrumentation consisted of a Waters 1515 isocratic HPLC pump, a Waters 717plus autosampler, two Waters ultrahydrogel linear columns, one Waters ultrahydrogel 250 column, a Wyatt MiniDAWN light scattering (LS) detector, and a Waters 2414 refractive index (RI) detector operating at a flow rate of 0.8 mL/min. The aqueous eluent was a ternary mixture of 54/23/23 (v/v/v) water/methanol/acetic acid with 0.1 M sodium acetate. Absolute molecular weight of the OEG macroCTA was determined with a d*n*/d*c* of 0.1156 mL/g determined offline using a Wyatt Opti-lab T-rEX differential refractometer. THF SEC was operated at 40 °C and a 1 mL/min flow rate using a Waters autosampler, a Waters 2410 RI detector, a Wyatt MiniDAWN LS detector, and three 5 μm PLgel Mixed-C columns. Relative molecular weights were determined using polystyrene standards.

10.6 Polymer Synthesis

MTEMA (3.75 g, 23.4 mmol), AIBN (39.8 mg, 0.242 mmol, 1 mol%), and toluene (38 mL) were added to a 100-mL, round-bottomed flask with a magnetic stir bar. The solution was purged with argon for 30 min and subsequently heated at 65 °C for 24 h. The polymer was precipitated from methanol and dried *in vacuo* at 60 °C for 24 h to obtain a white solid.

OEG (40.10 g, 82.7 mmol), CEP (868 mg, 3.30 mmol), V-501 (184 mg, 0.656 mmol), and DMSO (330 mL) were added to a 500-mL, round-bottomed flask with a magnetic stir bar. The solution was sparged with argon for 1 h and then heated at 70 °C for 250 min. The polymer was dialyzed against water (MWCO = 3,500 g/mol) for 2 d and subsequently lyophilized to obtain a yellow oil. Subsequent chain extension with MTEMA generated the desired diblock copolymer. Poly(OEG) macroCTA (268 mg, 0.02 mmol, 13,600 g/mol), V-501 (2.19 mg, 0.008 mmol), MTEMA (632 mg, 3.95 mmol), and dioxane (7.89 mL) were added to a 25-mL, round-bottomed flask with a magnetic stir bar. The solution was sparged with argon for 30 min and then heated at 70 °C for 4 h. The polymer solution was dialyzed against methanol (MWCO = 3,500 g/mol) for 2 d and then concentrated *in vacuo*. The polymer was dried *in vacuo* at 60 °C for 24 h.

Both polymers were quaternized following a similar protocol and the quaternization of poly(MTEMA) follows as an example. Poly(MTEMA) (504 mg, 3.15 mmol) was treated with 10 equivalents of methyl iodide (2.0 mL, 32.1 mmol) in 17 mL DMF for 48 h. The resulting solution was dialyzed against 0.1 M NaCl (MWCO = 3,500 g/mol) for 2 d to exchange the counterion to Cl^- and then dialyzed against water for 2 d. The polymer solution was lyophilized to obtain a white solid.

10.7 DNA Binding Assay

Plasmid DNA (0.2 μg, Aldevron, gWiz-Luc) was diluted into an appropriate amount of water to achieve a total volume of 28 μL after polymer addition. The polymer solution (1 mg/mL) was subsequently added to achieve various charge ratios (ratio of positively charged sulfonium in polymer to negatively charged phosphates in DNA). The polyplexes were incubated for 30 min and subsequently electrophoresed at 70 V for 30 min in a 1 wt% agarose gel stained with SYBR green I (6 μL). The gel was imaged using a MultiDoc-it Digital Imaging System (UVP).

10.8 Dynamic Light Scattering

Plasmid DNA (2.0 μg in 100 μL water) was complexed with the required amount of polymer solution for a specific charge ratio in 200 μL total water. The polyplexes were incubated for 30 min and subsequently diluted into 800 μL water or serum-free Opti-MEM (OMEM). Dynamic light scattering (DLS) using a Malvern Zetasizer Nano monitored polyplex hydrodynamic diameters over a 24 h period. All measurements reported were an average of three measurements. Serum stability required significantly higher pDNA concentrations to differentiate polyplexes from serum proteins in solution. pDNA (20.0 μg in 100 μL water) was complexed with the necessary amount of polymer to achieve a desired charge ratio in 200 μL total water. The resulting solution was incubated for 30 min and then diluted with 800 μL serum-containing Dulbecco's Modified Eagle Media (DMEM). DLS monitored polyplex hydrodynamic diameters over 24 h and each value reported was an average of three measurements.

10.9 Cell Culture

Human cervical cancer cells (HeLa cells) were obtained from ATCC and were cultured in serum-containing DMEM (10% FBS) with 100 U/mL penicillin and 100 μg/mL streptomycin in 95% humidity and 5% CO_2 at 37 °C. All reagents for subcultivation were obtained from MediaTech.

10.10 Luciferase and Cytotoxicity Assay

HeLa cells (500 μL, 100,000 cells/mL) were seeded in 24-well plates and incubated for 24 h. Polyplexes were prepared using pDNA (5 μg in 250 μL water) and the required amount of a polymer solution to obtain a total water volume of 500 μL at specific charge ratios. Jet-PEI polyplexes were prepared at a N/P ratio of 5 and applied to cells according to manufacturer's protocols. Each well was aspirated and washed with 300 μL HBSS. Serum-free OMEM (400 μL) or serum-containing DMEM (400 μL) was added to each well and then 100 μL of each polyplex solution was added to the wells (1 μg pDNA/well). The cells were transfected for 4 h and then the transfection media was aspirated and 500 μL serum-containing DMEM was added to each well. The cells were incubated for 44 h, rinsed with 300 μL PBS, and then lysed using 120 μL of a 1x Promega lysis buffer. Each plate was incubated for 30 min at 37 °C and subjected to two freeze-thaw cycles to fully lyse the cells. Luciferase activity was quantified using a Promega luciferase assay kit and a Promega GloMax 96 Microplate Luminometer. Total protein in the lysates was determined using a Pierce BCA protein assay kit following manufacturer protocols. Luciferase expression was normalized using the protein concentration and cell viabilities were determined based on the protein concentration relative to the cells only control. Experiments were performed in quadruplicate and the Student's t-test was utilized for statistical analysis.

10.11 *Results and Discussion*

10.11.1 Polymer Synthesis

Conventional free radical polymerization of MTEMA shown in **Scheme 10.1** readily synthesized a poly(MTEMA) homopolymer (THF SEC, M_n = 17,300 g/mol, PDI = 2.24). Higher molecular weights were possible to achieve, but toluene was chosen as the solvent to lower the molecular weight through chain transfer. Previous research has demonstrated the importance of molecular weight for delivery vehicles, wherein M_n's ideally are below 50,000 g/mol for optimal renal clearance and minimal toxicity. Reversible-addition fragmentation chain transfer (RAFT) polymerization enabled the synthesis of a thioether-containing diblock copolymer (**Scheme 10.2**). RAFT polymerization of OEG using a trithiocarbonate chain transfer agent (CTA) created a well-defined poly(OEG) macroCTA (Aqueous SEC, M_n = 13,600 g/mol, PDI = 1.04). Subsequent chain extension of the poly(OEG) macroCTA with MTEMA generated the desired diblock copolymer, poly(OEG-*b*-MTEMA). ^{1}H NMR determined the M_n of the MTEMA B block (12,800 g/mol) based on integration to the OEG A block, and aqueous SEC after alkylation of the diblock copolymer confirmed a well-defined diblock copolymer (PDI = 1.05). Thioethers typically require activated halides or other synthetic techniques to generate sulfonium cations due to the inherently poor nucleophilicity of thioethers. Quaternization of poly(MTEMA) and poly(OEG-*b*-MTEMA) with 10 equivalents of methyl iodide successfully generated a sulfonium-containing homopolymer, poly(2-methacryloxyethyldimethylsulfonium chloride) (poly(DMSEMA)), and a sulfonium-containing diblock copolymer, poly(OEG-*b*-DMSEMA). ^{1}H NMR determined quaternization levels of 90% and 87% for poly(DMSEMA) and poly(OEG-*b*-DMSEMA), respectively.

Scheme 10.1. Conventional free radical polymerization and subsequent quaternization to achieve a sulfonium-containing homopolymer, poly(DMSEMA).

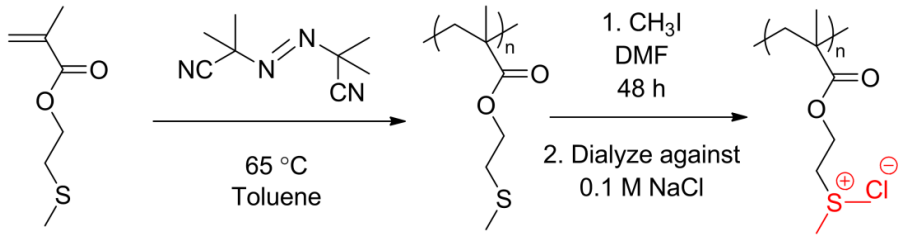

Scheme 10.2. RAFT polymerization and post-polymerization alkylation to generate a sulfonium-containing diblock copolymer, poly(OEG-*b*-DMSEMA).

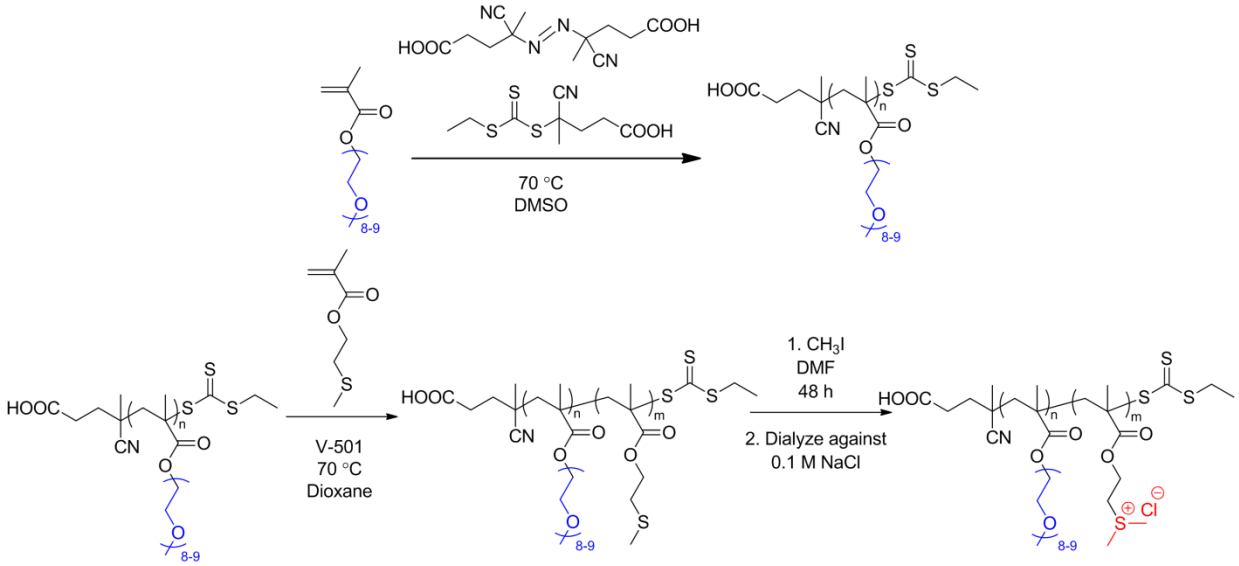

10.11.2 DNA Binding

DNA gel shift assays probed the ability of sulfonium-containing macromolecules to effectively bind pDNA. Classically, researchers utilize an N/P ratio to quantify nucleic acid binding of nitrogen-based systems wherein N corresponds to the moles of protonatable, protonated, or quaternized nitrogen atoms in the macromolecule while P corresponds to the moles of negatively charged phosphate units in the DNA backbone.[22] A charge ratio (+/- ratio) for other cation-based systems appropriately correlates the moles of cationic charge in the

polymer to the moles of negative charge in the DNA. **Figure 10.1** shows the DNA gel shift assays for poly(DMSEMA) and poly(OEG-*b*-DMSEMA). Both sulfonium macromolecules efficiently bound pDNA at a +/- ratio of 1.

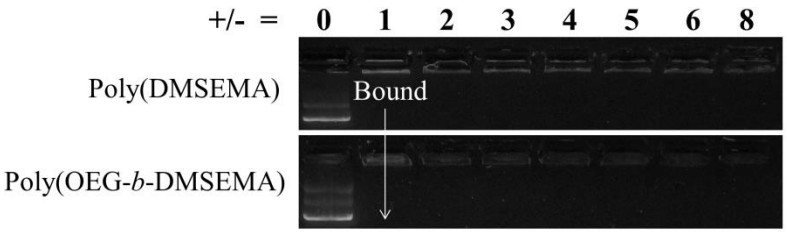

Figure 10.1. DNA gel shift assay demonstrating effective nucleic acid complexation at a charge ratio of 1 for both poly(DMSEMA) and poly(OEG-*b*-DMSEMA).

10.11.3 Transfection and Cytotoxicity

Luciferase transfections performed on HeLa cells in serum-free OMEM and serum-containing DMEM elucidated the delivery efficiency of sulfonium macromolecules compared to a common positive control, linear polyethyleneimine (Jet-PEI), and negative controls of cells or DNA only. **Figure 10.2** shows the normalized luciferase expression (RLU/mg protein) and cell viabilities of HeLa cells for serum-free OMEM transfections. Both poly(DMSEMA) and poly(OEG-*b*-DMSEMA) successfully displayed significantly higher luciferase expression compared to negative controls ($p < 0.05$). Poly(DMSEMA) required a lower +/- ratio of 6 to efficiently transfect HeLa cells compared to poly(OEG-*b*-DMSEMA), which required a higher +/- ratio of 10 to achieve similar transfection levels as poly(DMSEMA). Poly(DMSEMA) demonstrated significantly more cytotoxicity compared to poly(OEG-*b*-DMSEMA) and as expected, cytotoxicity increased as the charge ratio increased. Transfections using Jet-PEI resulted in significantly higher luciferase expression compared to sulfonium macromolecules. Jet-PEI and other delivery vehicles with protonatable sites rely on the proton sponge effect to

achieve endosomal escape for efficient transfection.[23] Both sulfonium macromolecules presumably struggled to escape the endosome due to their lack of protonatable sites, therefore lowering their transfection ability compared to Jet-PEI. Future incorporation of protonatable sites and other functionality will aim to improve the transfection of sulfonium macromolecules. Other potential hindrances for transfection using sulfonium macromolecules includes lower cellular uptake or low nucleic acid release in the cytosol. **Figure 10.3** illustrates the luciferase expression and cell viabilities of HeLa cells during serum transfections. The presence of serum during the transfection negatively affected the capability of both sulfonium macromolecules to delivery pDNA effectively. Serum typically hinders successful transfection due to association of negatively charged proteins to positively charged polyplexes and cationic free polymer in solution.[24] Serum transfections led to higher cell viabilities with all delivery vehicles displaying minimal cytotoxicity.

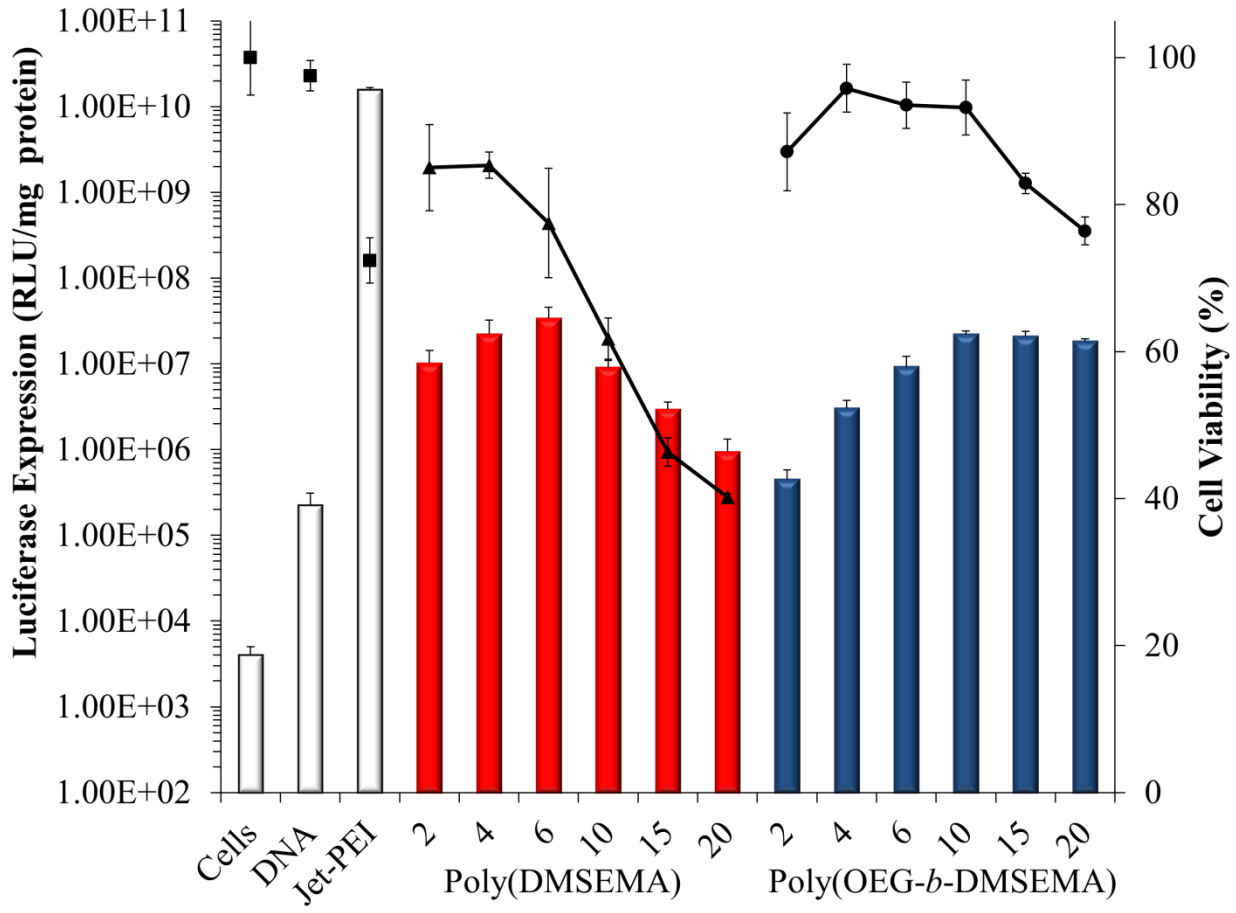

Figure 10.2. Luciferase expression and cell viability of HeLa cells for poly(DMSEMA) and poly(OEG-*b*-DMSEMA) under serum-free OMEM transfection conditions. The histogram bars correspond to the luciferase expression while the data points correlate to cell viability.

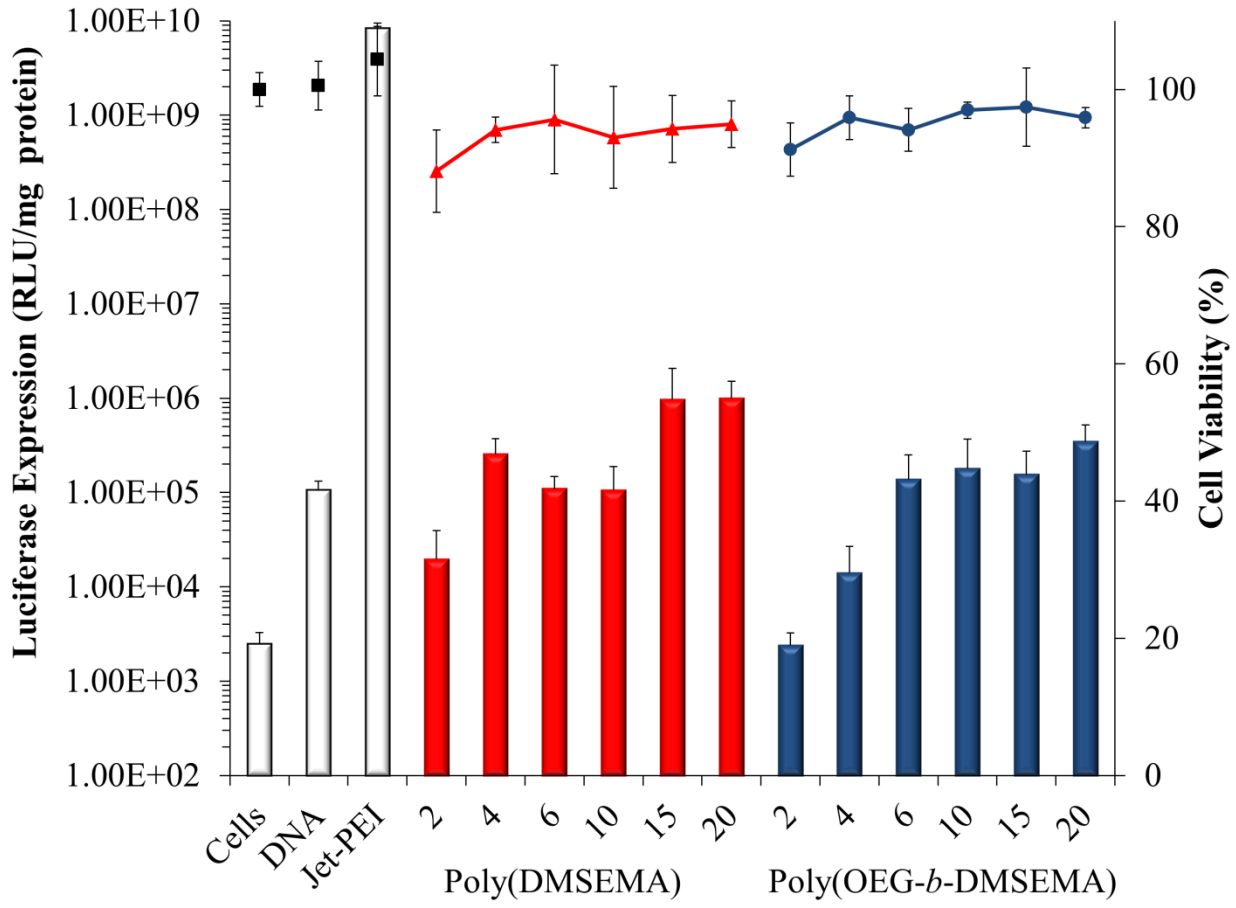

Figure 10.3. Luciferase expression and cell viability of HeLa cells for poly(DMSEMA) and poly(OEG-*b*-DMSEMA) under serum-containing DMEM transfection conditions. The histogram bars correspond to the luciferase expression while the data points correlate to cell viability.

10.11.4 Colloidal Stability

Nanoparticle colloidal stability is imperative for *in vivo* applications where nanoparticle size and surface chemistry directly influence circulation times and biodistribution.[25] Colloidal stability studies directly compared the colloidal stability of poly(DMSEMA) (+/- ratio = 6), poly(OEG-*b*-DMSEMA) (+/- ratio = 10), and Jet-PEI (N/P = 5) polyplexes at their optimal transfection formulation. Conditions examined for polyplex colloidal stability included water,

serum-free OMEM, and serum-containing DMEM. All three delivery vehicles exhibited colloidal stability in water, likely due to charge repulsion of the positively charged polyplexes (**Figure 10.4**). Zeta potentials for poly(DMSEMA) and poly(OEG-*b*-DMSEMA) were 22 mV and 18 mV, respectively.

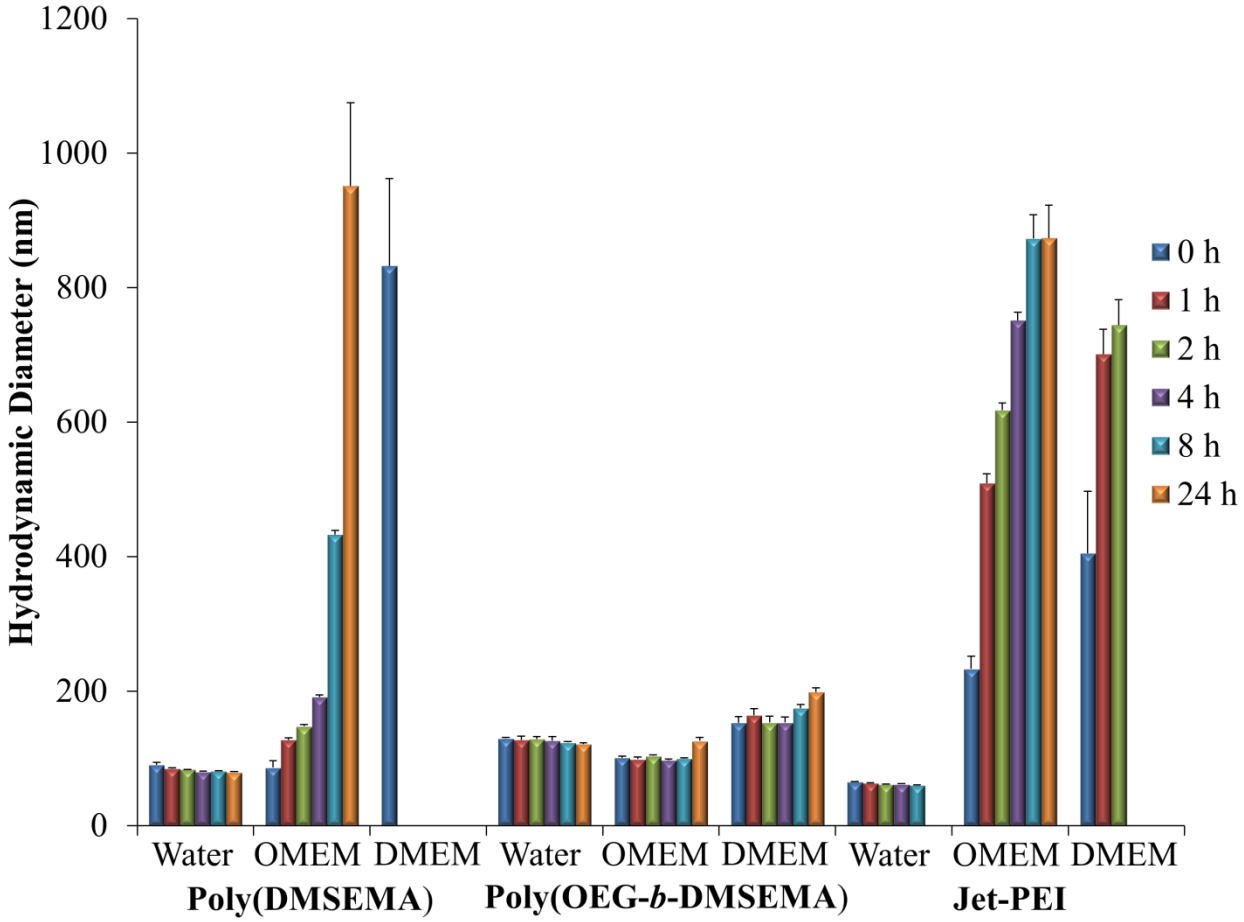

Figure 10.4. Colloidal stability of poly(DMSEMA) (+/- ratio = 6), poly(OEG-*b*-DMSEMA) (+/- ratio = 10), and Jet-PEI (N/P = 5) under various conditions (water, serum-free OMEM, and serum-containing DMEM).

Poly(DMSEMA) and Jet-PEI both demonstrated poor colloidal stability in serum-free OMEM, steadily increasing in hydrodynamic diameter over 24 h. The presence of salt neutralized the surface charge of the polyplexes, inducing aggregation.[26] Poly(OEG-*b*-

DMSEMA) polyplexes resisted aggregation under salt conditions due to the steric stabilizing OEG block and displayed excellent colloidal stability over 24 h. Serum conditions also induced polyplex aggregation for poly(DMSEMA) and Jet-PEI polyplexes due to the association of negatively charged proteins to the polyplex surface.[27] Poly(OEG-*b*-DMSEMA) polyplexes exhibited enhanced colloidal stability in serum conditions compared to poly(DMSEMA). The sulfonium diblock copolymer ultimately displayed outstanding colloidal stability under both salt and serum conditions.

10.12 *Conclusions*

Conventional and controlled radical polymerization with post-polymerization quaternization successfully synthesized a sulfonium-containing homopolymer and diblock copolymer. Sulfonium macromolecules were shown for the first time to efficiently complex nucleic acids and deliver them *in vitro* to HeLa cells. Poly(DMSEMA) and poly(OEG-*b*-DMSEMA) exhibited significantly higher luciferase expression under serum-free OMEM conditions compared to negative controls, demonstrating maximal transfection at charge ratios of 6 and 10, respectively. Higher charge ratios were necessary for poly(OEG-*b*-DMSEMA) to achieve similar luciferase expression compared to poly(DMSEMA). Poly(OEG-*b*-DMSEMA) displayed lower cytotoxicities compared to poly(DMSEMA). Serum lowered the transfection efficiency for both sulfonium macromolecules while improving cell viabilities. Both poly(DMSEMA) and Jet-PEI exhibited poor colloidal stability in salt and serum conditions while poly(OEG-*b*-DMSEMA) resisted aggregation and remained colloidally stable over 24 h. Future work will aim to broaden the sulfonium macromolecule library to provide buffering capacity and other functionality to enhance transfection.

10.13 *Acknowledgements*

The authors recognize Prof. Mark Van Dyke in the School of Biomedical Engineering and Sciences for access and use of his instrumentation. The authors gratefully thank Techulon, Inc. for financial and material support. This material is based upon work supported in part by the U.S. Army Research Office under grant number W911NF-07-1-0452 Ionic Liquids in Electro-Active Devices (ILEAD) MURI. This material is based upon work supported in part by the U.S. Army Research Laboratory and the U.S. Army Research Office under the Army Materials Center of Excellence Program, contract W911NF-06-2-0014. This material is based upon work supported by the Army Research Office (ARO) under Award No. W911NF-10-1-0307 (DURIP).

10.14 *References*

(1) Synatschke, C. V.; Schallon, A.; Jérôme, V.; Freitag, R.; Müller, A. H. E. *Biomacromolecules* **2011**, *12*, 4247.
(2) San Juan, A.; Letourneur, D.; Izumrudov, V. A. *Bioconjugate Chemistry* **2007**, *18*, 922.
(3) Pack, D. W.; Putnam, D.; Langer, R. *Biotechnology and Bioengineering* **2000**, *67*, 217.
(4) Funhoff, A. M.; van Nostrum, C. F.; Lok, M. C.; Fretz, M. M.; Crommelin, D. J. A.; Hennink, W. E. *Bioconjugate Chemistry* **2004**, *15*, 1212.
(5) Ahn, H. H.; Lee, J. H.; Kim, K. S.; Lee, J. Y.; Kim, M. S.; Khang, G.; Lee, I. W.; Lee, H. B. *Biomaterials* **2008**, *29*, 2415.
(6) Layman, J. M.; Ramirez, S. M.; Green, M. D.; Long, T. E. *Biomacromolecules* **2009**, *10*, 1244.
(7) Allen, M. H.; Green, M. D.; Getaneh, H. K.; Miller, K. M.; Long, T. E. *Biomacromolecules* **2011**, *12*, 2243.
(8) Koping-Hoggard, M.; Tubulekas, I.; Guan, H.; Edwards, K.; Nilsson, M.; Varum, K. M.; Artursson, P. *Gene Therapy* **2001**, *8*, 1108.
(9) Mintzer, M. A.; Simanek, E. E. *Chemical Reviews* **2009**, *109*, 259.
(10) Hemp, S. T.; Allen, M. H.; Green, M. D.; Long, T. E. *Biomacromolecules* **2012**, *13*, 231.
(11) Hemp, S. T.; Smith, A. E.; Bryson, J. M.; Allen, M. H.; Long, T. E. *Biomacromolecules* **2012**, *13*, 2439.
(12) Ornelas-Megiatto, C.; Wich, P. R.; Fréchet, J. M. J. *Journal of the American Chemical Society* **2012**, *134*, 1902.
(13) Bansal, R.; Tripathi, S. K.; Gupta, K. C.; Kumar, P. *Journal of Materials Chemistry* **2012**, *22*, 25427.
(14) Kramer, J. R.; Deming, T. J. *Biomacromolecules* **2012**, *13*, 1719.

(15) Hatch, M. J.; Meyer, F. J.; Lloyd, W. D. *Journal of Applied Polymer Science* **1969**, *13*, 721.
(16) Novak, B. M.; Hagen, E.; Hoff, S.; Viswanathan, A. *Macromolecules* **1994**, *27*, 1985.
(17) Bailey, F. E.; La Combe, E. M. *Journal of Macromolecular Science: Part A - Chemistry* **1970**, *4*, 1293.
(18) Toennies, G. *Journal of Biological Chemistry* **1940**, *132*, 455.
(19) Lu, S. C. *The International Journal of Biochemistry & Cell Biology* **2000**, *32*, 391.
(20) Bourgis, F.; Roje, S.; Nuccio, M. L.; Fisher, D. B.; Tarczynski, M. C.; Li, C.; Herschbach, C.; Rennenberg, H.; Pimenta, M. J.; Shen, T.-L.; Gage, D. A.; Hanson, A. D. *The Plant Cell Online* **1999**, *11*, 1485.
(21) Convertine, A. J.; Benoit, D. S. W.; Duvall, C. L.; Hoffman, A. S.; Stayton, P. S. *Journal of Controlled Release* **2009**, *133*, 221.
(22) Chan, P.; Kurisawa, M.; Chung, J. E.; Yang, Y.-Y. *Biomaterials* **2007**, *28*, 540.
(23) Behr, J.-P. *CHIMIA International Journal for Chemistry* **1997**, *51*, 34.
(24) Dash, P. R.; Read, M. L.; Barrett, L. B.; Wolfert, M. A.; Seymour, L. W. *Gene Therapy* **1999**, *6*, 643.
(25) Farokhzad, O. C.; Langer, R. *ACS Nano* **2009**, *3*, 16.
(26) Prevette, L. E.; Lynch, M. L.; Kizjakina, K.; Reineke, T. M. *Langmuir* **2008**, *24*, 8090.
(27) de Wolf, H. K.; Luten, J.; Snel, C. J.; Oussoren, C.; Hennink, W. E.; Storm, G. *Journal of Controlled Release* **2005**, *109*, 275.

Chapter 11: RAFT Polymerization of Temperature- and Salt-Responsive Block Copolymers as Reversible Hydrogels

(*In preparation* for submission)

Sean T. Hemp,[§] Adam E. Smith,[ψ] Clayton Bunyard,[†] Michael Rubinstein,[‡] and Timothy E. Long*[,§]

[§]*Department of Chemistry and Macromolecules and Interfaces Institute, Virginia Tech, Blacksburg, VA 24061*

[ψ]*Department of Chemical Engineering, The University of Mississippi, University, MS 38677*

[†]*Department of Material Science, Corporate Research & Engineering, Kimberly-Clark Corporation, 2100 Winchester Road, Neenah, WI 54956, USA*

[‡]*Department of Chemistry, University of North Carolina at Chapel Hill, Chapel Hill, NC 27599*

*To whom correspondence should be addressed. E-mail: telong@vt.edu. TEL: (540)231-2480 FAX: (540)231-8517

Keywords: RAFT polymerization, hydrogels, stimuli-responsive, block copolymers

11.1 *Abstract*

Reversible-addition fragmentation chain transfer (RAFT) polymerization enabled the synthesis of novel, stimuli-responsive, AB and ABA block copolymers. The B block was hydrophilic, and the A block displayed salt- and temperature-response, which was dependent on the diethylene glycol methyl ether methacrylate (DEG) and [2-(methacryloyloxy)ethyl]trimethylammonium chloride (TMA) molar ratio. Higher TMA content increased the critical micelle temperatures (CMT) in HPLC-grade water due to the increased hydrophilicity of the A block. Upon the addition of 0.9 wt% NaCl, the CMTs decreased

significantly due to the salt response of the TMA unit from 50 °C to 36 °C for poly(OEG-*b*-$DEG_{95}TMA_5$). ABA triblock copolymers displayed excellent hydrogel properties with salt- and temperature-dependent gel points. TMA incorporation increased the gel points for all triblock copolymers, and salt-response increased with TMA concentration. For example, poly($DEG_{98}TMA_2$-*b*-OEG-*b*-$DEG_{98}TMA_2$) formed a hydrogel at 40 °C and 26 °C in HPLC-grade water and 0.9 wt% NaCl in water, respectively. These salt- and temperature-responsive AB diblock and ABA triblock copolymers find applications as drug delivery vehicles, adhesives, and hydrogels.

11.2 *Introduction*

Stimuli-responsive macromolecules are an important area of advanced materials wherein the polymer properties change upon a response to different environmental conditions.[1] Various stimuli are investigated in the literature including temperature, pH, salt, light, and analyte concentrations.[2] Stimuli-responsive materials find a broad range of applications including drug delivery vehicles,[3] sensors,[4] hydrogels,[5] and smart surfaces.[6] Temperature-responsive macromolecules are widely reported as stimuli-responsive polymers for biomedical applications with a target-temperature response near physiological body temperature (37 °C).[7] Polymer families that display temperature-responsive properties include polyacrylamides,[8] polyacrylates,[9] polymethacrylates,[10,11] polyoxazolines,[12] polyethers,[13] and polypeptides.[14] Polymers that display lower critical solution temperatures (LCSTs) exhibit unique solubility properties in water wherein the polymer is soluble in water below the LCST, but upon heating above the LCST, the polymer precipitates and becomes water insoluble.[15]

Poly(*n*-isopropyl acrylamide) (PNIPAM) is the most widely studied LCST polymer due to an ideal LCST of 32 °C for biological applications.[16] The advent of controlled radical

polymerization enabled the design and synthesis of poly(NIPAM)-containing block copolymers. For instance, McCormick et al.[17] generated poly(dimethyl acrylamide-*b*-*n*-isopropyl acrylamide) and poly(dimethyl acrylamide-*b*-*n*-isopropyl acrylamide-*b*-dimethyl acrylamide) block copolymers utilizing reversible addition-fragmentation chain transfer (RAFT) polymerization and they demonstrated temperature-responsive micellization due to the poly(NIPAM) block. Acrylate and methacrylate polymers with LCST behavior recently received significant attention. Sumerlin et al.[18] synthesized poly(diethylene ethyl ether acrylate) (PDEGA) random and block copolymers with dimethyl acrylamide as a hydrophilic comonomer. The LCST behavior of the random copolymers linearly depended on the mol% incorporation of dimethyl acrylamide; LCSTs ranged from ~10 °C to 90 °C with the LCSTs increasing as the dimethyl acrylamide incorporation increased. The poly(DEGA-*b*-dimethyl acrylamide) diblock copolymers displayed thermoresponsive micellization behavior.

Oligoethylene glycol methacrylate monomers have received significant attention recently in the literature.[10,19] The length of the oligoethylene glycol side chain dramatically impacts LCST behavior.[20,21] Longer ether side chains result in higher LCSTs due to the enhanced hydrophilicity of the polymer. These macromolecules display LCST behavior due to the interplay between the hydrophobic polymer backbone and the hydrogen bonding of the ether groups to water.[10] Poly(diethylene glycol methyl ether methacrylate) with two ethylene glycol repeat units exhibits an LCST of 26 °C[22] and various researchers reported a broad range of block copolymers and random copolymers. Random copolymers containing hydrophilic monomers such as OEG,[22] 2-dimethylaminoethyl methacrylate (DMA),[23] or methacrylic acid[23] enables the tuning of the LCST. Multiple researchers examined poly(DEG-*b*-DMA) diblock copolymers for their temperature- and pH-responsive micellization behavior.[24,25] Müller et al.[26] synthesized

DEG and DMA star block copolymers with a DMA core and DEG shell. These triblock copolymers displayed pH-responsive and thermoresponsive hydrogel behavior. Lutz and coworkers examined DEG-containing covalently crosslinked hydrogels[11] and physically crosslinked hydrogels.[27] The covalently crosslinked hydrogels deswelled upon heating above the LCST of DEG while the DEG-containing star bock copolymers exhibited thermoresponsive gelation.

Polymers containing ionic groups commonly display a response to salt wherein salt triggers a change in solubility or polymer conformation.[28] For instance, polyelectrolytes display an extended conformation in solution due to electrostatic repulsion in the polymer backbone called the polyelectrolyte effect.[29] The addition of salt to the solution effectively screens the electrostatic repulsions in the polymer backbone, allowing the polyelectrolyte to adopt a random coil in solution.[30] Tuning solubility of polymers through salt concentration enables the generation of a broad range of materials suitable for biomedical and hygiene applications. Salt triggerable polymers display salt-dependent solubility where the addition of salt induces precipitation.[31] Bunyard et al.[32] examined the salt response of ammonium-containing polycaprolactones and they demonstrated the impact of salt concentration, salt identity, and ionic content in the polymer on the salt triggered solubility of the cationic polycaprolactones.

We report herein the synthesis and characterization of salt- and temperature-responsive diblock and triblock copolymers through the incorporation of LCST monomers and salt-triggerable monomers. RAFT polymerization enabled the well-defined synthesis of AB diblock and ABA triblock copolymers using monofuntional or difunctional trithiocarbonate chain transfer agents. The B block was hydrophilic while the A block displayed salt- and temperature-responsive character dependent on the relative incorporation of DEG and TMA. Dynamic light

scattering probed the micellization behavior of the AB diblock copolymers with a focus on their temperature response and salt response. Solution rheology studies using temperature ramp experiments probed the hydrogel behavior of the ABA triblock copolymers and elucidated the sol-gel transition (gel point) for all triblock copolymers. These salt- and temperature-responsive block copolymers are proposed for a broad range of utility in drug delivery, adhesive, and hydrogel applications.

11.3 *Experimental Section*

11.3.1 Materials

Oligo(ethylene glycol) methyl ether methacrylate (OEG) (485 g/mol) and diethylene glycol methyl ether methacrylate (DEG) (95%) were obtained from Sigma-Aldrich and the inhibitor was removed using a neutral alumina column prior to polymerization. [2-(methacryloyloxy)ethyl]trimethylammonium chloride (80 wt% in water) (TMA) was purchased from Sigma-Aldrich and used as received. 4,4′-Azobis(4-cyanopentanoic acid) (V-501) (>98%) was obtained from Sigma-Aldrich and recrystallized from methanol. 4-Cyano-4-(ethylsulfanylthiocarbonylsulfanyl)pentanoic acid (CEP)[33] and 1,6-bis(4-cyano-4-(ethylsulfanyl-thiocarbonylsulfanyl)pentanoic acid)hexane diamide (dCEP)[34] were synthesized according to previous literature procedures. All other solvents and reagents were purchased from Sigma-Aldrich.

11.3.2 Analytical Methods

Aqueous SEC was performed using a ternary mixture of 54/23/23 v/v/v water/methanol/acetic acid with 0.1 M sodium acetate as the eluent. The aqueous SEC instrumentation consisted of a Waters 1515 isocratic HPLC pump, a Waters 717plus

autosampler, two Waters ultrahydrogel linear columns, one Waters ultrahydrogel 250 column, a Wyatt MiniDAWN light scattering (LS) detector, and a Waters 2414 refractive index (RI) detector operating at a flow rate of 0.8 mL/min. Poly(OEG) and poly(DEG) displayed dn/dc values of 0.1156 mL/g and 0.1267 mL/g, respectively, in the aqueous SEC solvent. The dn/dc values for all block copolymers were estimated at 0.12 mL/g to enable calculation of molecular weights. Dynamic light scattering was performed using a Malvern Zetasizer Nano and enabled the determination of the critical micellization temperature. Polymer solutions (1 mg/mL in pure water or 0.9 wt% NaCl in water) were subjected to a temperature step protocol (2°C/step from 4 °C to 50 °C) and the hydrodynamic diameters were measured after a 5 min equilibration at each step. The critical micellization temperature was attributed to the temperature step where the polymers exhibited a shift in their hydrodynamic diameters from unimers (<10 nm) to micelles (>20 nm). Solution rheology using a TA Instruments DHR-2 strain-controlled rheometer with a 2° 40 mm cone and Peltier plate geometry directly probed hydrogel formation and overall gel strengths. Polymer solutions (25 wt% polymer in pure water or 0.9 wt% NaCl in water) were subjected to temperature sweep experiments using 1% oscillatory strains at 1 Hz with a heating rate of 0.5 °C/min from 4 °C to 50 °C. The gel point was determined using the TA Instruments TRIOS package and was defined as the crossover point of the storage and loss moduli.

11.3.3 Synthesis of poly(OEG) monofunctional macroCTA

A 500-mL, round-bottomed flask containing OEG (40.10 g, 82.7 mmol), CEP (868 mg, 3.30 mmol), V-501 (184 mg, 0.656 mmol), and DMSO (330 mL) was sparged with argon for 1 h. The resulting yellow solution was heated at 70 °C for 250 min and then dialyzed against water for 3 d (MWCO = 3,500 g/mol) to remove solvent and residual monomer. Lyophilization isolated a yellow polymer oil (M_n = 13,600 g/mol, PDI = 1.04).

11.3.4 Synthesis of salt- and temperature-responsive diblock copolymers

All diblock copolymers were synthesized according to a similar procedure. The synthesis of poly(OEG-*b*-$DEG_{99}TMA_1$) follows as a representative example. Poly(OEG) macroCTA (364.0 mg, 0.0268 mmol), DEG (978 μL, 5.30 mmol), TMA (12.5 μL, 0.0532 mmol), V-501 (3.74 mg, 0.0133 mmol), and DMF (10.268 mL) were added to a 25-mL, round-bottomed flask with a magnetic stir bar. The resulting yellow solution was sparged with argon for 15 min and subsequently heated at 70 °C for 6 h. The polymer solution was dialyzed against water (MWCO = 3,500 g/mol) and then subsequently lyophilized to obtain the diblock copolymer (M_n = 39.4 kg/mol, PDI = 1.03).

11.3.5 Synthesis of poly(OEG) difunctional macroCTA

The following is an example to synthesize a difunctional poly(OEG) macroCTA. OEG (0.995 g, 2.05 mmol), dCEP (8.34 mg, 0.0137 mmol), V-501 (1.54 mg, 0.00549 mmol), and DMSO (8.247 mL) were added to a 25-mL, round-bottomed flask with a magnetic stir bar. The resulting solution was sparged with argon for 30 min and then heated at 70 °C for 220 min. The polymer solution was dialyzed against water (MWCO = 3,500 g/mol) and lyophilized to obtain a yellow oil (Aqueous SEC: M_n = 74.6 kg/mol, PDI = 1.01).

11.3.6 Synthesis of salt- and temperature-responsive triblock copolymers

A representative procedure to synthesize poly(DEG_xTMA_y-*b*-OEG-*b*-DEG_xTMA_y) triblock copolymers follows with an example to feed 3 mol% TMA into the outer block. DEG (2.89 mL, 15.7 mmol), TMA (114 μL, 0.439 mmol), poly(OEG) macroCTA (523.9 mg, M_n = 64.9 kg/mol), and DMF (15.99 mL) were added to a 25-mL, round-bottomed flask with magnetic stir bar. The resulting solution was sparged with argon for 30 min and subsequently heated at 70

°C for 7 h. The polymer solution was dialyzed against water (MWCO = 3,500 g/mol) at 4 °C and lyophilized to obtain a slightly yellow polymer (Aqueous SEC: M_n = 230 kg/mol, PDI = 1.19).

11.4 *Results and Discussion*

11.4.1 Polymer Synthesis

Block copolymers containing a hydrophilic block and a salt- and temperature-responsive block enabled the examination of critical micellization temperatures and hydrogel formation of novel block copolymers. Specifically, an OEG block acted as the hydrophilic block while a random copolymer of DEG and TMA consisted as the salt- and temperature-responsive block. DEG homopolymers display an LCST of ~26 °C[22] and the incorporation of TMA was hypothesized to raise the LCST behavior to near body temperature while also providing a salt response. RAFT polymerization readily enabled the generation of salt- and temperature-responsive diblock and triblock copolymers as shown in **Scheme 11.1**. A monofunctional trithiocarbonate CTA, CEP, mediated the polymerization of OEG to synthesize a well-defined poly(OEG) macroCTA (M_n = 13.6 kg/mol, PDI = 1.04). Subsequent chain extension with DEG and TMA created the desired salt- and temperature-responsive diblock copolymers. **Figure 11.1** highlights the aqueous SEC analysis of the poly(OEG) macroCTA and all diblock copolymers showed a clear, monotonic shift in elution time upon chain extension. All diblock copolymers displayed similar M_n's of ~40 kg/mol with narrow molecular weight distributions as shown in **Table 11.1**. Molar feed ratios of DEG and TMA were controlled to examine the impact of TMA incorporation on critical micellization temperatures. Accurately determining the TMA

incorporations proved difficult due to the low TMA feed in the copolymerization. All block copolymer compositions reported correspond to the monomer feed ratios of DEG and TMA.

Scheme 11.1. RAFT polymerization of OEG and subsequent chain extension with DEG and TMA to synthesize doubly-responsive diblock copolymers.

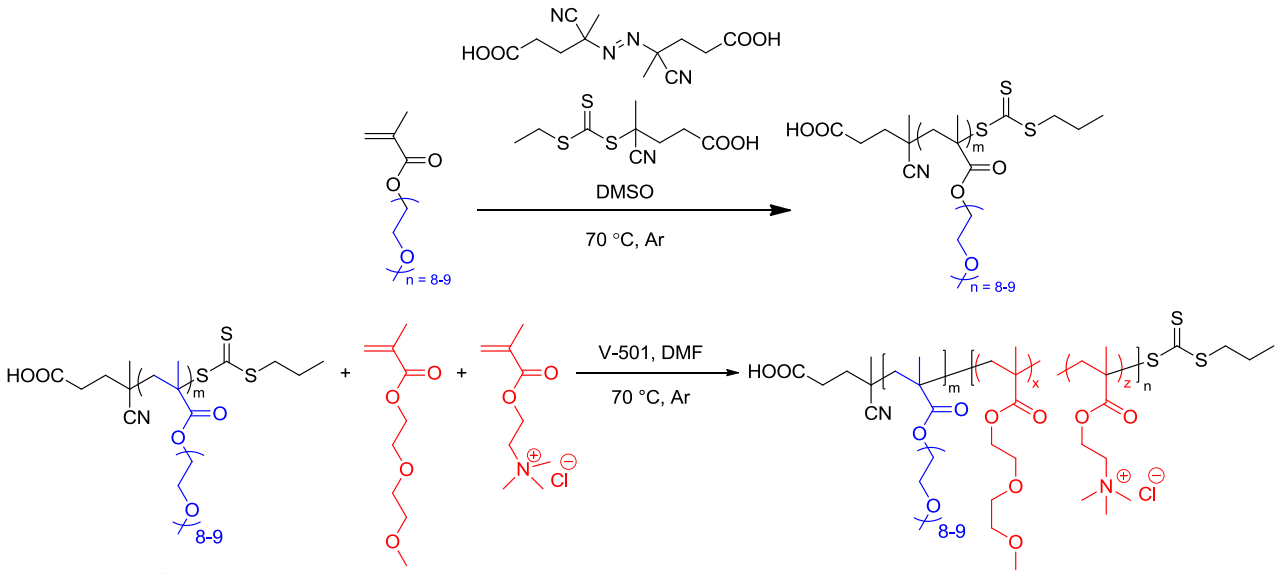

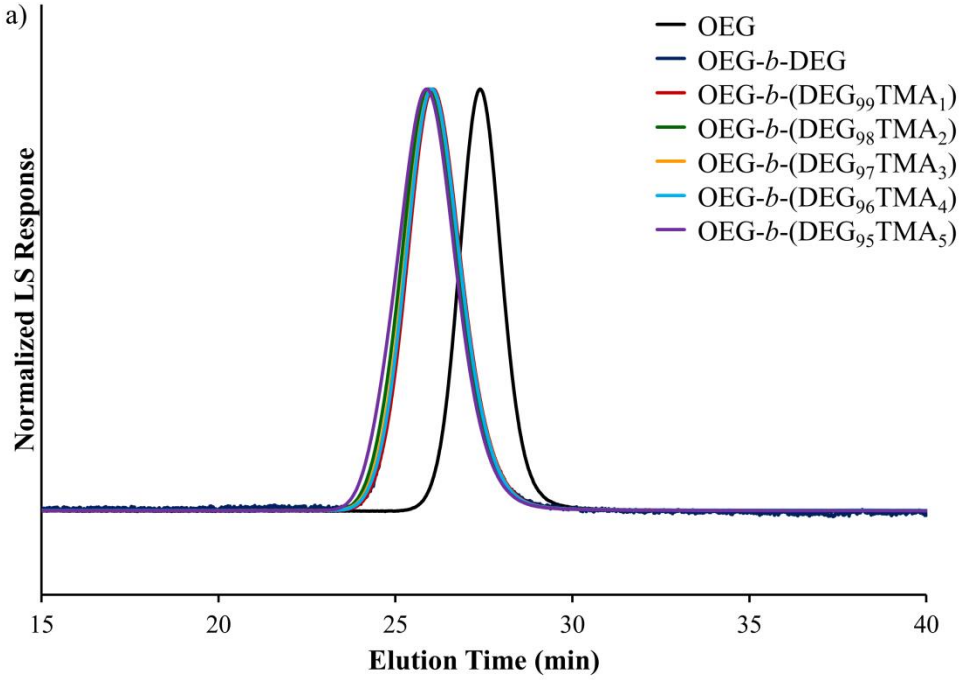

Figure 11.1. Aqueous SEC LS curves for the initial poly(OEG) macroCTA and the resulting poly(OEG-*b*-DEG$_x$TMA$_y$) diblock copolymers.

Table 11.1. Molecular weight analysis of the poly(OEG-*b*-DEG_xTMA_y) diblock copolymer series.

Polymer	M_n (kg/mol)	PDI	DP of A Block	DP of B Block
poly(OEG)	13.6	1.04	28	0
poly(OEG-*b*-DEG)	41.6	1.03	28	149
poly(OEG-*b*-$DEG_{99}TMA_1$)	39.4	1.03	28	137
poly(OEG-*b*-$DEG_{98}TMA_2$)	44.0	1.03	28	161
poly(OEG-*b*-$DEG_{97}TMA_3$)	41.2	1.02	28	147
poly(OEG-*b*-$DEG_{96}TMA_4$)	40.3	1.02	28	141
poly(OEG-*b*-$DEG_{95}TMA_5$)	41.7	1.03	28	149

ABA triblock copolymers display ideal properties for hydrogel materials wherein the A blocks act as physical crosslinks and the B block remains hydrophilic. Upon micellization, the A blocks associate to generate a physically crosslinked network bridged through the hydrophilic B block. Long and Allen et al.[35] recently published a novel difunctional trithiocarbonate, dCEP, suitable for the RAFT polymerization of methacrylate monomers. Since dCEP contains similar CTA functionality as CEP, dCEP enabled the synthesis of salt- and temperature-responsive ABA triblock copolymers in two synthetic steps similar to the diblock copolymer synthesis (**Scheme 11.2**). Polymerization of OEG first synthesized a precise poly(OEG) macroCTA (M_n = 64.9 kg/mol, PDI = 1.01). Subsequent chain extension with DEG and TMA in different molar feed ratios generated the desired dual responsive triblock copolymers with M_n's of ~230 kg/mol and PDIs ≤ 1.20 as shown in **Table 11.2**. Aqueous SEC confirmed a complete monotonic shift to shorter elution times upon chain extension (**Figure 11.2**).

Scheme 11.2. RAFT polymerization to synthesize temperature- and salt-responsive triblock copolymers.

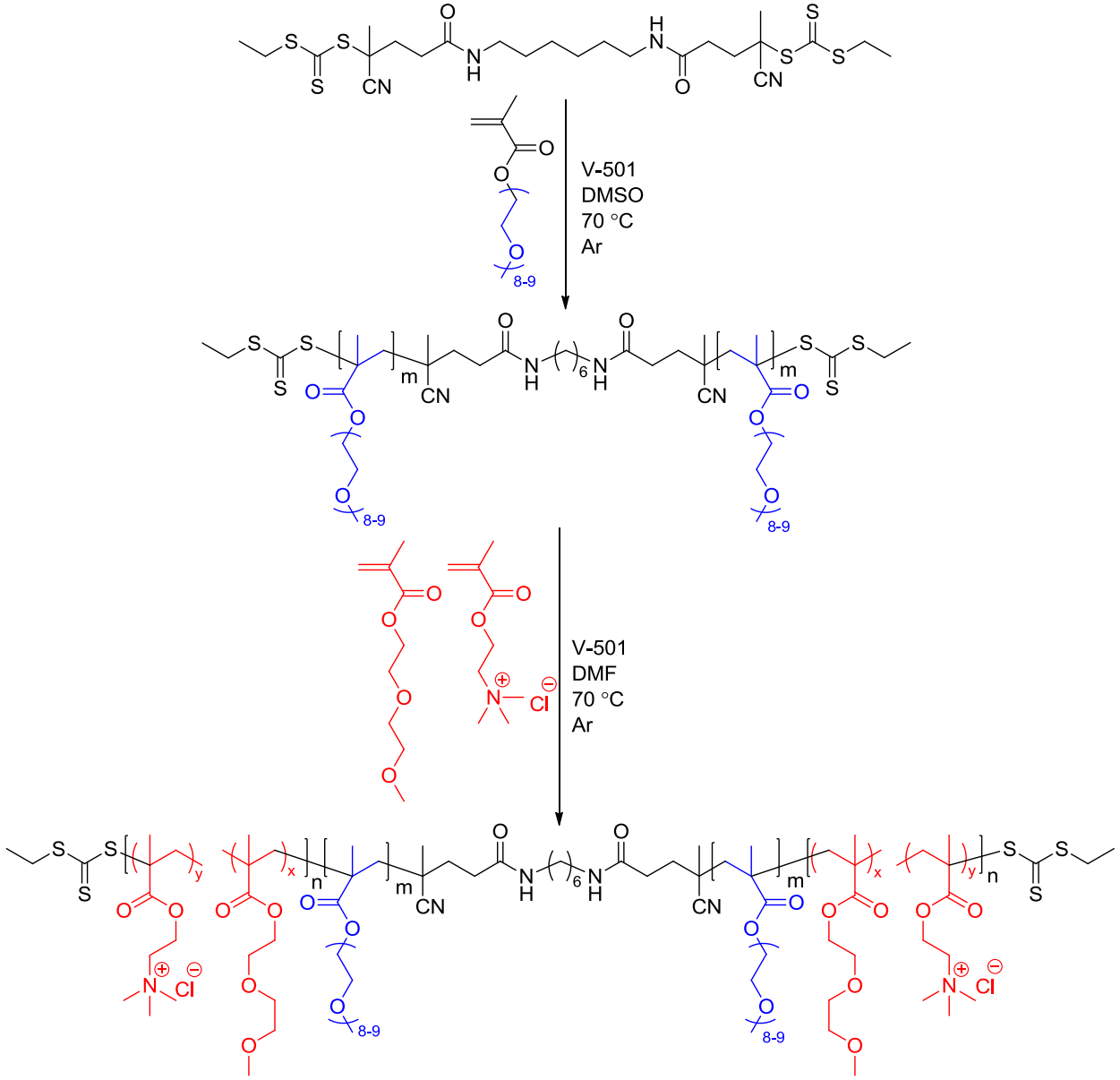

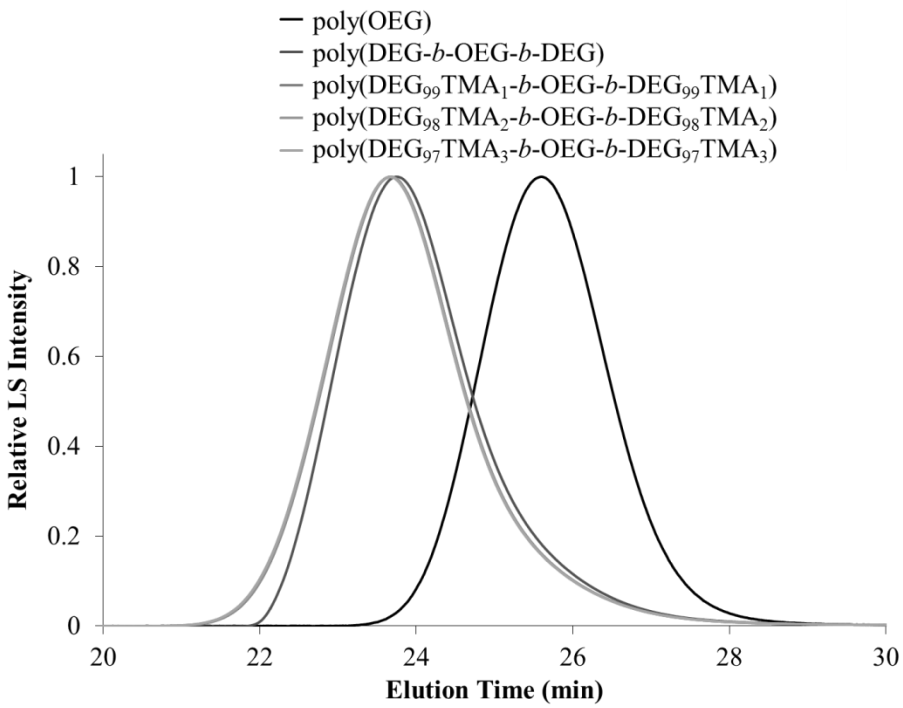

Figure 11.2. Aqueous SEC analysis of the difunctional poly(OEG) macroCTA and the resulting triblock copolymers poly(DEG_xTMA_y-*b*-OEG-*b*-DEG_xTMA_y).

Table 11.2. Molecular weight analysis of the poly(OEG) macroCTA and the resulting triblock copolymers poly(DEG_xTMA_y-*b*-OEG-*b*-DEG_xTMA_y).

Polymer	Block M_n (kg/mol)	Overall M_n (kg/mol)	PDI
poly(OEG)	64.9	64.9	1.01
poly(DEG-*b*-OEG-*b*-DEG)	84.6-*b*-64.9-*b*-84.6	234	1.14
poly($DEG_{99}TMA_1$-*b*-OEG-*b*-$DEG_{99}TMA_1$)	87.1-*b*-64.9-*b*-87.1	239	1.17
poly($DEG_{98}TMA_2$-*b*-OEG-*b*-$DEG_{98}TMA_2$)	82.1-*b*-64.9-*b*-82.1	229	1.20
poly($DEG_{97}TMA_3$-*b*-OEG-*b*-$DEG_{97}TMA_3$)	82.6-*b*-64.9-b-82.6	230	1.19

11.4.2 Salt- and temperature-responsive micelles

Dynamic light scattering elucidated the salt- and temperature-response of the diblock copolymers. Temperature step studies (2 °C/step) in HPLC-grade water or 0.9 wt% NaCl in water (physiological salt concentration) directly measured the critical micellization temperatures.

Figure 11.3 summarizes the DLS studies for all diblock copolymers in HPLC-grade water or salt solution. The critical micellization temperature was attributed to the temperature when the hydrodynamic diameter increased dramatically. After equilibration at higher temperatures, the micelles achieved a steady state size between 25 and 50 nm. Previous literature on PNIPAM diblock copolymers show a similar trend where a larger micelle occurs at the CMT with the formation of a smaller micelle at higher temperatures presumably due to dehydration of the PNIPAM core.[17] Poly(OEG-*b*-DEG) displayed a CMT of 30 °C in HPLC-grade water, higher than the LCST of poly(DEG) (26 °C) due to the attachment of the hydrophilic poly(OEG) block. Higher incorporations of TMA resulted in an increased CMT with poly(OEG-*b*-$DEG_{99}TMA_1$) displaying a CMT of 32 °C while poly(OEG-*b*-$DEG_{95}TMA_5$) displayed a CMT greater than 50 °C. Matyjaszewski et al. synthesized copolymers of DEG and DMAEMA that displayed increasing LCSTs as the DMAEMA content increased due to increased hydrophilicity.[23] The hydrophilicity of TMA primarily drove the increase in the LCST of the block copolymers containing TMA.

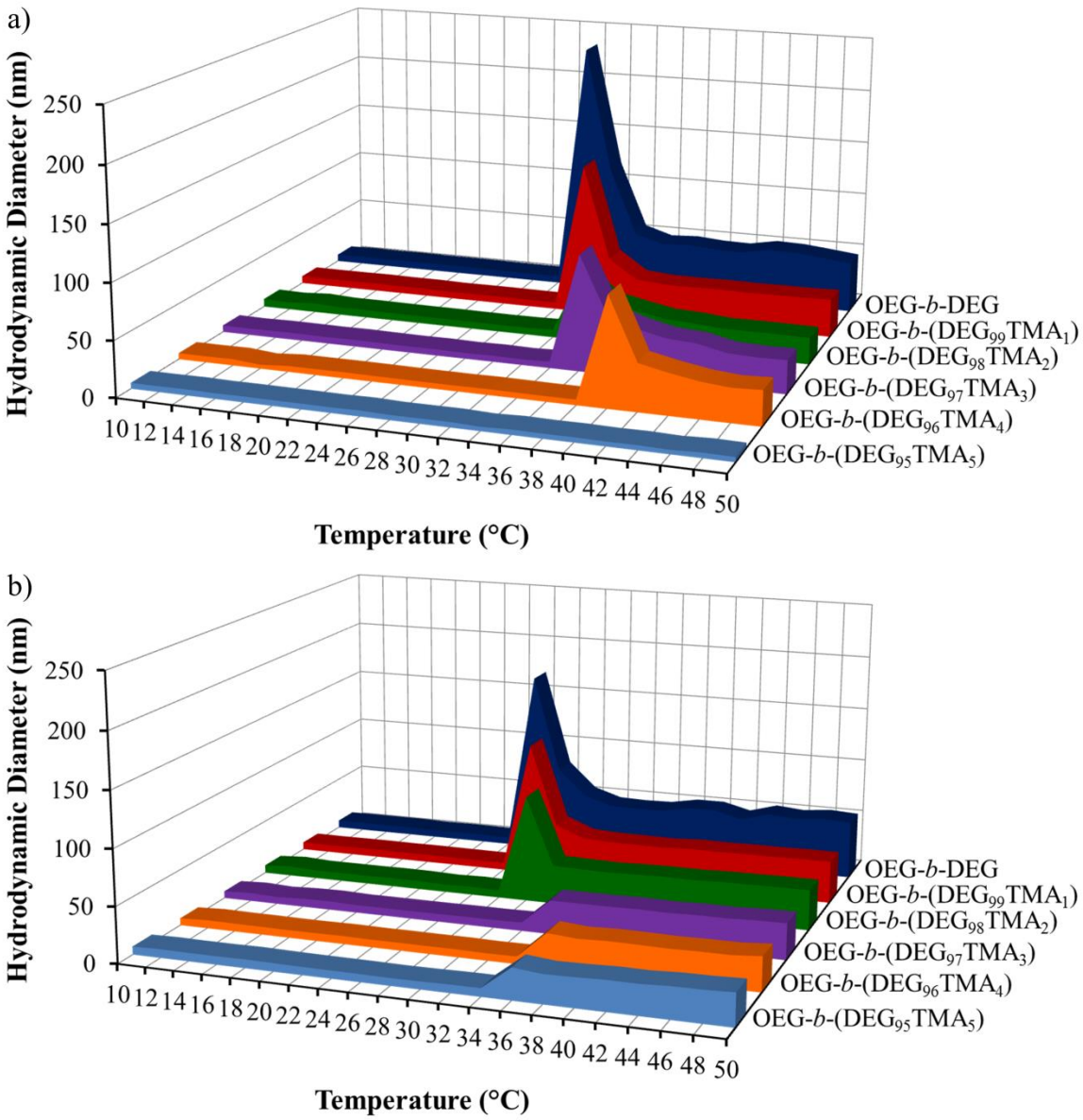

Figure 11.3. Temperature-responsive micellization of the poly(OEG-*b*-DEG$_x$TMA$_y$) diblock copolymer series in a) water and b) 0.9 wt% NaCl in water.

The addition of a physiological salt concentration (0.9 wt% NaCl in water) dramatically impacted the CMT behavior of all diblock copolymers (**Figure 11.3b**). Poly(OEG-*b*-DEG) exhibited a 2 °C shift to a lower CMT of 26 °C. Diblock copolymers containing higher TMA concentrations displayed a more dramatic shift in CMT behavior upon the addition of salt. For

example, poly(OEG-*b*-$DEG_{95}TMA_5$) exhibited a shift in CMT behavior from >50 °C to 36 °C upon the addition of salt. From a biological perspective, poly(OEG-*b*-$DEG_{96}TMA_4$) exhibited an ideal salt- and temperature-response wherein the CMT of the diblock copolymer in HPLC-grade water and 0.9 wt% NaCl in water was 40 °C and 34 °C, respectively. In the absence of both physiological salt and temperature, poly(OEG-*b*-$DEG_{96}TMA_4$) will exist as unimers in solution; biological conditions of 37 °C and 0.9 wt% NaCl will induce micellization.

11.4.3 Salt- and temperature-responsive hydrogels

ABA triblock copolymers exhibiting salt- and temperature-responsive A blocks with a hydrophilic B block enabled the generation of salt- and temperature-responsive hydrogels. The B block consisted of poly(OEG) and the A block consisted of poly(DEG) or poly(DEG_xTMA_y). Solution rheology in HPLC-grade water and 0.9 wt% NaCl in water probed the hydrogel behavior of all triblock copolymers. **Figure 11.4** highlights temperature ramp, oscillatory strain, solution rheology experiments to identify the gel point and overall gel strength of all ABA triblock copolymers in HPLC-grade water. The gel point occurred at the crossover point for storage and loss moduli. TMA concentration directly impacted the gel point in HPLC-grade water, increasing from 24 °C to >50 °C as the TMA feed ratio increased from 0 mol% TMA to 3 mol% TMA, respectively.

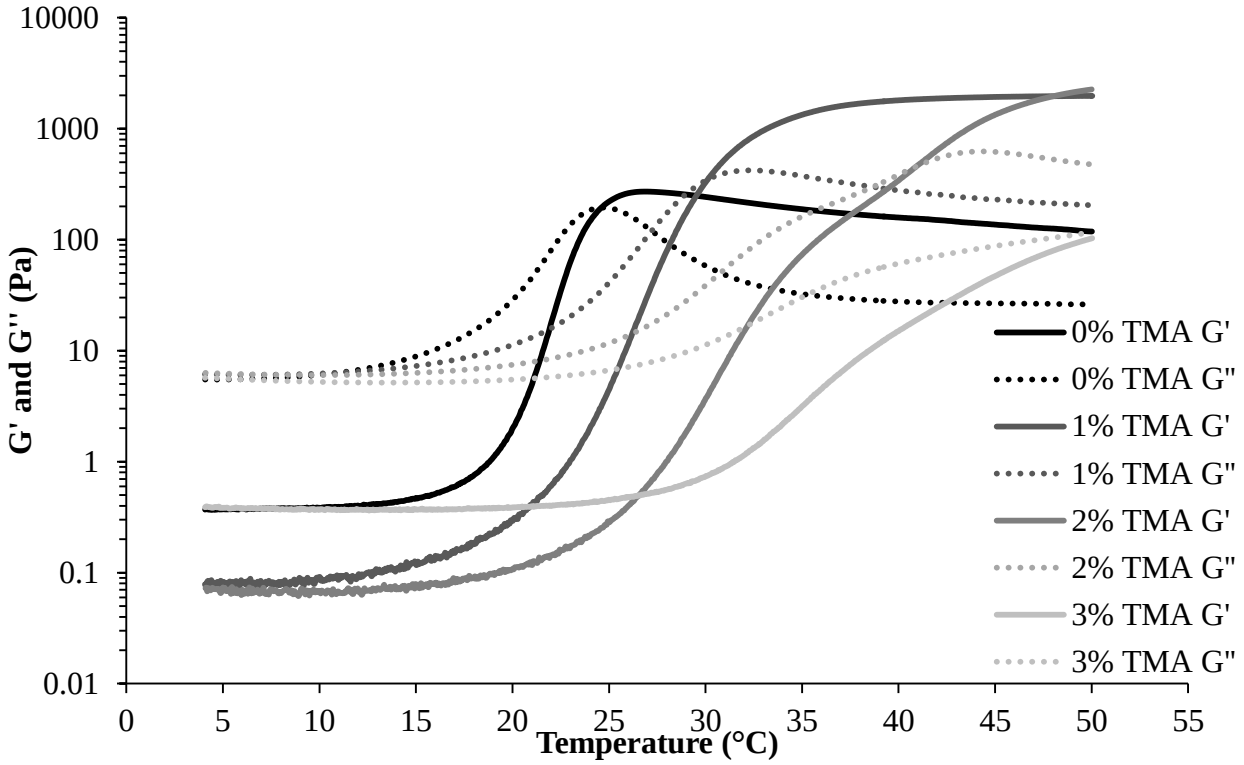

Figure 11.4. Solution rheology using a temperature sweep to determine the sol-gel transition for 25 wt% poly(DEG_xTMA_y-*b*-OEG-*b*-DEG_xTMA_y) in HPLC-grade water.

The presence of physiological salt concentrations dramatically impacted the gel points for all triblock copolymers. As the TMA concentration increased, the gel point decreased more significantly in the presence of 0.9 wt% NaCl. **Figure 11.5** highlights the solution rheology for poly($DEG_{97}TMA_3$-*b*-OEG-*b*-$DEG_{97}TMA_3$) in HPLC-grade water or 0.9 wt% NaCl in water. The gel point decreased substantially from >50 °C to 28 °C. A systematic increase in the gel point occurred as the TMA concentration increased in the 0.9 wt% NaCl solution as shown in **Figure 11.6**. **Table 11.3** summarizes the gel points for all triblock copolymers in HPLC-grade water and 0.9 wt% NaCl in water. Interestingly, all ABA triblock copolymers formed hydrogels at lower temperatures than compared to the AB diblock copolymer CMTs in both HPLC water or 0.9 wt% NaCl in water. McCormick et al.[36] demonstrated the significant impact of polymer

concentration on the gel points of poly(NIPAM-*b*-dimethyl acrylamide-*b*-NIPAM) triblock copolymers. Higher polymer concentrations resulted in lower gel points. Müller et al.[26] found similar results for their DEG and DMA star block copolymers. All rheology experiments were performed at 25 wt% polymer, suggesting a similar effect where the gel point decreased significantly compared to the CMT of the diblock copolymers at concentrations of 0.1 wt% polymer.

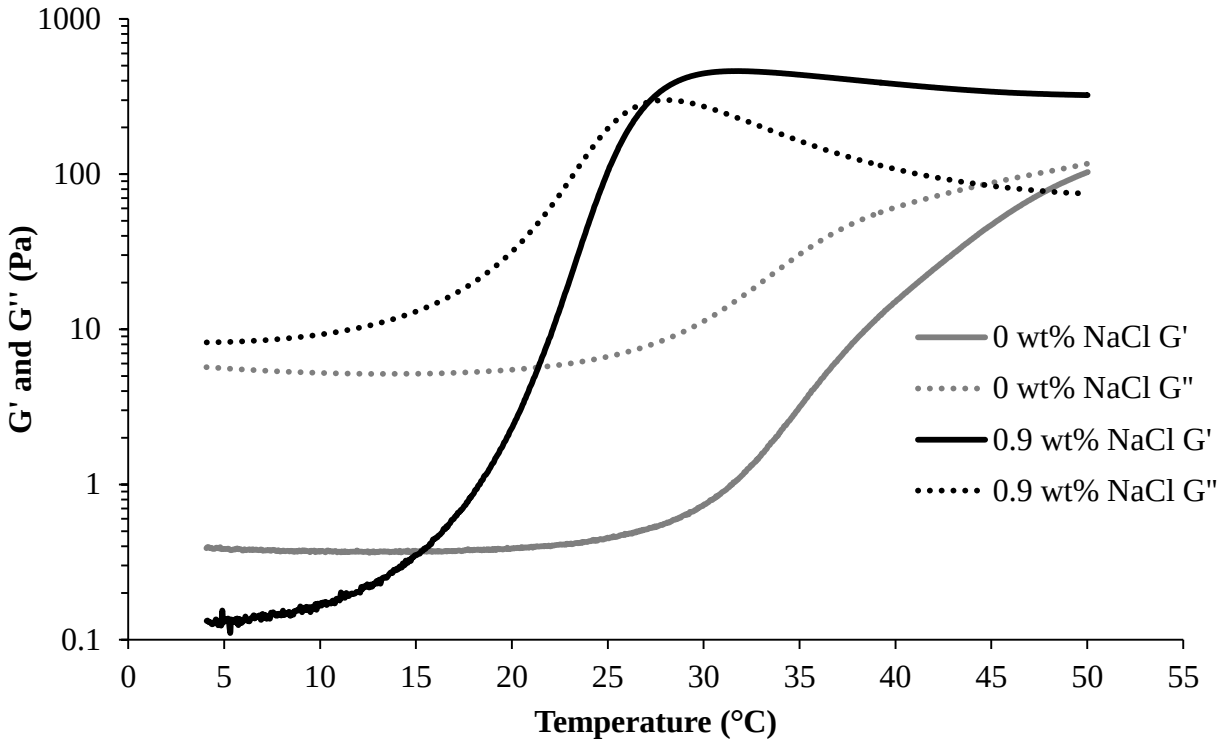

Figure 11.5. Temperature- and salt-responsive nature of poly($DEG_{97}TMA_3$-*b*-OEG-*b*-$DEG_{97}TMA_3$) probed using solution rheology with 25 wt% polymer in HPLC-grade water or 0.9 wt% NaCl in water.

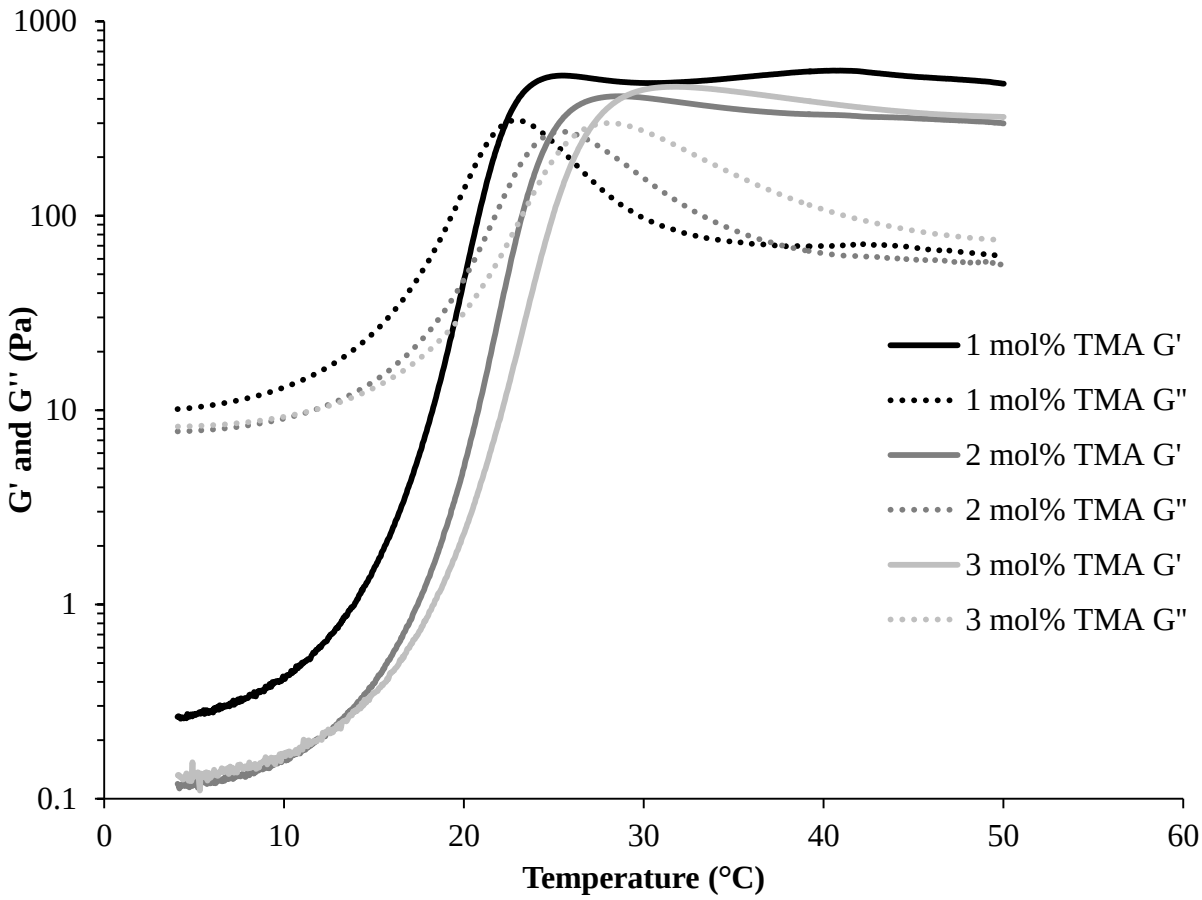

Figure 11.6. Impact of TMA concentration on sol-gel transitions for 25 wt% poly(DEG_xTMA_y-*b*-OEG-*b*-DEG_xTMA_y) in 0.9 wt% NaCl water solution.

Table 11.3. Sol-gel transitions for triblock copolymers with 25 wt% polymer in pure water or 0.9 wt% NaCl solutions.

Polymer	Gel Point No Salt (°C)	Gel Point 0.9 wt% Salt (°C)
poly(DEG-*b*-OEG-*b*-DEG)	26	22
poly($DEG_{99}TMA_1$-*b*-OEG-*b*-$DEG_{99}TMA_1$)	30	23
poly($DEG_{98}TMA_2$-*b*-OEG-*b*-$DEG_{98}TMA_2$)	40	26
poly($DEG_{97}TMA_3$-*b*-OEG-*b*-$DEG_{97}TMA_3$)	>50	28

Overall gel strengths for all triblock copolymer hydrogels were between 100 Pa and 2000 Pa at 25 wt% polymer. DEG and DMA star block copolymers from Müller et al. exhibited

higher gel strengths at 20 wt% polymer, presumably due to the multi-arm star topography that provided an inherently higher crosslink density.[26] Hysteresis experiments probed the reversibility of hydrogel formation. **Figure 11.7** shows the heating and cooling temperature ramps for poly($DEG_{98}TMA_2$-*b*-OEG-*b*-$DEG_{98}TMA_2$). Both heating and cooling curves displayed similar storage and loss moduli with the gel point occurring at a similar temperature of ~26 °C therefore showing minimal hysteresis.

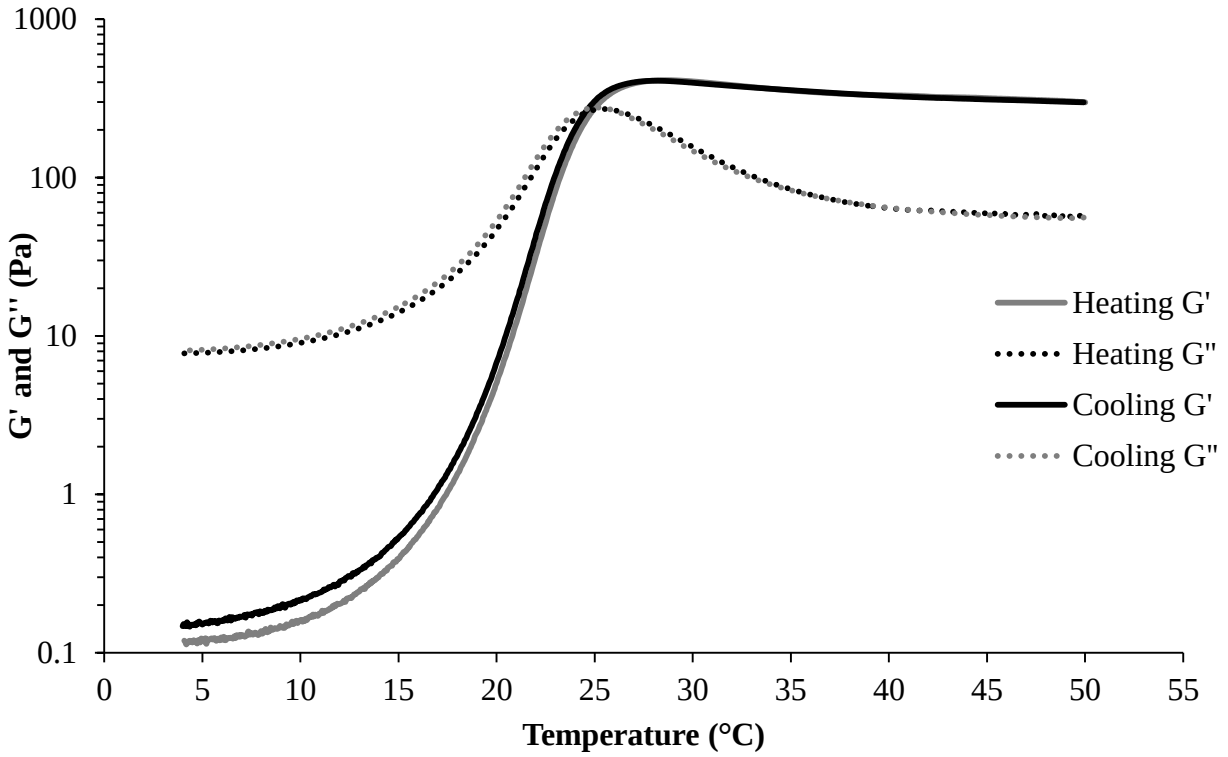

Figure 11.7. Hysteresis analysis of poly($DEG_{98}TMA_2$-*b*-OEG-*b*-$DEG_{98}TMA_2$) under heating and cooling cycles with 25 wt% polymer in 0.9 wt% NaCl water solution.

11.5 *Conclusions*

RAFT polymerization generated novel salt- and temperature-responsive AB diblock and ABA triblock copolymers in two synthetic steps. Aqueous SEC determined the molecular

weights of all block copolymers and confirmed successful chain extension. Dynamic light scattering studies probed the micellization behavior of the AB diblock copolymers. Higher TMA concentrations resulted in higher CMTs and the presence of 0.9 wt% NaCl decreased the CMT's of all diblock copolymers. Solution rheology examined the hydrogel behavior of the ABA triblock copolymers. TMA feed ratios from 0 mol% to 3 mol% increased the gel point from 26 °C to >50 °C, respectively. All ABA triblock copolymers exhibited significant salt response with poly($DEG_{97}TMA_3$-*b*-OEG-*b*-$DEG_{97}TMA_3$) exhibiting the largest shift in gel point from >50 °C to 28 °C. Hysteresis experiments using poly($DEG_{98}TMA_2$-*b*-OEG-*b*-$DEG_{98}TMA_2$) confirmed the reversibility of the hydrogel formation with minimal hysteresis. Ultimately, the designed AB and ABA triblock copolymers displayed tunable salt- and temperature-response with direct applications as drug delivery vehicles, adhesives, and hydrogels.

11.6 *Acknowledgements*

The authors gratefully thank Kimberly-Clark Corporation for financial and material support. This material is based upon work supported in part by the U.S. Army Research Office under grant number W911NF-07-1-0452 Ionic Liquids in Electro-Active Devices (ILEAD) MURI. This material is based upon work supported in part by the U.S. Army Research Laboratory and the U.S. Army Research Office under the Army Materials Center of Excellence Program, contract W911NF-06-2-0014. This material is based upon work supported by the Army Research Office (ARO) under Award No. W911NF-10-1-0307 (DURIP).

11.7 *References*

(1) Alexander, C.; Shakesheff, K. M. *Advanced Materials* **2006**, *18*, 3321.
(2) Kumar, A.; Srivastava, A.; Galaev, I. Y.; Mattiasson, B. *Progress in Polymer Science* **2007**, *32*, 1205.
(3) Schmaljohann, D. *Advanced Drug Delivery Reviews* **2006**, *58*, 1655.

(4) Ruan, C.; Zeng, K.; Grimes, C. A. *Analytica Chimica Acta* **2003**, *497*, 123.
(5) Madsen, J.; Armes, S. P. *Soft Matter* **2012**, *8*, 592.
(6) Nath, N.; Chilkoti, A. *Advanced Materials* **2002**, *14*, 1243.
(7) Alarcon, C. d. l. H.; Pennadam, S.; Alexander, C. *Chemical Society Reviews* **2005**, *34*, 276.
(8) Gilcreest, V. P.; Carroll, W. M.; Rochev, Y. A.; Blute, I.; Dawson, K. A.; Gorelov, A. V. *Langmuir* **2004**, *20*, 10138.
(9) Miasnikova, A.; Laschewsky, A. *Journal of Polymer Science Part A: Polymer Chemistry* **2012**, *50*, 3313.
(10) Lutz, J.-F. *Journal of Polymer Science Part A: Polymer Chemistry* **2008**, *46*, 3459.
(11) Lutz, J.-F.; Weichenhan, K.; Akdemir, Ö.; Hoth, A. *Macromolecules* **2007**, *40*, 2503.
(12) Diehl, C.; Schlaad, H. *Macromolecular Bioscience* **2009**, *9*, 157.
(13) Jia, Z.; Chen, H.; Zhu, X.; Yan, D. *Journal of the American Chemical Society* **2006**, *128*, 8144.
(14) Chen, C.; Wang, Z.; Li, Z. *Biomacromolecules* **2011**, *12*, 2859.
(15) Jeong, B.; Gutowska, A. *Trends in Biotechnology* **2002**, *20*, 305.
(16) Xia, Y.; Yin, X.; Burke, N. A. D.; Stöver, H. D. H. *Macromolecules* **2005**, *38*, 5937.
(17) Convertine, A. J.; Lokitz, B. S.; Vasileva, Y.; Myrick, L. J.; Scales, C. W.; Lowe, A. B.; McCormick, C. L. *Macromolecules* **2006**, *39*, 1724.
(18) De, P.; Sumerlin, B. S. *Macromolecular Chemistry and Physics* **2013**, *214*, 272.
(19) Lutz, J.-F.; Akdemir, Ö.; Hoth, A. *Journal of the American Chemical Society* **2006**, *128*, 13046.
(20) Han, S.; Hagiwara, M.; Ishizone, T. *Macromolecules* **2003**, *36*, 8312.
(21) Ishizone, T.; Seki, A.; Hagiwara, M.; Han, S.; Yokoyama, H.; Oyane, A.; Deffieux, A.; Carlotti, S. *Macromolecules* **2008**, *41*, 2963.
(22) Lutz, J.-F.; Hoth, A. *Macromolecules* **2005**, *39*, 893.
(23) Yamamoto, S.-i.; Pietrasik, J.; Matyjaszewski, K. *Macromolecules* **2008**, *41*, 7013.
(24) Pietsch, C.; Mansfeld, U.; Guerrero-Sanchez, C.; Hoeppener, S.; Vollrath, A.; Wagner, M.; Hoogenboom, R.; Saubern, S.; Thang, S. H.; Becer, C. R.; Chiefari, J.; Schubert, U. S. *Macromolecules* **2012**, *45*, 9292.
(25) Kostiainen, M. A.; Pietsch, C.; Hoogenboom, R.; Nolte, R. J. M.; Cornelissen, J. J. L. M. *Advanced Functional Materials* **2011**, *21*, 2012.
(26) Schmalz, A.; Schmalz, H.; Muller, A. H. E. *Soft Matter* **2012**, *8*, 9436.
(27) Fechler, N.; Badi, N.; Schade, K.; Pfeifer, S.; Lutz, J.-F. o. *Macromolecules* **2008**, *42*, 33.
(28) Wang, D.; Wu, T.; Wan, X.; Wang, X.; Liu, S. *Langmuir* **2007**, *23*, 11866.
(29) Dobrynin, A. V.; Colby, R. H.; Rubinstein, M. *Macromolecules* **1995**, *28*, 1859.
(30) McKee, M. G.; Hunley, M. T.; Layman, J. M.; Long, T. E. *Macromolecules* **2005**, *39*, 575.
(31) Yao, K.; Chen, Y.; Zhang, J.; Bunyard, C.; Tang, C. *Macromolecular Rapid Communications* **2013**, *34*, 645.
(32) Yao, K.; Tang, C.; Zhang, J.; Bunyard, C. *Polymer Chemistry* **2013**, *4*, 528.
(33) Convertine, A. J.; Benoit, D. S. W.; Duvall, C. L.; Hoffman, A. S.; Stayton, P. S. *Journal of Controlled Release* **2009**, *133*, 221.
(34) Allen, M. H.; Hemp, S. T.; Zhang, M.; Zhang, M.; Smith, A. E.; Moore, R. B.; Long, T. E. *Polymer Chemistry* **2013**.

(35) Allen, M. H.; Hemp, S. T.; Zhang, M.; Zhang, M.; Smith, A. E.; Moore, R. B.; Long, T. E. *Polymer Chemistry* **2013**, *4*, 2333.
(36) Kirkland, S. E.; Hensarling, R. M.; McConaughy, S. D.; Guo, Y.; Jarrett, W. L.; McCormick, C. L. *Biomacromolecules* **2007**, *9*, 481.

Chapter 12: Overall Conclusions

The conventional free radical polymerization of 9-vinylbenzyl adenine (VBA) and 2-(dimethylamino)ethyl methacrylate (DMAEMA) generated amine-containing macromolecules. Subsequent protonation using HCl generated adenine-containing polyelectrolytes. *In situ* FTIR confirmed a random copolymerization of VBA and DMAEMA. Adenine-containing polyelectrolytes displayed polyelectrolyte solution behavior in water and these copolymers were successfully electrospun to generate adenine-decorated nanofibrous mats. Ultimately, these electrospun mats will find applications focused on filtration or antimicrobial applications.

A library of ammonium- and phosphonium-containing polyelectrolytes synthesized using conventional free radical polymerization enabled a thorough structure-property examination. The library of polyelectrolytes included variations in the cationic atom, alkyl substituent lengths, and counterions. Phosphonium polyelectrolytes displayed significantly enhanced thermal stabilities compared to ammonium analogs. Ammonium polyelectrolytes primarily degraded through a reverse Menschutkin degradation mechanism. Counterion exchange to fluorinated, bulky counterions significantly improved the thermal stability of all polyelectrolytes, especially the ammonium polyelectrolytes. Bulkier counterions also depressed the glass transition temperatures of all polymerized ionic liquids. Longer alkyl substituent lengths also decreased the glass transition temperatures of the polyelectrolytes. Phosphonium polymerized ionic liquids exhibited enhanced ionic conductivities compared to ammonium analogs. Ultimately, phosphonium polymerized ionic liquids displayed enhanced thermal stabilities and ionic conductivities compared to ammonium analogs, suggesting potential applications such as fuel cell membranes and electroactive devices.

The water-soluble ammonium- and phosphonium-containing polyelectrolytes were also further examined for nonviral nucleic acid delivery applications to elucidate the impact of the cationic atom on nucleic acid binding and delivery. Phosphonium polyelectrolytes bound plasmid DNA at a +/- ratios of 2 whereas ammonium analogs bound plasmid DNA at +/- ratios of 4. Tributyl-containing polyelectrolytes exhibited the highest luciferase transfection compared to triethyl-containing polyelectrolytes. The phosphonium tributyl delivery vehicle displayed significantly improved transfection compared to the ammonium analog. All delivery vehicles failed to deliver nucleic acids in the presence of serum and they displayed significant cytotoxicity due to their 100% charge density. Ultimately, phosphonium macromolecules show significant promise for nonviral nucleic acid delivery due to their enhanced nucleic acid complexation and delivery compared to ammonium macromolecules.

Controlled radical polymerization synthesized novel AB diblock copolymers that contained a hydrophilic, colloidally stable A block and a phosphonium-containing B block. The A block consisted of oligo(ethylene glycol) methyl ether methacrylate or methacryloxyphosphoryl choline, both shown previously to impart colloidal stability to nanoparticles. All phosphonium diblock copolymers complexed nucleic acids efficiently at +/- ratios of 1. Dynamic light scattering studies at charge ratios of 2 in the presence of salt or serum highlighted the enhanced colloidal stability of all diblock copolymers compared to the phosphonium homopolymer. Phosphonium diblock copolymers displayed minimal cytotoxicity and they delievered nucleic acids efficiently to HepaRG cells in the presence of serum.

Step-growth polymerization of ditertiary phosphines and alkyl dibromides generated well-defined phosphonium ionenes. Short alkyl spacer lengths in the monomers preferentially led to the generation of oligomeric cyclics while long alkyl spacer lengths suppressed cyclization.

All phosphonium ionenes displayed high molecular weights shown using aqueous SEC. Phosphonium ionenes exhibited high thermal stabilities compared to ammonium ionenes. They also resisted degradation in alkaline environments compared to ammonium ionenes, which readily degrade in alkaline conditions. Glass transition temperatures decreased as the phosphonium ionene charge density decreased. Ultimately, the enhanced thermal stabilities and relatively low glass transition temperatures enabled a further understanding of polyelectrolyte melt flow dynamics using melt rheology. Phosphonium ionenes obeyed time-temperature superposition principles and they exhibited two major relaxations: one attributed to the glass transition temperature and one attributed to electrostatic relaxations. Charge density directly impacted flow activation energies with lower activation energies corresponding to lower charge densities.

Phosphonium gemini surfactants were readily synthesized using S_N2 substitution techniques and the alkyl spacer lengths were readily controlled based on the starting materials utilized. Phosphonium gemini surfactants demonstrated poor water solubility due to their hydrophobic head groups. Dilute aqueous solutions resulted in the self-assembly of phosphonium gemini surfactants into vesicles. Phosphonium gemini surfactants complexed nucleic acids efficiently, but they displayed poor transfection capabilities. They readily dissolved in chloroform and they self-assembled in chloroform solutions with increasing viscosities as the surfactant concentration increased. Phosphonium gemini surfactants with ethylene and propylene spacers were successfully electrospun to generate uniform fibers while the butylene spacer gemini surfactant and the monophosphonium surfactant failed to electrospin.

Conventional and controlled radical polymerization techniques generated a thioether-containing homopolymer and diblock copolymer, respectively. Alkylation using methyl iodide

generated a sulfonium-containing homopolymer and diblock copolymer. Both sulfonium macromolecules effectively complexed nucleic acids at a charge ratio of 1. They both delivered nucleic acids to HeLa cells *in vitro* in the absence of serum. The sulfonium diblock copolymer exhibited enhanced colloidal stability compared to the sulfonium homopolymer and polyethyleneimine. Ultimately, sulfonium macromolecules were shown for the first time to complex and delivery nucleic acids, which will expand the potential synthetic delivery vehicles possible for nucleic acid delivery.

Reversible addition-fragmentation chain transfer polymerization enabled the synthesis of AB diblock and ABA triblock copolymers with salt- and temperature-responsive character. The B block consisted of oligo(ethylene glycol) methyl ether methacrylate as the hydrophilic block while the A block was a random copolymer of diethylene glycol methyl ether methacrylate and an ammonium methacrylate monomer. AB diblock copolymers displayed salt- and temperature-responsive micellization behavior with increasing ammonium content leading to higher LCSTs and more pronounced salt triggerability. ABA triblock copolymers exhibited salt- and temperature-responsive hydrogel formation. Gel points depended significantly on the ammonium content in the triblock copolymer and the presence of physiological salt concentrations decreased the gel points due to their salt responsive character. Ultimately, AB diblock and ABA triblock copolymers with salt- and temperature-responsive character near physiological conditions were synthesized suitable for drug delivery and hydrogel applications.

Chapter 13: Suggested Future Work

13.1 *Phosphonium Macromolecules for Nonviral Gene Delivery*

Future work on the phosphonium diblock copolymers would primarily focus on further nanoparticle characterization and stability analyses. Static light scattering studies would enable the determination of the M_w of the polyplexes and provide insight into the cationic diblock and anionic nucleic acid composition within the polyplexes. Small angle neutron scattering with contrast matching experiments would enable further in depth studies allowing the determination of the shell and core size of the polyplexes. Ultimately, cryo-TEM coupled with the previous two experiments will visualize the polyplexes in their hydrated state. The goal would be to understand further the core-shell micelle assembly upon nucleic acid and cationic diblock copolymer complexation. Further understanding of salt stability concerning electrostatic complexation is also needed and would be an excellent avenue of research. The absence or presence of salt dramatically impacts electrostatic complexation and studies on coacervates will help detail the necessary structures to provide stabilization in a salt environment. The salt concentration and salt structure will also impact the electrostatic complexation, allowing a broad range of experiments focused on salt structure and the structure of the cationic and anionic macromolecules. Molecular weights of the macromolecules will influence the strength and nature of the electrostatic complexation also. Covalent crosslinking between the cationic and anionic macromolecule would also stabilize the coacervate in the presence of salt.

13.2 *Phosphonium Ionenes*

Previous phosphonium ionene work focused on examining the structure-property relationship based upon varying the alkyl spacers in between the ditertiary phosphine and

dibromide to control the phosphonium ionene charge density. **Scheme 13.1** highlights a logical extension of the phosphonium ionene project through the anion metathesis reactions to exchange the Br^- counterion to bulky, fluorinated counterions. These novel polymerized ionic liquids will display further enhanced thermal stabilities and the bulky counterions will reduce the glass transition temperatures of the phosphonium ionenes. Melt rheology studies will examine the impact of the counterion on melt flow dynamics and the ionic conductivities of the phosphonium ionenes can be examined using impedance spectroscopy. Further alkaline stability studies will also enable a further understanding of the base stability of phosphonium ionenes. Phosphonium ionenes with fluorinated anions will display significant water insolubility, enabling a base stability study of a film in a 1M KOH solution. The alkaline stability of phosphonium ionenes could also be probed at elevated temperatures in water, approaching conditions necessary for alkaline fuel cell membranes.

Scheme 13.1. Anion-exchange reactions to generate phosphonium ionenes with different counterions.

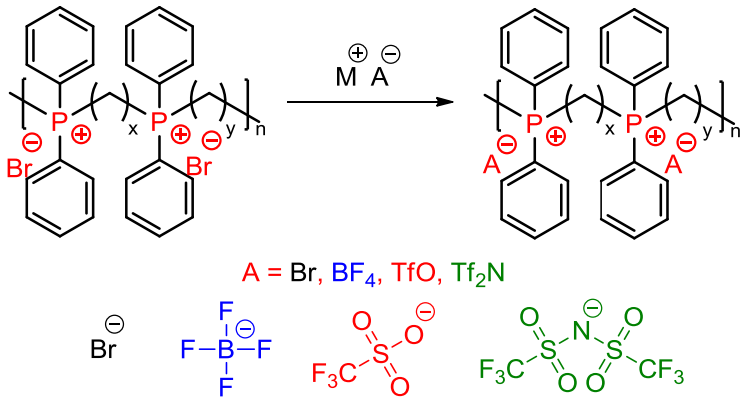

Preliminary studies focused on the anion exchange of 4P,12-ionene from bromide counterions to BF_4^-, TfO^-, and Tf_2N^- counterions. TGA analysis showed significantly improved thermal stabilities for all fluorinated counterions (≥400 °C). The glass transition temperatures for Br^-, BF_4^-, TfO^-, and Tf_2N^--containing 4P,12-ionene were 123 °C, 90 °C, 71 °C, and 19 °C,

respectively. **Figure 13.1** shows preliminary melt rheology analysis of 4P,12-ionene with different counterions. Both glass transition and electrostatic relaxations shift to shorter time scales upon anion exchange to more bulky, delocalized anions.

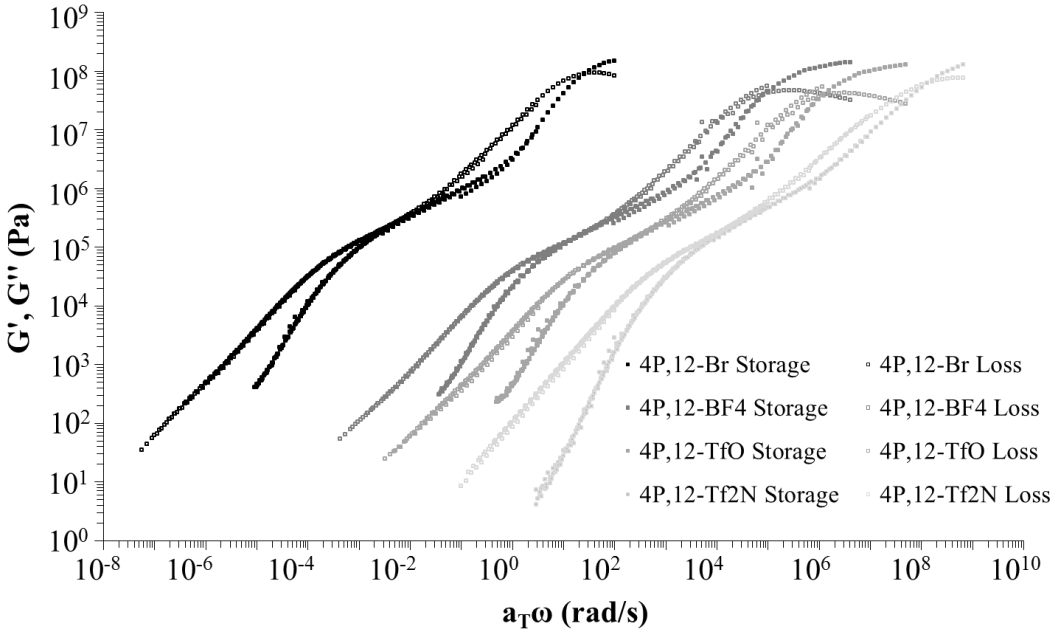

Figure 13.1. Melt rheology of 4P,12-ionene with various counterions showing a significant shift in both glass transition and electrostatic relaxations upon counterion exchange.

A further extension of the phosphonium ionene project will focus on the design and synthesis of segmented phosphonium ionenes with the goal to generate thermoplastic elastomers. **Scheme 13.2** depicts an example synthesis of a segmented phosphonium ionene. The hard segment content can be readily controlled through stoichiometry along with varying the ditertiary phosphines and chain extender dibromides utilized. The present example shows a poly(ethylene glycol) (PEG) dibromide as the soft segment monomer. A PEG soft segment will improve the water solubility of phosphonium ionenes, improving their potential for biological/aqueous applications. Ultimately, the soft segment can be modified to include poly(dimethyl siloxane) or polyethers such as poly(propylene glycol), which would be more suitable for thermoplastic

elastomers due to their enhanced hydrophobicity. Segmented phosphonium ionenes remain a rich area of research with a broad range of structures possible to generate unique macromolecular properties.

Scheme 13.2. Synthesis of segmented phosphonium ionenes using step-growth polymerization.

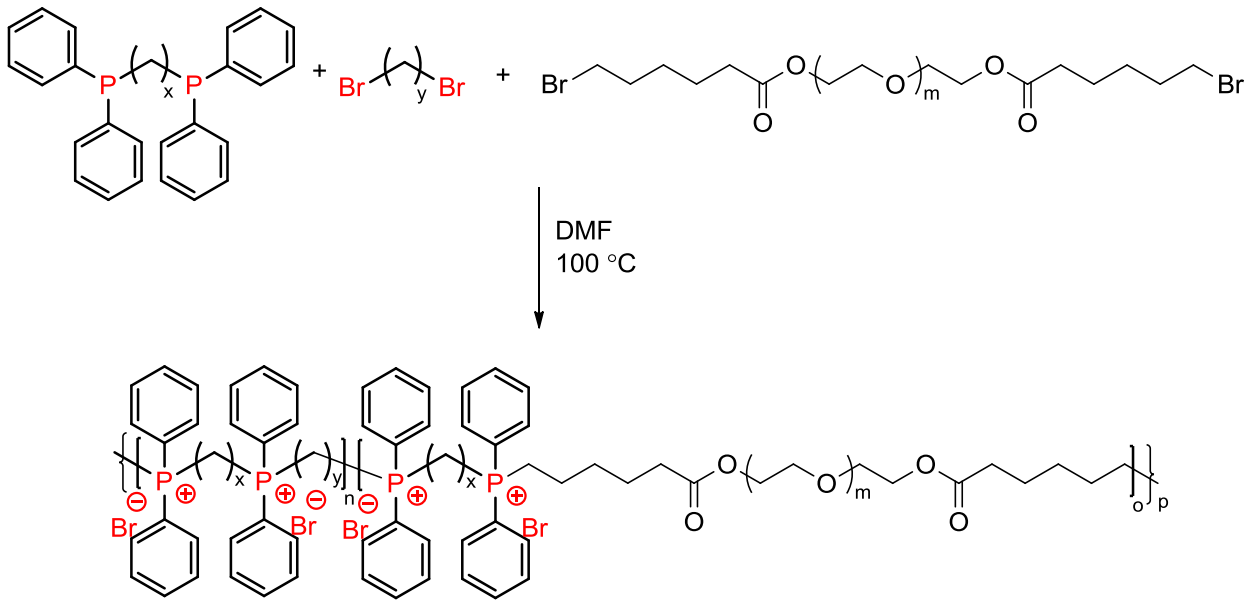

13.3 *Sulfonium Polyelectrolytes*

Sulfonium polyelectrolytes remain an immature area in macromolecular research, primarily stemming from synthetic difficulty and overall cation stability. Activated halides and other synthetic techniques should enable the synthesis of a broad range of sulfonium polyelectrolytes. Post-polymerization alkylation of poly(2-methylthioethyl methacrylate) will avoid potential monomer stability issues during polymerization and subsequent anion metathesis will expand the library of sulfonium polymerized ionic liquids possible as shown in **Scheme 13.3**. Due to the relatively unexplored research area, sulfonium polymerized ionic liquids exhibit a rich area of research potential. **Scheme 13.4** depicts the successful synthesis of a sulfonium polymerized ionic liquid wherein the glass transition temperature of the ionic liquid monomer

was -51 °C. Thermogravimetric analysis will probe overall sulfonium macromolecule stability with a focus on examining how the counterion impacts thermal stability. The goal would be to improve the overall cation stability to expand the potential applications possible for sulfonium macromolecules. Impedance spectroscopy will examine the ionic conductivities of sulfonium polymerized ionic liquids, enabling an understanding of how a sulfonium cation impacts ionic conductivity.

Scheme 13.3. Alkylation of poly(2-methylthioethyl methacrylate) utilizing a broad range of activated alkyl halides with subsequent counterion exchange to generate a large library of polymerized ionic liquids.

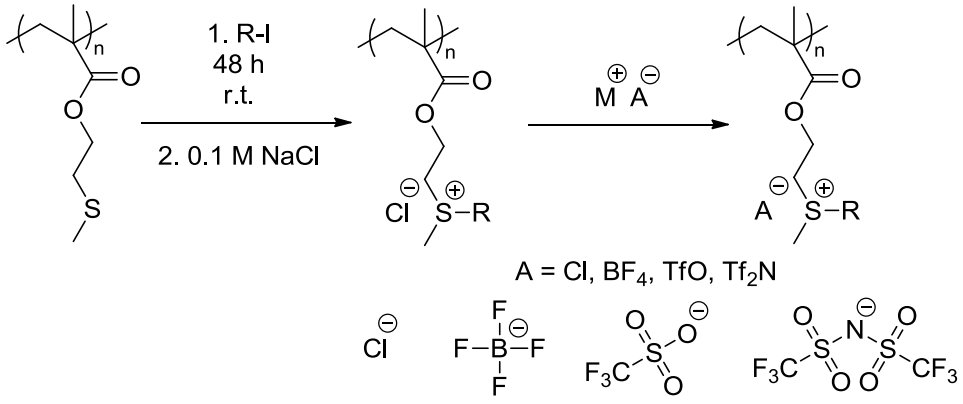

Scheme 13.4. Successful synthesis of a sulfonium polyermized ionic liquid.

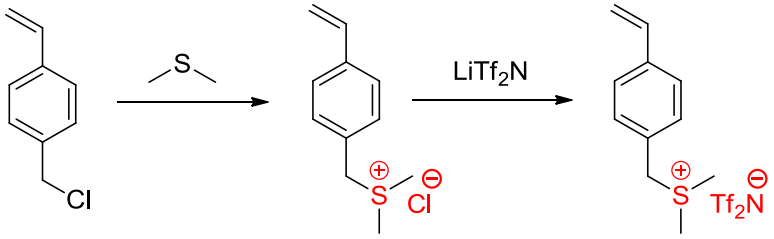

13.4 *Arsenium Macromolecules*

Arsenium macromolecules are not found in the literature due to the limited availability of tertiary arsines along with their potential toxicity and difficulty in handling. Triphenylarsine is

the commercially available and poses minimal risks due to the resonance stabilization of the arsine through the phenyl substituents. Unfortunately, triphenylarsine displays very poor nucleophilicity, hindering the potential synthesis of arsenium macromolecules. Trimethylarsine also is commercially available and should be suitable to generate novel arsenium monomers as shown in **Scheme 13.5**. Subsequent conventional free radical polymerization will create novel arsenium macromolecules, which can then be anion exchanged to generate polymerized ionic liquids. These macromolecules are completely unexplored and the proposed synthesis will enable the first characterization of arsenium macromolecules. Trimethylarsenium-containing macromolecules also will be directly compared to trimethylammonium- and trimethylphosphonium-containing macromolecules to elucidate the impact of the arsenic cationic atom on macromolecular properties.

Scheme 13.5. Synthesis of a novel arsenium monomer and arsenium macromolecules.

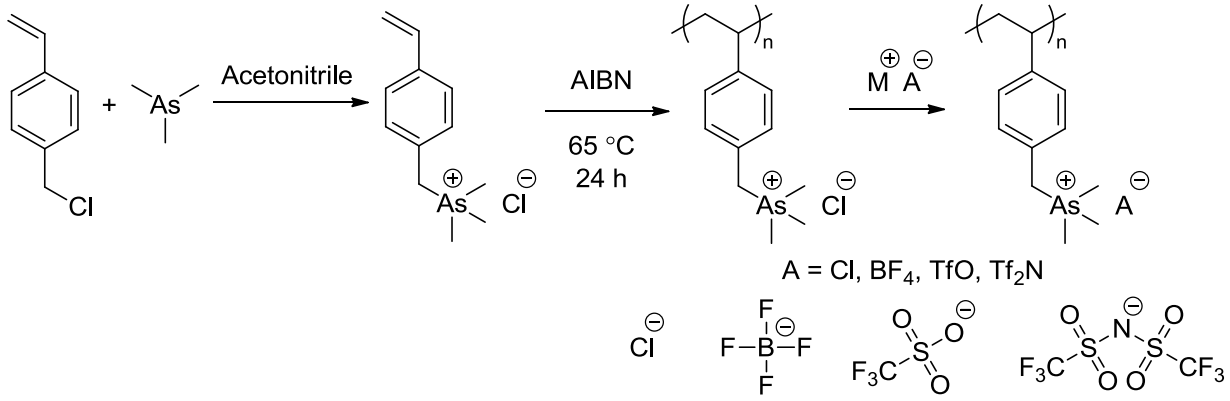

13.5 *Styrene Phosphine Macromolecules*

The reported ammonium and phosphonium polystyrenes relied solely on the attachment of the ammonium or phosphonium cation at the para benzylic position of the monomer and macromolecule. The benzylic position affords facile substitution and synthesis, but also results in thermal and chemical instability due to the acidity of the benzylic position. Shown previously

above, the benzylic position resulted in the thermal degradation of the ammonium polystyrenes through reverse Menschutkin degradation. 4-(diphenylphosphino)styrene is a commercially available monomer utilized in a broad range of materials.[1,2] **Scheme 13.6** depicts a proposed synthetic pathway that will generate a phosphonium-functionalized polystyrene wherein the phosphonium group will be attached directly at the para position. The removal of the benzylic position along with the initial neutral monomer will enable conventional free radical polymerization, controlled radical polymerization, and anionic polymerization to generate homopolymers and well-defined block copolymers. Due to the enhanced nucleophilicity of tertiary phosphines, the tertiary phosphine polystyrene could be alkylated with a broad range of alkyl halides to create a library of phosphonium polystyrenes.

Scheme 13.6. Polymerization of 4-(diphenylphosphino)styrene with subsequent alkylation to generate phosphonium polystyrenes.

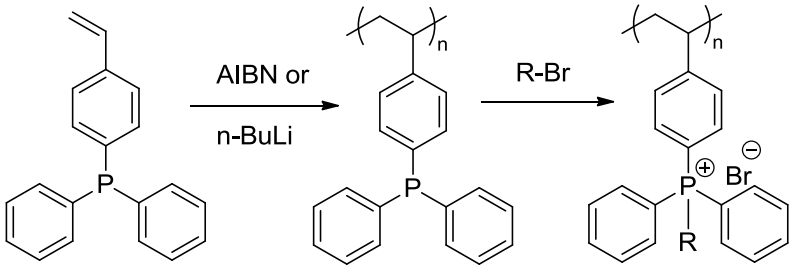

13.6 *References*

(1) Choi, M. K. W.; He, H. S.; Toy, P. H. *The Journal of Organic Chemistry* **2003**, *68*, 9831.
(2) Guino, M.; Hii, K. K. *Chemical Society Reviews* **2007**, *36*, 608.